TARGETING OF PROTEINS AND PROTEIN ANALOGS

TO METAL-CHELATING LIPID VESICLES

Thesis by

Deborah Rebecca Shnek

In Partial Fulfillment of the Requirements

for the Degree of

Doctor of Philosophy

California Institute of Technology

Pasadena, CA

1996

(submitted July 21, 1995)

iii

ACKNOWLEDGMENTS

As the first student on a demanding project, I have many people to thank for their support. First I would like to thank my advisor, Frances Arnold, for without her support this project would not be possible. I would like to thank all the past and present members of the Arnold group for their help. Although she has passed away, I will remember Chariklia Economou Tsapatsis for her cheerful demeanor which made my days bright. Especially helpful was my collaborator Dr. Darryl Sasaki, who was a talented chemist and also an inventor, always having many wonderful ideas and suggestions. Dr. Robert Johnson deserves many thanks for his support and for helpful discussions. My recent interaction with Dr. Litian Fu and Dr. Kevin Maloney has made the last months very enjoyable.

I thank the Baldeschweiler group, especially Dr. Mitsuko Fujiwara and Dr. Roxanne Male for their comments about my work. Many thanks to Dr. Soon-Sam Kim of JPL for the many days he spent teaching me ESR spectroscopy. Many thanks to Dr. Jean-Paul Revel and Jean Edens for their patient instruction in freeze-etch technique. I also appreciate the help of Dr. Jay Winkler at the Beckman Institute Laser Facility. My MIT cohorts Edye Udell and Kim Mislick deserve a special pat on the back for their support throughout all these years.

The person who deserves the greatest thanks is my husband Frode Stavehaug. He has unfailingly stood by me throughout the trials and tribulations of my Ph.D. He has provided wisdom and has always told me that I could accomplish my goals.

ABSTRACT

This investigation demonstrates that new metal-chelating lipids formed into mixed vesicles can bind to a variety histidine-rich ligands through metal coordination. Our results show the feasibility of metal-chelating lipids as a method for targeting histidine-rich compounds to lipid interfaces. Interesting metal chelating lipid materials for protein orientation studies, matching the surface distribution of surface residues, protein drug delivery, and for two-dimensional protein crystallization could be made with chelating-lipids. Engineered proteins containing a histidine "tag" or proteins with natural surface histidine residues are easily targeted to the interface using metal binding.

Both metal binding and histidine-rich ligand binding were investigated with mixed metal-chelating lipid vesicles. New metal-chelating lipids containing an iminodiacetate (IDA) chelating-moiety were formed into mixed vesicles and shown to bind transition metal ions through the lipid headgroup. Metal binding was characterized through calorimetry, freeze-etch microscopy, light scattering, ESR, and fluorescence studies. Fluorescently-labeled lipids containing iminodiacetate showed a large change in the fluorescence emission spectra upon metal binding, behavior which has proven useful for a vesicle-based metal sensor.

Metal-loaded vesicles bound a model protein specifically through surface-accessible histidines, as shown using ESR studies. Equilibrium binding measurements showed at least an order of magnitude increase in binding affinity of the protein for the membrane when metal was present. The association constants determined through isothermal titration calorimetry for a model bivalent histidine compound binding to metal-chelating lipid bilayers were of the order of 10^5 M^{-1}, while monovalent binding constants were of the order 10^3 M^{-1}.

Lipid re-organization upon ligand binding was probed with model histidine compounds and histidine polymers using fluorescently-labeled metal-chelating lipid

vesicles. The ability of lipids to form multivalent ligand-lipid complexes was investigated using the formation of lipid excimers, as demonstrated by fluorescence measurements of the E/M intensity ratio. Histidine content of model compounds determines the magnitude of the effect on the fluorescence emission spectra. Histidine polymers showed a larger increase of the E/M ratio than the smaller bivalent or monovalent compounds. Combining equilibrium binding results obtained with model complexes and results from fluorescence experiments, studies with metal-chelating vesicles support multivalent coordination and reorganization of the lipids by histidine-rich ligands.

TABLE OF CONTENTS

LIST OF FIGURES

Chapter 3.

Chapter 4.

Chapter 5.

LIST OF TABLES

Introduction

MULTIVALENT RECOGNITION AT INTERFACES

Many recognition events in biological membranes involve multivalent binding to create high affinity, high selectivity target-receptor complexes. Multivalent interactions often control the extent and specificity of binding and can govern the subsequent processes, such as signal transduction [1]. Multivalent binding involves the association of a ligand with multiple receptors to form a complex with higher affinity than the monovalent ligand-receptor complex. An excellent illustration of the benefits of multivalent ligand-receptor binding is the association between antigen, soluble IgE antibodies, and Fcε receptors present on human basophils, illustrated in Figure 0.1. Multiple soluble IgE antibodies are able to bind to different sites on an antigen. Both monovalent antigen-IgE and unbound IgE can bind reversibly to membrane-bound Fcε receptors with low ($K \approx 10^6$ M^{-1}) affinity (Figure 1.1,A) [2,3]. Upon antigen binding to multiple IgE antibodies in solution, the subsequent multivalent complex binds with much higher affinity ($K \approx 10^9$ M^{-1}) to the membrane Fcε receptors (Figure 1.1, B) than the monovalent IgE-Fcε complex. The $(IgE)_n$-antigen complex cross-links Fcε receptors. Upon formation of the membrane-bound multivalent receptor-ligand complex, a signal is sent: histamine granules are released from inside the cell (Figure 1.1, C). Monovalent binding results in no histamine release. The higher affinity of the multivalent complex results in signal transduction, while monovalent, lower affinity binding does not.

Enhancement of binding affinity through multivalent recognition is due to formation of multiple membrane contacts. It has been shown that the necessary condition for histamine release is that IgE is cross-linked in solution. Chemically dimerized IgE lacking antigen also triggers histamine release [4]. Thus, IgE must be pre-organized with antigen in a multivalent complex for signaling. The dimer of antigen cross-linked IgE consequently forms more receptor contacts, enhancing the affinity of binding and brings the receptors physically close together [5]. Cross-linking of the receptors changes the membrane

fluidity, resulting in histamine release. Many surface cellular receptors reorganize in the lipid bilayer upon ligand binding to form a higher-affinity multivalent ligand-receptor complex that participates in signal transduction [6,7]. Dimer complex formation acts as an on-off switch for the signal response between different receptors. Dimerization and activation of tyrosine kinase activity have been encountered with EGF surface receptors [8,9]. Specific cross-linking of membrane receptors to produce signal transduction is encountered for olfactory sensing [10] and peptide sensing [11,12]. Signal transduction is frequently mediated through GTP-binding proteins [7] or tyrosine kinases [13], usually occurring after a soluble ligand, such as a hormone, has bound to a receptor on the cell surface. These examples illustrate the effect of multivalent binding to mobile multiple receptors and how this higher-affinity binding results in biological events transduced after recognition.

Multiple ligand-receptor bonds to a fixed surface also confer favorable energetics of binding. For instance, fits of equilibrium binding experiments between polymers and a carbon surface yielded increased association constant when multiple surface contacts were included in the curve fitting procedure when compared to simple Langmuir fits [14,15]. Indeed multiple-point binding is important for adsorptive protein separations, such as ion exchange, on chromatographic supports [16,17]. As multiple bonds are formed and re-formed with the surface, molecules that are able to form a greater number of surface bonds are retained longer on the support. In liquid chromatography discreet multiple interactions can occur through electrostatic or affinity attachments to the surface. Chromatography supports have "receptors" that are fixed two-dimensionally. However, with lipid assemblies we have the potential to make receptors that are able to reorganize to form the maximum number of contacts with the ligand.

LIGAND-DRIVEN REORGANIZATION OF LIPID MEMBRANE SURFACES

We are interested in using multivalent ligands to make synthetic materials for biological recognition. A high-affinity multivalent complex analogous to a synthetic "receptor" could be made by forming multiple lipid-protein bonds, shown in Figure 0.2. The ability of the membrane components to re-organize to increase the number of lipid-ligand bonds would promote strong binding of interesting ligands. Lipid-based materials could be used for applications where it is desirable to target biological molecules to the interface. Targeting of proteins to membrane interfaces would be useful for controlled protein orientation on membrane surfaces and for two-dimensional crystallization of proteins on membrane interfaces. Or, membrane-bound proteins could be used for drug delivery *via* vesicles. If a lipid-ligand binding interaction is sufficiently strong to overcome the energetic penalty of lipid re-organization, the lipids should re-order to match the distribution of binding residues.

Lipid membranes provide a controlled architecture for biological recognition. Natural lipid membrane interfaces have evolved to serve numerous functions in the cell, including keeping desirable molecules such as DNA, proteins, and nutrients inside the membrane; transporting valuable nutrients inside, while also serving as a matrix for advertising the identity of the cell through surface proteins. The largest constituent of natural membranes is lipids. Many other compounds are present in natural membranes including glyco-lipids, membrane imbedded proteins that may extend to one face of the bilayer or through both, and links to the skeleton of the cell. Internal cell membranes participate in compartmentalization of the cell into specialized domains that contain specialized functions. Membrane components are not chemically linked together and are free to diffuse [18]. Diffusion of individual lipids allows many favorable dynamic events to occur on the membrane, such as re-organization.

Synthetic lipid assemblies maintain many of the features inherent in biological receptor systems such as self-assembly and rapid re-organization. In mixtures of greater than 25% water lipids naturally self-assemble into closed vesicles [19]. By varying the water content, a diverse family of lipid architectures can be created. Figure 0.3 shows some of the structures that lipids can form in excess water. The surface area and curvature of these species, especially closed spherical vesicles, vary greatly. Even though the closed lamellar superstructures are large (300-1000 nm), the individual lipids are free to diffuse in two dimensions. In fact, upon ligand binding in model membranes composed only of lipids, lipids have been observed using fluorescence microscopy to migrate to a location where specific macromolecule-lipid binding is occurring [20]. Thus, the lipids can easily re-organize to form multiple energetically favorable ligand-lipid bonds.

Often, natural lipids participate in protein binding. Glyco-lipids containing sugar groups linked directly to the lipid can bind to lectins when formed into model membranes [21]. Negatively-charged lipids are necessary for the redox action of cytochrome c, since the protein is only active when membrane-associated. Although electrostatic interactions are non-specific, the composition of the lipid bilayer can be used to modulate the activity of the protein through specific protein-lipid binding. Protein kinase c activity is also modified by lipid composition [22]. From these examples, it is obvious that lipid interfaces can function as receptors for recognition of biomolecules. More types of lipid-mediated recognition can be made possible by adding the recognition element to the chemical structure of the lipid.

Most natural lipids are similar to the general phospholipid structure shown in Figure 0.4. A glycerol molecule forms the basic structural building block for the lipid. Lipids ordinarily contain two aliphatic chains placed on the 1 and 2 positions of the glycerol. Presence of two hydrophobic alkyl chains longer than 12 carbons provides spontaneous organization into ordered repeating lamellar phases in water [23]. The 3 position is commonly linked to a phosphate ester. Phosphate ester substituents define the polar "head

group" portion of the phospholipid. These range from charged to uncharged, large (sphingolipid) and small (phosphatidic acid) polar groups which confer many interesting properties to the lipids due to inter-lipid interactions or association with ions. Lipid membranes are an important structural feature of life and possess many desirable characteristics as a synthetic receptor. Thus, model membranes composed of lipids are an ideal starting point for building synthetic receptors.

SYNTHETIC POLYMERIZED LIPID-BASED RECEPTORS

One possible application of lipid-based recognition is to create materials that match the surface distribution of residues on a protein's surface. This can be accomplished by a forming a pre-organized complex between a ligand, such as a protein, and multiple lipids to create a pre-organized multivalent protein-lipid complex. If the lipids are polymerizable, the ligand-lipid complex can be polymerized *in situ*, and after removal of the ligand, a synthetic receptor that matches the distribution of binding residues on the protein is created. This process is termed "template polymerization" and is illustrated in Figure 0.5. It requires, however, that the binding interaction between template and monomer be reversible. This strategy would be applicable to many types of biological molecules, such as peptides, proteins and viruses, since the mobility of the lipids allows re-organization to form multiple lipid-ligand contacts independent of the length scale. Additionally, the structure of the template need not be known, only matching recognition elements in the lipid-receptors need be present.

Ligand-driven re-organization followed by polymerization has been used to make synthetic receptors in solid polymers for small molecules [24]. Multiple contacts between the synthetic receptor monomer and target are pre-formed in solution; polymerization then fixes the three dimensional information about the orientation of the ligand-receptor

complex. Such templated polymers have shown selectivity for the target molecule over non-target molecules.

Previous template-polymerized materials are difficult to use with proteins due to mass-transport limitations and bio-compatibility of the polymer matrix and polymerization conditions. Making a material biocompatible is very difficult to achieve because proteins are stable only over a very small pH and temperature range, lose their activity upon exposure to organic solvents, and often unfold upon adsorption to hydrophobic surfaces. In contrast, lipid bilayers provide a charged, two-dimensional surface for protein binding. Diffusion limitations are removed by making the surface molecularly flat on the length scale of proteins (20-1000 Å diameter). The choice of lipid composition allows fine control over the charge and morphology of the surface [25]. To make use of these desirable features, we have developed a new lipid-based strategy for specific ligand recognition and binding.

PROTEIN TARGETING TO LIPID VESICLES

Synthetic "affinity lipids" have been constructed to target proteins to lipid interfaces for crystallization [26], specific orientation and recognition [27,28], redox processes [29], and drug delivery [30]. Since lipids are relatively easy to synthesize *de novo* compared to much larger natural receptors like proteins, lipids were a natural choice as a structural element to create synthetic receptors. Usually an affinity ligand, chemically linked to the polar group of the lipid, serves as the recognition element. An example of an affinity lipid that is widely used to orient proteins at the interface is the biotinylated lipid-streptavidin system [31]. The association of streptavidin for biotin is extremely high, ($\approx 10^{15}$ M^{-1}) so the binding interaction is essentially irreversible. This affinity interaction has been used to form crystallized protein monolayers [31], build supramolecular assemblies of multi-layered protein [27], and to make affinity vesicle precipitation systems [32]. Lipids with an antigen such as fluorescein linked to the lipid headgroup have been synthesized and shown

to bind proteins [33]. Lipids containing sugar residues in their headgroup region have been synthesized and shown to bind lectins [34]. Lipids containing co-factors for proteins have also showed specific protein binding [35]. Incorporation of an affinity group effectively targets a molecule to the interface. However, the lipid films are unstable in organic solvents and have limited stability over time.

Polymeric lipids have been investigated to make a more stable lipid film to target molecules specifically to the interface [36,37]. Polymerized lipid structures such as vesicles or monolayers can be made through chemical or light-initiated polymerization. Charych and coworkers [38] designed affinity lipids containing sialic acid and diacetylene acyl chains, then polymerized the lipids using UV light to form stable vesicles. Virus particles rich in sialic acid recognition sites were added to the vesicles, and a colorimetric shift was observed in the absorbance range from 400 to 680 nm that corresponded to a detection limit of 10^8 virus particles [39]. This colorimetric change is believed to be due to a reorientation in the conjugated fluorescent backbone of the lipid polymer due to binding at the head group. Although this system is very elegant in the signal transduction upon binding, it suffers from a lack of specificity, since all sialic acid binding proteins or viruses could potentially interact with the lipids.

Current affinity lipids made from naturally-occurring affinity ligands are severely limited in the number of proteins they can target. Affinity lipids that could bind to a much larger variety of proteins or peptides would be very desirable in order to generalize the types of biological molecules that could be targeted to the interface. We are also interested in making materials that can recognize a protein whose three dimensional structure is not necessarily known. Indeed, the number of publicly available protein structures is severely limited, and many therapeutic proteins or peptides will be expressed whose X-ray crystal structure is not known at the time. We would like to take a suitably versatile binding moiety, attach it to a lipid and create ligand-organized surface receptors for a wide range of biological targets.

We have synthesized versatile affinity lipids containing metal-binding moieties for protein recognition [40]. A small tridentate chelator, iminodiacetate (IDA), binds Cu^{2+} strongly with an association constant of 10^{11} M^{-1} [41]. After binding the metal ion the IDA chelating group leaves coordination site(s) available for formation of a ternary complex with protein. The Cu^{2+}-IDA complex binds imidazole with moderate affinity ($K \sim 10^{3.5}$ M^{-1}) in solution [42], while also being specific for electron-donating residues such as histidine on the protein surface. While proteins with a single accessible histidine bind with similar affinities to surfaces densely derivatized with Cu^{2+}-IDA [43], those with multiple surface histidines can adsorb much more strongly by forming multiple, simultaneous histidyl-Cu^{2+} coordination bonds. Studies with engineered protein variants containing as few as two surface-accessible histidines have shown that multipoint attachment results in apparent protein-binding constants greater than 10^6 M^{-1} [43]. Alternatively, proteins can be engineered to display high-affinity surface metal-binding sites [44] or metal-binding peptides at their N- or C-termini [45,46], useful for specific protein targeting and immobilization on metal-derivatized surfaces [47].

The metal-protein interaction is reversible under mild conditions. Several strategies exist: competitors such as imidazole, small quantities of acid, or strong chelating agents all effectively disrupt the protein-Cu^{2+}-IDA complex, releasing the bound protein [48]. Additionally, different metal ions can be bound to iminodiacetate, tailoring the metal binding to a particular protein surface. For instance, exchange inert metal ions can be used instead of copper to change the rate of formation of the metal to ligand bond. After using an appropriate redox reaction to oxidize Ru^{2+} to Ru^{3+}, the metal to protein bond is made irreversible on the time-scale of the experiment [49]. Such metals could be used to form "irreversible" links to the lipids. Thus, the metal-protein interaction is very general and can be used to target multiple protein-lipid bonds to bring the protein to the interface.

Diverse proteins could be targeted to interfaces using lipid-based materials. Recently, a protein labeled with a histidine peptide "tag" has been crystallized on lipid

monolayers containing metal-coordinating nitrilo-triacetate lipids [26]. Alternatively, the unique distribution of histidine residues on a protein surface can be exploited to design materials for selective recognition [50]. Metal-chelating membrane-based synthetic receptors could be used as new materials to fabricate sensors, diagnostic reagents, and chromatography supports for separations. It is with the general goal of targeting a diverse array molecules to lipid interface that we have proceeded.

PROJECT GOALS AND APPROACH

With an ultimate goal of creating a lipid-based receptor whose metal ion matches the surface distribution of histidine residues on a protein surface, we investigated iminodiacetate lipids and their properties upon metal ion, protein, peptide and small molecule binding. The most important condition necessary for protein-based synthetic receptor fabrication or protein immobilization strategies is that the target protein bind with high affinity to the membrane surface. The more contacts with the interface formed, the more energetically favorable the interaction becomes. Thus, one of the critical features of ligand-directed lipid re-organization is to show the formation of the ligand-lipid complex bound at multiple points to the surface. Therefore, we have sought to determine how the multivalent ligand-lipid complexes form. Two important aspects of lipid-ligand binding were probed. Upon strong ligand binding we expect the association constant for a multivalent ligand-lipid complex would be higher than a monovalent complex. Also, by forming the multivalent complex, the "receptor" lipids would be expected to be brought near each other by ligand relative to their free diffusion in the membrane.

Since metal binding is known to affect membrane properties such as permeability and thermotropic phase transition of mixed lipid systems [51], changes upon metal binding to new iminodiacetate lipids formed into vesicles were investigated in Chapter 2. Presence of metal ions at the interface and the effect of specific metal binding to the bilayers were

investigated using light scattering, scanning calorimetry, freeze-etch microscopy, and fluorescence microscopy. We wished to determine if any macroscopic changes of the membrane properties due to metal binding were different from previous lipid systems using new IDA-lipids [51]. Significant changes in the thermotropic properties for pure and mixed lipid systems were induced by metal binding to the lipid interface. Metal ion binding to fluorescently-labeled lipids caused a large change in the fluorescence emission spectrum [52].

To investigate whether metal-chelating assemblies displayed favorable binding affinity with histidine-rich proteins we added myoglobin to metal-loaded vesicles (Chapter 3). Equilibrium binding experiments and electron spin resonance spectroscopy were used to determine if a protein containing five surface accessible histidines could bind to copper-loaded mixed bilayers. The apparent association constant was quantified to determine if more than one surface histidine was participating in binding. The lower limit of the proteins binding constant was determined for Cu^{2+}-loaded mixed small unilamellar vesicles and found to be at least an order of magnitude higher than for protein binding to the vesicles lacking metal. ESR studies with histidine-blocked protein and native protein showed protein binding to liposome vesicles is consistent with coordination of histidine by lipid-chelated-Cu^{2+}.

Pyrene-labeled, metal-chelating lipids were used to investigate ligand-induced lipid re-organization in the bilayer (Chapter 4). Pyrene-labeled lipids have been used extensively to characterize membrane properties, such as lateral mobility or formation of microscopic phase separation [53]. The pyrene probe has interesting fluorescence properties in organic solution or in membranes. When pyrene is linked to the end of a hexadecyl chain, upon vesicle formation the probe is confined to the hydrophobic portion of the bilayer. Collisions ensuing between pyrene-lipids in the course of their diffusion result in excited state dimers or "excimers" [54]. Excimers have different fluorescence emission and lifetime properties compared to the monomer. The ratio of the maximum wavelengths of

the excimer and monomer intensity is very sensitive to changes in the membrane properties in a diffusion-controlled bilayer [55]. Specific ligand binding to labeled lipids would change the lipid dynamics in the bilayer if pyrene-labeled lipids were "re-organized" by the multivalent ligand. Therefore we have used pyrene-labeled metal-chelating lipids to target the ligand to the interface to study the changes induced in the lipid dynamics and distributions.

We wished to determine whether the excimer to monomer (E/M) fluorescence intensity ratio ($I_{470\ nm}$ / $I_{377\ nm}$) could be used to probe the re-organization of metal-chelating bilayers due to multivalent binding. Figure 0.6 shows the proposed mechanism for the increase in the E/M ratio upon coordination through multiple copper lipids. The ligand is expected to coordinate to multiple lipids because of the favorable binding energetics of metal-histidine coordination. The binding of Cu^{2+}-IDA to imidazole in solution is energetically favorable at room temperature [41]. However, it is necessary to investigate whether multivalent binding is still favorable for two-dimensional lipid systems because the surface is now mobile. The entropic cost of binding could be large because the ligand-coordination of the lipids would reduce their mobility and outweigh the enthalpic gain due to coordination. The excess collisions in the bilayer due to macromolecule binding should be reflected in the E/M ratio. Thus, the E/M ratio may allow us to monitor multiple lipid coordination of the ligands to the bilayer.

Binding of imidazole, model di-histidine compounds, peptides, and poly-L-histidine was investigated using pyrene-labeled, metal-chelating mixed vesicles. We investigated changes in the E/M ratio when ligands containing two or more histidine residues were added to mixed Cu^{2+}-loaded vesicles. The effects on the E/M ratio of single-histidine controls were used a reference for comparison. Histidine polymers were also investigated to determine if polymer binding involved multiple metal-complexing lipids.

To further ascertain if specific ligand binding promoted re-organization of lipid bilayers, we measured the binding affinity for a multivalent ligand compared to a

monovalent ligand. If ligand binding was strong enough to re-organize the bilayer, we would expect greater binding affinity where more membrane contacts were formed than when only a single lipid-ligand bond was formed. The equilibrium binding of model monovalent and bivalent compounds to metal-loaded vesicles was investigated in Chapter 5 with isothermal titration calorimetry (ITC) to determine the thermodynamic parameters of association. Binding of model complexes imidazole and 1,4-bis-imidazole to metal-loaded vesicles were investigated to quantify both the enthalpy and entropy of binding for bivalent (1,4-bisimidazole) and monovalent (imidazole) studies. By using this technique, we could compare the entropic cost of bivalent lipid coordination and compare these results with the fluorescence binding studies.

As a strategy for construction of synthetic membrane receptors, metal-chelating lipids offer many advantages. Proteins can be endowed with membrane-binding capacity by attaching a histidine "tag" at their N- or C-terminus if the proteins do not contain at least two surface accessible histidines. Or, the natural distribution of surface histidines can be used to target proteins to the interface. These lipid-based materials would offer advantages for membrane-based two-dimensional crystallization studies, selective protein orientation for direct imaging using atomic force microscopy (AFM), and as a general model for affinity based signaling interactions occurring on natural membranes. The metal-binding interaction is reversible and mild, ideal for protein-based separations. The metal-chelating lipid system is useful for many different types of proteins and may proffer many advantages over more conventional strategies such as natural affinity receptors or immunoglobulins linked to lipids. Smaller metal-chelating headgroups can recognize potentially many more ligands than lipid-linked proteins since the lipids can naturally re-organize to form high-affinity "receptors". From these studies, lipid systems composed of metal-chelating lipids and a matrix lipid are evaluated as a new type of surface for protein binding.
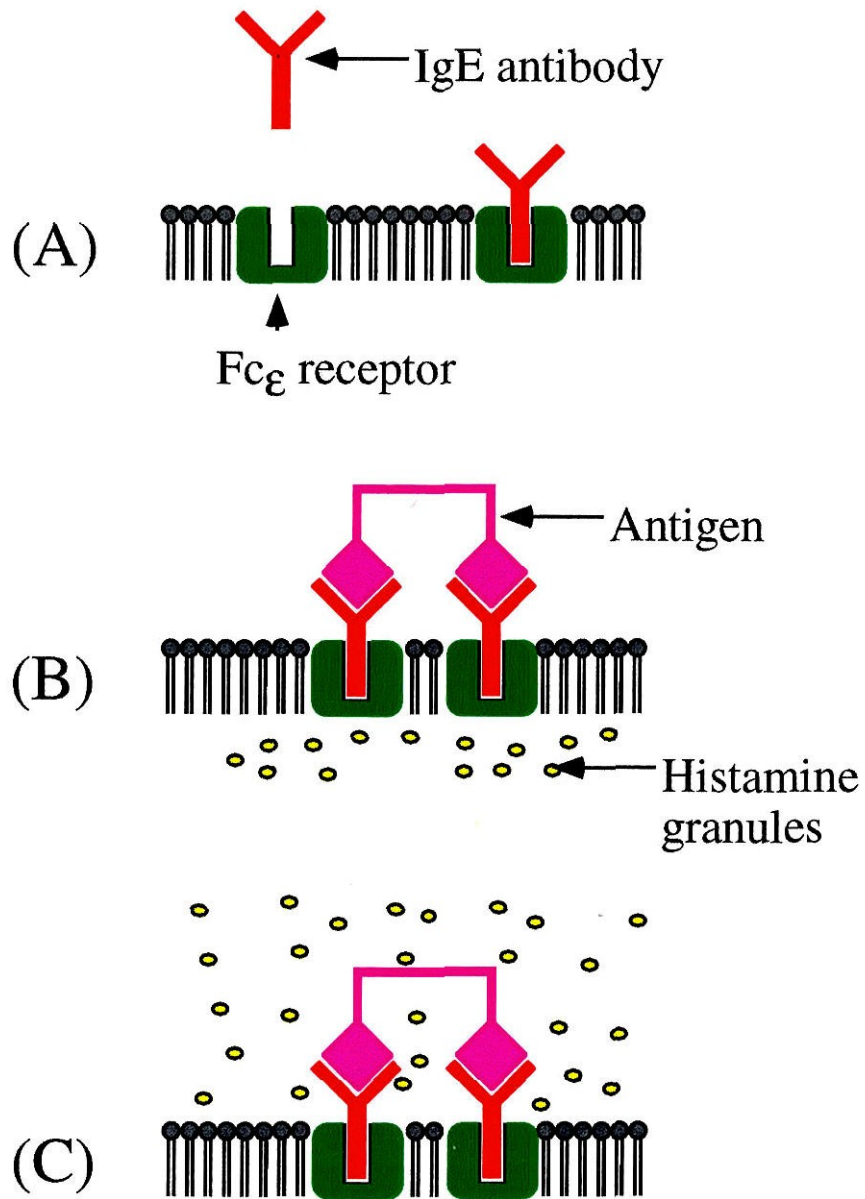
Figure 1.1. IgE binding to soluble antigen causing cross-linking of IgE to form dimer. Dimer associates with Fcε receptor on human basophil surfaces (B). Histamine release occurs after dimerization of Fcε receptors (C).
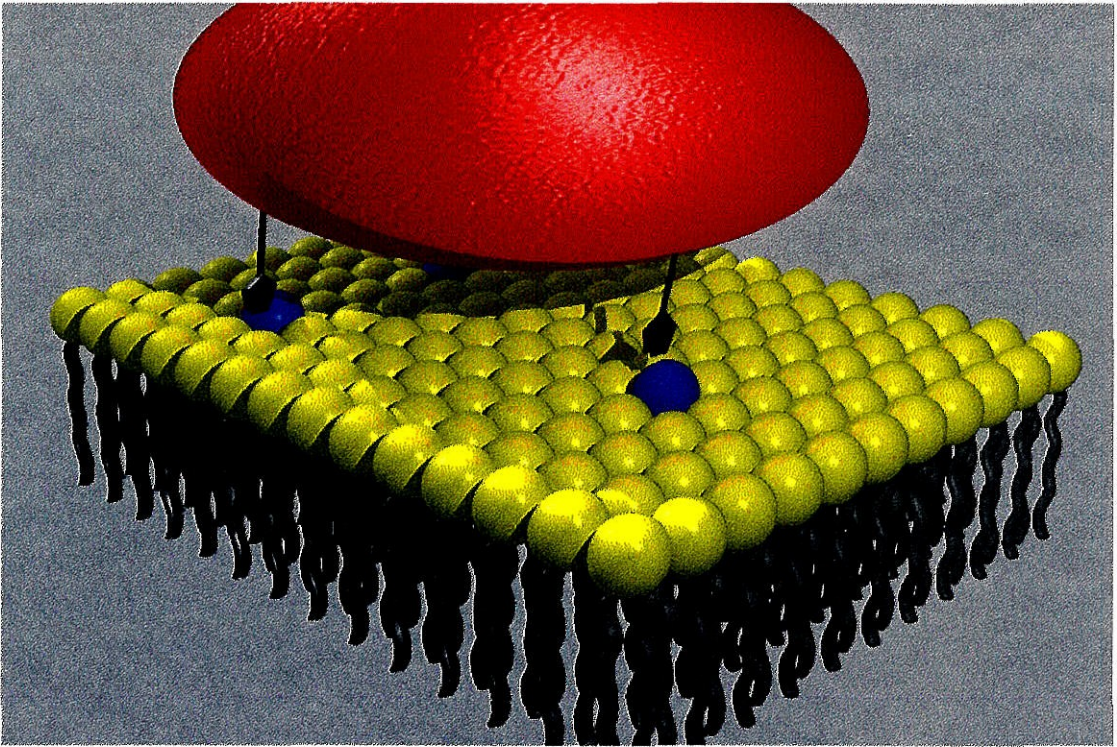
Figure 1.2. Schematic diagram showing a protein organizing the lipid bilayer through specific coordination to lipids. The protein would pre-organize the bilayer by forming multiple contacts.

Lipid morphology

Closed vesicle (lamellar)   Tubules

LB film on substrate
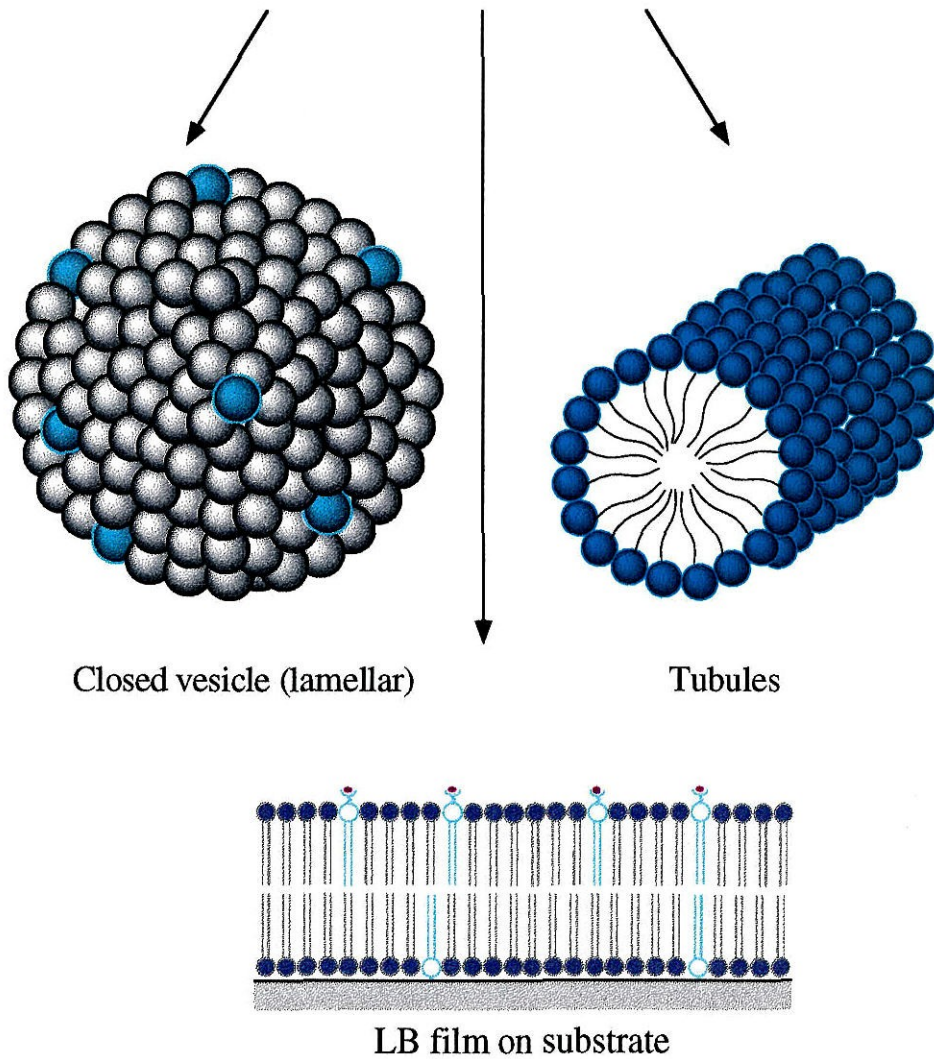
Figure 1.3. Some structures natural phospholipids adopt when mixed with water.
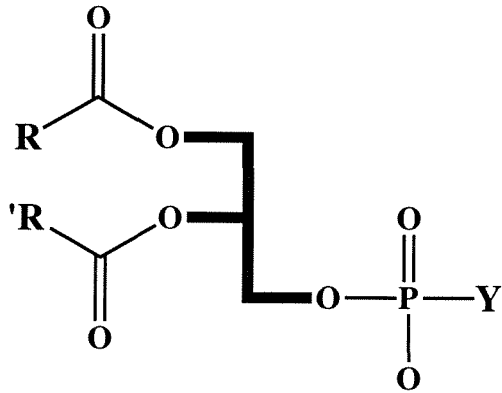
Y :	phosphatidylcholine	$—OCH_2CH_2N(CH_3)_3$
	phosphatidylserine	$—OCH_2CHNH_2$ $\quad\quad\quad	$ $\quad\quad\quad COOH$
	phosphatidic acid	$—OH$
	phospatidylethanolamine	$—OCH_2CH_2NH_2$
	phosphatidylglycerol	$—OCH_2CHCH_2OH$ $\quad\quad\quad	$ $\quad\quad\quad OH$
R,R':	$CH_3-(CH_2)_n-$	$n = 12,...,24$

Figure 1.4. Chemical structure of some natural phospholipids. Glycerol backbone is indicated by boldface along with numbering nomenclature. Various natural headgroups are indicated.
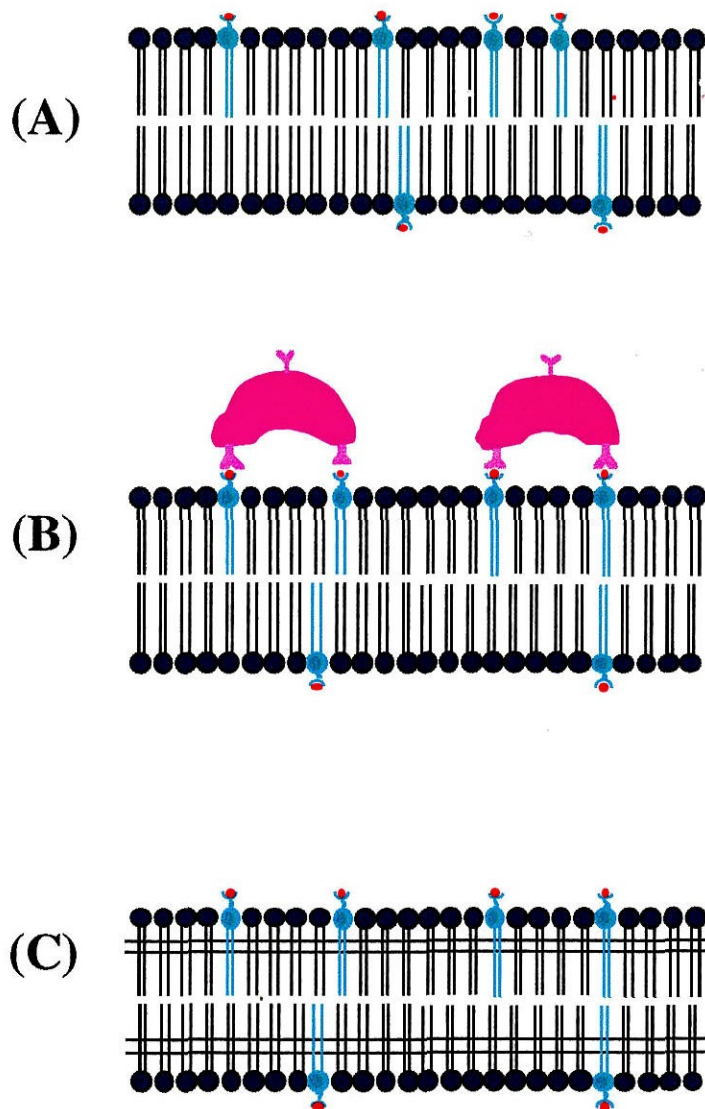
Figure 1.5. Mixed bilayer composed of metal-chelating lipids and matrix lipid (A). Protein pre-organizes bilayer through formation of histidine-metal coordination (B). Polymerization of complex and removal of protein affords synthetic receptor with matching distribution of metal ions (C).

No ligand

$(E/M)_O$
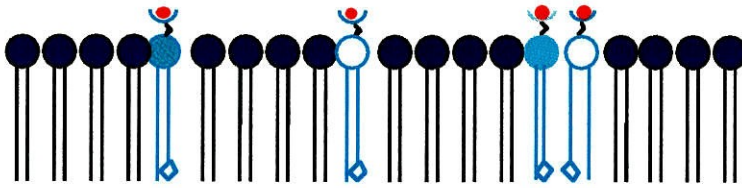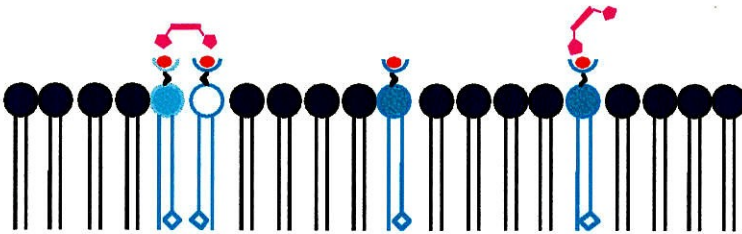
+ ligand

E/M

Figure 1.6. Fluorescently-labeled metal-chelating lipids mixed with matrix lipid used to determine the effect of ligand binding on monomeric and dimeric lipids. Pyrene-labeled lipid bilayers contain monomer (M) and excited state dimer "excimer" (E) fluorescent species. Binding of a multivalent ligand is expected to show an increase in the amount of excimer lipids.
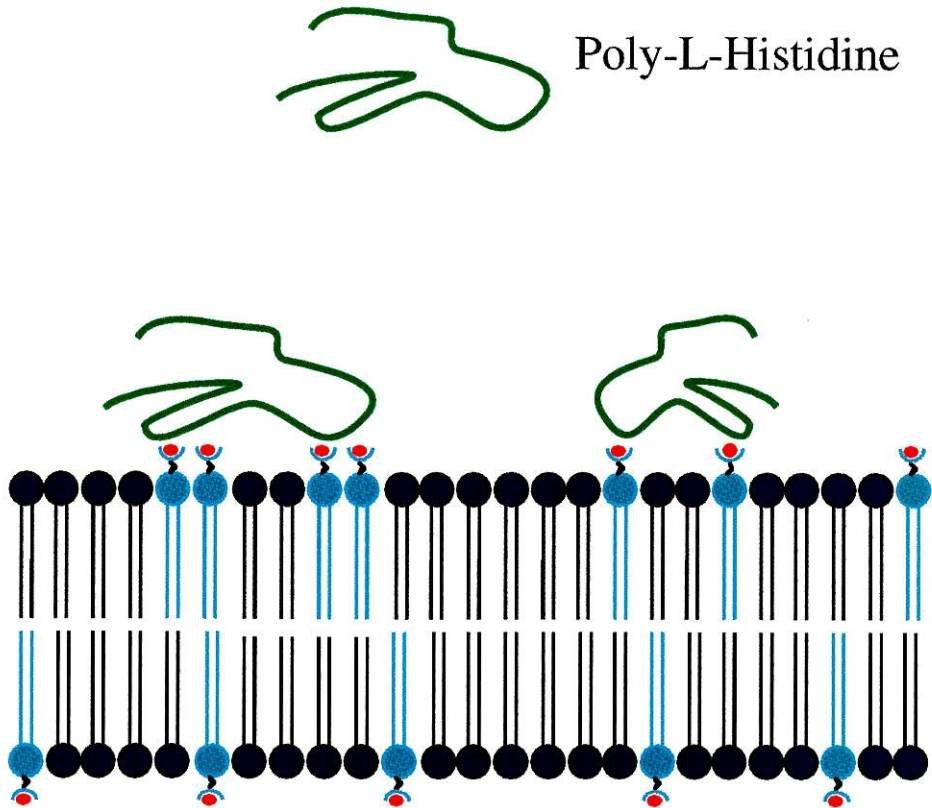
Figure 1.7. Schematic representation of poly-L-histidine organizing the lipid bilayer by simultaneous binding to multiple metal-chelating lipids. Note that the polymer enhances excimer-producing collisions.

REFERENCES

1. Dower, S. K.; Titus, J. A.; Segal, D. M. In *Cell Surface Dynamics: Concepts and Models*; A. S. Perelson, C. DeLisi and F. W. Wiegel, Eds.; Marcel Dekker, Inc.: New York, 1984; pp 277-328.

2. Becker, K.E.; Ishizaka, T.; Metzger, H. Ishikaza, K.; Grimley, P.M. *J. Exp. Med.* **1973**, 138, 394-409.

3. Siraganian, R.P.; Hook, W.A.; Levine, B.B. *Immunochemistry* **1975**, 12, 149-157.

4. Kagey-Sobotka, A.; Dembo, M.; Goldstein, B.; Metzger, H.; Lichtenstein, L. M. *J. Immunology* **1981**, *127*, 2285-2286.

5. McCloskey, M. A.; Liu, Z. Y.; Poo, M. M. *J. Cell. Biol.* **1984**, *99*, 778-787.

6. Eichmann, K. *Angew. Chem. Int. Ed. Engl.* **1993**, 32, 54-63.

7. Shimohigashi, Y.; Costa, T.; Chen, H.-C.; Rodbard, D. *Nature* **1982**, *297*, 333-335.

8. Boege, F.; Neumann, E.; Helreich, E. J. M. *Eur. J. Biochem.* **1991**, *199*, 1-15.

9. Mohammadi, M.; Honegger, A.; Sorokin, A.; Ullrich, A.; Schlessinger, J.; Hurwitz, D. R. *Biochemistry* **1993**, *32*, 8742-8748.

10. Lancet, D. and Ben-Arie, N. *Current Biol.* **1993**, *3*, 668-674.

11. Brenner, M. B.; Trowbridge, I. S.; Strominger, J. L. *Cell* **1985**, *40*, 183-190.

12. Sharon, M.; Klausner, R. D.; Cullen, B. R.; Chizzonite, R.; Leonard, W. J. *Science* **1986**, *243*, 859-863.

13. Ullrich, A. and Schlessinger, J. *Cell* **1990**, *61*, 203-212.

14. Frisch, H.L. and Simha, R. *J. Chem. Phys.* **1957**, *27*, 702-706.

15. Frisch, H.L.; Hellman, M.Y.; Lundberg, J.L. *J. Polym. Sci.* **1959**, *38*, 441-449.

16. Helfferich, F. *Ion Exchange* McGraw-Hill: New York, 1962.

17. *Separation processes in Biotechnology*; Asenjo, J.A., Ed.; Marcel Dekker, Inc.: New York, 1990; Vol. 9, pp 33-59.

18. Singer, S.J. and Nicolson, G.L. *Science* **1972**, 175, 720-731.

19. Bangham, A. D.; Standish, M. M.; Watkins, J. C. *J. Mol. Biol.* **1965**, *13*, 238.

20. McCloskey, M. A.; Poo, M.-M. *J. Cell. Biol.* **1986**, *102*, 2185-2196.

21. Yamazaki, N.; Kodama, M.; Gabius, H.-J. In *Methods* **1994**, *242* ; 56-65.

22. Newton, A. C. *Annu. Rev. Biophys. Biomed. Struct.* **1993**, *22*, 1-25.

23. Fendler, J. H. *Membrane Mimetic Chemistry;* 1 ed.; John Wiley & Sons: New York, 1982, pp 1-522.

24. Dhal, P.K. and Arnold, F.H. *Macromolecules* **1992**, *25*, 7051-7059.

25. Jones, M. N. *Adv. Coll. Interf. Sci.* **1995**, *54*, 93-128.

26. Kubalek, E. W.; Legrice, S. F. J.; Brown, P. O. *J. Struct. Biol.* **1994**, *113*, 117-123.

27. Fischer, B.; Heyn, S. P.; Egger, M.; Gaub, H. E. *Langmuir* **1993**, *9*, 136-140.

28. Laukkanen, M.-L.; Alfthan, K.; Keinanen, K. *Biochemistry* **1994**, *33*, 11664-11670.

29. Groves, J. T.; Fate, G. D.; Lahiri, J. *J. Amer. Chem. Soc.* **1994**, *116*, 5477-5478.

30. Lasic, D. *Amer. Sci.* **1992**, *80*, 20-31.

31. Blankenburg, R. ;. Meller, P.; Ringsdorf, H.; Salesse, C. *Biochemistry* **1989**, *28*, 8214-8221.

32. Tortorella, D. ; Ulbrandt, N. D. ; London, E. *Biochemistry* **1993**, *32*, 9181-9188.

33. Grainger, D. W. ;. A., M.; Reichart, A.; Ringsdorf, H.; Salesse, C.; Herron, J.N.; Lim, K. *J. Contr. Rel.* **1992**, *19*, 201-218.

34. Yamazaki, N. ;. Kim, M.; Gabius, H.-J. In *Meth. Enzym.* **1994**; 242, 56-65.

35. Hamachi, I. ;. Nogata, K.; Fujita, A.; Kunitake, T. *J. Am. Chem. Soc.* **1993**, *115*, 4966-4970.

36. Ringsdorf, H. ;. S., B.; Venzmer, J. *Angew. Chem. Int. Ed. Engl.* **1988**, *27*, 113-158.

37. Kobayashi, S.; Uyama, H. *Polish J. Chem.* **1994**, *68*, 417-444.

38. Charych, D. H. ;. Nagy, J.O.; Spevak, W.; Bednarski, M.D. *Science* **1993**, *261*, 585-588.

39. Reichert, A.; Nagy, J. O.; Spevak, W.; Charych, D. *J. Amer. Chem. Soc.* **1995**, *117*, 829-830.

40. Shnek, D. R. ;. Pack, D.W.; Sasaki, D.Y.; Arnold, F.H. *Langmuir* **1994**, *10*, 2382-2388.

41. Martell, A. E., Smith, P.M. *Critical Stability Constants*; Plenum Press: New York, 1974; Vol. 6.

42. Sinha, P.C.; Saxena, P.K.; Nigam, N.B.; Srivastava, M.N. *Indian J. Chem.* **1989**, 28A, 335-336.

43 Todd, R. J.; Johnson, R. D.; Arnold, F. H. *J. Chromatography* **1994**, *662*, 13-26.

44. Arnold, F. H.; Haymore, B. L. *Science* **1991**, *252*, 1796-1797.

45. Hochuli, E.; Bannwarth, W.; Dobeli, H.; Gentz, R.; Stuber, D. *Bio/technology* **1988**, *6*, 1321-1325.

46. Smith, M. C.; Cook, J. A.; Furman, T. C.; Gesellchen, P. D.; Smith, D. P.; Hsiung, H. *ACS Symp. Ser.* **1990**, *427*, 168-180.

47. Ill, C. R.; Keivens, V. M.; Hale, J. E.; Nakamura, K. K.; Jue, R. A.; Cheng, S.; Melcher, E. D.; Drake, B.; Smith, M. C. *Biophys. J.* **1993**, *64*, 919-924.

48.   Porath, J.; Carlsson, J.; Olsson, I.; Belfrage, G. *Nature* **1975**, *258*, 598.

49.   Muheim, A.; Todd, R. J.; Casimiro, D. R.; Grey, H. B.; Arnold, F. H. *J. Amer. Chem. Soc.* **1993**, *115*, 5312-5313.

50.   Mallik, S.; Plunkett, S.D.; Dhal, P.K.; Pack, D.W.; Shnek, D.; Arnold, F.H. *New. J. Chem.* **1994**, *18*, 299-304 .

51.   Cevc, G. *Bioc. Biophys. Acta* **1991**, 293-307.

52.   Sasaki, D. Y.; Shnek, D. R.; Pack, D. W.; Arnold, F. H. *Angew. Chem. Int. Ed. Engl.* **1995**, *34*, 905-907.

53.   Galla, H. J.and Hartmann, W. *Chem. Phys. Lipids.* **1980**, *27*, 199-219.

54.   Förster, Th. and Kasper, K. *Z. Phys. Chem.* **1954**, *1*, 275-277.

55.   Galla, H.-J. and Sackmann, E. *Bioc. Biophys. Acta* **1974**, *339*, 103-115.

Chapter 2. Metal binding to iminodiacetate lipid vesicles

INTRODUCTION

Ligand binding to membrane surfaces is an intrinsic feature in many biological processes such as signaling [1] or membrane fusion [2]. Metal ion association with model lipid membranes has been studied to understand the role of metal ions in modulating membrane permeability [3] and isothermal phase separation [4]. Metal ions often bind specifically to biological membranes through lipid head groups causing large-scale lipid reorganization such as crystallization [5], or phase separation [6,7], depending on the lipid composition. Although the natural biological membrane's response to metal ion binding is difficult to reproduce because metal ion binding involves many membrane proteins as well as links to the endo-skeleton of the cell, model systems such as lipid vesicles have been used as a cell substitute for metal-binding studies.

Incorporation of metal-chelating lipids in vesicles would allow placement of metal ions at the interface to participate in catalysis [8], electron transfer [9], or protein binding [10]. Lipids may be mixed together and formed into supramolecular assemblies such as spherical vesicles or tubules with controlled surface characteristics (Figure 1.3) [11]. The surface density of metal ions can be controlled by the mole fraction of added metal-chelating lipid. Thus, to make an organized surface containing metal ions requires synthesizing just one component which can be formed with minimal effort into thin films or colloidal dispersions with very large surface areas.

Most metal-chelating lipids have metal-chelating moieties placed on the polar part of the lipids structure to make the binding portion accessible to the solvent. Some metal binding groups which have been linked to lipids are imidazole [7], porphyrins [12], dithiocarbamate [13,14], cyclam [15,16], iminodiacetate [17], crown ethers [18], and non-cyclic crown analogs [19]. Ions are not expected to associate significantly with the hydrophobic portion of the bilayer since they have charges which must be solvated. Reporter groups such as azobenzene [20] and pyrene [21] can be placed in the apolar hydrophobic portion of the lipid molecule to produce a signal upon metal binding.

We have designed a model vesicle system in which a transition metal ion is chelated specifically by a single lipid. Such chelated metal complexes provide a new type of lipid head group which can bind to a wide variety of proteins through histidine, cysteine and lysine residues present on the protein surface [10]. Small chelating agents such as iminodiacetate (IDA) have large association constants for transition metals. Additionally, the metal can be easily removed by changing pH or using soluble chelators with higher affinity for the metal ions than iminodiacetate. Our desire to organize bilayers led us to develop optically-labeled metal-chelating lipids containing iminodiacetate (IDA) to study coordination of lipids to histidine-rich molecules. In the course of our studies we discovered that the optically-labeled metal-chelating vesicles reorganized upon metal binding, producing a signal that could be used as a metal ion sensor.

Metal ion sensors have been formulated from lipid components [14,20,22,23]. An optical signal is usually modulated by specific metal binding to the polar head group. Alternatively, other components such as porphyrins [9] are added to the lipid architecture to transduce the signal. Effective strategies to formulate sensors for metal ions include using changes in the electrostatic potential of the membrane surface [23], UV spectrum changes upon metal binding [20], and changes in rates of fluorescence emission versus electrostatic potential [24]. Ease of fabrication of lipid coatings onto surfaces or into colloidal suspension bestows an advantage upon lipid-based sensors compared to conventional ion-selective electrodes [25] or photo-induced electron transfer sensors [24].

Metal ion binding to interfaces can have profound effects on the lipid packing resulting in interesting methods to transduce a signal upon metal ion binding. For instance, millimolar Ca^{2+} induces a contraction in a phosphatidic acid lipid monolayer, decreasing molecular area by 10% [26,27]. Such a large change in area at the molecular scale may play an important role in cell fusion since higher membrane surface tension is a result of the metal ion binding. Since these changes are effected isothermally, there is no need for complex regeneration procedures to return the system to its initial state, such as temperature

cycling [22], only the metal ion need be removed. For instance, phosphatidic acid bilayers are very strongly affected by Ca^{2+} binding to the ionized phosphate head group [28,29]. The temperature of the gel to liquid-crystalline transition, T_m, of the lipid system increases quite dramatically, and the lipids phase separate into distinct regions [30,31]. Metal ion binding usually affects the temperature of the gel to liquid-crystalline phase transition of the bilayer, determined from differential scanning calorimetry [32]. The change in T_m reflects both the change in the lipid packing and also electrostatic changes upon the transition due to the presence of the bound metal ion. In such cooperative systems, the T_m of the mixed bilayer can increase by as much as 100 °C, due to a "cross-linking" of the head groups by the metal ion, as seen for Ca^{2+} binding to phosphatidylserine vesicles [32]. Metal ion binding can be observed by changes in the thermal transitions, vesicle morphology, co-diffusion of lipids, and fluorescence spectra of labeled lipids. Physical characterization of metal binding to vesicles yields insight into the molecular events occurring between lipids.

The effect of Cu^{2+} ions on bilayers containing two new iminodiacetate chelating lipids developed in this laboratory was investigated. The iminodiacetate lipids were formed into vesicles containing a binary mixture of phosphatidylcholine and metal-chelating lipid. Transition metal ions were found to have profound effects on mixed membranes containing fluorescently-labeled, metal-chelating lipids and also on pure unlabeled metal-chelating lipids. The effect of the metal ions was investigated using several different techniques including quasi-elastic light scattering, differential scanning calorimetry, freeze-etch microscopy, and fluorescence spectroscopy.

These new iminodiacetate metal-chelating lipids were found to have properties that differ from previous natural and synthetic metal-binding lipids. As a result of these studies, we found conditions under which pyrene-labeled iminodiacetate lipids mixed with phospholipids and formed into vesicles function as a fluorescent sensor for transition metal ions. The fluorescence spectrum of the pyrene-labeled metal-chelating vesicles changes

when metal is added to the vesicles. The change in the emission spectrum is believed to reflect an inversion in an aggregated population of labeled lipids into a more dispersed state. The fluorescent change occurs with transition metal ions that have affinity for iminodiacetate, showing that it is the specific binding driving the fluorescence change. The concentration at which the fluorescence change occurs reflects the affinity of transition metal ions to iminodiacetate. Indeed, the sensor showed high selectivity for copper over calcium. The metal binding is reversible with EDTA. This metal sensor has characteristics that are very desirable, including the fact that the vesicles can be freeze dried and stored for long periods of time.

RESULTS

Vesicle formation and size characterization by light scattering

Two new metal-chelating lipids were synthesized; the chemical structures and names are shown in Figure 2.1. Natural zwitterionic phospholipids, shown in Figure 2.2, were mixed with metal-chelating lipids to make stable lipid vesicles. Either PSIDA (5 mole %) or DSIDA (2 mole %) was mixed with di-stearoyl phosphatidylcholine (DSPC) or DSPC/cholesterol, respectively, and formed into small unilamellar vesicles using probe tip sonication. Sonication is known to produce vesicles with sizes below 100 nm [33]. Small unilamellar vesicles (SUV) have large surface areas. 34% of the total lipid is located on the inner lamella, inaccessible to the solvent [34]. The amount of exposed lipid may be estimated more easily with SUV-type vesicles than vesicles with many lipid bilayers, such as a multilamellar vesicle (MLV).

Quasi-elastic light scattering was used to determine the vesicle size distribution of selected vesicle samples. Light scattering was used to verify that the mean vesicle size was in the small unilamellar regime. Additionally, the effect of metal binding on vesicle fusion was also probed using light scattering. Vesicle sizes measured by quasi-elastic light scattering are reported in Table 2.1. The distribution width is provided to show how

disperse the vesicle distribution is. These parameters are derived from the manufacturer's fitting algorithm for auto-correlation of the signal over time taken at 90° scattering angle [35]. As can be seen from Table 2.1, vesicle aggregates larger than a vesicle diameter are present for dialyzed, metallated 2% DSIDA/ 48% DSPC/ 50% cholesterol vesicles. Although these vesicles had free metal removed by dialysis, aggregation occurs after the vesicles have remained in solution for at least 24 hr. When a slight excess of metal is present at sonication, 5% PSIDA/ 95% 1-stearoyl-2-oleayl-3-phosphocholine (SOPC) vesicles do not show this behavior and remain in solution for weeks. All vesicle solutions lacking metal show no precipitation over time. Both unmetallated PSIDA/DSPC and DSIDA/DSPC vesicles have mean diameters below 50 nm, which indicates that they are small unilamellar vesicles. The large size distributions indicates the vesicle distribution is polydisperse.

Thermal transitions show mixing properties of metal-chelating lipids and phospholipids

The effect of metal ions on the thermal transitions of metal-chelating lipids formed into multilamellar vesicles was investigated to determine if phase separation was occurring. Multilamellar vesicles (MLVs) were used since they show excellent reproducibility of multiple scans and large endothermic transitions between the gel phase and the liquid-crystalline phase of lipid bilayers. Small unilamellar vesicles have high surface curvature compared to multilamellar vesicles, which reduces the overall enthalpy of transition, and sometimes have a slightly lower transition temperature (T_m) [36]. Also, SUV vesicles often fuse during the course of a calorimetry experiment, causing poor reproducibility between consecutive experiments [36]. Small unilamellar vesicles were used in measurements where the surface concentration of chelating lipid had to be known, since a great deal of the chelating-lipid is contained within the lamellae of MLV vesicles. Thus, although SUV's may have a slightly shifted ΔH value, the overall effect of metal ions on T_m will be

represented by the microcalorimetry of MLV's and can be used to interpret the mixing of lipids in SUV systems.

Very slow scan rates were used to prevent kinetic effects on the equilibrium lipid transition from gel phase to liquid-crystalline. Although scan rates as high as 45 °C/hr showed no appreciable difference in the T_m of the transition, scan rates of 10 °C/hr were always run for comparison. The data for pure metal-chelating lipid components are shown in Figure 2.4 and Figure 2.5. The saturated DSIDA lipids had to be sonicated with metal present to obtain a continuous suspension. PSIDA-Cu^{2+} samples were also sonicated slightly to be sure that the inner lamellae were metallated. Metal addition to pure components greatly changes the solubility of the vesicles, causing the vesicles to settle to the bottom of the tube.

After the thermal properties of the pure components were established, mixing studies were done with the optically-labeled, chelating-lipid PSIDA and DSPC. Figure 2.6 shows the calorimetric traces for different mixtures of the two lipids. Metal was added to similar compositions of vesicles to produce thermal data shown in Figure 2.7. The vesicles were visibly blue before the cells were filled. Metal binding to PSIDA pure and mixed vesicles resulted in a complete removal (Figure 2.7) of the calorimetric peak compared to the same vesicle composition lacking metal (Figure 2.6). Since metal binding to mixed MLV's of PSIDA and DSPC has the strange effect of removing the transition, enthalpies were not calculated.

Freeze-etch microscopy

Vesicles containing metal-chelating lipids were checked by freeze-etch microscopy to determine the change metal binding induces in the mixed vesicle morphology. Large multilamellar vesicles (MLV) with concentric layers were investigated instead of small unilamellar vesicles (SUV), since the length scale of transmission electron microscopy is limited to features approximately 50 nm. Since small unilamellar vesicles have length

scales near 50 nm, freeze-etch microscopy would not successfully image the features of the smaller vesicles. Freeze-etching is a sample preparation method used for imaging the inner and outer lamellae of vesicles in the same sample. The distribution of surface features such as ripples, smoothness, and also shape of the vesicles yields information about the lipid packing which is determined by the lipid phase state. Freeze-etch microscopy is especially useful for determining whether the lipids are below or above their gel to liquid crystalline phase transition.

The change induced in the lipid surface upon metal binding was investigated at pH 7.5 using microscopy to image gross surface structural changes. Multi-lamellar vesicles (MLV) were formed, sandwiched between special copper holders and frozen in liquid nitrogen slush to get cooling rates that are very fast (100°C/min.) allowing no disruption of the equilibrium structures due to water crystallization [37]. The vesicles are fractured using standard procedures under high vacuum at 77 °K after a short (60 sec.) period of sublimation the surfaces are coated with platinum, then carbon to make replicas of the surfaces while maintaining 77 °K temperature. The replicas are cleaned and images taken at high magnification (x15-80,000) using transmission electron microscopy. If the procedure is done correctly, replicas of the lipid lamellae can be observed at high (50 nm) resolution.

Figure 2.8 through Figure 2.12 show representative pictures of DSPC, PSIDA, PSIDA-Cu^{2+}, and 5% PSIDA-Cu^{2+} /95% DSPC multilamellar vesicles. The phase transition temperature of pure DSPC and mixed PSIDA/DSPC vesicles is well above room temperature and thus the surfaces show ripples corresponding to the gel phase. Pure PSIDA and PSIDA-Cu^{2+} multilamellar vesicles did not show ripple structures. Some PSIDA-Cu^{2+} vesicles adopted tube-like shapes rather than spherical morphology, which can be seen in Figure 2.10. Since PSIDA-Cu^{2+} pure MLV vesicles aggregated and fell out of solution, the pictures might be representative of an aggregate of tubes. Since the solubility of the PSIDA-Cu^{2+} multilamellar vesicles were decreased compared to the

PSIDA, light microscopy images did not show tube-like structures because the vesicle aggregates adsorbed to the glass slides (data not shown).

Metal binding to fluorescently-labeled metal-chelating vesicles.

The binding of metal ions to chelating complexes in solution is commonly measured by potentiometry [38] and, less often, by fluorescence [39]. We found that transition metal binding affected the fluorescence emission intensity of mixed PSIDA/DSPC vesicles very strongly. The binding of the metal ions to 5% PSIDA/ 95% DSPC vesicles has an striking effect on the value of the intensity ratio between excimer (470 nm) to monomer (377 nm) emission. Excimer emission results when an excited state monomer collides with a ground state monomer to form a complex [40]. Figure 2.13 shows the effect of $CuCl_2$ on 5% PSIDA/ 95% DSPC fluorescence emission spectrum of small unilamellar vesicles. Note that the emission intensity in Figure 2.13 (curve A) before metal addition has a large featureless band at 470 nm which is attributed to excimer fluorescence. Vesicles lacking metal have an E/M ratio of 1.2 for fresh vesicles, which can go as high as 1.8 upon standing for several days. Upon addition of copper, the E/M ratio decreases to 0.4 as can be seen in Figure 2.13, (curve B). This change is so dramatic that with much more concentrated vesicles [0.2 mM total lipid] it can be observed with the naked eye under UV lamp illumination (365 nm).

Figure 2.15 shows the presence of an isosbestic point at 424 nm during metal ion addition. These data were acquired with $MnCl_2$ ions [0.1 M concentrated solution in 0.1M NaCl] from the concentration range 10^{-6} to 10^{-3} M total added metal to 5% PSIDA/ 95% DSPC vesicles at 25°C. Aggregation of the vesicles was assumed not to occur since the vesicles were very dilute [~6 μM total lipid]. The presence of an isosbestic point could be reproduced for $MnCl_2$ quite easily, and less often for Cu^{2+} and Ni^{2+}. Since Cu^{2+} is known to induce aggregation of the vesicles, vesicle dilution must be very high (1:1000 or higher) to observe the isosbestic point during metal ion titration.

The change in the scaled excimer (470 nm) to monomer (377 nm) intensity ratio $(E/M)/(E/M)_o$ is also induced isothermally by binding of different metal ions to the 5% PSIDA/ 95% DSPC vesicles but at different concentrations (Figure 2.16). Concentrated metal ion solutions in 0.1M NaCl were added to dilute vesicles [~0.2 μM] to generate the curves shown in Figure 2.16. For $MnCl_2$ ions, the concentration at the halfway point of the E/M curve is estimated to be 3×10^{-4} M, corresponding to an apparent association constant of 3×10^3 M^{-1}. The association constant for $MnCl_2$ binding to 5% PSIDA/ 95% SOPC vesicles [~8 mM total lipid concentration] was found to be 3.32×10^4 M^{-1} using isothermal titration calorimetry (Chapter 5).

E/M can be modulated by substituting different matrix lipids or changing the pH.

Since the excimer to monomer concentration is known to be influenced strongly by the phase state of the vesicles [40], the effects of matrix lipids with the same phosphatidylcholine head group with varying acyl chain composition on the E/M ratio were investigated before and after metal binding to the vesicles, shown in Figure 2.17-Figure 2.20. The transition from the ordered gel state to the more disordered liquid crystalline state occurs at the melting temperature T_m. Thus, at room temperature if the T_m is greater > 25 °C the lipid bilayer will be in the gel state, and if T_m is lower than 25°C, the lipids will be in the liquid-crystalline phase. Diffusion and permeability of the membranes are strongly affected by the membrane phase [41]. The results of varying the matrix lipid are shown in Table 2.3. To show the effect of the E/M due to metal binding, the E/M values without and with metal are indicated.

The effect of ionization of the lipid headgroup using 5% PSIDA/ 95% DSPC vesicles was also investigated. 5% PSIDA/ 95% DSPC vesicles in 0.1M NaCl buffer were made and placed in different buffer solutions from the pH range 3 to 10. Phosphatidylcholine is uncharged between the pH range 3-10, so the only contribution of ionized lipids is due to the PSIDA lipid [42,43]. Figure 2.21 shows that a large change in

the E/M ratio can also be induced by varying the pH. The curve goes through a minimum reflecting the less lipid-aggregated state for vesicles at pH values less than 6.0. The aggregated state with E/M ratio of 1.2 is present between pH 7 and 8. Metal binding studies were not investigated because the metal hydroxide forms above pH 8 [38].

Changing the matrix lipid charge should also change the initial aggregation state of the PSIDA lipid if electrostatics are affecting the mixing of the neutral phosphatidylcholine with the negatively-charged PSIDA lipid. The charge of the head group is expected to influence solubility of the vesicles, determine the pH range of operation, and to affect the pH at which the excimer to monomer ratio is highest. Figure 2.19 shows a decrease in the excimer emission (curve a) due to metal binding (curve c) in a mixed vesicle containing 5 mol% PSIDA and 95 mol% DSPA. In the negatively-charged vesicles there is a larger population of excimers as evidenced by the high initial E/M value. This system showed a decrease in the E/M ratio from 7 to 3 after roughly 1:1 addition on metal ions to PSIDA. A consequent increase in monomer intensity is not observed. Addition of greater than stoichiometric metal resulted in an unchanging E/M ratio of 3.0 at which point the vesicles visibly precipitated. Negatively-charged lipids are known to be easily cross-linked and subsequently precipitated by metal ions.

Fluorescence lifetime measurements

To determine whether the mechanism of changes in fluorescence could be due to quenching of the probe by a transition metal ion, lifetimes of the excimer and monomer were measured using pulse lifetime measurements. Short pulses of laser light are used to excite the fluorophore, and then the time decay is sampled at different times (Figure 2.22). The lifetime of a fluorophore follows a simple exponential decay after excitation by a pulse of laser light [44].

$$\frac{dN(t)}{dt} = -(\gamma + k)N(t)$$

N is the population of fluorophores, γ is the emissive rate of the fluorophore and k is the rate of non-radiative decay. By integrating this expression with the initial condition $N = N_o$ at t = 0 we get a simple expression containing the lifetime τ.

$$N(t) = N_o e^{-t/\tau}$$

The lifetime decay is then deconvoluted from the response of the system to scattered light, in this case, 100% SOPC small unilamellar vesicles at the same concentration. A bi-exponential lifetime was used because there is a second, faster lifetime. The integral that is evaluated using a minimization algorithm is shown below. L(t) is the instrument response function, τ_1 and τ_2 are the two lifetimes, and α_1 and α_2 are the amplitude coefficients of each decay.

$$R(t) = \int_0^t L(t - \mu)[\alpha_1 e^{-\mu/\tau 1} + \alpha_2 e^{-\mu/\tau 2}]d\mu$$

The vesicles were diluted 1:1000 and excited by a pulsed 355 nm YAG laser over a 1.25 μs acquisition time. The resulting decay curves are shown in Figure 2.23. Metal ion binding and the changes induced in the lifetime were measured at 25°C with stirring. The effect of copper was to decrease the lifetimes of the excimer and monomer. The excimer lifetime was longer than the monomer lifetime and more strongly affected by copper addition. The plot of the excimer lifetime with respect to metal concentration is shown in Figure 2.24.

DISCUSSION

Vesicle size changes upon metal ion binding

Metal-chelating vesicles made by probe tip sonication were tested by quasi-elastic light scattering to determine the mean vesicle size. Two formulations of mixed vesicles were formed, one from cholesterol, DSPC (Figure 2.2) and small amounts of DSIDA (Figure 2.1) or DSPC and small amounts of PSIDA (Figure 2.1). An important consideration in vesicle formulation in our binding studies was whether the vesicles fused due to metal ion addition. Thus, the mean value of the distribution was compared to infer if the vesicles had fused and become larger, assuming they maintain spherical geometry.

After metal is added to DSIDA vesicles, precipitates of vesicles are created as seen in Table 2.1. These larger particles were observed only with metallated vesicles. Even though these aggregates are very large, approximately 70% of the total vesicles are in the SUV regime and the mean is not significantly shifted. Thus, the metal does not seem to enhance fusion since the mean would be enlarged. One explanation for this phenomenon is that DSIDA lipids from different vesicles form inter-vesicle, EDTA-like complexes when the metal concentration is lower than the total exposed IDA lipid. Since EDTA is chemically two iminodiacetate residues linked together through a flexible spacer, it is not surprising that the vesicles can cross-link, because this is predicted to be energetically favorable [38]. Due to the cross-linking of vesicles over time, all studies with metallated vesicles were done with freshly metallated vesicles.

Another metal-chelating lipid, fluorescently-labeled lipid PSIDA shown in Figure 2.1, was also sized using quasi-elastic laser light scattering Table 2.1. This lipid has a pyrene group on one of the acyl tails which endows it with interesting fluorescence properties. The head group contains an iminodiacetate group which can bind divalent transition metal ions. We wished to characterize vesicles containing these new lipids using light scattering to show they were also in the small unilamellar regime. PSIDA/DSPC vesicles lacking metal also were found to be in the small unilamellar regime. Mixed 5%

chelating lipid vesicles lacking metal are typically in the 40 nm range, and the distribution is very large indicating poly-dispersity. Since the mean vesicle size is below 50 nm we assume that the vesicles have adopted unilamellar morphology [34].

Mixing properties of metal-chelating lipids in other lipids

Deviations from ideality of mixing between lipid components in aqueous-binary lipid mixtures can be resolved using differential scanning calorimetry (DSC). Presence of multiple transitions can be easily determined using scanning calorimetry [45]. The presence of multiple transitions in a binary lipid mixture indicate phase separation of lipid components into regions with different state properties. A schematic diagram showing a typical DSC trace is shown in Figure 2.3. Scanning microcalorimetry yields thermodynamic information about the thermal transitions of aqueous dispersions of lamellar lipids between the gel phase and liquid-crystalline phases [46]. A scanning calorimeter measures the difference in heat capacity between a reference cell containing buffer and a lipid dispersion of vesicles. The scan-rate normalized heat capacity curve is integrated to obtain the heat of the transition. The heat capacity changes endothermally upon a phase transition of the lipid mixture yielding a sharp, symmetric C_p peak for most natural phospholipids. Multilamellar phospholipid vesicles exhibit two transitions, a small pre-transition and a larger sharp main transition [47]. Both phase transitions are highly cooperative and reversible for multilamellar vesicles [48].

Thermal transitions for pure metal-chelating lipids were investigated using DSC because metal-binding was expected to change the conformation of the lipid headgroup and therefore alter lipid-lipid packing. The phase transition temperatures of the pure components must be known to determine if the mixing is ideal or non-ideal. The thermodynamic parameters for vesicles made up of the pure components are shown in Table 2.2. Thermotropic phase transitions with and without copper for two chelating lipids were investigated to detect multiple peaks upon metal binding. Chemically attaching a

pyrene-labeled acyl chain to the 2-position on the glycerol-backbone of DSIDA to form PSIDA (Figure 2.1) decreases the transition temperature by 42 °C (Table 2.2). Metal binding to saturated vesicles containing DSIDA increased the transition temperature (Figure 2.4). In contrast, addition of metal to PSIDA multilamellar vesicles (Figure 2.5) either totally abolishes or places the phase transition temperature out of the range of the instrument (range 5-110 °C). Scans were run to 80 °C for PSIDA-Cu^{2+} multilamellar vesicles, so it is possible that the transition might be greater than 80 °C. Metal-binding to the same lipid head group had two different effects on the thermal transition of the pure lipids, either increasing or removing the transition, which was not expected since the mechanism of metal binding to these lipids is presumed to be the same.

Metal ion association to pure or mixed membranes is often accompanied by an increase in the phase transition temperature, T_m [49]. An increase in the phase transition temperature usually indicates dehydration of the lipid head groups by metal binding [50]. Specific metal-ion binding is often followed by a large change in the permeability of the vesicles due to metal-ion headgroup association [51]. Cu^{2+} binding probably causes dehydration of the DSIDA lipid headgroup, since a tri-dentate chelate between the carbonyl oxy-anions and lone-pair of the nitrogen to the metal ion is formed, releasing the carbonyl-solvating waters. Completely dehydrated natural phosphatidylcholines melt between 110 and 120 °C, much higher temperature than the solvated lipid in bilayers (23 °C for DMPC (Table 2.3)) [52]. Thus, changes in the amount of bound water can shift the transition temperature very much, as observed for specific Cu^{2+}-DSIDA binding. The loss of the thermal transition upon Cu^{2+} binding to PSIDA vesicles is less straightforward to explain, without further information determined from higher temperature calorimetry studies using conventional scanning calorimetry.

PSIDA and DSPC multilamellar mixtures were investigated using microcalorimetry since they have interesting fluorescence properties, especially at low (5%) PSIDA mole fractions. The extreme difference in phase transition temperature indicates that the pure

components would not mix well. However, multiple peaks were not observed until ratios greater than 40% PSIDA were approached (Figure 2.6). These multiple peaks are just slightly larger than the baseline, the total enthalpy of the transition being greatly reduced and broadened. The presence of a single peak for 5% PSIDA/ 95% DSPC multilamellar vesicles indicates that there is no macroscopic phase separation into pure components at 5% PSIDA, which is consistent with freeze-etch microscopy experiments (see below). Mixing studies of pyrene-labeled metal-chelating lipids in phosphatidylcholine (DSPC) vesicles shows similar scanning calorimetry results as calorimetry studies done by Somerharju with pyrene-labeled phosphatidylcholine and DPPC, also a phosphatidylcholine [53]. The T_m of a pure pyrene-labeled phosphatidylcholine is 26 °C lower than saturated, unlabeled lipids with the same chain length, even though they have exactly the same headgroup. Thus, the presence of the pyrene label on the acyl tails greatly disturbs the lipid packing.

Addition of Cu^{2+} to mixed PSIDA/DSPC vesicles removes the main transition at PSIDA-Cu^{2+} compositions greater than 30% (Figure 2.7). Although consistent with the pure components behavior, these calorimetry results yield very little information about what might be happening to the mixed-lipid system upon to metal binding. In fact, the transition may have been lowered or increased out of the range of aqueous micro-calorimetric investigations (T_{max} = 110 °C). Extremely large changes in T_m have been reported for association of Mg^{2+} and Ca^{2+} to mixed vesicles containing phosphatidylglycerol and phosphatidylserine lipids. Even in mixed DSPC/PSIDA vesicles, specific Cu^{2+} binding to PSIDA is dramatic and has a very large effect on the melting transition.

Morphology of metal-chelating vesicles

To determine how transition metal ions affect the morphology of vesicles containing iminodiacetate lipids, replicas of vesicle surfaces were prepared using freeze-etch microscopy. Most phospholipids form lamellar phases when mixed with less than 25% water or buffer [54]. Phospholipids spontaneously form multilamellar vesicles when

buffer is added above the phase transition of the lipid [55,56]. These closed spherical colloids contain many onion-like layers, or lamellae, of phospholipid bilayers. Freeze-etch microscopy exploits the large size of multilamellar vesicles and repeating nature of the lamellae by cracking open these vesicles and creating metal replicas of the vesicle surface. The phase of the lipid is preserved by this technique since ice crystals are prevented from forming by rapid freezing rates, preventing the lipids from reordering. The transmission electron microscopy technique is very desirable because the gross structures afforded by formation of a thin platinum layer are representative of the actual lipid packing.

Freeze-fracture electron microscopy has been used to image directly the surface structure of lamellar phospholipids. Correlation of data from X-ray measurements [57] or ESR spin label experiments [58] at a specific temperature with micrographs obtained with freeze-etch microscopy have shown surface features consistent with lipid geometry predicted from these measurements [59]. These surface features have dimensions consistent with the dimensions measured from X-ray diffraction data. For instance, certain phases with a "ripple" structure are often observed in the TEM images. The ripples are believed to be an ordered phase, the P_β' phase corresponding to a change in the headgroups of the lipids [60]. "Rippled" surface features occur below the phase transition temperature, due to the gel phase packing of phospholipids [61].

For our purposes, we sought information showing microscopic changes in lipid packing induced by metal binding. The length scales probed using transmission electron microscopy (TEM) after platinum shadowing can be as low as 50 nm which can yield information about domain formation on that scale. Other macroscopic thermodynamic measurements such as scanning calorimetry or fluorescence sometimes cannot detect very small, microscopic domain formation. Microscopy allows us to look at a single vesicle, imaging both the hydrophilic and hydrophobic surfaces in the same sample, rather than the whole system of vesicles. It is sometimes possible to detect two types of domains co-existing within the same vesicle, indicating phase separation [62]. Thus, from known

characteristics of phases shared by lamellar vesicles, we wished to determine the qualitative effect of the metal ion on the vesicle surfaces at 25 °C from which the vesicles were frozen.

Pure DSPC vesicles were used as a control and compared to pure metallated and unmetallated PSIDA multilamellar vesicles. The images obtained from freeze fracture prepared DSPC vesicles were typical of vesicles in the gel phase. Small rippled surfaces can be seen in Figure 2.8 which have been documented to be characteristic of either the gel phase or the pre-transition phase [57]. The faces of individual lamellae are visible. Note from the size bar that the approximate ridges are longer than the expected dimension of a bilayer lamella (< 40 Å for DSPC). Once freeze-etch samples of the control vesicles had been successfully prepared, freeze-etch samples of chelating lipids were made.

Since the pure PSIDA lipids were found to have interesting characteristics when mixed with other phospholipids, their vesicle morphology was investigated. Pure PSIDA vesicles adopt a spherical geometry, although individual lamella are not easily visible on the length scale (1000 nm) probed (Figure 2.9). This phase is characterized by a smooth appearance when imaged using freeze-etch microscopy. Because the phase transition temperature of PSIDA vesicles is lower than room temperature, these vesicles would be expected to exist in the liquid-crystalline phase. Smooth lamellae surfaces are expected since the liquid-crystalline phase of lipids is more disordered than the gel phase [58]. PSIDA-Cu^{2+} vesicles seemed to form tube-like structures along with spherical structures. Thus, Cu^{2+} may induce a change in the PSIDA vesicle morphology.

The effect of metal ions on the morphology of mixed PSIDA/DSPC vesicles was not dramatic (Figure 2.11) when compared to addition of metal to pure PSIDA vesicles (Figure 2.10). Freeze-etch micrographs of multilamellar vesicles composed of 5% PSIDA-Cu^{2+} and 95% DSPC showed ridges typical of phospholipids in the gel phase. The vesicles are expected to be in the gel phase at 25 °C (T_m = 54.4 °C) from calorimetry experiments. Metal binding does not produce a new surface morphology at the resolution of the microscopy experiment. The freeze-etch microscopy did not show any tubules

forming upon metal addition to mixed vesicles, indicating that mixed vesicles have properties more similar to natural phospholipids. Coexistence of another phase with the liquid-crystalline phase would show two regions in freeze-etch microscopy, as McConnell has observed [62]. It seems that the vesicles containing small amounts of the metallated lipid are not micro-phase separated, since the rippled appearance was found on all vesicle surfaces. Thus, while metal ion binding may be able to change the vesicle morphology in pure metal-chelating systems, it does not have a large effect on imaged features in mixed vesicles.

The effect of Cu^{2+} on IDA mixed vesicles is different than for other metal-binding systems. For instance, Van Dijck found that Ca^{2+} induced an isothermal phase change upon addition to 35% DPPS (di-palmitoyl phosphatidylserine) mixed with DPPC (di-palmitoyl phosphatidylcholine) [3]. Additionally, Ca^{2+} binding to the headgroup induced cylindrical structures to form. Large isothermal phase transitions were found for Ca^{2+} binding to DPPA/DPPC multilamellar vesicles. Since only one thermal transition from calorimetry was found for 5% PSIDA-Cu^{2+}/ 95% DSPC multilamellar vesicles, the freeze-etch results also supports the existence of only one type of region (rippled) and no microscopic phase separation at 25 °C, the temperature from which the vesicles were frozen.

Fluorescence changes due to metal ion binding

PSIDA (Figure 2.1) was designed as an optical probe for lipid-protein binding studies using fluorescence spectroscopy. The pyrene fluorescence probe was directed to the central portion of the bilayer by its placement at the end of the lipid tail. The presence of this bulky group was found to have profound consequences on the phase transition temperature. Presence of a pyrene group chemically linked to a lipid seems to have this effect on the melting transition in general. For instance, Somerharju made pyrene-labeled lipids with the most common phospholipid head groups [53]. The transition temperature of

these pyrene-labeled lipids are much lower (10-20 °C) than saturated, unlabeled lipids with the same chain length, even though they were designed to mimic natural lipids in all other respects. Even though the lipid head-group interactions are maintained, the lipids have significantly different mixing properties due to pyrene moiety. Although the pyrene-labeled metal-chelating lipids have very different melting properties, they do not phase separate at low mole percent (5%) as evidenced by calorimetry (Figure 2.6).

Binding of transition metal ions to the headgroup of the labeled lipid dramatically affects the PSIDA fluorescence emission spectrum (Figure 2.13). Mixed lipid bilayers containing PSIDA can bind $CuCl_2$, as evidenced by calorimetry (Figure 2.7) and their blue color (pure PSIDA-Cu^{2+}). The dramatic change upon metal ion binding in the fluorescence emission spectrum for mixed bilayers containing only a small percent of PSIDA was unexpected, since the charge of the IDA group in solution studies is neutralized upon metal binding. The change in E/M is similar to the change that might be expected upon ionization of a lipid. The E/M change can be explained by a reversible shift between aggregated PSIDA lipids to disperse, well-mixed PSIDA lipids upon metal binding. The presence of the pyrene moiety causes the labeled chelating-lipid to form enriched domains at low mole fractions when mixed with phosphatidylcholine lipids with much higher phase transition temperature. Thus, PSIDA lipids are near each other due to aggregation, increasing the number of collisions between labeled-lipids [21]. The E/M ratio is increased since there are more excimer-yielding collisions. By adding the metal, the aggregates are broken up by some difference in the lipid charge or lipid packing and the E/M ratio drops to a low value.

The metal-ion driven change in the fluorescence emission spectrum occurs with transition-metal ions that have affinity for iminodiacetate in solution. The metal concentration at which the E/M value begins to change correlates with the strength of binding for the metal ion to the head group of the pyrene lipid (Figure 2.16). For $MnCl_2$ ions this is estimated to be 3×10^{-5} M from the halfway point of $(E/M)/(E/M)_o$ change. The affinity of $MnCl_2$ for 5% PSIDA/ 95% SOPC vesicles was found to be 3.32×10^4 M^{-1}

using isothermal titration calorimetry (Chapter 5). The concentration at which half of the lipids are occupied with metal (Figure 2.16) is $K_d = 3 \times 10^{-5}$ M, therefore coincides with the onset of the change in the scaled $(E/M)/(E/M)_0$ ratio. The binding constant obtained from ITC, although measured for a different matrix lipid, is an order of magnitude lower than the solution binding constant for Mn^{2+} to iminodiacetate ($K_a = 10^{5.5}$ M^{-1}) [38]. This apparent binding may be vesicle concentration dependent. Therefore, changes in the E/M ratio may reflect more than just the binding affinity for Mn^{2+} for the lipid headgroup, since the changes occur after more than half the lipids would be bound to metal.

Upon changing the pH of the vesicle solution, a pronounced increase or decrease of the E/M ratio much like the change due to metal binding, is observed (Figure 2.21). Thus, the lipid charge must play a role in the E/M ratio reversal due to metal binding. The E/M ratio decreases at pH values lower than 7, mimicking the effect of the metal ion on the PSIDA lipid. Thus, assumptions about the charge of the PSIDA lipid must be included to explain the behavior of PSIDA lipids mixed with DSPC. The maximum in the E/M ratio probably represents an aggregated form of PSIDA [21], but it is not known whether the components are interacting with one another through hydrogen bonding or charge-charge interactions. For other negatively-charged mixed-lipid systems, the effect of divalent cations on the mixture is not wholly described by Gouy-Chapman-Stern theory if the binding is specific [32]. In fact the theory does not fully predict changes in the thermal melting transition, and considerations of the lipid packing must be included.

The transduction of metal binding into a fluorescent signal, as seen in the dramatic shift of the E/M value from a value greater than one to a much lower value, can be modulated by the matrix lipid. Membrane properties are expected to be very sensitive to the matrix lipid, since it comprises 95% of the total membrane. For instance, the diffusion constants of lipid membranes change abruptly at the gel to liquid crystalline phase transition and are strongly influenced by matrix lipids [41]. To show how the chain length affects the E/M ratio, di-palmitoyl phosphatidylcholine (DPPC), a lipid containing 16 carbon tails,

was substituted for DSPC (Figure 2.17). The E/M ratio before metal addition to 5% PSIDA/ 95% DPPC vesicles is lower than for 5% PSIDA/ 95% DSPC vesicles (0.6 versus 1.2). By further decreasing the phase transition temperature of the matrix lipid, we expect to see an even lower E/M ratio before metal is added. Matrix lipids with a phase transition around room temperature (Table 2.3) in fact show a much smaller E/M ratio before metal addition. Indeed, binding of metal ions to DMPC vesicles results in a small shift in the E/M ratio (from 0.3 to 0.2) indicating that the acyl chain mismatch is important in the segregation of the lipid into domains. Mixtures of PSIDA and a lower melting lipid, 1-stearoyl-2-olealyl-3-phosphocholine (SOPC), had a change in E/M upon metal binding that is also a smaller change than in DSPC/PSIDA mixtures, although the acyl chains are the same length. From these examples, the E/M value before metal addition is related to the phase of the lipid mixture. Both DMPC or SOPC lipid formulations will be in the liquid-crystalline phase at 25 °C. Thus, the PSIDA lipid, due to its low phase transition temperature, is better mixed in liquid-crystalline phase vesicles, resulting in a lower E/M ratio.

Longer phosphatidylcholine lipids, in contrast, have a larger effect on the E/M ratio change upon metal binding, since the transition temperature mismatch between PSIDA and the matrix lipid is even larger than for DSPC/ PSIDA mixtures. A synthetic phosphatidylcholine matrix lipid with 24 carbons in the acyl chains, DBPC, was mixed with PSIDA to determine the effect on E/M (Figure 2.19). The E/M ratio before metal addition is higher than PSIDA/DSPC vesicles and decreases significantly upon metal binding. Thus, the melting transition temperature also correlates with the E/M ratio value without and with Cu^{2+}. Aggregation of the pyrene-labeled lipid induced by the matrix lipid has been observed with matrix lipids which having a higher T_m than the pyrene-labeled lipid [53,63,64].

Changing the phospholipid headgroup also should affect the E/M ratios before and after metal addition. Changing the matrix-lipid headgroup alters the ionization of the

chemical groups located at the interface and thus the charge per lipid. For instance, changing the matrix lipid to phosphatidic acid greatly increases the value of E/M without metal to between 7 and 9. The addition of metal decreases the ratio to about 2. The phosphatidic acid headgroup will be negatively-charged at pH 7.5 if the bulk pH is assumed to be the same as the interfacial pH. Since the acyl chains were chosen to have the same length as DSPC (18 carbons), the negatively-charged headgroup also must have a strong affect on the lipid aggregation, making PSIDA less soluble in the matrix lipid. The charge of the headgroup may actually be more important in modulating the E/M ratio than the acyl chain length. Since the vesicle system can be used as a metal sensor, the choice of matrix lipid can be used to design the pH and sensitivity of the sensor operation.

Thus, the high E/M value found for PSIDA in DSPC can be removed by changing to a matrix lipid that at 25 °C would be in the liquid-crystalline phase. If a larger change upon metal binding is desired, a higher-melting, matrix lipid in the gel phase could be used. The E/M value is affected by phase transition temperature for the same matrix lipid headgroup (Table 2.3). From the pH effects on E/M as well as changes in E/M with acyl chain length, the effect of metal binding on the PSIDA mixing properties seems to be a combination of both electrostatic effects and lipid-mixing effects.

Fluorescence lifetime and metal binding

To further explore the mechanism of the metal-induced changes on the mixed bilayer, fluorescence lifetime studies were initiated. Changes in lifetime of fluorescence are induced by association of a paramagnetic metal ion either with the ground state of the fluorescent molecule (static quenching) or the excited state fluorophore (dynamic quenching) [44]. Many metal sensors composed of a chelating moiety attached to a fluorescent group show dynamic quenching, known as collision quenching, upon addition of metal ion [39]. However, perylene has been described as forming a resonance energy transfer complex with Co^{2+} in lipid bilayers [65]. The mechanism of quenching is usually

inferred by the effect of the quencher on the lifetime of the fluorescent complex [44]. Thus, we investigated the effect of increasing Cu^{2+}, our strongest binding metal, on the fluorescence lifetimes 5% PSIDA/SOPC vesicles.

PSIDA/DSPC vesicles had fluorescence lifetimes shorter than the minimum resolution of the instrument ($\tau > 5$ ns). PSIDA/SOPC vesicles had lifetimes in the range of 40 ns for the monomer and 90 ns for the excimer. The lifetime was strongly affected by copper (Table 2.4). Plots of the excimer lifetime data show a decrease in the lifetime upon addition of less than stoichiometric copper [~3.3 µM total lipid]. However, to determine the mechanism of quenching the approximate behavior of the lifetime with increasing quencher must be determined. If the lifetime decreases linearly upon metal addition, collisional quenching is occurring. Other quenching phenomena such a Dexter resonance-energy transfer have an exponential decrease upon metal addition [65]. Dexter-type quenching has been observed for Co^{2+} association with lipid headgroups to perylene dissolved in lipid bilayers. Our data showed a more exponential type decrease in the lifetime, although the linearity of the response is determined almost wholly by the first point lacking metal. Since the effect of the metal ion caused a decrease in the E/M ratio well below stoichiometric copper (~150 nM), the E/M effect is not clearly Stern-Volmer quenching and could be Dexter resonance-energy transfer.

CONCLUSIONS

Metal-chelating lipids containing iminodiacetate moieties were formed into stable vesicles that had interesting metal-binding properties. Metal ions interacted strongly and specifically with mixed vesicles, determined using fluorescence spectroscopy, freeze-etch microscopy, and calorimetry. The binding of the metal ion causes an interesting increase of the gel to liquid crystalline phase transition for pure DSIDA metal-chelating vesicles. However, addition of excess metal resulted in a complete removal of the transition for PSIDA metal-chelating vesicles with the same IDA head group. Direct examination of the

pure and mixed vesicle surfaces by freeze-etch microscopy showed very little change in the pure chelating-lipid vesicle surface upon metal binding for the fluorescently-labeled vesicle.

Addition of metal ions to pyrene-labeled, metal-chelating vesicles had a profound effect on the fluorescence emission spectrum. The excimer to monomer ratio reflected the specificity of iminodiacetate for different metal ions. The metal ion driven fluorescence change is also affected by the length and charge of the matrix phospholipid, so electrostatic and lipid packing effects are influencing this change. Similar changes in E/M ratio could be caused by changing the pH of the vesicles. Since an isosbestic point was present it seems that a population inversion from aggregated to less aggregated lipid state is occurring. Measurements of the fluorescence lifetimes showed a strong effect due to metal ion binding. This could be due to an energy transfer mechanism, since Ca^{2+} also causes the same effect on the E/M ratio and because metal ions are not expected to penetrate the bilayer below the phase transition temperature.

EXPERIMENTAL

Lipids

DSIDA [10] and PSIDA [66] was synthesized by Dr. Darryl Sasaki according to the published procedure. Stock solutions in chloroform were made in 10 or 5 ml volumetric flasks and stored in the freezer wrapped with Teflon tape. PSIDA was stored at 4 °C in dilute chloroform solutions, being careful to keep the solution protected from light. DSPC, SOPC, and DBPC were obtained (>99% purity) from Avanti Polar Lipids (Birmingham, AL). Synthetic DSPA, DPPC, DBPC were obtained from Sigma Chemicals (St. Louis, MO). DMPC was obtained from Coatasome (Nippon Oil & Fats, Japan) Lipid solution volumes were measured using either volumetric pipettes and by Hamilton gas-tight syringes. All glassware to be used with vesicle solutions was cleaned in a bath sonicator using RBS-35 detergent and rinsed extensively with dH$_2$O, then oven dried.

Vesicle preparation

Lipids were dissolved in chloroform to make concentrated stock solutions. 12 ml glass centrifuge tubes were coated with 10 μmoles total lipid under a stream of argon gas. The coated tubes were dried for 12 hr under vacuum and hydrated with 3 ml of 20 mM MOPS, 100 mM NaCl, pH 7.5 buffer. The liposomes were vortexed at 50 °C and then probe tip sonicated (Heat Systems model 375) at 4 °C for 15 min. at 15-25% power output. Titanium fragments were removed by filtration on a 0.2 mm syringe filter. For experiments with DSPC vesicles at pH 7.5 it was impossible to get vesicles with a mean of lower than 30 nm in MOPS buffer. Thus, this larger mean is most likely due either to the sonicator performance or the type of lipid formulation. For instance, pure phosphatidylcholine vesicles sonicated in pure ddH$_2$O form a very clear suspension indicating small unilamellar vesicles.

Freeze fracture microscopy

3 mM total lipid (10 µmoles in 3 ml buffer) were made into multilamellar vesicles at 55 °C with no degassing [54]. If metallated samples were desired, the metal was added along with the buffer. The multilamellar vesicles were concentrated by centrifuging at 5,000 rpm for 10 minutes. The solution above the pellet was removed and the pellet re-suspended by pipetting. Copper "hats" were scored with clean forceps and a drop of lipid solution placed into the center of the hats. The hat was frozen in a liquid N_2 slush prepared by taking liquid nitrogen and placing it in a vacuum chamber and evacuating. This procedure should yield cooling rates that are very fast (100 °C/s) since the samples are extremely small (≤ 0.1 ml). The frozen samples were placed in liquid N_2 cooled sample holder being careful to keep the sample under liquid N_2 at all times. Standard procedures were followed to transfer the samples onto a liquid N_2 cooled stage. The samples were fractured, ice was sublimated, and the sample shadowed by Pt (~500 nm) and then carbon (several micron) according to standard procedures [37]. The prepared samples were placed in commercial bleach and the replicas floated off. The replicas were transferred to pure ddH_2O and then to 50% MeOH/50% H_2O. The samples were washed again in pure H_2O and transferred to Formvar coated TEM girds (Ted Pella, Inc.). The grids were imaged on a transmission electron microscope by Jean Edens and Dr. Jean-Paul Revel.

Data selection was difficult for pure PSIDA-Cu^{2+} vesicles due to problems in preparing replicas. The copper metallated vesicles fell out of solution, and it was very difficult to get good replicas that contained vesicle features. One of the few replicas obtained is shown in Figure 2.10. However, I believe some replicas may be representative of a clump of PSIDA-Cu^{2+} vesicles rather than free floating particles. When possible the vesicle samples were allowed to sit over 24 hr. so that they would form equilibrium structures before pelleting.

DSC experiments

Experiments to measure the thermal transitions of lipid vesicles were done using a Microcal MCS differential scanning calorimeter. The DSC was computer-controlled by a 486 Ambra clone computer using the commercial software Microcal Observer™ supplied by Microcal. The cell were cooled using a Neslabs RTE-110 water bath that had a RS-232 interface that was also computer controlled. Calibration of T_m was periodically checked with paraffin standards supplied by Microcal. Scan rates of 45°C/hr were used for calibration and ddH$_2$O was placed in each cell prior to inserting the standards. Periodically, the cells were cleaned with conc. HCl or HNO$_3$ and the water-water baseline checked for reproducibility.

The experiments were performed after stirred degassing of the vesicle samples for 20 minutes under aspirator vacuum. MOPS buffer was transferred into the reference cell by using a syringe while carefully removing bubbles from the capillary neck. Vesicles were transferred in the same way into the sample cell. The scans were started at 5 °C and data acquisition started at 10 °C due to the equilibration procedure used by the software. The scan rate was set at 10°C/hr (0.18 °C/min.) to prevent kinetic limitations of the phospholipid transition [67]. 15 psi N$_2$ atmosphere was kept over the cells to prevent boiling and to promote reproducibility. The amount of available PSIDA lipid was small and low concentrations of lipid (1-3 mM) had to be used and the experiments could not be repeated. Two consecutive scans were run to show reversibility, which was found for all vesicle suspensions at both 45 and 10 °C/hr scan rates. Since the baseline was reproducible for every run after the first, the second scan was used for data analysis. The vesicle concentration was assumed to be the same as the initial concentration (no loss of solvent). DPPC multilamellar vesicles made in MOPS buffer were also run as a control and found to have T_m and ΔH_{cal} values that were nearly identical to published values [69].

The experimental scan was analyzed by subtracting a cubic baseline from the scan. Flat baselines were regularly obtained for pure degassed H_2O and MOPS buffer. The maximum value of ΔC_p was taken to be T_m since baseline subtraction can shift the ΔCp curve if there is a difference in the intrinsic heat capacity of the gel and liquid-crystalline state. For most lipid systems studied, especially phospholipids, the ΔC_p returned to the starting value after the main transition. For most lipid mixtures, the transition was found to be cooperative, thus the curves were integrated and the total enthalpy divided by the concentration to obtain the calorimetric enthalpy of the transition.

Fluorescence experiments

Vesicles were diluted 1:150, 1:500 or 1:1000 for fluorescence experiments to prevent inter-vesicle cross linking. A Shimadzu RF-540 spectrofluorimeter fitted with temperature controlled bath was used for fluorescence intensity measurements. For a typical experiment, the vesicles were diluted in MOPS buffer to a final volume of 3 ml and placed in a quartz cuvette. The excitation wavelength was 346 nm with excitation and emission slits set at 5 nm. The scan speed was 8 mm /min. The signal to noise of the machine was periodically checked and found to be S/N $\approx$ 100 (Raman band of H_2O). The water Raman emission band did not exceed the emission intensity of pyrene for any lipid concentration used. Similar fluorescence emission spectra were also obtained on a SLM 4800 instrument.

Metal salts were added directly to the same sample cell, and the intensities at 377 nm and 470 nm measured from the analog (paper) output. Vesicles were metallated during fluorescence binding experiments since the effect on E/M was found to be directly proportional to metal binding. The error in the experiment was by averaging the initial E/M values of vesicle samples with the same composition. Oxygen quenching of fluorescence was found to be very small and neglected for all experiments. Experiments duplicated under N_2 atmosphere showed the same E/M behavior with metal-ion concentration.

Measurement of fluorescence lifetimes

A YAG laser fitted with an oscillating shutter was used for pulsed lifetime experiments [44]. The instrument response at 25°C was acquired using 100% SOPC vesicles diluted 1:1000 in MOPS buffer to account for light scattering. The excitation was set at 355 nm. Monomer lifetime was acquired by using emission wavelength 397 nm with a 385 nm cutoff filter and neutral density filters with slits 1 mm in the double beam monochromator. Excimer lifetime was acquired using an emission wavelength of 470 nm with 385 nm cutoff and neutral density filters with 0.5 mm slit on the outside and 1 mm slit in the middle monochromator slit. Metal salt solution was added to the cell with rapid stirring.

The data were deconvoluted using a bi-exponential decay with the instrument response function. The minimum lifetime deemed faster than the response time of the machine is 5 nanoseconds [68]. Thus, lifetimes lower than 5 nanoseconds are artifacts of the fitting algorithm or correspond to a faster lifetime. A bi-exponential decay was chosen because there is a faster component of the lifetime due to light scattering during the acquisition time. Measurements with χ^2 values of less than 4×10^{-4} (mV) were deemed acceptable.

Table 2.1. Sizes of vesicles determined through quasi-elastic light scattering in MOPS buffer at pH 7.5 using Microtrac Fine Particle Analyzer (Leeds & Northrop) taken at least 24 hr after vesicle formation. Parameters are taken from data output of fitting algorithm used to determine vesicle size distribution. Vesicles were assumed to be spherical, reflecting scatterers at 25 °C.

vesicle composition	median diameter [nm, (% total volume fraction)]	distribution width (nm)
5% PSIDA/ DSPC	47 (100%)	59
2.5% DSIDA/ 47.5% DSPC/50% cholesterol	44 (99%)	15
2.5% DSIDA-Cu^{2+} / 47.5% DSPC /50% cholesterol	41 (91%) 130 (7%)	42 64

Table 2.2. Thermodynamic parameters obtained from scanning microcalorimetry of multilamellar vesicles. Scans taken in MOPS buffer [20 mM MOPS, 100 mM NaCl, pH 7.5). ΔH_{cal} determined by integration of baseline-subtracted, concentration normalized ΔC_p curve. ΔS_{cal} calculated from $\Delta S_{cal} = \Delta H_{cal} / T_m$. The chemical structures of PSIDA and DSIDA are shown in Figure 2.1. The chemical structures of DSPC and SOPC are shown in Figure 2.2. SOPC thermodynamic parameters obtained from [69].

lipid (acronym)	T_m (°C)	ΔH_{cal} (kcal/mol)	ΔS_{cal} (cal/°K mol)
SOPC	3-7	5.2 ± 0.2	19
DSPC	54.5 ± 0.2	11.1 ± 0.5	33.9
DSIDA	54.9 ± 0.2	21.1 ± 0.5	64.3
DSIDA-Cu^{2+}	70.1± 0.1[b]	10.8 ± 0.5[b]	31.5
PSIDA	13.4 ± 0.2	7.1 ± 0.5	24.8
PSIDA-Cu^{2+}	no transition	---------	---------

[a] 2X excess Cu^{+2}

[b] DSIDA was sonicated with Cu^{+2} for 10 min. to metallate inner lamellae.

Table 2.3. Effect of excess copper [1.5 µM] on fluorescence E/M intensity ratio 5% PSIDA lipid mixed with different matrix phospholipids at 25°C in pH 7.5 MOPS buffer. Intensity ratio calculated from excimer intensity, 470 nm; monomer intensity, 377 nm. Pre-formed vesicles diluted 1:200 in MOPS buffer [~20 µM total lipid].

5% PSIDA mixed with 95%	# Acyl chain carbons	E/M (no metal)	E/M (+ CuCl$_2$)[a]	T$_m$ (°C) [69]
SOPC 1-stearoyl-2-olealyl-3-phosphocholine	18	0.3 ± 0.05	0.2	3-7
DMPC 1,2-myristoyl-3-phosphocholine	14	0.3 ± 0.1	0.2	23.5
DPPC 1,2-palmitoyl-3-phosphocholine	16	0.6 ± 0.1	0.3	41.4
DSPC 1,2-stearoyl-3-phosphocholine	18	1.2 ± 0.1	0.4	54.5
DBPC 1,2-behenoyl-3-phosphocholine	24	4.3 ± 0.2	2.9	80.1
DSPA 1,2-stearoyl-3-phosphatidic acid	18	7.5 ± 0.5	2.4[b]	—

[a] 1.5 µM CuCl$_2$

[b] precipitation of vesicles observed

Table 2.4. Fluorescence lifetime data of 5% PSIDA/ 95% SOPC vesicles at 25 °C, pH 7.5. $CuCl_2$ metal addition to vesicles is compared with unmetallated vesicles. Lifetime parameters obtained from bi-exponential fluorescence decay curve fit with deconvolution of machine response function taken with same dilution of 100% SOPC vesicles.

5% PSIDA/ 95% SOPC vesicles + $CuCl_2$ (nM)	τ, machine response (nanoseconds)	τ, lifetime (nanoseconds)
no metal	3.5	89.7
19	3.1	57.2
38	2.9	55.2
56	2.5	46.9
75	3.1	47.3
93	2.9	47.5
114	2.6	44.3
133	2.8	41.3

Table 2.5. Fluorescence lifetime data showing lifetime from bi-exponential fits of monomer fluorescence (397 nm) of 5% PSIDA/ 95% SOPC vesicles at 25 °C, pH 7.5. Curves fitted with bi-exponential fluorescence decay with deconvolution of machine response function taken with same dilution of 100% SOPC vesicles at 365 nm.

5% PSIDA/ 95% SOPC vesicles + $CuCl_2$ (nM)	τ, machine response (nanoseconds)	τ, lifetime (nanoseconds)
no metal	N.A.	N.A.
19	2.5	39.9
38	2.5	35.8
56	2.4	36.5
75	2.3	34.4
93	2.5	34.3
114	2.6	34.5
133	2.6	32.9
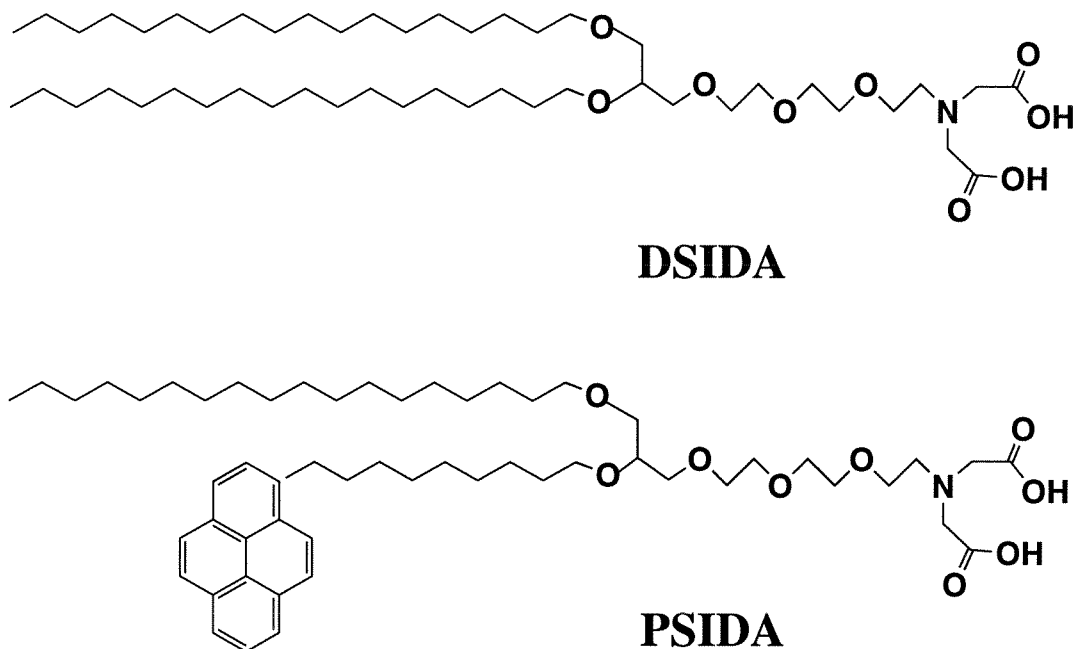
DSIDA

PSIDA

Figure 2.1. Synthetic metal-chelating 1-Octadecyl-2-(9-(1-pyrene)nonyl)-*rac*-glycero-3-(8-(3,6-dioxy)octyl-1-amino-N,N-diacetic acid) (PSIDA) and 9-[2,3-Bis(octadecyloxy)propyl]-3,6,9-trioxynonyl-1-iminodiacetic acid (DSIDA) lipid used to form pure and mixed vesicles. The alkyl chains of these lipids are ether linked for stability.

DMPC

DPPC

SOPC

DSPC

DBPC

DSPA
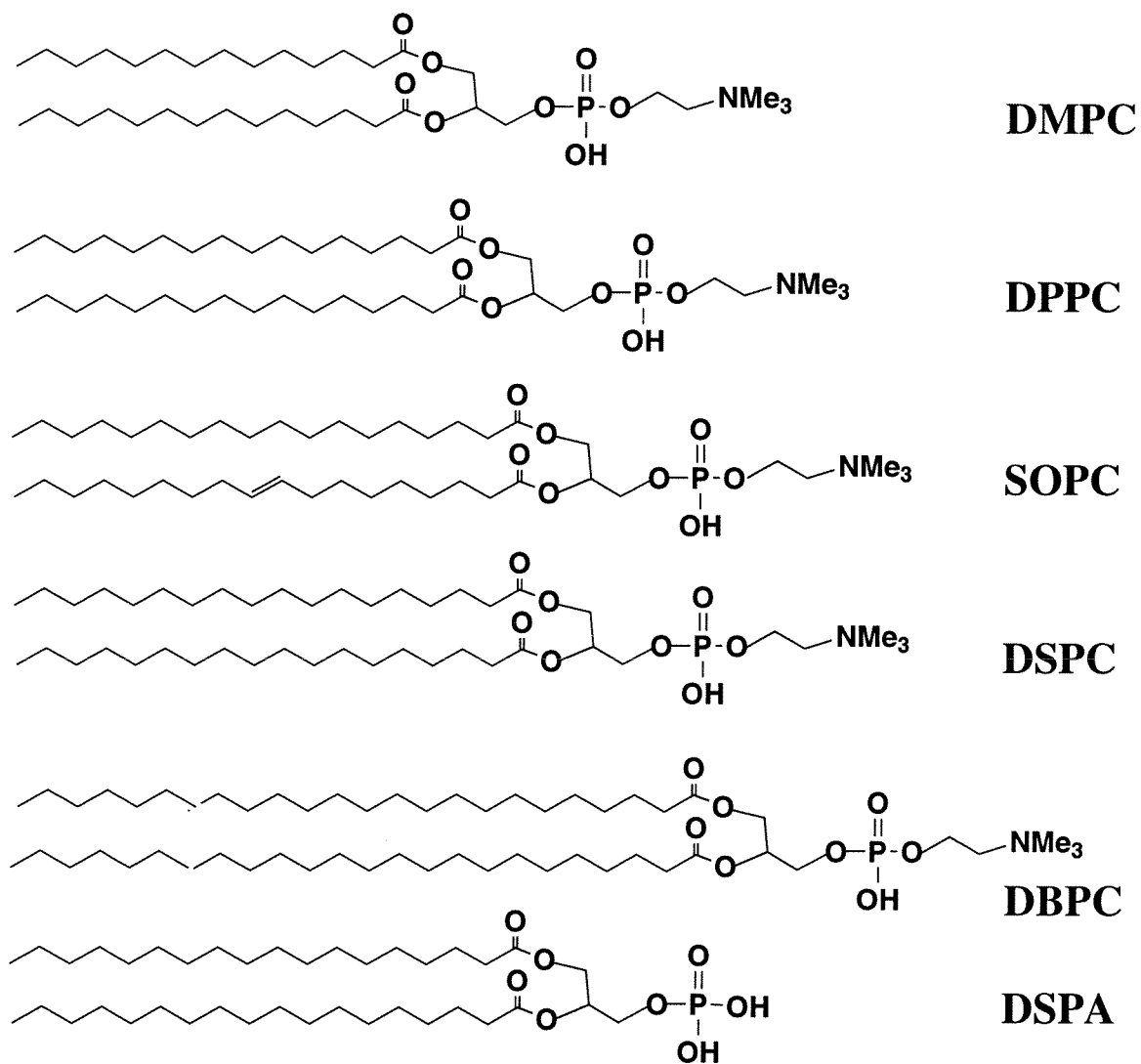
Figure 2.2. Natural phospholipids used to form mixed metal-chelating vesicles. The acyl chain length varies from 14 carbons (DMPC) to 24 carbons (DBPC).

62
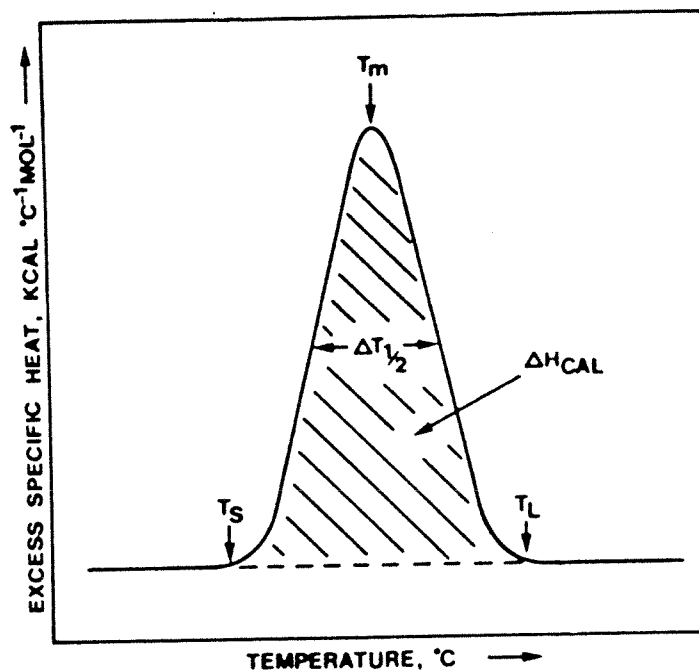
Figure 2.3. Schematic diagram illustrating typical data obtained from scan rate normalized differential scanning calorimetry. ΔH_{cal} is the calorimetric enthalpy, T_m is the maximum temperature, $\Delta T_{1/2}$ is obtained from the value of $1/2 C_{p,max}$ as indicated graphically. Schematic ΔC_p versus temperature curve reproduced from McElhaney [47].
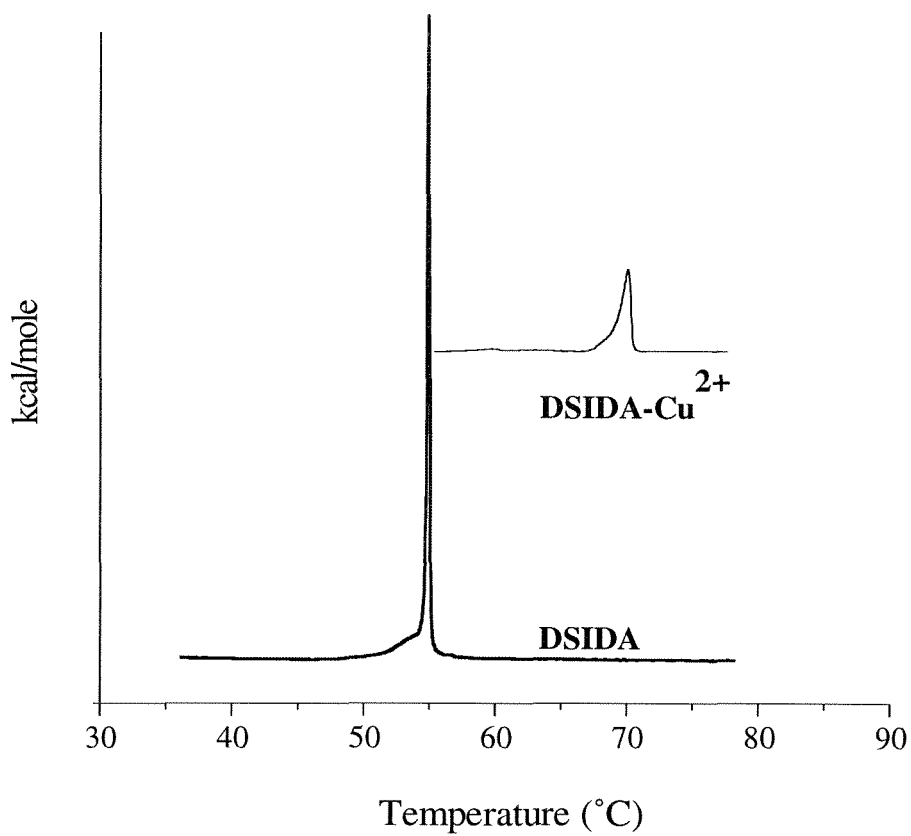
Figure 2.4. Thermal transitions of pure DSIDA lipids with and without copper added to vesicles in [20 mM MOPS, 100 mM NaCl, pH 7.5] buffer using 0.18 °C/min. scan rate. Total integrated enthalpy divided by total lipid present to get ΔH_{cal}. Four-fold excess of $CuCl_2$ added to metallate vesicles.
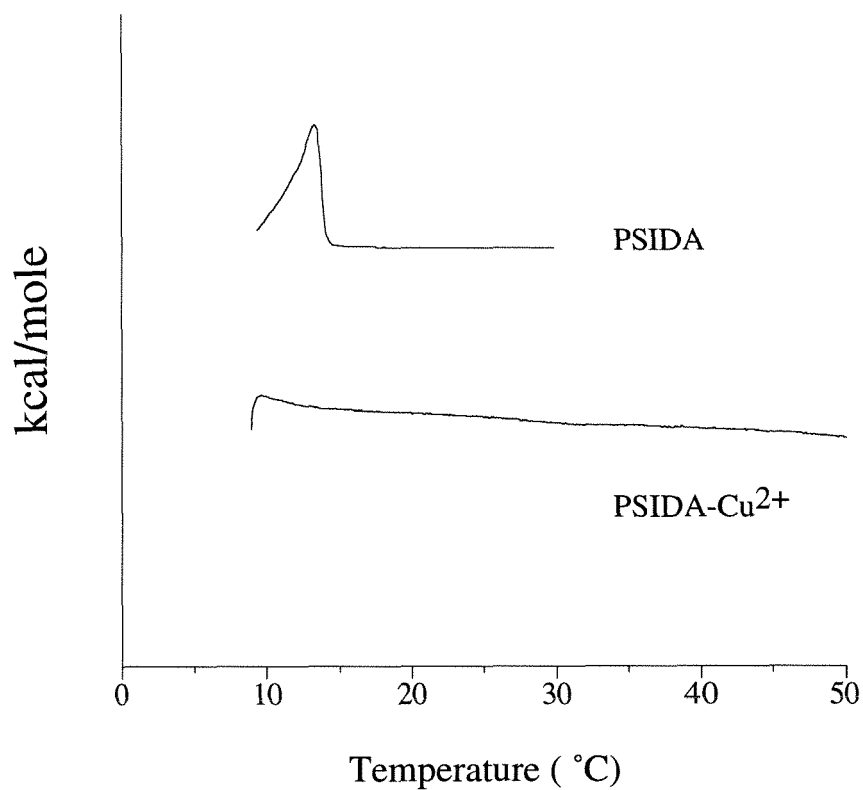
Figure 2.5. Thermal transitions of pure PSIDA and PSIDA-Cu^{2+} multilamellar vesicles determined using 0.18 °C/min. scan rate in [20 mM MOPS, 100 mM NaCl, pH 7.5] buffer. Four-fold excess of $CuCl_2$ added to metallate vesicles.
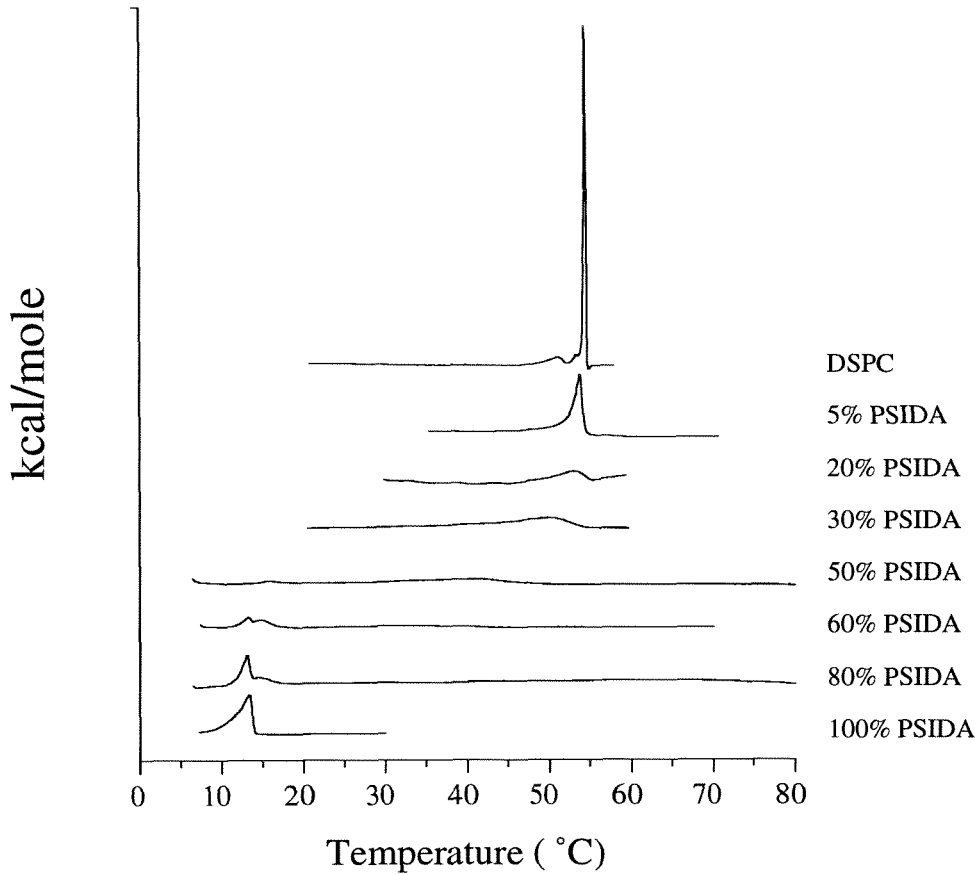
Figure 2.6. Effect of PSIDA lipid composition on thermal transition of mixed multilamellar vesicles containing DSPC. Scan rate was 0.18°C/min. in [20 mM MOPS, 100 mM NaCl, pH 7.5] buffer.
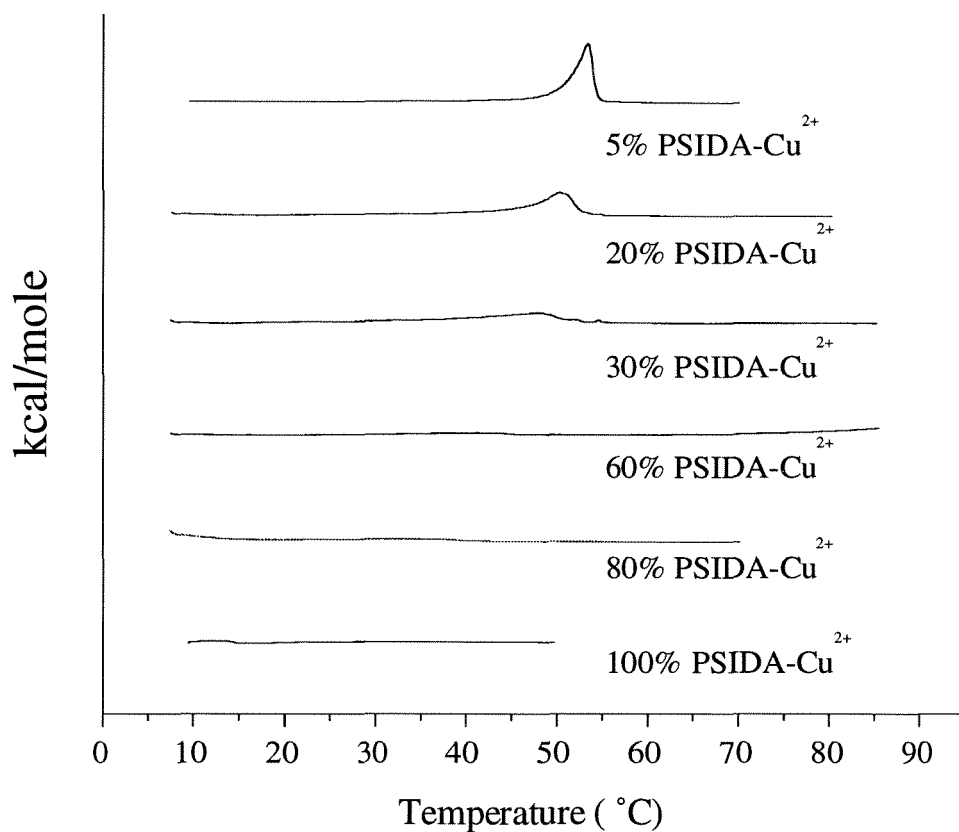
Figure 2.7. Effect of PSIDA-Cu^{2+} composition on thermal transitions of DSPC multilamellar vesicles. Scan rate was 0.18 °C/min. in [20 mM MOPS, 100 mM NaCl, pH 7.5] buffer.

Figure 2.8. Transmission electron micrograph showing freeze-etch prepared DSPC multilamellar vesicles. Magnification is 18,500x; size bar is indicated.
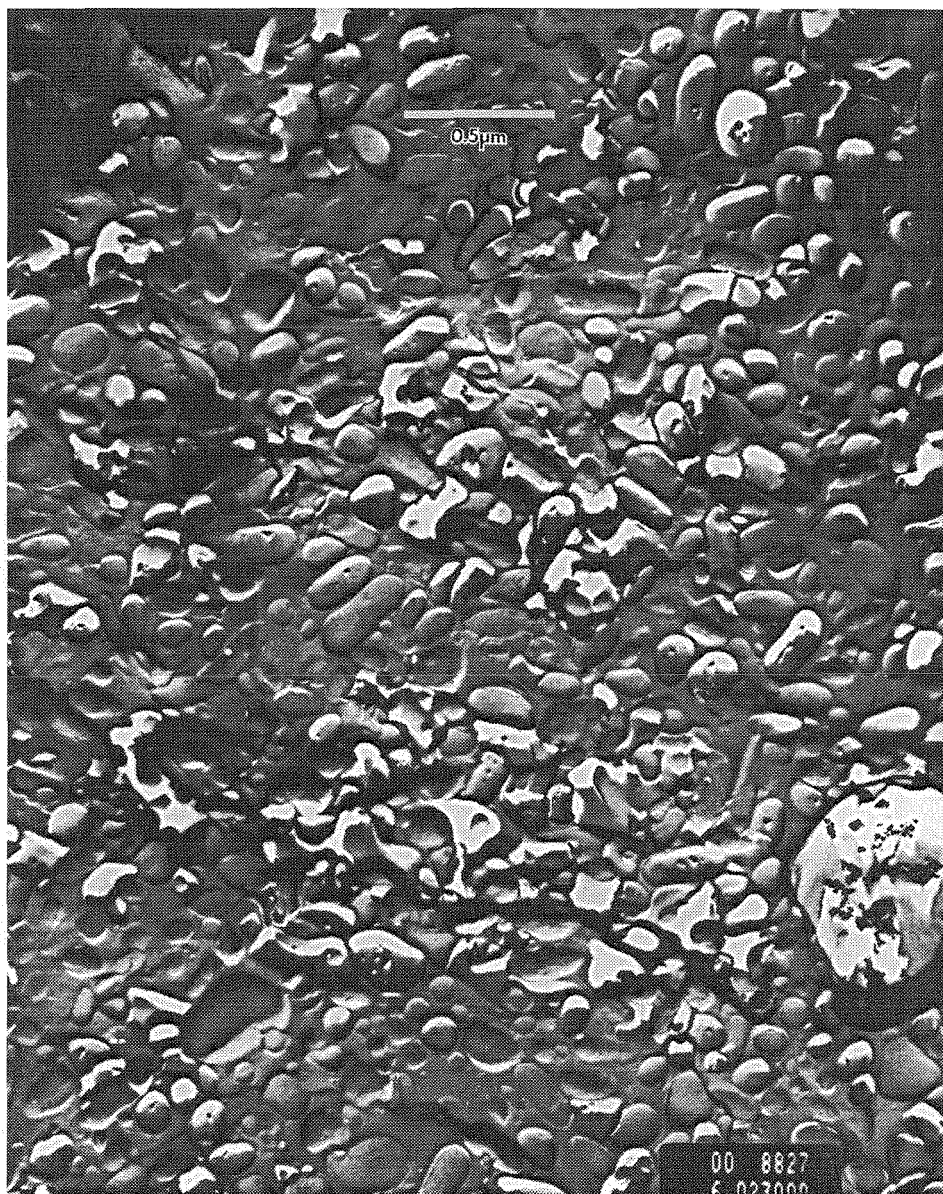
Figure 2.9. Transmission electron micrograph showing freeze-etch prepared PSIDA multilamellar vesicles. Magnification is 15,800x; size bar is indicated.
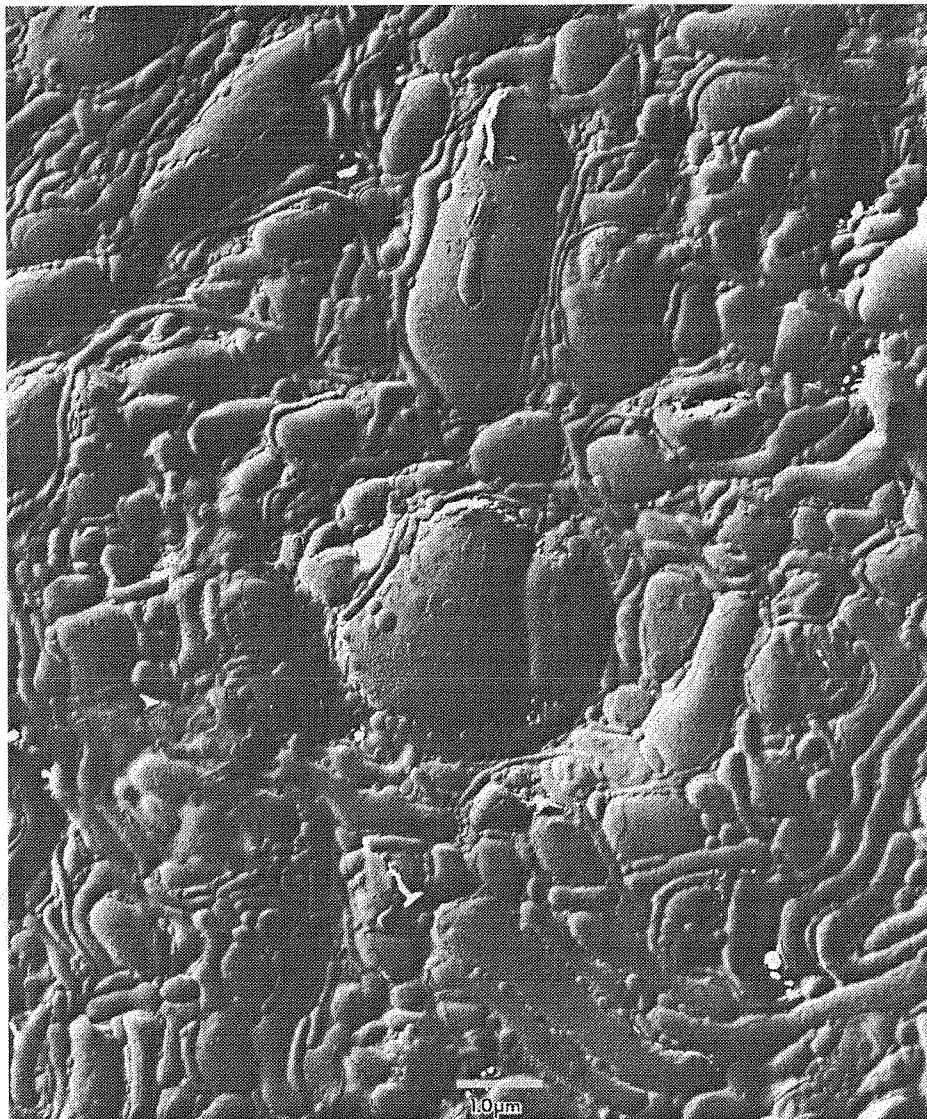
Figure 2.10. Transmission electron micrograph showing freeze-etch prepared 5%

PSIDA-Cu^{2+} multilamellar vesicles. Magnification is 15,800x; size bar is indicated.

Figure 2.11. Transmission electron micrograph showing freeze-etch prepared 5% PSIDA-Cu^{2+} / 95% DSPC multilamellar vesicles. Magnification is 15,800x; size bar is indicated.
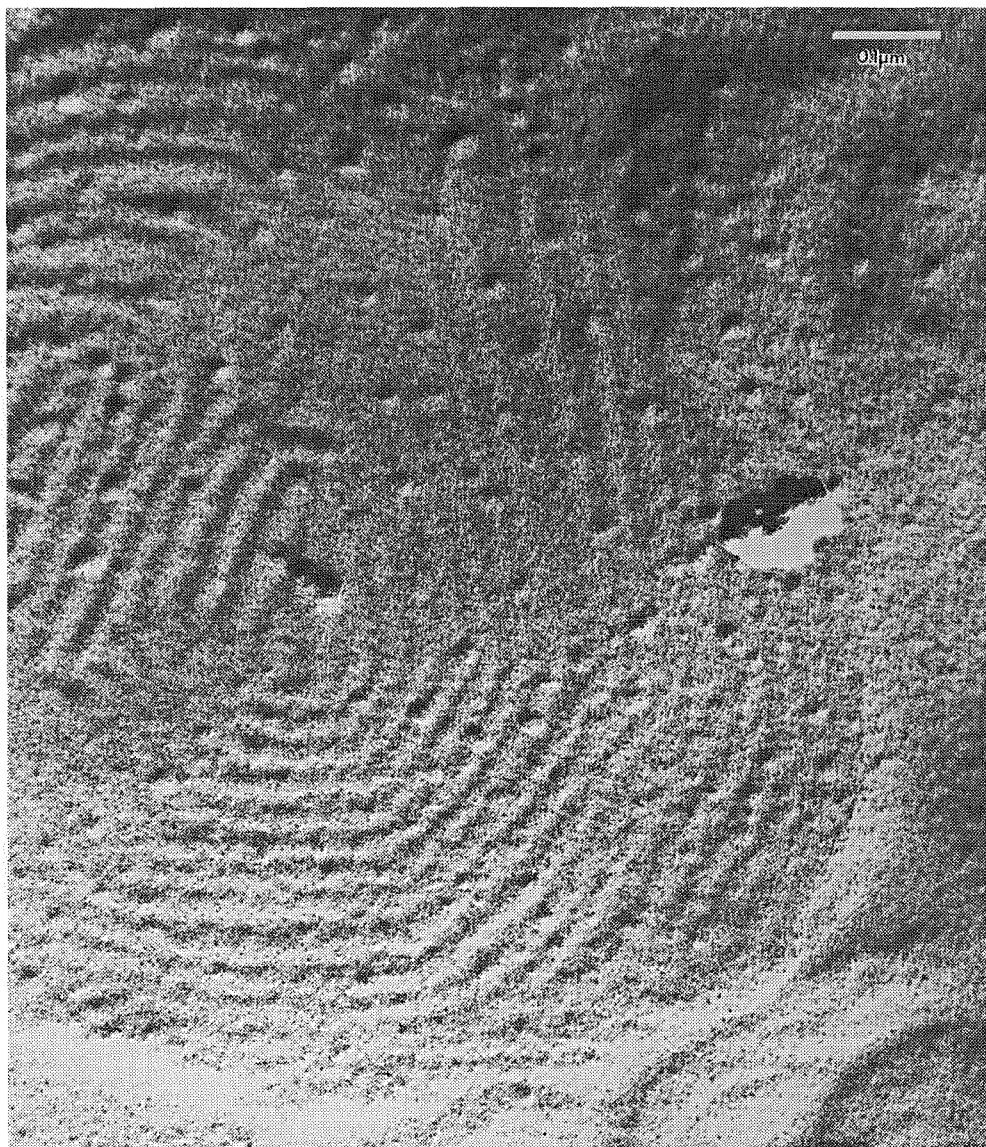
Figure 2.12. Transmission electron micrograph showing higher magnification image of ripple feature of 5% PSIDA-Cu^{2+} / 95% DSPC multilamellar vesicles. Magnification is 56,600x; size bar is indicated.
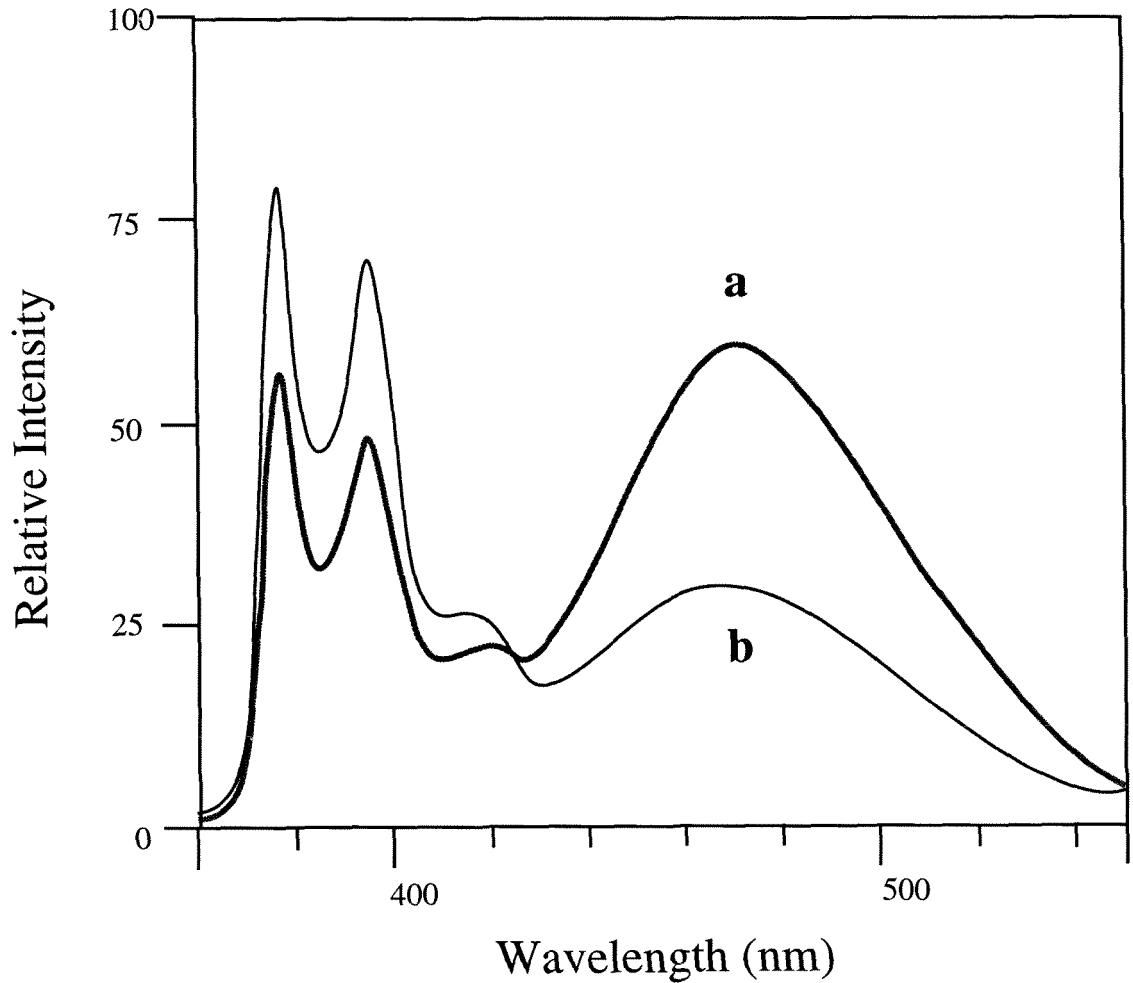
Figure 2.13. CuCl$_2$ addition to 5% PSIDA/95% DSPC small unilamellar vesicles results in a change in excimer (470 nm) to monomer (377 nm) intensity values in the fluorescence emission spectrum. E/M value changes from 1.1 (curve a) to 0.4 (curve b) upon addition of 0.14 µM CuCl$_2$ in MOPS buffer, 25°C. Vesicle concentration was 2.9 µM total lipid.
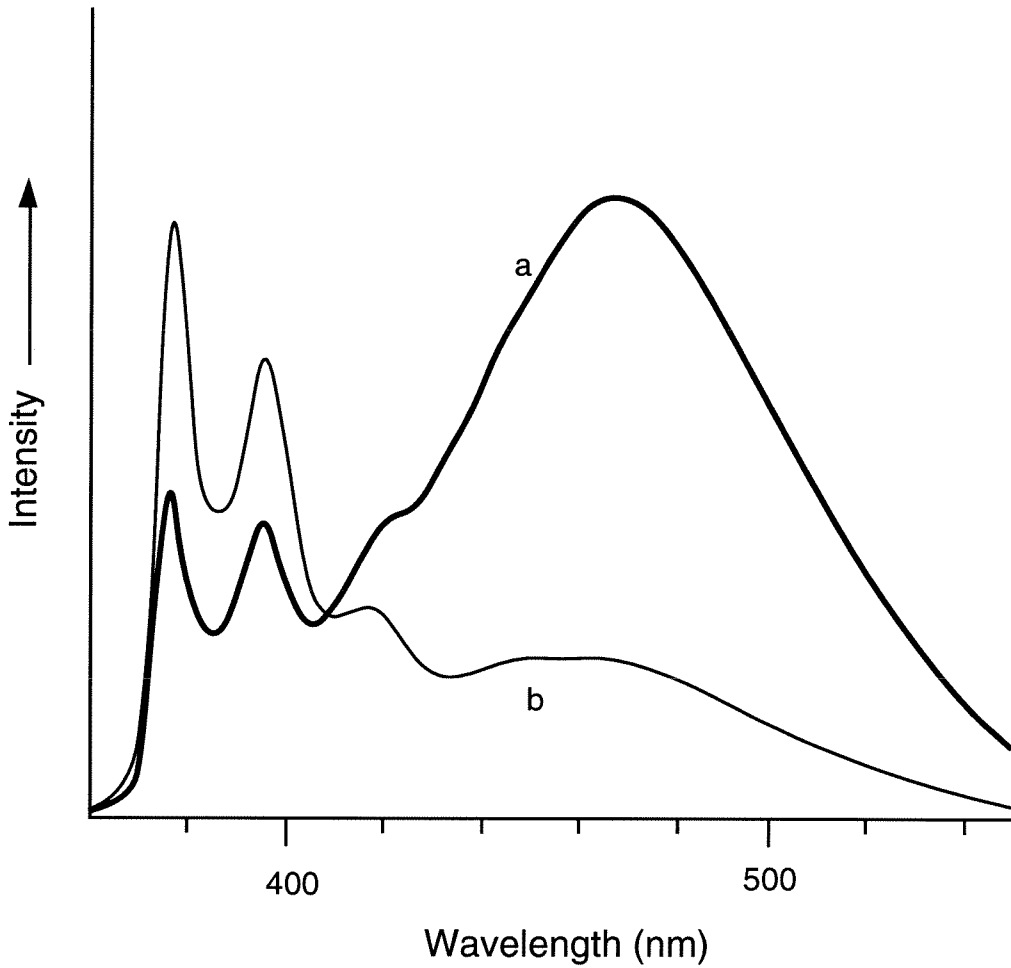
Figure 2.14. Fluorescence emission spectra showing effect of two matrix lipids composition on 5% PSIDA /95% matrix lipid. Curve (a) contains 5% PSIDA/ 95% DSPC vesicles, curve (b) contains 5% PSIDA/ 95% SOPC vesicles at 25 °C in MOPS buffer pH 7.5.
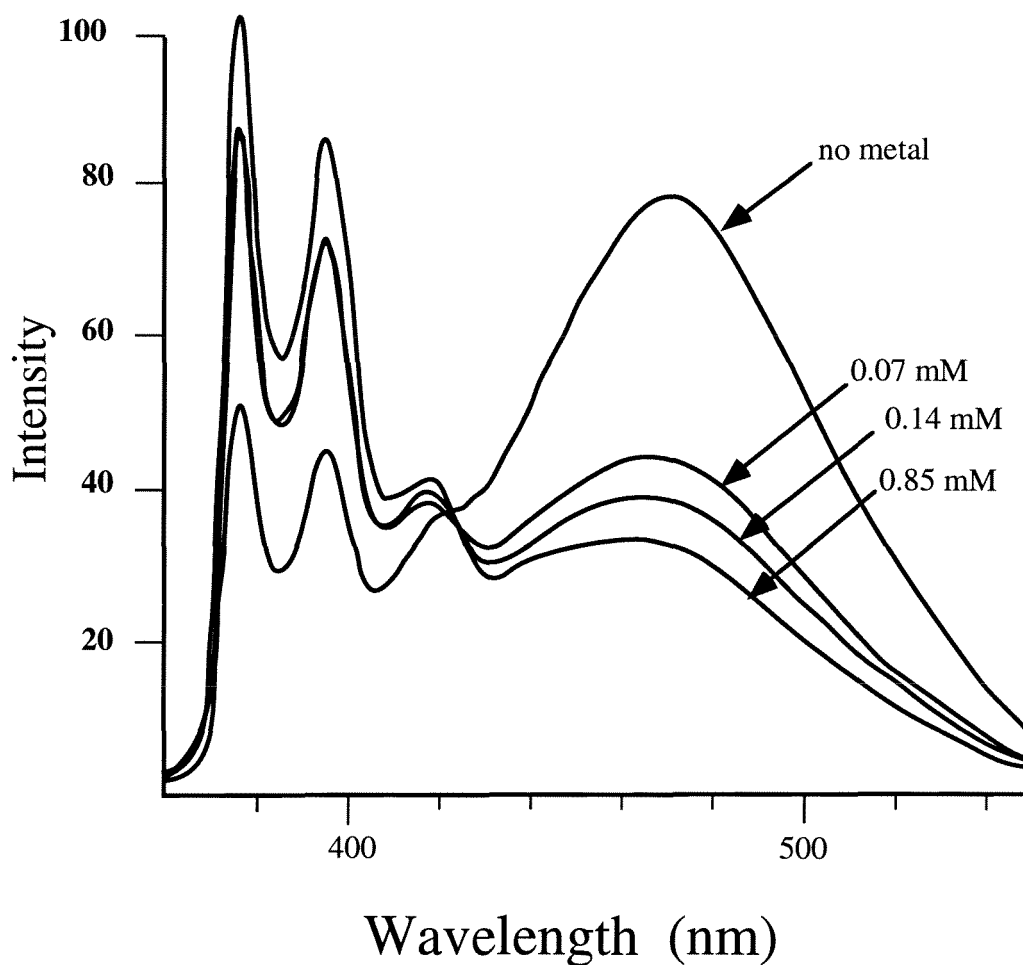
Figure 2.15. MnCl$_2$ addition to 5% PSIDA/ 95% DSPC small unilamellar vesicles in [20 mM MOPS, 100 mM NaCl, pH 7.5] buffer at 25 °C. Fluorescence spectra taken at λ_{ex} = 346 nm, 5 nm slit widths. Note presence of isosbestic point at 424 nm. Vesicle concentration is ~15 µM total lipid.
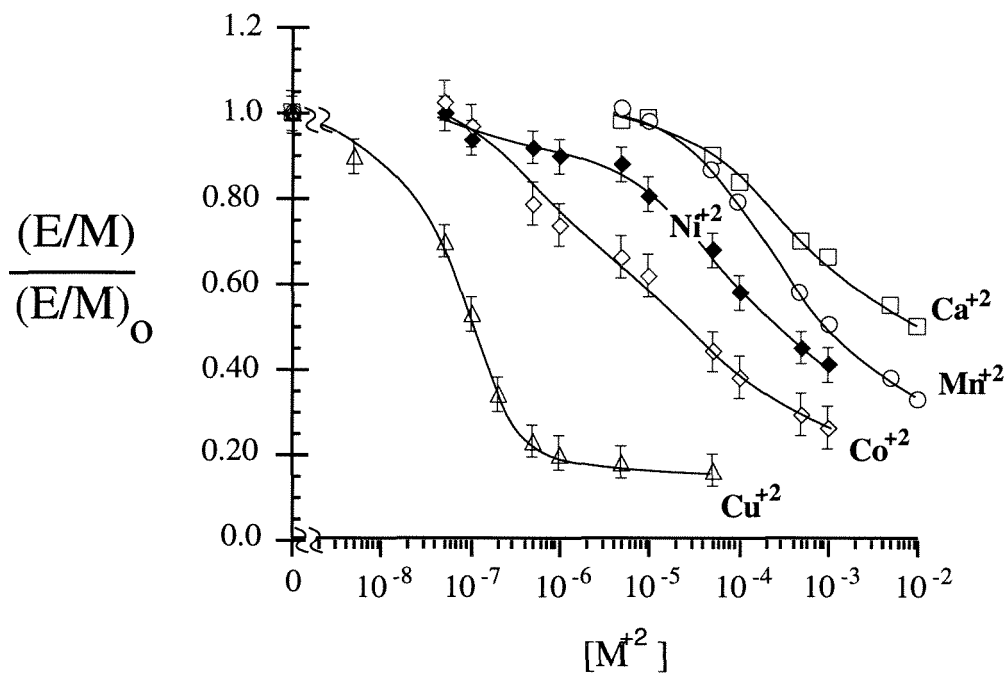
Figure 2.16. Fluorescence E/M values (normalized by E/M without added metal) for 5% PSIDA/ 95% DSPC vesicles at 25 °C, pH 7.5 in MOPS buffer. The metals were added as the chloride salt in 0.1 M NaCl. Curve fits are for the benefit of the reader. The curves approximately follow the order of metal ions for IDA in solution [Cu > Ni > Co > Mn > Ca] determined from ordering of stability constants [38].
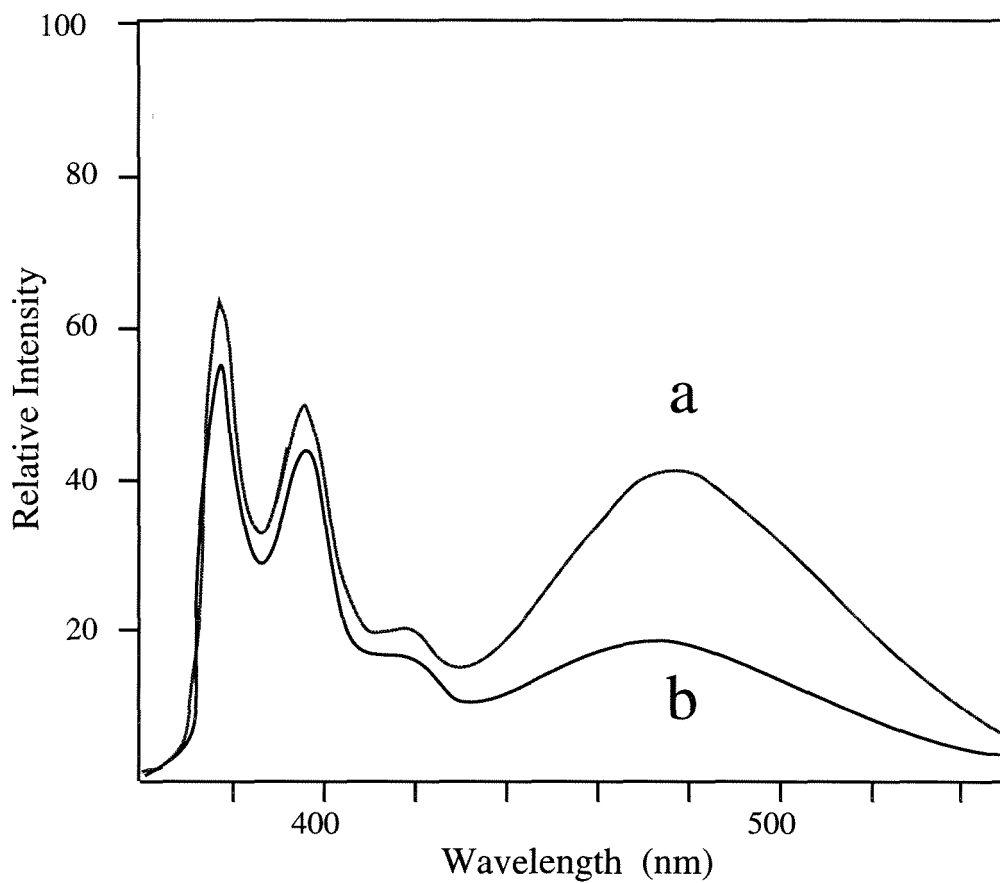
Figure 2.17. Fluorescence emission spectra showing $CuCl_2$ addition to 5% PSIDA/ 95% DPPC vesicles at 25 °C in pH 7.5 MOPS buffer. Curve (a) shows vesicles without metal, curve (b) shows vesicles with 1.5 µM $CuCl_2$.
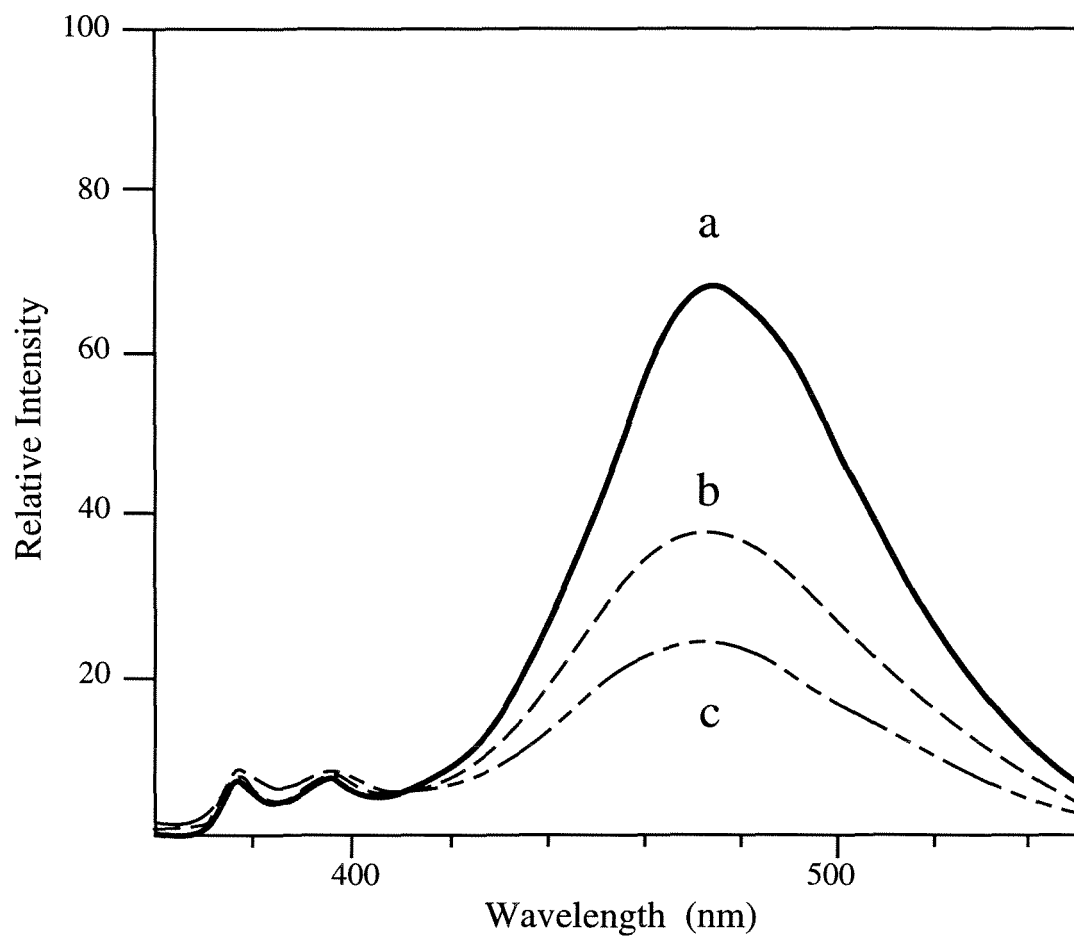
Figure 2.18. Fluorescence emission spectra showing 5% PSIDA/ 95% DSPA small unilamellar vesicles lacking metal (curve a), with 0.8 mM $CuCl_2$ (curve b), and 1.5 mM $CuCl_2$ (curve c) in pH 7.5 MOPS buffer.
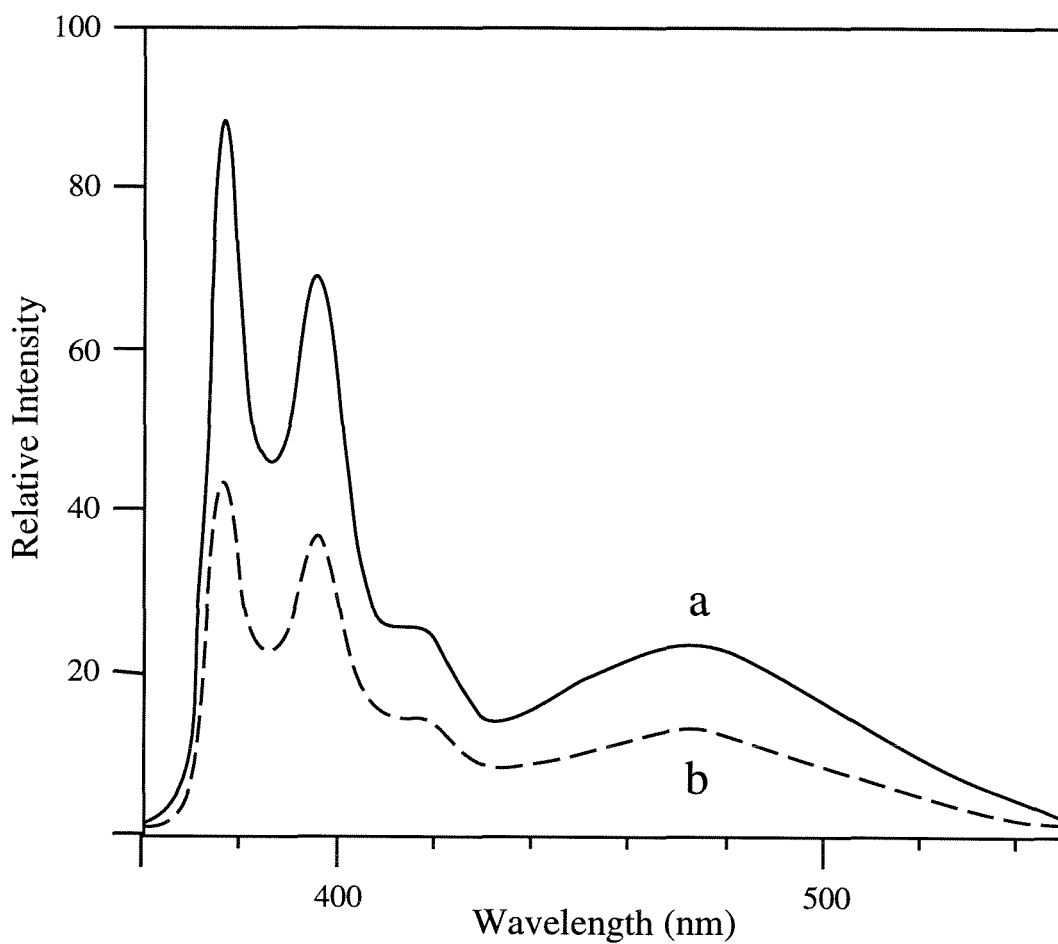
Figure 2.19. Fluorescence emission spectra showing 5% PSIDA/ 95% dimyristoyl phosphatidyl choline (DMPC) vesicles without copper (curve a) and with 0.7 mM $CuCl_2$ added (curve b) in MOPS buffer pH 7.5, at 25°C.
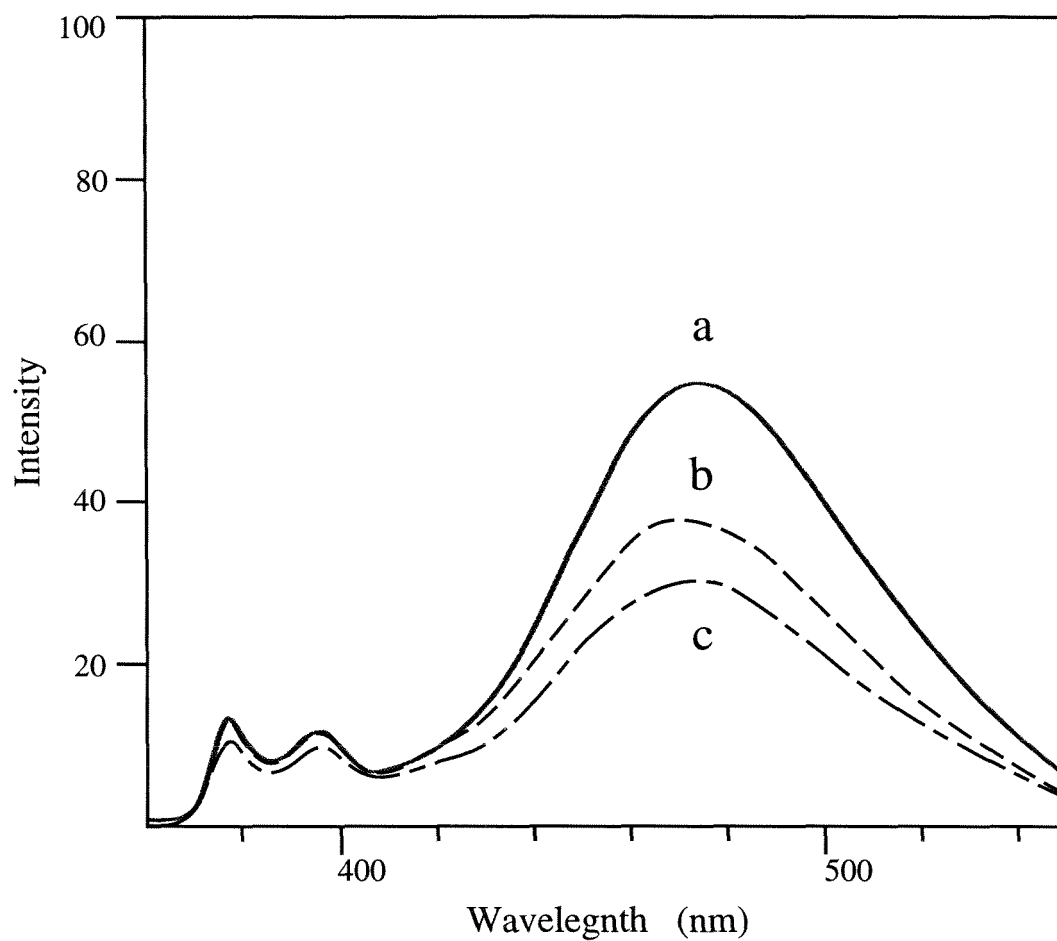
Figure 2.20. Fluorescence emission spectrum showing 5% PSIDA / 95% di-behenoyl phosphatidylcholine (DBPC) small unilamellar vesicles lacking metal (curve a), with 0.7 μM added $CuCl_2$ [in 0.1 M NaCl] (curve b), and 1.4 μM added $CuCl_2$ [in 0.1 M NaCl] (curve c) in MOPS buffer pH 7.5, at 25 °C.
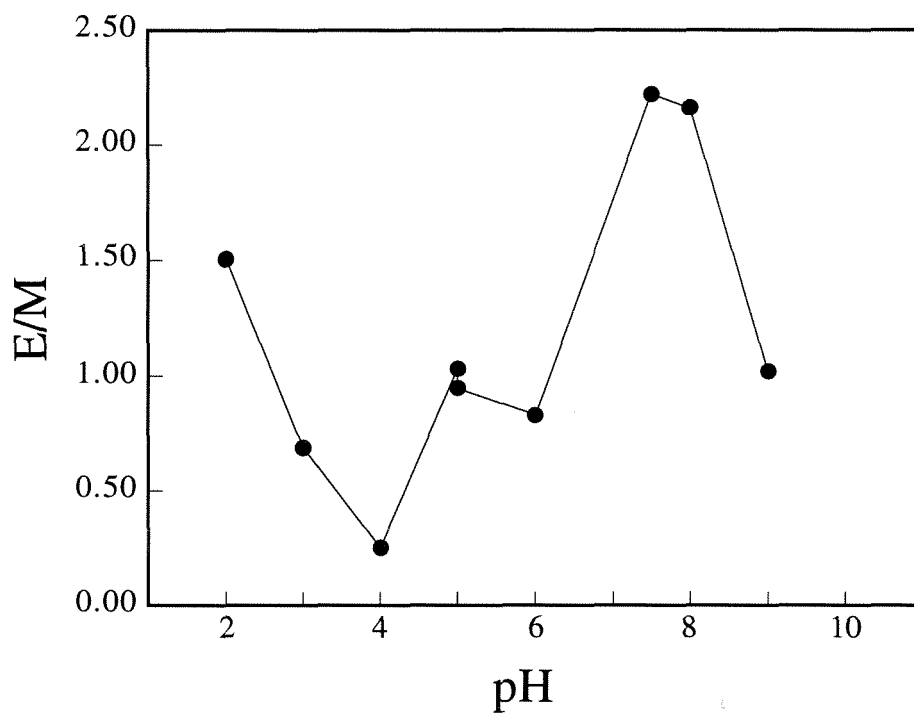
Figure 2.21. Changing pH affects E/M ratio of 5% PSIDA/ 95% DSPC vesicles. Vesicles were diluted 1:200 in buffered 0.1 M NaCl to achieve a desired pH and E/M ratio measured at 25 °C from fluorescence emission spectrum. Vesicle concentration ~7 μM total lipid.
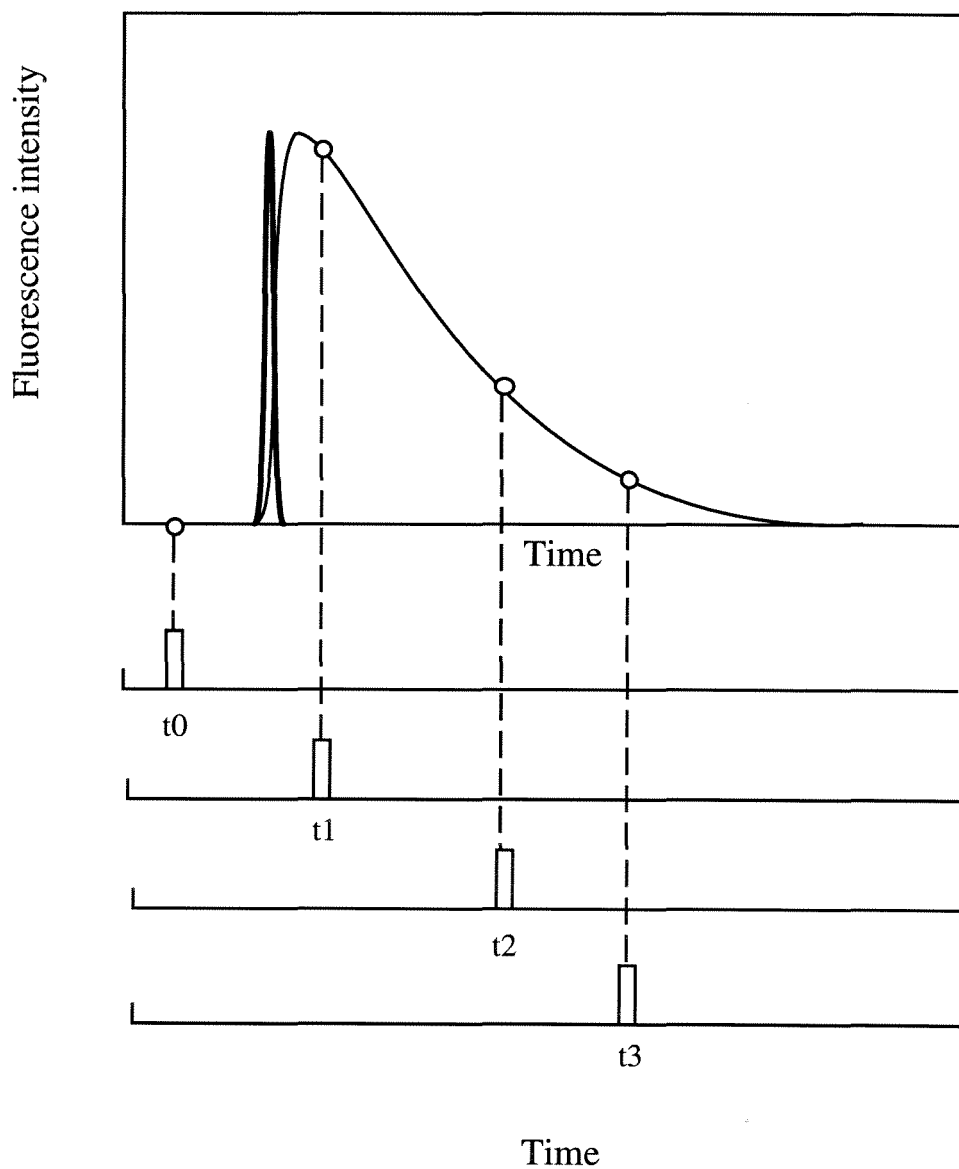
Figure 2.22. Schematic diagram showing pulsed-laser fluorescence decay used to obtain fluorescence lifetime. Initial pulse of laser light at 355 nm is indicated by boldface. At different times after the pulse, the intensity signal is sampled to obtain a decay curve. Decay curve data are fitted to obtain fluorescence lifetime. Reproduced from Lakowicz [44].
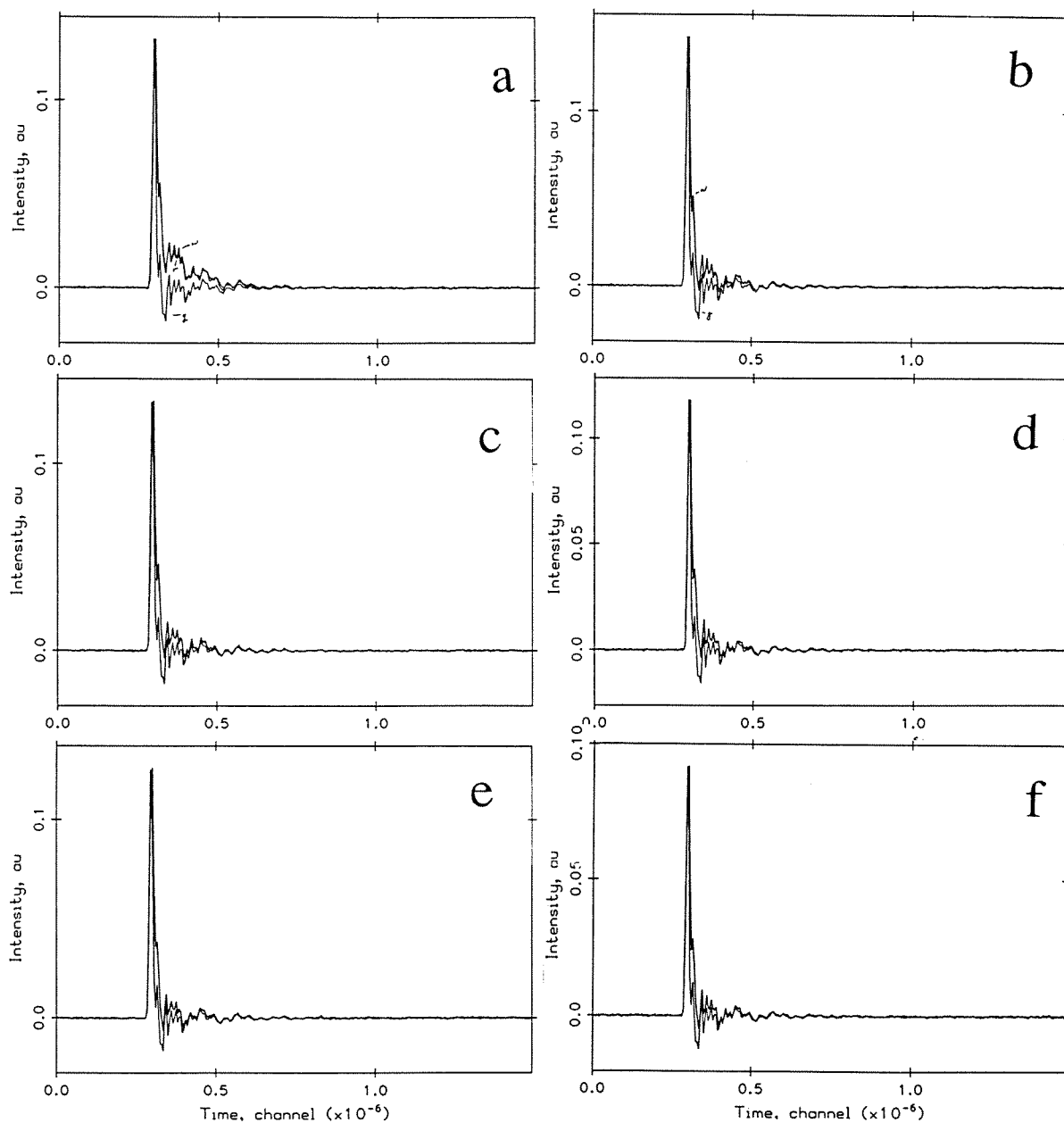
Figure 2.23. Pulsed laser lifetime data at 470 nm obtained with 5% PSIDA/ 95% SOPC vesicles in MOPS buffer, pH 7.5. Sample (a) contains no metal and total lipid concentration of 3.2 μM. $CuCl_2$ is added to vesicles in (b) 19 nM $CuCl_2$, (c) 38 nM $CuCl_2$, (d) 56 nM $CuCl_2$, (e) 75 nM $CuCl_2$, (f) 93 nM $CuCl_2$.
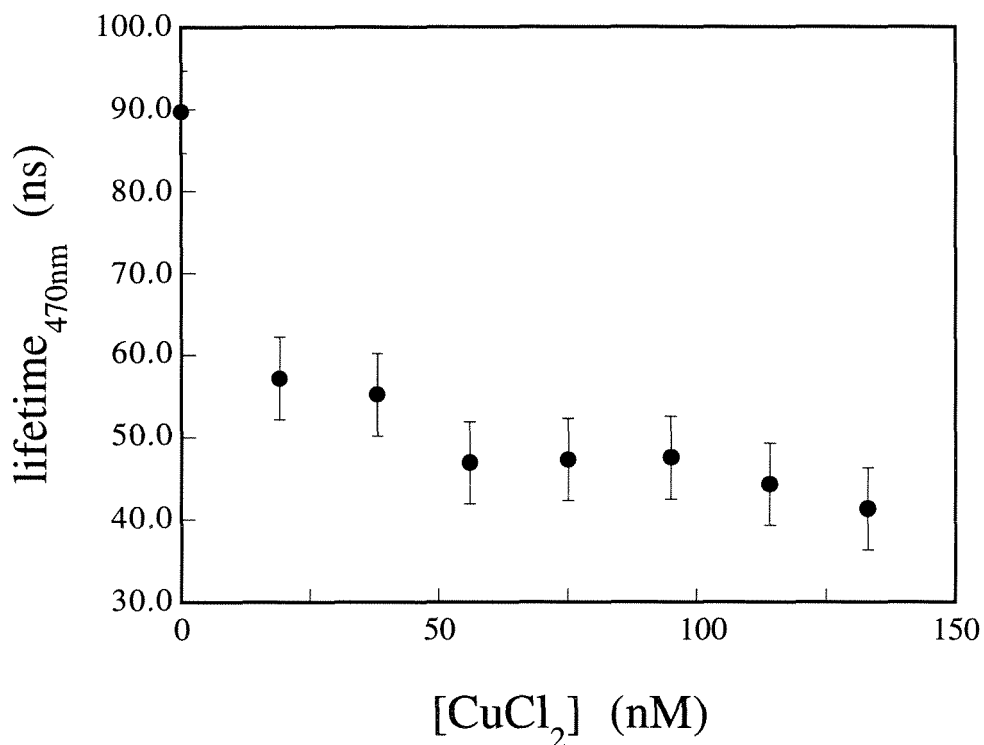
Figure 2.24. Excimer lifetime of 5% PSIDA/ 95% SOPC vesicles (470 nm) is decreased by addition of $CuCl_2$. Data taken using pulsed YAG laser excitation at 355 nm with 385 cutoff filter. Total acquisition time was 1.25 μs with a response time of the system of 5 ns. The estimated concentration of total chelating groups is 0.05(3.3 μM total lipid concentration) = 165 nM.

REFERENCES

1.   Eichmann, K. *Angew. Chem. Int. Ed. Engl.* **1993**, *32*, 54-63.

2.   Zimmerberg, J.; Vogel, S. S.; Chernomordik, L. V. *Annu. Rev. Biophys. Biomol. Struct.* **1993**, *22*, 433-466.

3.   Van Dijck, P. W. M.; Ververgaert, P. H. J. T.; Verkleij, A. J.; Van Deenen, L. L. M.; De Gier, J. *Biochim. Biophys. Acta* **1975**, *406*, 465-478.

4.   Cevc, G. *Biochim. Biophys. Acta* **1991**, 293-307.

5.   Heywood, B. R.; Mann, S. *Chem. Mat.* **1994**, *6*, 311-318.

6.   Cevc, G. *Biochemistry* **1987**, *26*, 6305-6310.

7.   Vanesch, J. H.; Nolte, R. J. M.; Ringsdorf, H.; Wildburg, G. *Langmuir* **1994**, *10*, 1955-1961.

8.   Meldrum, F. C.; Heywood, B. R.; Mann, S. *J. Coll. Interf. Sci.* **1993**, *161*, 66-71.

9.   Groves, J. T.; Fate, G.D.; Lahiri, J. *J. Amer. Chem. Soc.* **1994**, *116*, 5477-5478.

10. Shnek, D. R.; Pack, D.W.; Sasaki, D.Y.; Arnold, F.H. *Langmuir* **1994**, *10*, 2382-2388.

11. Ringsdorf, H.; Schlarb, B.; Venzmer, J. *Angew. Chem. Int. Ed. Engl.* **1988**, *27*, 113-158.

12. Tsuchida, E.; Komatsu, T.; Arai, K.; Nishide, H. *J. Chem. Soc.* **1993**, *9*, 730-732.

13. Budach, W.; Ahuja, R. C.; Mobius, D. *Langmuir* **1993**, *9*, 3093-3100.

14. Budach, W.; Ahuja, R. C.; Mobius, D.; Schrepp, W. *Thin Sol. Films* **1992**, *210*, 434-436.

15. Kunitake, T.; Ishikawa, Y.; Shimoumura, M.; Okawa, H. *J. Am. Chem. Soc.* **1986**, *108*, 327.

16. Ishikawa, Y.; Kunitake, T. *J. Macromol. Sci. Chem.* **1990**, *A27*, 1157-1166.

17. Furhop, J.-H.; Koesling, V.; Schonberger, G. *Liebigs. Ann. Chem.* **1984**, *10*, 1634-1640.

18. Munoz, S.; Mallen, J.; Nakano, A.; Chen, Z. H.; Gay, I.; Echegoyen, L.; Gokel, G. W. *J. Amer. Chem. Soc.* **1993**, *115*, 1705-1711.

19. Yanagi, M.; Tamamura, H.; Kurihara, K.; Kunitake, T. *Langmuir* **1991**, *7*, 167-172.

20. Shimomura, S. and Kunitake, T. *J. Amer. Chem. Soc.* **1982**, *104*, 1757-1759.

21. Galla, H.-J. and Sackmann, E. *Biochim. Biophys. Acta* **1974**, *339*, 103-115.

22. Singh, A.; Tsao- L.-I.; Markowitz, M.; Gaber, B. *Langmuir* **1992**, *8*, 1570-1577.

23. Budach, W.; Ahuja, R. C.; Mobius, D.; Schrepp, W. *Thin Sol. Films* **1992**, *210*, 434-436.

24. Bissell, R. A.; Desilva, A.P.; Gunaratne, H.Q.N.; Lynch, P.L.M.; Maguire, G.E.M.; Mccoy, C.P.; Sandanayake, K.R.A.S. *Topics Current Chemistry* **1993**, *168*, 223-264.

25. Belli, S. L. and Zirino, A. *Anal. Chem.* **1993**, *65*, 2583-2589.

26. Ohki, S. *Biochim. Biophys. Acta* **1982**, 689, 1-10.

27. Ohki, S. *J. Memb. Biol.* **1984**, *77*, 265-275.

28. Eklund, K.K.; Vuorinen, J.; Mikkola, J.; Virtanen, J.A.; Kinnunen, P.K.J. *Biochemistry* **1988**, *27*, 3433-3437.

29. Ito, T. and Ohnishi, S.-I. *Biochim. Biophys. Acta* **1974**, *352*, 29-37.

30. Jacobson, K. and Papahadjopoulos, D. *Biochemistry* **1975**, *14*, 152-161.

31. Welti, R.and Glaser, M. *Chem. Phys. Lipids.* **1994**, *73*, 121-137.

32. Hauser, H. *Chem. Phys. Lipids* **1991**, *57*, 309-325.

33. Huang, C. *Biochemistry* **1969**, *8*, 344-352.

34. *Liposomes: A Practical Approach;* New, R.R.C., Ed.; Oxford University Press: New York, 1990.

35. Microtrac Ultrafine Paricle Analyzer Manual. Leeds & Northrop,

36. Biltonen, R. L. and Lichtenberg, D. *Chem. Phys. Lipids* **1993**, *64*, 129-142.

37. Willson, J. H. M. *Replica, Shadowing and Freeze-etch Technique*; North Holland Pub. Co.: New York, 1980; Vol. 8.

38. Martell, A. E., Smith, P.M. *Critical Stability Constants*; Plenum Press: New York, 1974; Vol. 6.

39. Fabbrizzi, L.; Licchelli, M.; Piersandro, P.; Perotti, A.; Sacchi, D. *Angew. Chem. Int. Ed. Engl.* **1994**, *33*, 1975-1977.

40. Galla, H. J. and Hartmann, W. *Chem. Phys. Lipids.* **1980**, *27*, 199-219.

41. Tocanne, J.-F.; Dupou-Cézanne, L.; Lopez, A. *Prog. Lipid Res.* **1994**, *33*, 203-237.

42. Tocanne, J.-F. and Teissie, J. *Biochim Biophys. Acta* **1990**, 1031, 111-142.

43. Hauser, H. and Philips, M.C. *Prog. Surf. Membr. Sci.* **1979**, *13*, 297-413.

44. Lakowicz, J. R. *Principles of Fluorescence Spectroscopy*; Plenum Press: New York, 1983, pp 1-429.

45. Sturtevant, J. M. *Ann. Rev. Phys. Chem.* **1987**, 38, 463-488.

46. McElhaney, R. M. *Chem. Phys. Lipids* **1982**, *30*, 229-259.

47. Mabrey, S. and Sturtevant, J.M. *Proc. Natl. Acad. Sci U.S.* **1976**, *73*, 3862-3866.

48. Chowdhry, B. Z. and Cole, S.C. *Trends Biot.* **1989**, **1989** 7, 11-18.

49. López-Garcia, F.; Villalan, J.; Gómez-Fernandez, J. C. *Biochim. Biophys. Acta* **1994**, *1190*, 264-272.

50.   Hauser, H. *Chem. Phys. Lipids* **1991**, *57*, 309-325.

51.   Van Dijck, P. W. M.; Ververgaert, P.H.J. Th.; Verkleij, A.J.; Van Deenen, L.L.M.; De Gier, J. *Biochim. Biophys. Acta* **1975**, *406*, 465-478.

52.   Ladbrooke, B.D. and Chapman, D. *Chem. Phys. Lipids* **1969**, *3*, 304-367.

53.   Somerharju, P. J.; Virtanen, J.A.; Eklund, K.K.; Vainio, P.; Kinnunen, P.K.J. *Biochemistry* **1985**, *24*, 2773-2781.

54.   Bangham, A.D. and Horne, R.W. *J. Mol. Biol.* **1964**, *8*, 660-668.

55.   Bangham A.D. *Chem. Phys. Lipids.* **1972**, *8*, 386-392.

56.   Bangham, A.D.; De Gier, J.; Greville, G.D. *Chem. Phys. Lipids.* **1967**, *1*, 225-246.

57.   Ververgaert, P. H. J. T.; Verkleij, A.J.; Elbers, P.F.; Van Deenen, L.L.M. *Biochim. Biophys. Acta* **1973**, *311*, 320-329.

58.   Grant, C. W. M.; Wu, S.H.-W.; McConnell, H.M. *Biochim. Biophys. Acta* **1974**, *363*, 151-158.

59.   Krull, U. J.; Brown, R. S.; Vandenberg, E. T.; Heckl, W. M. *J. Electron Micr. Tech.* **1991**, *18*, 212-222.

60.   Yeagle, P. *The Structure of Biological Membranes*; CRC Press: Boca Raton, 1992; Vol. 1, pp 123.

61.   Verkleij, A. J.; Ververgaert, P.H.-J.; van Deenen, L.L.M; Elbers, P.F. *Biochim. Biophys. Acta* **1972**, *311*, 320-329.

62.   Kleeman, W. and McConnell, H.M. *Biochim. Biophys. Acta* **1974**, *345*, 220-230.

63.   Hresko, R. C.; Sugar, I. P.; Barenholz, Y.; Thompson, T. E. *Biochemistry* **1986**, *25*, 3813-3823.

64.   Lehtonen, J. Y. A. and Kinnunen, P.K.J. *Biophys. J.* **1995**, *68*, 525-535.

64. Lehtonen, J. Y. A. and Kinnunen, P.K.J. *Biophys. J.* **1995**, *68*, 525-535.

65. Birch, D. J. S.; Suhling, K.; Holmes, A.S.; Salthammer, T.; Imhof, R.E. *Pure & Appl. Chem .***1993**, *65*, 1687-1692.

66. Ng, K.; Pack, D.W.; Sasaki, D.Y.; Arnold, F.H. (submitted for publication to *Langmuir*)

67. Hinz, H.-J. and Sturtevant, J.M. *J. Biol. Chem.* **1972**, 247, 6071-6075.

68. *personal communication*, Winkler, J., California Institute of Technology.

69. Marsh, D. *Handbook of Lipid Bilayers*; CRC Press: Boca Raton, 1990, pp 149.

Chapter 3. Binding of proteins to metal-chelating, mixed-lipid vesicles

INTRODUCTION

Specific targeting of proteins to interfaces is important for applications in biomedicine, structure determination, sensors and devices, synthesis of materials with defined, highly-ordered molecular architectures, as well as for model studies of protein interactions in biological membranes. The organization of proteins on artificial lipid membranes can be mediated by interactions with specific lipid-bound receptors or affinity ligands, a widely cited example of which is the orientation and two-dimensional crystallization of streptavidin on biotin-functionalized membranes [1]. Although the biotin-streptavidin system exhibits very strong and specific binding, the range of proteins that can be bound to the membrane surface and the types of molecular architectures produced are limited. Other affinity ligands that have been used to target proteins to model membranes and surfactant assemblies include haptens for antibodies [2,3,4,5], antibodies for specific proteins [6,7], inhibitors/effectors for enzymes [8], and the heme prosthetic group for apomyoglobin [9]. Unfortunately, no convenient natural affinity ligands have been identified for many proteins with interesting biological, optical, electrical or catalytic properties. A versatile, generally-applicable affinity system for targeting and orienting functional proteins at membranes would be extremely useful.

We are also interested in the template-directed patterning of metal ions in lipid assemblies. Using the technique of template polymerization, or 'molecular imprinting', we have prepared macroporous polymers capable of recognizing bis-imidazole "protein analogs" [10,11]. These polymers were synthesized using the desired target compound as a template to position metal-containing monomers such that they complement the template's metal-coordinating groups. The goal is to create a binding cavity in the final material with a specific arrangement of metal ions that matches the template. We are currently extending this template polymerization concept to mixed lipid assemblies in order to prepare metal-chelating lipid monolayers and bilayers patterned at the nanometer scale [12]. The metal coordination interaction should be sufficiently strong to direct the placement of metal-

chelating lipids in monolayer or bilayer assemblies; this pattern could be 'fixed' by polymerization and cross-linking of the lipid tails.

The imidazole moieties of histidyl residues on the surfaces of proteins readily coordinate to divalent transition metal ions such as Cu^{2+}, Ni^{2+} and Zn^{2+} [13]. When immobilized onto solid supports via appropriate chelating agents, metal ions can serve as affinity ligands for protein purification by metal-affinity chromatography [14,15] and for protein immobilization [16]. The chelating group should bind the metal ion tightly yet leave coordination site(s) available for formation of a complex with the protein. A tri-dentate chelator widely used in metal-affinity chromatography, iminodiacetate (IDA), binds Cu^{2+} with an association constant of 10^{11} M^{-1} [17]. The Cu^{2+}-IDA complex in turn binds imidazole with moderate affinity ($K \sim 10^{3.5}$ M^{-1}) in solution [18] and at the surface of a chromatographic support [19]. While proteins with a single accessible histidine bind with similar affinities to surfaces densely derivatized with Cu^{2+}-IDA, those with multiple surface histidines can adsorb much more strongly by forming multiple, simultaneous histidyl-Cu^{2+} coordination bonds. Studies with engineered protein variants containing as few as two surface-accessible histidines have shown that multipoint attachment results in apparent protein binding constants greater than 10^6 M^{-1} [19]. Alternatively, proteins can be engineered to display high-affinity surface metal-binding sites [20,21] or metal-binding peptides at their N- or C-termini [22], either of which can be used for specific protein immobilization on metal-derivatized surfaces [20]. The metal-protein interaction is reversible under mild conditions: competitors such as imidazole, small quantities of acid, or strong chelating agents all effectively disrupt the protein-Cu^{2+}-IDA complex, releasing the bound protein [14].

Chelating amphiphiles have been prepared for studies of metal ion binding to monolayers and artificial bilayer membranes. Porphyrins [23], dithiocarbamate [24,25], cyclam [26,27], iminodiacetate [28], imidazole [29] crown ethers [30], and non-cyclic crown analogs [31] have been incorporated into the polar headgroup regions of these

materials to study the ion-binding properties and the anisotropic organization of metal-chelates in monolayers and bilayers [26], to make metal ion sensors [24], and to control the orientation and packing of membrane components [31]. For the purpose of targeting proteins to monolayer and bilayer assemblies we have synthesized a lipid with an IDA moiety in the headgroup. When loaded with Cu^{2+}, small quantities of this IDA-lipid in small unilamellar vesicles of di-stearoyl phosphatidylcholine (DSPC) effectively bind a small, histidine-rich protein, myoglobin.

Horse heart myoglobin (M_r = 17,641) contains eleven histidines, at least four of which can coordinate to Cu^{2+}IDA [32]. We report herein on myoglobin binding to vesicles of DSPC and an IDA-lipid (Figure 3.1) containing Cu^{2+} and Ca^{2+}. Because imidazole is not a good ligand for Ca^{2+} (K_a = 1.2 M^{-1}) [33], this divalent ion provides a non-coordinating surface for comparison. Measurements of protein binding to vesicles loaded with Cu^{2+}, Ca^{2+} and lacking metal was investigated to determine the extent of protein binding.

The specificity of metal coordination on lipid bilayers was investigated by electron spin resonance (ESR) spectroscopy. Cu^{2+} contains an unpaired electron spin when coordinated to ligands. Ligand exchange of electron-rich, nitrogen ligands for oxygen ligands often changes the ESR spectral parameters of Cu^{2+} [34]. Model compound studies of Cu^{2+}IDA and imidazole show that imidazole coordination affects the spectral parameters $g_{\parallel}$ and $A_{\parallel}$. Features in the superhyperfine region of the ESR spectrum indicate the identity of the ligand in certain cases [35]. Superhyperfine features from imidazole ligands were observed in the ESR spectra for model-complex studies of Cu^{2+}IDA. ESR analyses of Cu^{2+}-containing vesicles in the presence of unmodified and diethylpyrocarbonate (DEPC)-modified protein indicate that myoglobin binding to these artificial membrane assemblies is significantly enhanced by coordination of surface histidines to Cu^{2+} ions immobilized at the membrane surface.

93

RESULTS

Characterization of vesicles

Metal-chelating and non-coordinating lipids used to form small unilamellar vesicles are shown in Figure 3.1. Metal-chelating small unilamellar vesicles (SUVs) (mean size 35-48 nm, distribution width 15-30 nm) were made from DSPC and cholesterol incorporating a small amount of the chelating lipid DSIDA [2 mol % DSIDA, 48 mol % DSPC and 50 mol % cholesterol]. Cholesterol was incorporated to prevent metal-induced aggregation. In vesicles composed of negatively-charged lipids, cholesterol greatly decreases metal-induced aggregation [36]. Assuming cholesterol is buried in the hydrophobic region of the bilayer [37], the chelating IDA function represents 4 % of the accessible headgroups at the membrane surface.

The vesicles were metallated with the appropriate metal chloride, followed by dialysis to remove free metal (for Cu^{2+}). DSIDA/DSPC vesicles upon metallation form aggregates that cannot be dispersed by dialysis (data not shown). Quasi-elastic light scattering (QELS) measurements showed that the mean vesicle size was not altered by metallation if cholesterol was present (**Table 2.1**). Since some lipid is lost during filtration to remove titanium particles after sonication, the vesicle samples were analyzed for total phosphate to establish lipid concentration [38]. The average phosphate concentrations were 2.82 ± 0.25 mM for vesicles without metal and 2.49 ± 0.18 mM for the metallated vesicles after dialysis. Cu^{2+} concentrations measured for selected batches of vesicles by ICP-MS were found to be 105 ± 5 μM. This value agrees well with the expected metal concentration calculated from the phosphate concentration and the known composition of chelating lipid DSIDA. Therefore, the vesicles can be assumed to be fully loaded with Cu^{2+} under the experimental conditions.

Protein binding experiments

A model protein, horse heart myoglobin, was added to metal-chelating mixed vesicles loaded with Ca^{2+} and Cu^{2+}. Horse heart myoglobin contains at least 4 accessible histidines [39] with the accessible surface area shown in Table 3.1, calculated using Insight II. The unbound protein was separated from the vesicle-bound protein by analytical ultracentrifugation at 200,000g. Figure 3.2 shows a photograph of vesicle-protein mixtures after ultracentrifugation containing either Ca^{2+} or Cu^{2+}-loaded vesicles with identical total protein. The concentrations of the metal ions added to saturate the chelating-lipids; $[Cu^{2+}] = 105$ µM, $[Ca^{2+}] = 1$ mM, was different because the affinities of iminodiacetate for the two metals is very different (10^{11} vs. $10^{4.1}$ M^{-1}, respectively) [17]. The pellet at the bottom of the centrifuge tube (Tube A) is darker for Cu^{2+}-loaded vesicles, indicating increased protein binding compared to the Ca^{2+}-loaded vesicles (Tube B).

In Figure 3.3, the binding of horse myoglobin (normalized by the total phospholipid content of the sample) to copper-containing vesicles is compared to vesicles with no bound metal and ones that contain Ca^{2+}. Nonspecific binding of myoglobin to pure DSPC vesicles is similar to the unmetallated DSPC/DSIDA vesicles. Although myoglobin has been reported to exhibit negligible adsorption to zwitterionic phosphatidylcholine vesicles [40] and monolayers [9,41] at neutral pH, we do observe nonspecific binding to DSPC vesicles and to the mixed DSPC/DSIDA vesicles that is not altered by the presence of Ca^{2+}. Monolayer studies with pure and mixed DSIDA lipids also indicate that myoglobin interacts nonspecifically with pure and mixed DSIDA, even in the presence of Ca^{2+} [42].

Apparent association constants for myoglobin binding to the metallated and unmetallated vesicles were obtained by fitting the data in Figure 3.3 to a Langmuir isotherm. Myoglobin binding to the copper-containing vesicles is so strong that only a lower limit on the association constant could be obtained from these measurements: $K_a > 2.9 \times 10^6$ M^{-1}. The association is weaker by at least a factor of ten for binding to vesicles

without copper: $K_a = 2.5 \pm 1.5 \times 10^5$ M^{-1}. The Cu^{2+}-vesicles exhibit a maximum loading of 0.0075 moles of protein per mole phospholipid (0.18 mol protein / mol DSIDA), while the unmetallated vesicles and those loaded with Ca^{2+} bind less than half that.

ESR experiments

ESR data were acquired using frozen (77 °K) aqueous samples containing Cu^{2+}IDA and also with dialyzed Cu^{2+}-loaded, metal-chelating vesicles. The spectral parameters were determined for comparison of mixtures containing model complexes of Cu^{2+}IDA and imidazole, to metal-loaded vesicles [2.5% DSIDA-Cu, 47.5% DSPC, and 50% cholesterol] and horse myoglobin. Table 3.2 shows the spectral parameters obtained for mixtures of Cu^{2+}IDA and imidazole using the equation for resonance of an electron spin in an applied magnetic field [43].

$$g\beta H = h\nu_{el}$$

The component of electron magnetic moment parallel to the magnetic field, $g_{\parallel}$, is expected to be an average of the $g_{\parallel}$ values for each electronically different copper species in solution. The value of $g_{\parallel}$ is very sensitive to the exchange of imidazole for water in the ligand field of Cu^{2+}IDA (Table 3.2). Figure 3.4 shows the change in each spectrum as the ratio of imidazole to copper is increased. The number of super-hyperfine lines can be discerned in the region 3100-3300 Gauss for Cu^{2+}IDA-Im-H$_2$O complexes. The increase in the number of super-hyperfine lines can be interpreted as increasing the number of nitrogen ligands and shows the increased splitting the spin of the electron by the nuclear spin of nitrogen ligands. Table 3.3 shows the calculated equilibrium concentrations of the expected imidazole-Cu^{2+}IDA complexes determined from potentiometric titration data (Table 3.4). The concentrations of these species was used to interpret the $g_{\parallel}$ values. Thus, the presence of imidazole in the ligand field of copper can be detected through ESR spectroscopy by a decrease in $g_{\parallel}$.

Protein was blocked with diethylpyrocarbonate (DEPC) to provide a control for non-specific effects on the ESR spectrum due to the presence of the heme and also to show $g_\parallel$ parameters are not affected by chemically-blocked myoglobin histidines. DEPC -blocked histidines are not expected to coordinate to chelated Cu^{2+} because the nitrogen lone pair is chemically bound to DEPC. Horse heart myoglobin contains at least four surface-accessible histidines which we wished to block with DEPC [44]. The UV absorption at 240 nm and 410 nm was measured and the concentration ratio of blocked histidines determined using published molar extinction coefficients after chemical modification [45]. By calculating the concentration ratio measured from spectrophotometry using the published extinction coefficients, the measured ratio was found to be five. If the ratio of blocked histidines was larger than five, protein precipitate was observed. The precipitate is most likely unfolded protein since the heme moiety is held in place non-covalently by coordination to histidine residues [46]. Presumably when more than five surface histidines are chemically blocked, the heme is no longer coordinated in the binding pocket, and the protein unfolds to form a precipitate. Thus, the five blocked histidines were assumed to be the surface-accessible histidines.

Figure 3.5 shows the ESR spectra (77 °K) of 2.5% DSIDA-Cu^{2+} /47.5% DSPC/ 50% cholesterol vesicles with histidine-blocked and native protein. The vesicles were loaded with Cu^{2+} and dialyzed against buffer to remove free metal, which might complicate the spectrum. Arrows show the field position used to calculate the spectral parameters shown in Table 3.5. The first ESR spectrum of vesicles lacking protein (Figure 3.5, A) is slightly broadened compared to the model chelate, Cu^{2+}IDA, showing features in the superhyperfine region. ESR measurements with DEPC-blocked protein mixed with copper-loaded vesicles (Figure 3.5, B) show that adding 2-fold excess of histidine-blocked protein did not affect the value of $g_\parallel$, although the hyperfine coupling constant ($A_\parallel$) did change (Table 3.5). The addition of native protein to 2.5% DSIDA-Cu^{2+}/ 47.5% DSPC/ 50% cholesterol vesicles (Figure 3.5, C) caused a shift in the $g_\parallel$ value similar to the model

complexes (Table 3.2). A separate ESR measurement of frozen protein showed that the Fe^{3+} ESR signal of the heme did not overlap significantly with the Cu^{2+} spectrum at 77 °K.

DISCUSSION

Protein binding experiments

Protein binding was investigated by measuring vesicle-bound protein and free protein for vesicles loaded with Ca^{2+}, Cu^{2+} and no metal. The data were fitted with a Langmuir isotherm to determine the apparent association constant. The affinity for myoglobin was increased at least an order of magnitude when the vesicles were loaded with copper compared to vesicles loaded with calcium. Assuming that the phosphatidylcholine lipid headgroups occupy 70 $Å^2$/molecule at the vesicle surface [47], the average surface area of a Cu^{2+}-chelating vesicle per myoglobin molecule at maximum loading is estimated to be ~ 70/0.0075 = 9300 $Å^2$, an area significantly larger than the largest dimensions of the globular protein (44 x 44 x 25 Å) [27]. The maximum protein loading therefore corresponds to less than monolayer coverage, assuming that myoglobin does not undergo a significant conformational change upon interaction with the vesicles.

When loaded with Cu^{2+}, the 19:1 DSPC:DSIDA vesicles interact strongly with myoglobin. Adding copper greatly enhances both the amount of myoglobin targeted to the interface and the strength of binding. The myoglobin loading observed for these vesicles corresponds to roughly five DSIDA-Cu^{2+} per protein molecule, which equals the maximum number of surface-accessible histidines. It is possible that all the DSIDA-Cu^{2+} is bound to surface histidines, which could result from myoglobin-induced cross-linking and aggregation of the vesicles upon standing or during sedimentation. Histidine-rich proteins such as horse heart myoglobin can act as affinity crosslinkers of the vesicles since they are able to link two vesicles together. Precipitation of copper-loaded vesicles is in fact induced by myoglobin. Vesicles lacking copper remain suspended over the same time periods in the presence of the protein. Similar effects have been reported for biotin-containing SUV's

and streptavidin, a protein with four biotin binding sites [48]. Other affinity-functionalized vesicles have been investigated as affinity precipitant systems and shown to effectively precipitate proteins with multiple binding sites for the affinity ligand [49,50].

Myoglobin, with five binding sites, is readily precipitated by Cu^{2+}-IDA-derivatized polyethylene glycols; the resulting precipitate contains a stoichiometric amount of metal to surface-accessible histidines, indicating that histidine-to-copper coordination is the dominant cross-linking interaction [51]. Precipitation is minimized when proteins with engineered high-affinity metal-chelating sites are used or by blocking 'excess' histidines after adsorption to the vesicles.

Recently, HIV protease, containing a hexa-histidine peptide, was crystallized using this strategy at Ni^{2+}-chelating lipid monolayer interfaces [52]. Binding of the engineered protein was investigated using a phospholipid-based chelating nitrilo-triacetate lipid loaded with Ni^{2+}. Use of polyhistidine "tag" provided specific targeting as well as specific orientation, shown through formation of two-dimensional crystals. Precipitation in a vesicle-based system would be prevented by using a "tagged" protein, since the peptide "tail" would be sterically prevented from coordinating to two vesicles simultaneously.

Specificity of protein binding characterized through ESR

ESR studies of model Cu^{2+}IDA-imidazole complexes and protein binding to Cu^{2+}-loaded chelating-vesicles were used to determine if the surface histidine residues were coordinating to vesicle-chelated copper. Exchange in the ligand field of a transition metal ion affects the unpaired spin of the transition metal ion through coupling of the electron spin angular momentum and orbital angular momentum to the spin angular momentum of the ligand nuclei [53]. Chemical exchange of ligands is often reflected in changes in the spectral parameters obtained from ESR measurements. Theoretically, the identity of the ligand can be determined from the nuclear super-hyperfine coupling in ESR spectroscopy, although for most applications the super-hyperfine region is too broadened to determine the

number of ligands [54]. Ligand nuclei splitting is reflected in the number of lines observed in the super-hyperfine region (3100-3300 Gauss for $Cu^{2+}IDA$), a result of the spin pairing of the ligand nucleus and the electron spin interacting in the ligand field. If the nuclear spin of a ligand interacts with the electron spin, then the number of superhyperfine lines is equal to $2S+1$ where S is the spin of the nucleus [55,43]. If the nuclear super-hyperfine region can be distinguished in an experimental ESR spectrum, then the identity of a ligand can be determined directly. Superhyperfine features observed for $Cu^{2+}IDA$ should be due to the nuclear spin of ^{14}N from the deprotonated imidazole lone pairs. We hoped to determine the number of ligands involved in protein binding to copper chelated to the membrane surface from the ESR spectrum. For model $Cu^{2+}IDA$ complexes, the number of superhyperfine lines was not counted because multiple $Cu^{2+}IDA\cdot Imid$ species were contributing to each spectra.

The effect of chemical exchange was also determined by measuring the ESR spectral parameters $g_{\parallel}$, $g_{\perp}$ and $A_{\parallel}$. ESR spectral parameters, g and A, are similar to chemical shift and coupling constant, respectively, encountered in NMR measurements [55]. For Cu^{2+} ions chelated on mixed vesicles or in model complexes, ligand exchange typically affects $g_{\parallel}$ and $A_{\parallel}$ more strongly than the other parameters (Table 3.2). This corresponds with previous results with mixed oxygen-nitrogen-copper model complexes where the presence of electron-rich nitrogen ligands, such as imidazole, can be detected from their effects on $g_{\parallel}$ and $A_{\parallel}$, the nuclear hyperfine splitting from the ^{63}Cu nucleus [34].

A model system composed of $Cu^{2+}IDA$ and imidazole was investigated by ESR spectroscopy to investigate the changes in the spectral parameters due to imidazole displacement of water. From X-ray crystal structures, $Cu^{2+}IDA$ has three sites/positions available for ligand coordination, two of which are coordinated to imidazole [56]. In a buffered solution lacking nitrogen ligands, coordination sites are occupied by water or hydroxide ions, depending on the pH of the mixture. Free copper in water $[Cu(H_2O)_6]^{2+}$ at pH 7.0 has a $g_{\parallel}$ value of 2.400 and an $A_{\parallel}$ value of 0.06 cm^{-1} [54]. We can conclude that

there is not much free copper present since the metallated vesicles have significantly different spectral parameters ($g_\parallel$= 2.284) than for the $[Cu(H_2O)_6]^{2+}$ species. Thus, dialysis of the vesicles effectively removes the unbound metal which would make the $g_\parallel$ value closer to 2.400.

Previously determined stability constants between $Cu^{2+}IDA$ and imidazole (Table 3.4) show that exchange of a water for a nitrogen-rich ligand is favored energetically (ΔG_{bind} = 5.0 kcal/mole) at pH 7.5 [18]. The spectral parameters obtained with model compounds imidazole and $Cu^{2+}IDA$ (Table 3.2) were interpreted in terms of the species predicted by the stability constants obtained from potentiometry. The concentration normalized by total added metal of the mono-imidazole and bis-imidazole species were compared to the changes in $g_\parallel$ and $A_\parallel$. Table 3.3 can be compared to Table 3.2 to show that a decreasing $g_\parallel$ value indicates the ligand-exchange of imidazole for water in the first solvent shell of $Cu^{2+}IDA$. The decrease in $g_\parallel$ upon adding imidazole to $Cu^{2+}IDA$ is consistent with previous measurements showing a decrease in $g_\parallel$ upon imidazole coordination to Cu^{2+} [56,57,58]. Changes in $g_\parallel$ are also consistent with previous ESR measurements made for $Cu^{2+}IDA$-styrene and benzylimidazole compounds in methanol [11]. New features in the superhyperfine regions are present as the imidazole to copper ratio is increased, providing strong support for imidazole coordination to $Cu^{2+}IDA$.

The ESR experiment was repeated using horse myoglobin that had been chemically modified with diethylpyrocarbonate (DEPC) to block the surface-accessible histidines. Myoglobin and hemoglobin have been shown to bind free copper through histidines present on their surfaces [34]. The protein was found to be modified with DEPC at five histidines using spectrophotometric characterization [45]. The vesicle ESR spectrum in the presence of excess DEPC-myoglobin is very similar to that of the vesicles without any protein. For example, the $g_\parallel$ values of vesicles with added blocked protein and those lacking protein are almost identical. The presence of the paramagnetic heme in myoglobin may have affected the $A_\parallel$ values, however (Table 3.5). The value of $g_\parallel$ decreased in the

presence of native protein as it did for Cu^{2+}IDA complexes interacting with imidazole. It is reasonable to conclude that the changes in the spectral line positions of the vesicle-bound Cu^{2+} in the presence of unmodified myoglobin are due to histidine coordination (Table 3.5). No clear ligand superhyperfine features were distinguishable in the protein-vesicles ESR spectra (Figure 3.5), possibly due to the anisotropic environment of Cu^{2+} on the vesicle surface or chelated Cu^{2+}-Cu^{2+} interactions.

CONCLUSIONS

A new chelating affinity lipid, DSIDA-Cu^{2+}, was found to bind a histidine-rich protein, horse myoglobin, when formed into mixed vesicles. Proteins bound specifically to chelated Cu^{2+} on the membranes through their surface histidines. Metal ion coordination is a promising strategy for targeting proteins to artificial membranes, monolayers at a gas-water interface, and molecular assemblies deposited or self-assembled on solid substrates. Small, stable, inexpensive metal-chelate affinity ligands can be incorporated into membrane components by a variety of chemical routes. The strength and kinetics of the interactions with proteins or other biological materials can be tailored through the choice of the metal ion and the chelating ligand [12]. A wide range of natural proteins can be targeted in this way, while more specific protein targeting and orientation at the interface could be achieved by engineering specific metal-binding site(s) into the protein surface.

EXPERIMENTAL

Materials

Phospholipids were obtained from Avanti Polar Lipids (>99% purity). DSIDA was synthesized by Dr. Darryl Sasaki according to the published procedure [42]. Cholesterol was obtained from Sigma. All other chemicals were of the highest purity available.

Preparation of vesicles

Lipids were dissolved in chloroform (48 mol % DSPC, 50 mol % cholesterol and 2 mol% lipid DSIDA). 12 ml glass centrifuge tubes were coated with 10 μmoles total lipid under a stream of argon gas. The coated tubes were dried for 12 hr under vacuum and hydrated with 3 ml of 20 mM MOPS, 100 mM NaCl, pH 7.5 buffer. The vesicles were vortexed at 50 °C and then probe tip sonicated (Heat Systems model 375) at 4 °C for 15 min. at 15-25% power output. Titanium fragments were removed by filtration on a 0.2 μm syringe filter. A two-fold molar excess of $CuCl_2$ [stock solution 5 mM $CuCl_2$ in 100 mM NaCl] was added, and excess copper was removed by dialysis against MOPS buffer (12 ml vesicles/1 L) using tubing with a MW cutoff of 3500. Cu^{2+} concentrations were determined by inductively-coupled plasma mass spectrometry (ICP-MS) on a Perkin Elmer Elan 5000 ICP-MS using copper standards in 1% HNO_3 (Sigma). 0.2 ml of vesicles were hydrolyzed in 0.4 ml of perchloric acid at 190 °C in heating blocks to make homogenous solutions prior to ICP-MS. The resulting hydrolyzate was diluted with ddH_2O to 2 ml in volumetric tubes. Liposome samples were prepared daily and used within 48 h, since precipitation of copper-containing vesicles was observed beyond this time. Liposome sizes were measured by quasi-elastic laser light scattering (QELS) using a Microtrac Ultrafine Particle Analyzer (Leeds & Northrop) at 25 C, in MOPS buffer in Chapter 2 (Table 1).

Protein binding to vesicles

Horse myoglobin was dissolved (0.1-0.3 mM) in MOPS buffer with stirring and filtered on 0.2 μm syringe filters. 1 ml of prepared vesicle solution was added to a 5 ml volumetric flask, and varying amounts of concentrated protein solution and MOPS buffer were added to achieve final protein concentrations of 4-40 μM. After equilibration for 1 hour, the samples were ultracentrifuged at 45,000 rpm (200,000 g) for 4 hr at 25°C. Phosphate analysis [38] of a vesicle sample before and after centrifugation showed that 95% of the vesicles were sedimented. The vesicle pellets could not be fully re-suspended by mechanical dispersion. Bound protein was determined from a mass balance on the total protein added to the sample minus the free protein remaining after sedimentation. The supernatant was decanted without disturbing the vesicle pellet and the protein concentration determined spectrophotometrically at 409 nm using the extinction coefficient of 160 mM^{-1} cm^{-1}[59]. The total protein added was determined from identically treated protein samples containing no vesicles. For the binding studies involving Ca^{2+}-vesicles, a concentrated solution of CaCl$_2$ (93 mM CaCl$_2$, 100 mM NaCl) was added to the vesicle-protein mixture to achieve a final Ca^{2+} concentration of 1 mM.

DEPC modification of horse myoglobin

Horse heart myoglobin was chemically modified with DEPC according to a published procedure [45] to block histidine nitrogens. Myoglobin was dissolved in 100 ml buffer [10 mM phosphate, 0.1 mM EDTA, pH 6.0] to 20 μM concentration. DEPC was added [0.12 M in anhydrous. EtOH] in 6.0 molar ratio to surface histidines (assuming 5 accessible histidines per protein), and the reaction was allowed to proceed for 1 hr with stirring. Histidine modification was quantified spectrophotometrically at 240 nm, using an extinction coefficient of 3.2 mM^{-1} cm^{-1} [45]. The reaction mixture was concentrated at 4 °C by ultrafiltration with a 10,000 MW cutoff filter. 150 ml MOPS buffer [20 mM MOPS, 100 mM NaCl, pH 7.5] was added and the sample was concentrated again at 4 °C. The

samples were kept refrigerated until used. The modified protein could not be separated from protein fractions containing less than five blocked surface histidines on an IMAC column (Pharmacia Sepharose IMAC gel) since the presence of copper causes removal of the DEPC label. The protein solution was mixed quickly with metallated vesicles prior to ESR and frozen immediately in liquid N_2 to prevent copper-induced deprotection.

ESR experiments

Electron spin resonance (ESR) experiments were performed on a X-band Bruker ESP 300 spectrometer operating at 9.2 GHz. A Hewlett Packard 5342A microwave frequency counter was used to measure the microwave frequency. Spectral line positions were measured with a homemade proton gaussmeter. Spectra were recorded with the following parameters: scan range, 1000 G; time constant, 0.16 sec; scan time, 480 sec; modulation amplitude, 6.3 G; microwave power, 4.9 mW; modulation frequency, 100 kHz; temperature, 77 ° K. Each spectrum was scan averaged three times.

Imidazole was dissolved in buffer [20 mM MOPS, 100 mM NaCl, pH 7.5] to make a concentrated (~100 mM) stock solution. $CuCl_2$ (> 99% purity, both isotopes) and iminodiacetic acid were weighed out and combined to make a 1.032 mM stock solution in a volumetric flask using MOPS buffer. Imidazole was added to 0.5 ml of Cu^{2+}IDA solution to achieve a total molar ratio of imidazole to Cu^{2+}. 0.5 ml of the solution was placed in an ESR tube (Wilmad Glass). All samples were frozen in liquid nitrogen and immersed into a liquid N_2-filled ESR dewar and the ESR spectrum measured with the parameters above.

Concentrated [0.2 mM] native and DEPC-modified horse myoglobin was added to 0.3 ml metallated vesicles at ratios of protein to Cu^{2+} above 2.0. All samples (0.5 ml) were frozen immediately in liquid nitrogen and immersed into a liquid N_2-filled ESR dewar. While in the spectrometer cavity, the dewar was purged with nitrogen gas to prevent condensation during spectral acquisition. $g_\parallel$, $A_\parallel$ values were calculated from the spectral line positions [43].

Table 3.1. Calculated accessibility of surface histidines from crystal structure of horse heart myoglobin [46]. The accessible surface area is reported by Robert Johnson [60] to be total Conolly area at either nitrogen accessible to a probe the size of $Cu^{2+}IDA$ (1.93 Å radius [61]). Percent accessibility is calculated with respect to surface area of imidazole. The pKa of each histidine is taken from Cocco et al. [62].

histidine	Accessible surface area ($Å^2$)	percent accessibility	pKa
36	7.9	27	7.8
48	14.5	49	5.46
81	17.1	58	6.65
97	6.1	20	N.A.
113	17.6	60	5.37
116	12.0	41	6.70
119	6.6	23	6.39

Table 3.2. ESR spectral parameters determined for mixtures of copper(II) iminodiacetate ($Cu^{2+}IDA$) and imidazole at 77 °K, pH 7.5. The ratio represents total imidazole added to $Cu^{2+}IDA$ at pH 7.5. $A_\perp$ was not clearly determined from the spectra. $[Cu^{2+}IDA] = 1.032$ mM in MOPS buffer [20 mM MOPS, 100 mM NaCl, pH 7.5].

total added [Cu²⁺IDA: Im]	$g_\parallel$	$A_\parallel$ (G)	$g_\perp$
1:0	2.285	159	2.052
1:0.5	2.271	152	2.052
1:1	2.268	157	2.050
1:2	2.265	170	2.049
1:4	2.262	180	2.046
1:10	2.261	183	2.047

Table 3.3. Calculated species from equilibrium formation constants [17] at pH 7.5 using the FORTRAN program SPE.FOR [63]. The amount of added $Cu^{2+}IDA$ was kept constant and imidazole was added to get the desired ratio. The percent of each species containing imidazole was determined by dividing that concentration by the total amount of $Cu^{2+}IDA$ added to each sample. The stability constants used in SPE.FOR are contained in Table 3.4. The percentage of $[Cu^{2+}Im_n]$ does not add up to 100 since imidazole is normalized by total $Cu^{2+}IDA$. $[Cu^{2+}IDA] = 1.032$ mM in [20 mM MOPS, 100 mM NaCl, pH 7.5] buffer.

$[Cu^{2+}IDA: Imidazole]_T$	% CuIDA.Im	% CuIDA.Im$_2$	% unbound Im
1: 0	0	0	0
1:1	35	11	33
1:2	42	29	76
1:4	33	56	191

Table 3.4. Equilibrium formation constants (T = 25 °C) used for calculation of $(Im)_nCu^{2+}IDA$ equilibria. Species distribution calculated with SPE program [63].

log K [17]	ΔH (kcal/mole)	IDA	Cu	Im	H$^+$
9.34	—	1	0	0	1
11.89	—	1	0	0	2
10.57	-4.5	1	1	0	0
16.54	-10.9	2	1	0	0
3.00	—	1	1	0	-1
14.37	-12.1	1	1	1	0
7.01	—	0	0	1	1
4.35	-7.6	0	1	1	0
7.75	-14.0	0	1	2	0
10.30	-19.0	0	1	3	0
11.80	-23.0	0	1	4	0

Table 3.5. ESR spectral parameters for complexes of 2% DSIDA-Cu^{+2} mixed vesicles (48 % DSPC and 50 % cholesterol) loaded with native and DEPC-modified horse myoglobin (hMb).[a]

Cu^{2+} vesicles mixed with:	$g_{\parallel}$	$A_{\parallel}$ (Gauss)
no protein	2.287	160
DEPC-modified hMb	2.288	152
hMb	2.264	177

[a] > 2-fold molar excess of protein to total copper.

Table 3.6. Equilibrium binding data for horse heart myoglobin and 2% DSIDA/ 48% DSPC/ 50% small unilamellar vesicles. Data taken at 25 °C in 20 mM MOPS, 100 mM NaCl, pH 7.5 buffer. Bound protein is normalized by total phosphate in each sample. Total volume of each sample was 5 ml.

no metal (2.82 μmole PO$_4$/tube)		1 mM CaCl$_2$ (2.82 μmole PO$_4$/tube)		105 μM CuCl$_2$ (2.49 μmole PO$_4$/tube)	
free hMb (μM)	bound hMb/PO$_4$ x10^{-3}	free hMb μM	bound hMb/PO$_4$ x10^{-3}	free hMb μM	bound hMb/PO$_4$ x10^{-3}
0	0	0	0	0.0	0.00
3.66	1.63	3.02	1.31	1.16	6.26
3.82	0.82	3.86	1.80	1.34	5.94
4.88	2.44	4.86	2.19	2.88	6.78
7.72	1.95	5.85	1.97	3.14	6.58
11.14	2.52	8.15	2.00	5.22	6.62
12.78	3.19	9.23	2.37	10.7	7.63
17.96	3.19	12.20	2.85	15.4	6.79
39.12	2.48	21.66	2.73	19.3	7.67
		33.69	3.04	20.8	6.74
				32.9	8.38
				42.4	7.91

Table 3.7. Binding data for pure DSPC small unilamellar vesicles for horse heart myoglobin. Data taken at 25 °C in 20 mM MOPS, 100 mM NaCl, pH 7.5 buffer. Total volume of initial sample was 5 ml. Phosphate per measurement was 2.94 µmoles.

free hMb (µM)	bound hMb (nmoles)
12.5 ± 0.01	10.4 ± 0.7
18.47 ± 0.4	9.0 ± 2
46.76 ± 0.8	15.6 ± 2
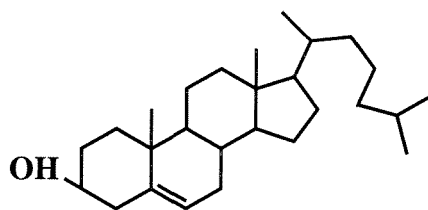
Cholesterol
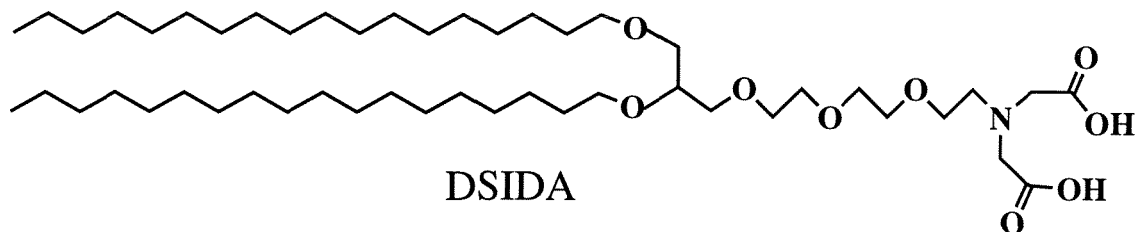
DSIDA
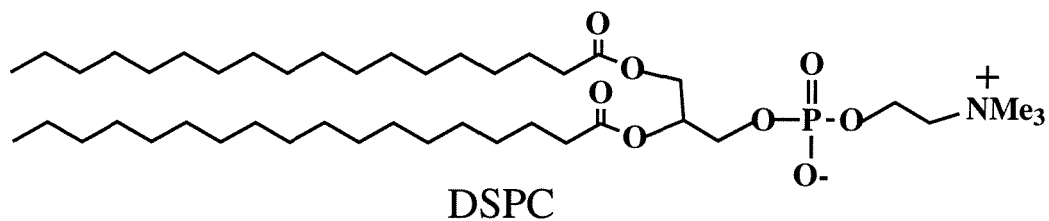
DSPC

Figure 3.1. Chemical structures of components used to form small unilamellar vesicles.
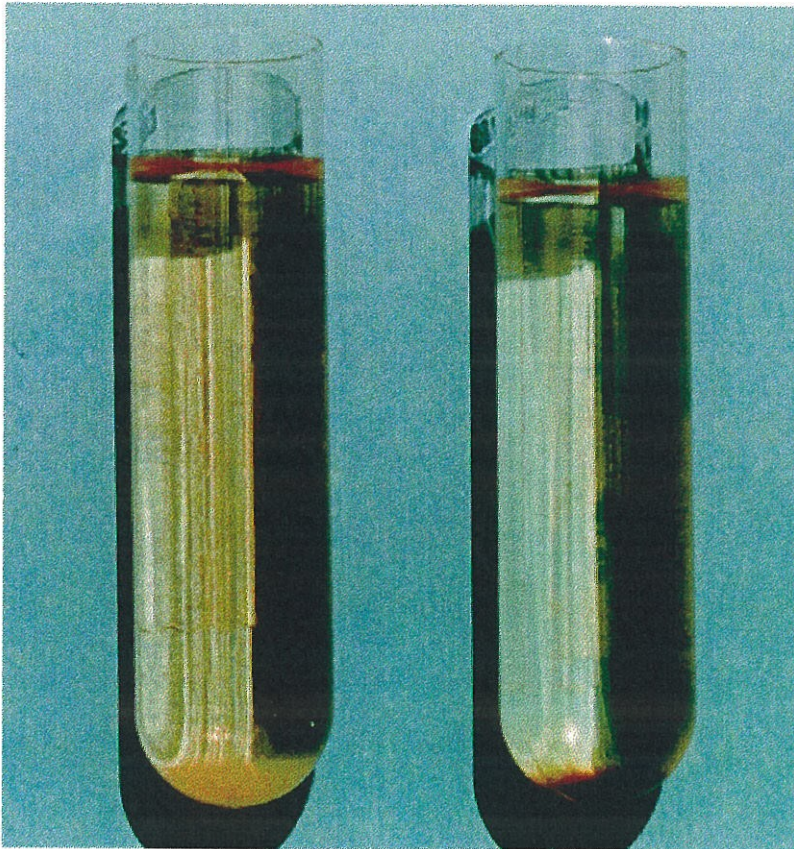
Figure 3.2. Photograph of equilibrium binding experiments to determine protein binding. Dark pellet on tube A shows vesicles loaded with Ca^{2+} with bound myoglobin. Tube B shows identical Cu^{2+} loaded vesicles with same total added protein showing much less protein binding.
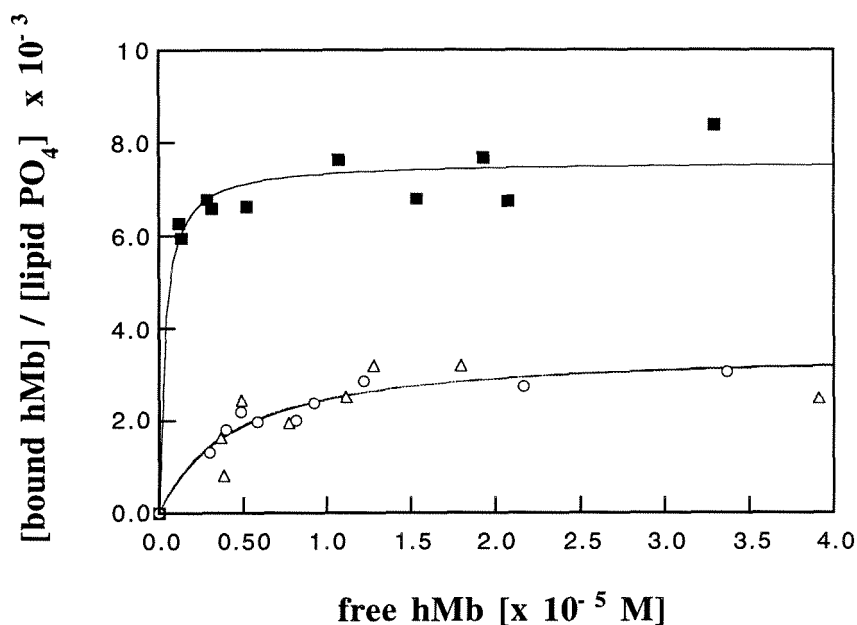
Figure 3.3. Binding of horse myoglobin to mixed vesicles containing 2 % DSIDA-Cu^{2+} (48% DSPC and 50 % cholesterol) (■), to mixed vesicles containing 2 % DSIDA-Ca^{2+}, (o), and to mixed vesicles containing DSIDA with no metal (Δ) at 25 °C in 20 mM MOPS, 100 mM NaCl, pH 7.5. Solid lines represent best fits to a Langmuir isotherm. The apparent binding constants determined from fits for Cu^{2+} were K$_a$ > 2.9 ± 1.2 x 10^6 M^{-1} and for Ca^{2+}, 2.5 ± 1.5 x 10^5 M^{-1}.
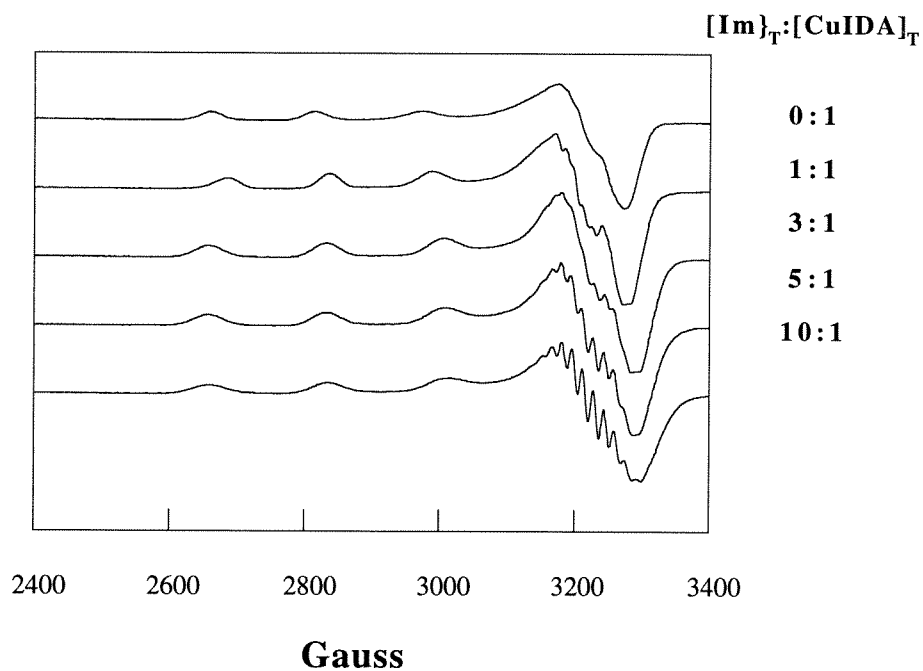
Figure 3.4. ESR spectra of Cu^{2+}IDA showing changes in spectral line positions with increasing imidazole concentration at pH 7.5 in MOPS buffer at 77 °K. Super-hyperfine features are present in the region 3100-3300 Gauss. Ratio of added Cu^{2+}IDA to imidazole is indicated next to each spectrum, $[Cu^{2+}IDA] = 1.03$ mM.

116
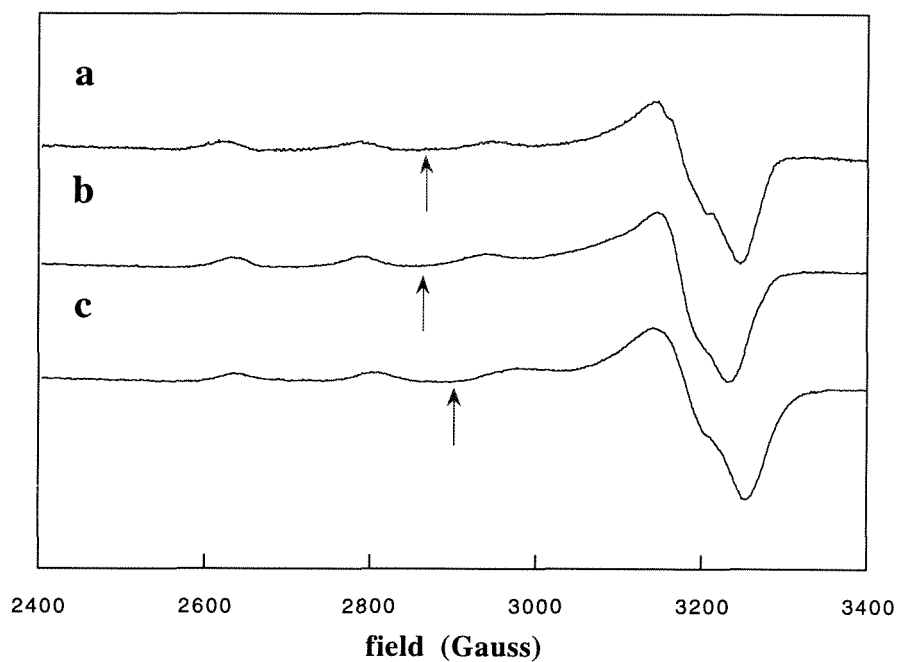
Figure 3.5. ESR spectra of metal loaded vesicles composed of 2.5 mol% DSIDA-Cu^{2+}, 47.5 mol % DSPC, and 50 mol% cholesterol with (a) no protein, (b) DEPC-modified horse myoglobin, (c) native horse myoglobin. Protein is roughly 2-fold excess of vesicle-bound Cu^{2+}. Arrows indicate field positions used to calculate $g_{\parallel}$ values.

REFERENCES

1. Blankenburg, R.; Meller, P.; Ringsdorf, H; Salesse, C. *Biochemistry* **1989**, *28*, 8214-8221.

2. Uzgiris, E. E.; Kornberg, R. D. *Nature* **1983**, *301*, 125-129.

3 McCloskey, M. A. and Poo, M.-M. *J. Cell Biol.* **1986**, *102*, 2185-2196.

4 Ahlers, M; Grainger, D. W.; Herron, J. N.; Lim, K.; Ringsdorf, H.; Salesse, C. *Biophys. J.* **1992,** *63*, 823-838.

5 Tamm, L. K. *Biochemistry* **1988**, *27*, 1450-1457.

6. Ribi, H. O.; Reichard, P.; Kornberg, R. D. *Biochemistry* **1987**, *26*, 7974-7979.

7 Lebeau, L., Regnier, E., Schultz, P., Wang, J. C.; Mioskowski, C.; Oudet, P. *FEBS Lett.* **1990**, *267*, 38-48.

8. Grainger, D. W.; Reichert, A.; Ringsdorf, H.; Salesse, C. *FEBS Lett.* **1989**, *252*, 73-82.

9. Hamachi, I.;. Nakamura, K.; Fujita, A.; Kunitake, T. *J. Am. Chem. Soc.* **1993**, *115*, 4966-4970.

10. Dhal, P. K.; Arnold, F. H. *J. Amer. Chem. Soc.* **1991**, *113*, 7417-7418.

11. Dhal, P. K.; Arnold, F. H. *Macromolecules* **1992**, *25*, 7051-7059.

12. Mallik, S.; Plunkett, S. D.; Dhal, P. K.; Johnson, R. D.; Pack, D. W.; Shnek, D. R.; Arnold, F. H. *New J. Chem.* **1994,** *18*, 299-304.

13. Sundberg, R. J. and Martin, R. B. *Chem. Rev.* **1974**, *74*, 471-517.

14. Porath, J.; Carlsson, J.; Olsson, I.; Belfrage, G. Nature **1975**, *258*, 598-599.

15 Arnold, F. H. *Bio/technology* **1991**, *9*, 151-156.

16. (a) Ill, C. R.; Keivens, V. M.; Hale, J. E.; Nakamura, K. K.; Jue, R. A.; Cheng, S.; Melcher, E. D.; Drake, B.; Smith, M. C. *Biophys. J.* **1993**, *64*, 919-924.
(b) Piesecki, S.; Teng, W.-Y.; Hochuli, E. *Biot. Bioeng.* **1993**, *42*, 178-184. (c)

Smith, M. C.; Cook, J. A.; Furman, T. C.; Gesellchen, P. D.; Smith, D. P.; Hsiung, H. *ACS Symp. Ser.* **1990**, *427*, 168-180.

17. Martell, A. E.; Smith, P. M. *Critical Stability Constants*; Plenum Press: New York, 1974; Vol. 6.

18. Sinha, P. C.; Saxena, V. K.; Nigam, N. B.; Sriastava, M. N. *Ind. J. Chem.* **1989**, *28A*, 335-336.

19. Todd, R. J. ; Johnson, R. D. ; Arnold, F. H. *J. Chromat.* **1994**, *662*, 13-26.

20. Arnold, F. H. and Haymore, B. L. *Science* **1991**, *252*, 1796-1797.

21. Todd, R. J.; Van Dam, M. E.; Casimiro, D.; Haymore, B. L.; Arnold, F. H. *Prot. Struct. Funct. Gen.* **1991**, *10*, 156-161.

22. Hochuli, E.; Bannwarth, W.; Dobeli, H.; Gentz, R.; Stuber, D. *Bio/Technology* **1988**, *6*, 1321-1325.

23. Tsuchida, E.; Komatsu, T.; Arai, K. *J. Chem. Soc. Ch.* **1993**, *9*, 730-732.

24. Budach, W.; Ahuja, R. C.; Möbius, D. *Langmuir* **1993**, *9*, 3093-3100.

25. Budach, W.; Ahuja, R. C.; Möbius, D.; Schrepp, W. *Thin Solid Films* **1992**, *210*, 434-436.

26. Ishikawa, Y.; Kunitake, T. *J. Am. Chem. Soc.* **1986**, *108*, 8300-8302.

27. Ishikawa, Y.; Kunitake, T. J. *Macromol. Sci.-Chem.* **1990**, *A27*, 1157-1166.

28. Furhop, J.-H. and Mathieu, M. *Angew. Chem. Int. Ed. Engl.* **1984**, *23*, 100-113.

29. Vanesch, J. H.; Nolte, R. J. M.; Ringsdorf, H.; Wildburg, G. *Langmuir* **1994**, *10*, 1955-1961.

30. Munoz, S.; Mallen, J.; Nakano, A.; Chen, Z.; Gay, I.; Echegoyen, L.; Gokel, G. W. *J. Am. Chem. Soc.* **1993**, *115*, 1705-1711.

31. Yanagi, M.; Tamamura, H.; Kurihara, K.; Kunitake, T. *Langmuir* **1991**, *7*, 167-172.

32. Wuenschell, G. E.; Wen, E.; Todd, R.; Shnek, D.; Arnold, F. H. *J. Chromat.* **1991**, *543*, 345-354.

33. Schubert, J. *J. Am. Chem. Soc.* **1954**, *76*, 3442-3446.

34. Peisach, J., Blumberg, W.E. *Arch. Biochem. Biophys.* **1974**, *165*, 691-708.

35. Abragam, A. and Bleaney, B. *Electron Paramagnetic Resonance of Transition Metal Ions*, Clarendon Press, Oxford, 1970.

36. Papahadjopoulos, D.; Poste, G.; Schaeffer, B. E.; Vail, W. J. *Biochim. Biophys. Acta* **1974**, *352*, 10-28.

37. *Liposomes: A Practical Approach;* New, R.R.C., Ed.; Oxford University Press: New York, 1990; p. 19.

38. Morrison, W. R. *Anal. Biochem.* **1964**, *7*, 218-224.

39. Louie, G.V. and Brayer, G.D. *J. Mol. Biol.* **1990**, *214*, 527-555.

40. Bergers, J. J.; Vingerhoeds, M. H.; van Bloois, L.; Herron, J. N.; Janssen, L. H. M.; Fischer, M. J. E.; Crommelin, D. J. A. *Biochemistry* **1993**, *32*, 4641-4649.

41. Hamachi, I.; Honda, T.; Noda, S.; Kunitake, T. *Chem. Lett.* **1991**, 1121-1124.

42. Shnek, D.R., Pack, D.W., Sasaki, D.S., Arnold, F.H. *Langmuir* **1994**, *10*, 2382-2388.

43. Wertz, J.E., Bolton, J.R. *Electron Spin Resonance: Elementary Principles and Practical Applications*, Chapman & Hall, New York, 1972, pp ii.

44. Johnson, R.D. *Ph.D. Thesis*, California Institute of Technology, Pasadena, CA, 1995, p227.

45. Konopka, K.; Waskell, L. *Biochim. Biophys. Acta.* **1988**, *954*, 189-200.

46. Evans, S.V. and Brayer, G.D. *J. Mol. Biol.* **1990**, *213*, 885-897.

47. A typical surface area for DMPC SUVs is ~ 70 Å^2/molecule (Fendler, J. H.,"Membrane Mimetic Chemistry," John Wiley & Sons, New York **1982**, p.

137). This area will of course be further increased by the incorporation of cholesterol.

48.   Tortorella, D., Ulbrandt, N.D., London, E. *Biochemistry* **1993**, 32, 9181-9188.

49.   Powers, D. D. ;. C., R.G.; Kilpatrick, P.K. *Biotech. Bioeng.* **1994**, *44*, 509-522.

50.   Powers, D. D. ;. W., B.L.; Carbonell, R.G.; Kilpatrick, P.K. *Biotechn. Prog.* **1992**, *8*, 436-453.

51.   Van Dam, M.; Wuenschell, G. W.; Arnold, F. H. *Biotechnol. Appl. Biochem.* **1989**, *11*, 492-502.

52.   Kubalek, E. W.; Legrice, S. F. J.; Brown, P. O. *J. Struct. Biol.* **1994**, *113*, 117-123.

53.   Figgis, B.N. *Introduction to Ligand Fields* Robert E. Krieger, Malabar, 1986.

54.   Froncisz, W., Hyde, J.S. *J. Chem. Phys.* **1980**, *73*, 3123-3131.

55.   Knowles, P.F.; Marsh, D.; Rattle, H.W.E. *Magnetic Resonance of Biomolecules.* John Wiley & Sons, London, 1976, pp. 168-207.

56.   Dung, N.-H.; Viossat, B.; Busnot, A.; Zafra, A.G.; Gonzalez-Perez, J.M.; Gutierrez, J.N. *Inorg. Chim. Acta* **1990**, *169*, 9-12.

57.   Bonomo, R. P. ;. C., V.; D'Alessandro, F.; Immpellizzeri, G.; Maccarrone, G.; Vecchio, G.; Rizzarellie, E. *Inorg. Chem.* **1991**, *30*, 2708-2713.

58.   Plesch, G.;. F., C.; Svajlenova, O.; Krätsmar-Smogrovic, J. *Polyhedron* **1991**, *10*, 893-898.

59.   Breslow, E. *J. Biol. Chem.* **1964**, *239*, 486-496.

60.   Johnson, R.D. *Ph.D. Thesis*, California Institute of Technology, Pasadena, CA, 1995, p227.

61.   Mrabet, N.T. *Biochemisty* **1992**, *31*, 2690-2702.

62. Cocco, M.J.; Kao, Y.H.; Philips, A.T.; Lecomte, J.T.J. *Biochemistry* **1992** ,*31*, 6481-6491.

63. Martell, A.E. and Motekaitis, R.J. **1988** *The Determination and Use of Stability Constants*, VCH Pub. Inc., New York, NY.

Chapter 4. Multivalent binding of histidine compounds to metal-chelating

fluorescently-labeled lipid bilayers

INTRODUCTION

Ligand-directed organization of lipid membrane surfaces drives many biological processes such as transmembrane signaling [1] and recognition [2]. Targeting of ligands to membrane interfaces followed by assembly can be used to form interesting supramolecular architectures [3]. Ligand-directed lipid assemblies have been formed by oriented binding [4] and receptor-complex formation [5] on natural and synthetic membranes. "Affinity" lipid components provide convenient targeting of interesting ligands to the interface through formation of specific lipid-ligand bonds [2]. A lipid-ligand complex can be created by subsequent re-organization of the lipids to form a high-affinity, multivalent complex.

Organized, two-dimensional protein assemblies would be extremely useful for protein orientation, catalysis, and preparation of biosensors. Thus, we have developed affinity lipid-based materials to make two-dimensional synthetic lipid surfaces used for ligand-directed binding. Our research goals include making pre-organized assemblies that can form a high-affinity "receptor" for a single ligand, protein or a small molecule. Multivalent binding of the ligand to multiple lipids will be used to two-dimensionally organize or "pattern" the bilayer. If the lipids are fixed after ligand binding, interesting patterned surfaces could be formed [6].

Many investigators have developed techniques to form nanometer-scale patterns on surfaces. These include labor intensive scanning-tunneling electron microscopic (STEM) deposition of individual atoms [7], micro-lithography [8] and molecular "printing" using self-assembled monolayers [9]. Lipids formed into vesicles or tubules provide an organic surface to make patterned interfaces. Lipid bilayer assemblies also have spacing between lipids of less than 10 nm between lipid molecules, set by the size of the lipid. An interesting property of lipid bilayers compared to mechanically patterned surfaces, is that lipids can easily re-organize upon ligand binding [10].

Thus, it is critical to determine if a multivalent ligand can re-organize the interface through specific binding to affinity lipids. To promote understanding of ligand-directed re-organization of membrane interfaces, we have sought to find a lipid-based system that provides a convenient method of measuring the organization of lipid "receptors" by a ligand with multiple binding moieties. Upon ligand binding to multiple lipids, a signal must be sent that reflects ligand-induced lipid re-organization.

Lipids modified with a fluorescent probe will be used to examine the organization of the lipid bilayer upon ligand binding. A charge transfer-like complex can form when a pyrene moiety in the ground-state collides with an excited state pyrene [11]. This complex undergoes non-radiative fluorescence emission to release the absorbed energy [12]. Excimer complexes have distinct fluorescence properties when compared to the monomer, including a red-shifted fluorescence emission and a different fluorescence lifetime. When pyrene is covalently attached to the acyl chain of a lipid and formed into model membrane, the probe lipids collide to form excimer complexes. Changes in the ratio of fluorescence intensity at the excimer and monomer wavelengths have been used to probe events occurring in and on the bilayer [13].

In the absence of ligands that perturb the lipid bilayer, the E/M ratio is proportional to the total concentration of the probe, the diffusivity of the probe in the bilayer, and the lifetime of the excimer [12]. A local increase in the concentration of the probe lipid is readily observed in the fluorescence emission spectrum, in the form of the excimer to monomer (E/M) intensity ratio. Previous fluorescence studies using pyrene-labeled lipids have been used to infer effects of changing the headgroup of lipids [14], cholesterol [13,15], and protein association [16,17,18,19,20] on mixed model membranes. Pyrene-labeled lipids have also been used to directly demonstrate that polyethylene glycol-conjugated lipids undergo phase separation [21].

The effect of ligand-directed re-organization of pyrene-labeled affinity lipids using the E/M ratio has not been extensively studied due to the scarcity of pyrene-labeled affinity

lipids. Previously studied labeled lipids consist chiefly of natural pyrene-labeled phospholipid analogues. These pyrene-labeled lipids usually do not have high binding affinity for proteins, since the headgroups interact with the protein only through electrostatic binding. Non-specific, electrostatic binding of proteins to negatively-charged membranes has been studied primarily to demonstrate protein-induced changes in the bilayer properties to pyrene-labeled lipids [19,22]. Although these studies were useful in showing that macromolecules such as proteins can have large effects on the membrane phase properties, the presence of ligand-induced isothermal organization of the bilayer has still largely not been demonstrated using labeled-lipids.

To test our hypothesis that multifunctional ligands can induce specific lipid re-organization in lipid bilayers, new metal-chelating, pyrene-labeled lipids were synthesized. Metal-chelating lipids have been designed to target proteins, peptides, and small molecules to model membrane interfaces [23,24,25]. Metal ions provide useful interactions for protein recognition, with relatively high binding affinities and specificity for residues on the surfaces of proteins, depending on the choice of metal ion [26]. Such metal-chelating lipid systems could be used to target proteins to the interface for assembly studies. Or, proteins can be engineered to contain a histidine "tag" to target the protein to the interface [24]. To target ligands to the interface for these studies, a pyrene-labeled metal-chelating lipid, PSIDA (Figure 2.1) has been synthesized which contains an iminodiacetate (IDA) metal-chelating head group. When PSIDA is metallated with Cu^{2+}, this compact headgroup is able to bind to electron-rich residues on the protein surface and is effective for targeting proteins to the lipid interface [23].

We intend to determine changes in the excimer to monomer fluorescence intensity ratio due to ligand binding to metal-chelating, pyrene-labeled lipids in mixed lipid bilayers. As a multivalent ligand coordinates to multiple Cu^{2+}-chelating lipids through surface-accessible histidine residues [23], an increase in the local concentration of labeled lipids is expected. This local increase in the pyrene-labeled lipid concentration should result in more

lipid collisions, and a higher E/M. The E/M ratio when ligand is present can be compared to the initial state lacking ligand $(E/M)_o$, to give a quantitative measure of the excess collisions induced by ligand binding, $\Delta E/M$. Thus, the increase in the excimer intensity and a decrease in the monomer intensity could be used to monitor multisite binding.

We have investigated the fluorescence spectra of small amounts of copper chelating, pyrene-labeled lipids in mixed synthetic vesicles. Metal-chelating fluorescently-labeled lipids were shown to have special properties upon transition metal ion binding [Chapter 2]. Metal binding caused the excimer to monomer ratio to decrease to a very low value. We have also shown that protein binding occurs chiefly through Cu^{2+} chelated on the lipid headgroup coordinating to histidine residues [Chapter 3]. Based on these previous studies with histidine-rich molecules and unlabeled metal-chelating mixed vesicles, we expect that histidine-rich molecules will affect the fluorescent emission spectra of mixed vesicles containing PSIDA reflecting multiple lipid coordination by multivalent ligands.

Since the number and geometry of co-planar surface-accessible histidines are known for the chosen model compounds, this investigation will provide a comparison of the effects of monovalent, bivalent, trivalent and polyvalent histidine compounds on the fluorescence emission spectra of metal-loaded membranes. Monovalent histidine compounds were added to metal-loaded bilayers and found to have a small effect on the fluorescence emission spectra. In contrast, a homopolymer of poly-L-histidine was found to cause the E/M ratio to increase and then decrease back to the initial E/M value for Cu^{2+}-loaded vesicles at higher polymer concentrations. Several biologically active histidine-containing peptides were also studied to investigate the changes in the excimer and monomer ratio.

CALCULATIONS

The schematic shown in Figure 4.1 indicates the expected equilibrium species for bivalent ligand binding to mobile lipid receptors located in a model membrane. We will

assume that the excess E/M ratio (ΔE/M = E/M - E/M$_o$) is proportional to the fraction of ligand simultaneously bound to two metallated lipids. Equations relating the fraction of bivalent bound lipid to concentration of free bivalent ligand are developed and used to interpret the experimental data.

Equilibrium binding between bivalent ligand L and one or two chelating lipids, M, was assumed. Single-site adsorption of the bivalent ligand assuming isolated sites is developed as a function of binding constants and concentration of free and total ligand added to the vesicles. Another model, originally developed by Perelson & DeLisi for bivalent ligand-receptor binding, assuming sequential binding of the bivalent ligand to two different lipids, was also used to interpret the data [27]. The excess steady-state fluorescence emission ratio ($I_{470\ nm}/I_{377\ nm}$ = E/M) of dilute (5 mole %) probe lipid in vesicles versus total ligand concentration was fitted using the software Kaleidagraph^{TM} with Equation 2 to determine apparent association constants using the software's non-linear, least-squares Marquadt algorithm.

Single-site adsorption

If the experimental measurement is proportional to the fraction of bivalent bound species, a simple Langmuir isotherm can be developed to describe the equilibrium between bivalent ligand-bound lipids (bis sites) on the surface of vesicles and the bifunctional ligand L in solution. We have applied this model at very low loading of bivalent ligand to total metal-chelating lipid where single point binding is not favored. Two lipids with matching distance to the target ligand L comprise the M_{bis} site and the ligand contains two histidines.

$$M_{bis} + L \leftrightarrow M_{bis}L \qquad K_{app} = \frac{[M_{bis}L]}{[L][M_{bis}]} \qquad [1]$$
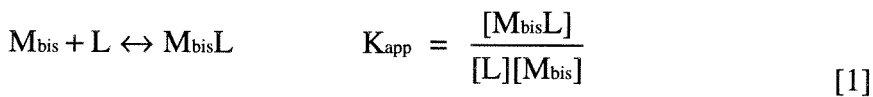
Combining the mass balance for total lipid and the equilibrium expression yields a binding isotherm between the total concentration of ligand L and the bound Q(L) concentration of ligand to two lipids, equivalent to the well-known Langmuir isotherm.

If the free concentration cannot be approximated by the total concentration, Equation 1 and the mass balance can be rewritten in terms of the total amount of ligand and metal added. The bivalent binding isotherm can be rewritten in terms of total ligand added relative to total metallated lipid .

$$\frac{(M_t + L_t + K_D) - \sqrt{(M_t + L_t + K_D)^2 - 4M_tL_t}}{2M_t} = \frac{[M_2L]}{M_t} = \frac{Q(L)}{Q_{max}} \qquad [2]$$

$[M_{bis}L]/M_t$ is the fraction of M involved in bivalent compound bound to the vesicle surface, proportional to the change in the E/M ratio. M_t is the amount of metal, which is assumed to be fully bound by chelating lipid. Since two lipids bind to each ligand to form $M_{bis}L$, the total number of bis sites is approximated by the total accessible chelating lipid concentration divided by 2. Plots of excess excimer to monomer ratio versus total bivalent added were fitted with Equation 2 to determine the binding parameter $K_{app} = (1/K_D)$.

Sequential two-point binding

Equilibrium expressions for sequential two-point binding can be written as a stepwise adsorption of each of the bifunctional residues of the ligand L to form the bivalent bound species M_2L [27]. Figure 4.1 shows a pictorial illustration of the various equilibrium species that are formed and used in the development of this model.

$$M + L \leftrightarrow ML$$
$$ML + M \leftrightarrow M_2L$$

$$K_1 = \frac{[ML]}{[M][L]}$$

$$K_2 = \frac{[M_2L]}{[ML][M]}$$

[3]
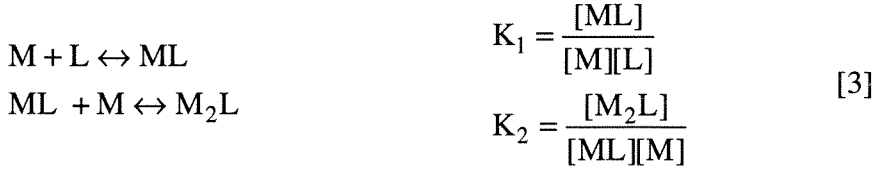
For binding of a bivalent ligand L to receptors located on the surface of a cell, equilibrium models like Equation 4 have been used to quantify the equilibrium number of cross-linked lipids as a function of ligand concentration. If we assume that the bivalent ligand concentration is not significantly depleted ($[L] \gg M_T$), then the equations have been solved analytically for the equilibrium concentration of cross-linked $[M_2L]$ lipids [27]. Using a mass balance for the total number of lipids, an expression can be obtained which contains two apparent binding constants K_1, K_2 and the normalized equilibrium bivalent bound ligand-lipid complex, $[M_2L]/M_T = \overline{M}$; in terms of a dimensionless concentration parameter β , the initial concentration of chelating lipids M_T, and both binding constants, K_1, K_2.

$$\beta = \frac{K_1 L}{(1 + K_1 L)}$$

$$\overline{M} = \frac{1 + 2\beta(1 - \beta)K_2 M_T - \sqrt{1 + 4\beta(1 - \beta)K_2 M_T}}{4\beta(1 - \beta)K_2 M_T}$$

[4]

Each chelating lipid receptor loaded with a copper ion, M, is able to bind to ligand L monovalently. Reversible binding of a bis-functional receptor L to both lipids is also assumed. The theory can be generalized for any number of identical multivalent attachments to multiple lipid receptors. Unfortunately, the condition $[L] \gg M_T$ or $L_T \approx [L]$ was not satisfied over the whole binding regime ($L_T \sim 10^{-7}$-10^{-5} M) investigated. To use the sequential binding model [27], the first binding constant K_1 from solution to the bilayer is assumed from other measurements or included in the fit, while the dimensionless cross-

linking binding constant K_2M_T is determined from fits of excess E/M versus concentration of added ligand. The model is included because it helps in interpretation of the qualitative $\Delta E/M$ behavior since a monotonic increase to a maximum value ($\Delta E/M(L_{max}) = 1/K_1$) followed by a symmetric decrease to zero is predicted. For $\Delta E/M$ data that display this behavior, the concentration at maximum value can be compared and interpreted using this model.

Excess E/M

The fluorescence spectra of pyrene-labeled lipids formed into vesicles have distinct peaks which correspond to monomers and excited state dimers (excimers), as shown in Figure 4.2. The steady state E/M ratio (I_E/I_M) without ligands is proportional to quantum yield ratio (Φ_e/Φ_m) and has the form below [12,13].

$$\frac{\Phi_E}{\Phi_M} = \kappa \frac{I_E}{I_M} = \kappa \frac{k_{f,E}}{k_{f,M}} \cdot \tau_{o,E} \cdot k_a \cdot c \qquad [5]$$

$\tau_{0,E}$ is the excimer lifetime, c is the total concentration of pyrene-labeled lipid, κ is an experimental ratio of the quantum yields, and the rate constants for fluorescence decay and collision are shown in Figure 4.2. We are interested in determining the excess collisions produced by ligand binding to the bilayer as a function of the concentration of ligand added in order to obtain the fraction of lipid brought together by the ligand. The ratio of excimer to monomer intensities is proportional to the concentration of pyrene-labeled lipid in a diffusion-controlled bilayer [13]. As the ligand binds to multiple lipids the number of labeled-lipid collisions should be enhanced. These collisions would result in more excimer fluorescence, since more excimer complexes would be formed.

We have assumed that the excess E/M ratio reflects these excess collisions induced by ligand-lipid binding, shown schematically in Figure 4.3. Figure 4.4 shows the kinetic

scheme for excimer and monomer formation upon bivalent ligand binding. It is not known whether the bivalent bound species forms an excimer directly while bound to the lipids or enhances excimer collisions by causing a local increase in the pyrene-labeled lipid after the ligand desorbs. However, the effect on the steady state E/M ratio would be the same. We have fitted plots of ΔE/M assuming it is proportional to the increase in the amount of bivalent bound caused by ligand binding (Figure 4.3).

Certain assumptions about the effect of the ligand on the fluorescence kinetics must be made for the steady-state experimental excess E/M ratio to represent the fraction of multiply bound ligand. The rates of monomer fluorescence excitation and emission are assumed to be unaffected by binding of small bivalent ligands since the fluorophore is buried in the hydrophobic region. The only effect of bivalent ligand on the bilayer is to increase the total number of excimer collisions. Fluorescence intensity remains the same if the ligand binding does not affect the fluorescence rate parameters. Thus, our most important assumption is that ligand binding does not affect fluorescence kinetics. We also assume that the lifetimes of the excimer and monomer do not change upon ligand binding, since this could also effect the E/M ratio (Equation 5) [11].

At a given time, not all of the fluorescently-labeled lipids are in the excited state. Instead they exist in the non-fluorescent ground-state (Figure 4.3) and could be bound to a bivalent histidine compound. Obviously, the ground-state lipid is not observable in a fluorescence experiment, yet is able to participate in the binding equilibria. No difference in the binding kinetics between excited-state and ground-state lipids is assumed. Therefore, the excess E/M ratio can be used to determine association behavior. Also, the binding valency state of a lipid is not expected to affect the diffusivity of the lipids for small ligands. Larger ligands, such as poly-L-histidine, may alter the diffusivity of the lipids upon binding.

Studies of pyrene dissolved in hexane have shown that every excimer collision results in fluorescence emission [28]. Therefore, every collision between labeled chelating

lipids is assumed to result in excimer emission. With these assumptions investigating the excess E/M ratio will help understanding of lipid reorganization due to multivalent ligands.

Excess E/M ratio was investigated for imidazole (monovalent), 1,4-bisimidazole (bivalent), porcine renin tetra-decapeptide (bivalent), human renin tetra-decapeptide (trivalent), and poly-L-histidine (multivalent) binding to pyrene-labeled, metal-chelating lipids in bilayer assemblies. Plots of excess E/M as a function of the model divalent compound, 1,4-bisimidazole, concentration were fitted with Equation 2 in order to extract association constants for comparison to ligands containing multiple histidine residues.

RESULTS

N-acetyl histidine binding to fluorescently-labeled vesicles

Compounds containing a single histidine were added to vesicles made from PSIDA and various phospholipids (Figure 4.5) to determine whether monovalent binding affects the excess excimer to monomer ratio (ΔE/M). Increasing the head group size by histidine coordination might alter the lipid diffusivity and lower the E/M value [13]. The stability of four imidazoles complexed to copper is comparable to that of Cu^{2+}IDA ($K_{Cu(Im)4} \approx 10^{12.6}$ versus $K_{CuIDA} \approx 10^{10.5} M^{-1}$) [29]. For a large excess of histidine or imidazole to copper (>1000 times the copper concentration), complexes of four histidine ligands coordinated to one copper ion start to form. However, in fluorescence experiments we did not exceed the estimated concentration necessary to strip the metal out of the bilayer $[Imidazole]_{max} \leq 1$ mM, $[Cu]_T \sim 1\text{-}2 \ \mu M$.

N-protected histidine was added to mixed vesicles composed of 5% PSIDA and 95% phospholipid. Figure 4.6 shows that the E/M ratio increases only very slightly with N-protected histidine concentration for 5% PSIDA-Cu^{2+}/95% DSPC vesicles. The slight positive slope could be due to binding, or other unrelated effects such as drift in the machine detection. The E/M value of mixed SOPC vesicles changed when exposed to excitation light over long periods (3 hr) (Appendix). Therefore, the shutter was kept closed

between experiments. For N-acetyl histidine binding to 2.5% PSIDA/ 47.5% DSPC/ 50% cholesterol bilayers in Figure 4.7, the E/M behavior increased slightly with increasing ligand concentration. Both imidazole and N-acetyl histidine was added to SOPC bilayers to determine if the E/M ratio changed for a bilayer in the more fluid liquid-crystalline state. Figure 4.8 shows the effect of N-acetyl histidine on copper-loaded 5% PSIDA/ 95% SOPC vesicles. Only a very small increase in the E/M ratio for imidazole addition (Appendix) was also observed for the more fluid PSIDA/SOPC system.

Effect of 1,4-bisimidazole on fluorescently-labeled vesicles

We expect that binding of a bivalent ligand to two pyrene-labeled lipids would enhance the number of excimer yielding collisions by bringing lipids near each other. An observable decrease in the monomer intensity and consequent increase in the excimer intensity would be observed according to the diffusion-controlled model developed by Galla [30].

Vesicles loaded with 5 mM $CaCl_2$ concentration were used as a control for 1,4-bisimidazole studies. We presume the bilayer will be charge neutral upon metal saturation. Since Ca^{2+} has a binding constant of $10^{4.1}$ (M^{-1}) to iminodiacetate in solution, millimolar added Ca^{2+} will effectively saturate the metal-chelating lipids [29]. Otherwise, the bilayer would bear negatively-charged lipids which can bind non-specifically to positively charged ions and residues. The stability constant for imidazole complexed to Ca^{2+}IDA is very low compared to the stability constant for imidazole to Cu^{2+}IDA in solution and therefore the Ca^{2+} loaded vesicles should not coordinate imidazole [29].

The behavior of the ΔE/M ratio with 1,4-bisimidazole (Table 4.1) concentration is shown in Figure 4.10 for 5 mol% PSIDA/ 95 mol% DPSC vesicles. The excess E/M values with copper present have a larger ΔE/M$_{max}$ than the Ca^{2+} controls or N-protected histidine binding (Figure 4.6). Controls where Ca^{2+} is present show primarily a linear decrease or increase, similar to the effect of histidine on the Cu^{2+}-lipid membranes. The

specific change in E/M is just larger than the experimental error and is observed mainly as a decrease in the monomer intensity while the excimer intensity remains constant. Addition of 50 mol% cholesterol made the absolute change in $\Delta E/M$ much smaller than the PSIDA-Cu^{2+}/ DSPC vesicles. Figure 4.11 shows E/M behavior with 1,4-bisimidazole concentration for 2.5 % PSIDA/ 47.5% DSPC/ 50% cholesterol vesicles.

Bis-imidazole binding to metal-chelating bilayers in the liquid-crystalline phase was also investigated. Figure 4.12 shows E/M behavior for 5% PSIDA/ 95 % SOPC vesicles at 25°C . SOPC vesicles showed an even smaller $\Delta E/M$ increase ($\Delta E/M_{max} \approx 0.02$) due to bis-imidazole coordination than the other two vesicle compositions. Since there was such a small effect beyond the Ca^{2+}-control (experimental error $\pm$ 0.006) due to 1,4-bisimidazole, the fits for PSIDA/SOPC data were not reported.

Effect of 1,4-bisimidazole binding on E/M ratio of 10 mol% PSIDA/DSPC vesicles

To investigate whether the excess E/M ratio was dependent on the mole fraction of PSIDA lipid, the PSIDA lipid was increased to 10 mol% in DSPC mixed vesicles. Figure 4.13 shows the behavior of 10% PSIDA mixed with DSPC vesicles. There was no increase in the $\Delta E/M$ ratio relative to the vesicle composition of 5% PSIDA and 95% DSPC. However, the $\Delta E/M$ values increased to a maximum and then decreased back to baseline with increasing 1,4-bisimidazole concentration. The concentration where $\Delta E/M$ reaches a maximum decreased to ~0.10 μM for 10% PSIDA-Cu^{2+} mole fraction.

Scanning calorimetry of 1,4-bisimidazole binding to SUV loaded with copper

Scanning microcalorimetry was used to investigate the effect of 1,4-bisimidazole on the lipid packing of the bilayer. The melting transition from gel to liquid-crystalline phase can be affected by the binding of ligands to the headgroup or hydrophobic region of the lipids [31]. Unfortunately, due to software constraints on starting temperatures, measurements below 7 °C were not attainable on the calorimeter. Binding of 1,4-

bisimidazole to 5 mol% PSIDA/ 95 mol% SOPC small unilamellar vesicles did not show an effect on the T_m above 7 °C, as seen in Figure 4.14. The major transition is below 7 °C. Since the main transition is expected to occur between 4-7 °C [37], there is not a large shift to higher temperature. Similarly, Figure 4.15 shows the scanning calorimetry of 5% PSIDA-Cu/ 95% DSPC small unilamellar vesicles with 1.5 equivalents of 1,4-bisimidazole added. For the same composition of multilamellar vesicles lacking ligand the transition temperature lacking macromolecule was found to be 54.3 ± 0.3 °C for metallated vesicles (Chapter 2). The T_m of the transition with ligand present was 54.04 ± 0.2 °C. Thus, 1,4-bisimidazole binding did not shift the T_m significantly.

Effect of Porcine Renin Tetra-decapeptide on E/M ratio

To investigate another compound capable of bivalent coordination to Cu^{2+}-chelating pyrene-labeled lipids, a model peptide containing two histidines was added to pre-formed metal-chelating pyrene-labeled vesicles. A natural peptide, porcine renin substrate, contains two histidines separated by two amino acids, one of which is a proline residue. The linear structure of the peptide is shown in Table 4.1. The amino terminus of the peptide was obtained N-protected. Thus, we expect the peptide to bind through its two histidines, similar to 1,4-bisimidazole.

Figure 4.16 shows the titration of 5% PSIDA/ 95% DSPC vesicles with the peptide. A linear dependence of the $\Delta E/M$ with porcine renin peptide is observed for vesicles without metal. Saturation of the $\Delta E/M$ value is observed for Cu^{2+}-loaded PSIDA/DSPC vesicles. The magnitude in $\Delta E/M_{max}$ is larger than for previous experiments because the vesicles are more concentrated and may be aggregated by the peptide. The saturation $\Delta E/M$ value occurs at the same concentration of porcine renin peptide as for saturation of the 1,4-bisimidazole complex. Saturation was also observed for PSIDA/DSPC/cholesterol vesicles (Figure 4.17).

Liquid-crystalline 5% PSIDA/ 95% SOPC vesicles showed a very small change in E/M ratio as porcine renin substrate was added to Cu^{2+}-loaded vesicles (Figure 4.18). The change in magnitude of $\Delta E/M$ is consistent with the change in $\Delta E/M$ measured for 1,4-bisimidazole binding experiments. Since there were few initial points for all three vesicle compositions, the data were not fitted with the models developed in Calculations.

Effect of Human Renin Tetra-decapeptide on E/M values

A peptide containing three histidines was added to 5% PSIDA mixed vesicles. The sequence of human renin peptide (Table 4.1) is similar to the sequence of porcine renin substrate, except that a third histidine is present near the COOH terminus of the peptide. Figure 4.19 shows the E/M dependence on the three-histidine peptide concentration for 5% PSIDA/ 95% DSPC vesicles. Qualitatively, the $\Delta E/M$ behavior with Cu^{2+}-loaded vesicles is the same as for the two-histidine peptide. The curve was fitted with the single-site isotherm to determine the apparent association constant for comparison with 1,4-bisimidazole data. The binding constant of $2.5 \pm 0.3 \times 10^6$ M^{-1} using single-site fits is similar within experimental error to the binding constant obtained for bis-imidazole binding to the same composition of vesicles (Table 4.3).

Vesicles composed of 5 mol% PSIDA and 95 mol% SOPC showed a much smaller effect on $\Delta E/M$ with increasing concentration of human renin substrate shown in Figure 4.20. Ca^{2+}-loaded vesicles controls showed a linear increase in the $\Delta E/M$ ratio with increasing total peptide added. The binding constant obtained from single-site fits was $9.4 \pm 2.5 \times 10^6$ M^{-1} (Table 4.3).

Effect of poly-L-histidine on E/M values

We wished to check how increasing the number of histidines changed the magnitude and dependence of the $\Delta E/M$ ratio. Poly-L-histidine can be commercially obtained in linear polymers of the (L)-amino acid with molecular weights ranging from

11,000 to 14,000. The number of histidines per polymer is between 80-90. We expected that poly-L-histidine would show a larger increase in the $\Delta E/M$ ratio than the divalent or trivalent histidine molecules since many histidines could bind simultaneously.

The $\Delta E/M$ behavior of mixed 5% PSIDA-Cu^{2+} vesicles was investigated with increasing poly-L-histidine concentration. Figure 4.21-Figure 4.26 show poly-L-histidine added to metal-loaded vesicles of 5% PSIDA lipid mixed with different matrix lipids. The controls containing no metal and Ca^{2+} showed a roughly linear $\Delta E/M$ dependence with poly-L-histidine concentration. This behavior is consistent with previous results for control vesicles combined with histidine-containing compounds. The change in $\Delta E/M$ measured using Ca^{2+} or unmetallated vesicle controls was larger than other multivalent histidine compounds added to the vesicles ($\Delta E/M_{max} \approx$ -0.05).

In contrast, when Cu^{2+} was present, the poly-L-histidine caused a much larger increase in the $\Delta E/M$ ratio at a much lower concentration than for the 1,4-bisimidazole or peptides. Moreover, the E/M value increased steeply with total poly-L-histidine concentration and returned to the starting E/M value, except for DSPC mixed vesicles, where it remained at an intermediate value. The polymer consistently caused a decrease in the monomer intensity and a slight increase in the excimer intensity.

Since the polymer could bind at many sites, two dilutions of vesicles ($\approx$ 15 μM and 6 μM) were used to determine if vesicle-vesicle cross-linking was occurring. The concentration for which poly-L-histidine caused an increase in the E/M ratio decreased upon vesicle dilution. Vesicles near 2-6 μM had a maximum change in the $\Delta E/M$ between 5-10 nM poly-L-histidine, compared to vesicles at 20-10 μM lipid concentrations which had a maximum change near 100 nM poly-L-histidine.

Fluorescence lifetime measurements

The fluorescence lifetimes of 5% PSIDA-Cu^{2+}/ 95% SOPC vesicles was measured with added imidazole and bis-imidazole to determine any changes. Short pulses of laser

light are used to excite the fluorophore, and then the time-resolved fluorescence decay is sampled (Figure 2.22). A single fluorophore lifetime follows a simple exponential decay after excited by a pulse of laser light [32].

$$\frac{dN(t)}{dt} = -(\gamma + k)N(t)$$

N is the population of fluorophores, γ is the emissive rate of the fluorophore and k is the rate of non-radiative decay. By integrating this expression with the boundary condition N = N_o at t = 0 we get a simple expression containing the lifetime τ.

$$N(t) = N_o e^{-t\pi}$$

The lifetime decay is then deconvoluted from the response of the system to scattered light, in this case, 100% SOPC small unilamellar vesicles at the same concentration. A bi-exponential lifetime was used because there was a second faster lifetime than the resolution of the instrument (5 ns). The integral that is evaluated using a minimization algorithm is shown below. L(t) is the instrument response function, τ_1 and τ_2 are the two lifetimes, and α_1 and α_2 are the amplitude coefficients of each decay.

$$R(t) = \int_0^t L(t - \mu)[\alpha_1 e^{-\mu/\tau 1} + \alpha_2 e^{-\mu/\tau 2}]d\mu$$

The vesicles were diluted 1:1000 and excited by pulsed 355 nm YAG laser over a 1.25 μs acquisition time. Metal ion were added to cuvette with the vesicles and the changes induced in the lifetime were measured at 25°C with stirring.

Imidazole was added to 5% PSIDA-Cu^{2+}/95% SOPC vesicles [5.2 µM] to compare the difference in lifetimes to 1,4-bisimidazole at [2.0 µM]. Imidazole did not increase the lifetime of the excimer (470 nm) or monomer (397 nm) within experimental error. Addition of 1,4-bisimidazole to the vesicles did cause an increase in the excimer and monomer lifetimes of 15-20 nsec.

DISCUSSION

Vesicles were formed from fluorescently-labeled, metal-chelating lipid PSIDA and two zwitterionic phospholipids. Different compositions of mixed lipid vesicles were investigated because the E/M ratio of pyrene-labeled lipids is very sensitive to the lateral mobility of the probe in the mixed membrane [30]. The phospholipids SOPC and DSPC (Figure 4.5) differ only in the saturation of the acyl chains. This small structural difference has very large consequences for the mobility of lipids in vesicles formed from these natural phospholipids, as observed in the diffusivity of the lipids [37] and the difference in E/M value before metal addition (Chapter 2). The frequency of collisions between excited state pyrene-labeled lipids with ground state pyrene lipids is dependent on the diffusivity of the probe. For instance, high concentration of cholesterol decreases the lateral mobility of lipids in model membranes which shows up as a decrease in the E/M ratio [13]. To control for effects of lipid lateral mobility on specific lipid-ligand binding, the temperature was kept constant and the composition of matrix lipid was varied, rather than investigating different temperatures, which would also have a large effect on the affinity of macromolecules for the bilayer.

In Chapter 2, significant effects of the bilayer phase on the (E/M)$_o$ ratio of PSIDA were observed. The E/M ratio was higher for DSPC lipid bilayers in the gel phase, reflecting aggregation of the probe, and smallest for bilayers in the liquid-crystalline phase. 5% PSIDA and 95% DSPC bilayers have a phase transition temperature of 54.4 °C and are in the gel phase at room temperature. 5% PSIDA and 95% SOPC vesicle have a phase

transition temperature of < 7 °C and are in the liquid-crystalline phase at room temperature. 2.5% PSIDA, 47.% DSPC and 50% cholesterol vesicles have no phase transition temperature [31,33], and have approximately the same surface concentration of chelating lipid as the other two systems since cholesterol is buried in the hydrophobic portion of the bilayer.

E/M ratio and monovalent binding

The small effect of monovalent ligands, N-acetyl-histidine and imidazole, on metal-chelating pyrene-labeled bilayers indicates that the E/M ratio is not strongly affected by monovalent binding (Figure 4.6-7, Figure 4.9). If the excess E/M ratio strongly reflected binding of singly-bound histidine, we would expect a non-linear change in the ratio for added imidazole near the dissociation concentration of imidazole to $Cu^{2+}IDA$ ($K_d \approx 1$ x 10^{-4} M) [26]. Small changes in $\Delta E/M$ at this concentration and beyond for N-acetyl histidine concentration were obtained for all vesicle compositions studied. Thus, for the concentration regimes investigated, the excess E/M ratio of N-acetyl-histidine ($\Delta E/M = E/M - (E/M)_o$) provides a reference for comparison with multivalent binding.

Since the three vesicle compositions spanned a wide regime of lipid bilayer fluidity, changes in the lipid diffusivity by single point binding is probably negligible for small ligands. Otherwise, if the fractional loading of monovalent ligand had a large effect on the dynamics of the bilayer, the E/M value would be expected to change dramatically as it does for the transition from liquid-crystalline to gel phase [30]. If phase separation of the chelating lipids occurred due to monovalent histidine coordination, a large increase in the E/M ratio would be observed since the pyrene lipids would form a region with higher mole fraction and therefore larger excimer signal.

Further experiments to measure the fluorescence lifetime upon imidazole addition show no effect on the lifetime within experimental error, supporting a negligible effect of

imidazole on the membrane dynamics. Thus, the ΔE/M ratio is only slightly affected by monovalent binding to the lipid headgroup below 1 mM.

E/M ratio and multiple lipid coordination by bivalent histidine compounds

Previous studies of multiple lipid coordination to proteins by monitoring pyrene-labeled lipids have shown very small effects on the E/M ratio due to the protein-binding [17,19]. Jones and Lentz [19] have investigated the changes of prothrombin I binding to negatively-charged vesicles with the pyrene-labeled phosphatidyl glycerol (pyr-PG) in unsaturated mixed vesicles. There was no phase separation due to protein binding (the E/M value changed only slightly, ΔE/M = 0.004), even though the protein is known to associate with the bilayer. The E/M ratios were also not altered by addition of $CaCl_2$ which would be expected to prevent the protein from binding.

Protein-associated pyrene-labeled lipids show a decrease in the E/M ratio if the protein binds the lipids hydrophobically [20]. The hydrophobic protein associates directly with the pyrene lipid, decreasing the total number of excimer yielding collisions. Binding of vesicular stomatis virus matrix M protein to mixed vesicles containing pyrene-labeled phosphatidyl glycerol was investigated using the E/M ratio [17]. The effect of protein binding on the E/M ratio was small both in gel phase bilayers and liquid crystalline bilayers. However, the E/M ratio increased due to protein binding during the gel-to-liquid-crystalline phase transition. Since it is not easy to extract effects of the gel-to-liquid-crystalline phase transition from the effect of the protein binding by scanning temperature instead of added ligand, conclusions about the specificity of the protein binding on the E/M ratio cannot be made. Both these studies may have had small changes in the E/M ratio because the lipid-protein interaction was weak or there is a critical number of pyrene-labeled lipid-protein interactions required to observe protein binding using E/M ratios.

A molecule having two imidazole ligands was synthesized in our laboratory for model studies of bivalent binding to 5% PSIDA and 95% phospholipid mixed vesicles.

The structure of the bis-imidazole molecule is shown in Table 4.1. 1,4-bisimidazole contains a carbonyl side chain that would be charged in the pH ranges used for metal binding. The charged side-chain should keep the otherwise neutral, slightly hydrophobic molecule from inserting into the bilayer, and enhances the solubility of the molecule in aqueous solutions. The distance between the lone pair of the unprotonated nitrogens was determined previously using Insight II by Dr. Sanku Mallik and found to range between 7 and 8 Å [34]. These distances may be compared to the known spacing of phospholipids formed into small unilamellar vesicles. For small (20 nm) unilamellar di-myristoylphosphatidylcholine (DMPC) vesicles at 25°C, the surface-area on the outer lamellae has been found to be 70.7 $Å^2$/molecule [35]. Lipid area/molecule is strongly dependent on the saturation of the acyl tails on the lipids as well as the type of lipid headgroup. Assuming a square lattice packing of lipids, the distance between phospholipids would be 8.4 Å for pure DMPC vesicles. Even though this distance is longer than the expected spacing of the nitrogen residues on 1,4-bisimidazole, the 1,4-bisimidazole should be able to coordinate two metal ions due to the 4-5 Å tri(ethylene oxide) spacer between the lipid tails and the headgroup.

We have found that the overall change in the excess E/M ratio after adding bivalent model histidine compounds to Cu^{2+}-loaded mixed bilayers is small ($\Delta E/M_{max}$ = 0.02-0.2), compared to the change in E/M due to metal binding ($\Delta E/M_{max}$ = 0.2-0.9). For 1,4-bisimidazole binding to Ca^{2+}-loaded controls there could be non-specific binding since we observe an increase (SOPC or cholesterol/DSPC) much like the monovalent binding experiments or a decrease (DSPC vesicles). A small increase in the $\Delta E/M$ ratio appears to occur for all vesicles containing 5% PSIDA-Cu^{2+}, although the changes in $\Delta E/M$ are just slightly above the controls containing Ca^{2+}-loaded vesicles. However, the change in excess E/M for cholesterol and SOPC vesicles is much lower than for the DSPC system ($\Delta E/M$ values 0.03 versus 0.2). Differences in the E/M value are due to the presence of the high cholesterol mole fraction in the bilayer, which other investigators have described as

decreasing the lateral mobility of the lipids in the bilayer [30]. Figure 4.11 shows saturation of the $\Delta E/M$ ratio when 1,4-bisimidazole is added to Cu^{2+}-loaded cholesterol vesicles. Similar to the fluid cholesterol-vesicles, a very small increase in the E/M ratio ($\Delta E/M_{max} = 0.02$) was observed for 1,4-bisimidazole binding to PSIDA-Cu^{2+}/SOPC vesicles (Figure 4.12). The smaller increase compared to PSIDA/DSPC vesicles may be due to the larger mean spacing of the PSIDA/SOPC lipids or an increase in the lateral diffusion of the lipids since the bilayer is in the liquid-crystalline phase [36]. X-ray diffraction measurements in the Lα phase show an increase in the mean molecular area for mono-unsaturated SOPC (64.3 Å^2) over DSPC (54.7 Å^2) at 25°C [37]. In any event, the maximum change in $\Delta E/M$ for SOPC vesicles is smaller than the change observed in the cholesterol/DSPC/PSIDA vesicles and an order of magnitude smaller than for PSIDA/DSPC vesicles.

Simple models were used to fit the 1,4-bisimidazole $\Delta E/M$ data for comparison of equilibrium binding parameters for different lipid compositions. The excess E/M values were fitted with Equation 2 developed in Calculations and the fitting parameters reported in Table 4.2. Only for cholesterol containing vesicles did the binding data clearly show non-linear dependence of $\Delta E/M$ with increasing 1,4-bisimidazole concentration. The association constant of a single imidazole coordinating to Cu^{2+}IDA at pH 7.5 is $K_a \approx 5.2$ x 10^3 M^{-1} from calorimetry (Chapter 5) or potentiometry [26]. The binding constants obtained from single-site fits for Cu^{2+}-loaded cholesterol/DSPC or saturated DSPC measurements have apparent binding constants of between 1-2 x 10^6 (M^{-1}) (Table 4.2). Thus, if the $\Delta E/M$ ratio is strongly affected by bivalent binding, a saturation near 2 μM could indicate increased affinity for 1,4-bisimidazole over monovalent association.

Increasing the mole fraction of PSIDA-Cu^{2+} lipid in the bilayer might increase the excimer-yielding collisions if more lipids are present to form bivalent complexes. 1,4-bisimidazole was added to 10% PSIDA-Cu^{2+} / 90% DSPC vesicles to determine if this was the case. Figure 4.13 shows that the maximum $\Delta E/M$ increase was the same magnitude as

for 5% bilayers. The data could not be fitted to the sequential binding model or the single-site model. However, the concentration of ligand at which the ΔE/M reaches saturation is an order of magnitude lower than the 5% PSIDA vesicles. The local concentration of lipids seems to have a large effect on the apparent association constant.

Although ΔE/M increased as 1,4-bisimidazole concentration was increased, this effect could be explained by increases in fluorescence lifetimes of either monomer or excimer upon coordination to the protein-analog. Since the excimer to monomer intensity ratio is proportional to excimer lifetime itself (Equation 5) [38], a change in the excimer lifetime would directly effect the E/M ratio. The fluorescence lifetime of 5% PSIDA/ 95% SOPC vesicles with 2 μM 1,4-bisimidazole present showed an increase (Table 4.4) in the lifetime of both excimer and monomer. Thus, the ΔE/M change could also be due to a specific change in the lifetime of excimer species [13]. When imidazole was added to the vesicles, no change in the lifetimes was observed. Therefore, the change in ΔE/M could be either explained by lipids being held physically near each other to result in more collisions or a change in the diffusivity of the bilayer, caused by specific binding.

Scanning calorimetry of mixed PSIDA small unilamellar vesicles did not show a change in the bilayer thermotropic phase transition when 1,4-bisimidazole was added. For a liquid-crystalline bilayer composed of 5% PSIDA/ 95% SOPC, there was no increase in the ΔCp peak between 7 and 60 °C. Since the main transition is expected to occur between 4-7 °C, no shift to higher temperature is observed. Therefore, there was no increase in the phase transition temperature due to the macromolecule binding. However, the melting transition could be lowered out of the instrument range. For 5% PSIDA-Cu^{2+}, 95% DSPC vesicles there was also negligible effect on the lipid melting transition, 54.04 $\pm$ 0.3 °C for vesicles loaded with bis-imidazole compared to 54.4 $\pm$ 0.3 °C for metallated-vesicles lacking ligand (Chapter 2) . Thus, the association of 1,4-bisimidazole does not lower the melting transition for the saturated vesicles. Scanning calorimetry studies were investigated to show any regions of phase-separated lipid domains induced by specific ligand binding.

Since the calorimetry showed no changes, ligand-induced crystallization of the bilayer is not important for interpretation of 1,4-bisimidazole binding studies to metal-loaded vesicles.

A peptide, porcine renin substrate, containing two histidine residues was added to 5% PSIDA vesicles to determine whether the maximum change in $\Delta E/M$ would be affected in the same manner as for 1,4-bisimidazole. If the excess E/M ratio was determined only by multivalent attachment to histidine residues, a peptide containing two accessible, non-chelating residues could have the same effect on the $\Delta E/M$ ratio as the synthetic 1,4-bisimidazole molecule. The excess E/M ratio increased when the peptide was contacted with 5% PSIDA-Cu^{2+}, 95% DSPC bilayers. The maximum change in E/M was slightly larger than for 1,4-bisimidazole. However, the vesicles are at higher concentration than for the bis-imidazole studies. Due to limited size of the data set, the binding parameters of peptide association were not determined.

Trivalent binding to labeled vesicles

Human renin substrate peptide, containing three histidine residues, was also added to 5% PSIDA vesicles loaded with Cu^{2+} and Ca^{2+}. The $\Delta E/M$ ratio increased with increasing peptide concentration when Cu^{2+} was present and a smaller increase (roughly linear) was observed when Ca^{2+} was present. The association constants obtained from fits of the data did not increase significantly compared to 1,4-bisimidazole binding (Table 4.3). However, for 5% PSIDA-Cu^{2+} / 95% SOPC vesicles, the association constant was larger than for 5% PSIDA-Cu^{2+}/ DSPC vesicles. This difference may be due to differences in the diffusivity of the SOPC matrix lipid or higher affinity for the peptide for these mixed vesicles [36].

Any subsequent increases in the $\Delta E/M$ ratio due to the trivalent peptide were compared to the bivalent 1,4-bisimidazole data. It is intuitively obvious that lipids brought adjacent to each other by multivalent ligand binding will form more excimer collisions than

labeled lipids that are not brought adjacent, but instead are spaced by several intervening matrix lipids. Two-point binding to adjacent lipids may have as large an effect on the ΔE/M ratio as trivalent binding with imidazole moieties spaced several lengths larger than a lipid dimension, because the third residue does not directly induce an excimer collision. However, ΔE/M$_{max}$ did increase compared to 1,4-bisimidazole, which might also indicate more collisions due to trivalent attachment. This result provides more evidence that the ΔE/M ratio is sensitive to multivalent histidine compounds and provides an effective method to probe the effects of lipid organization. An alternative explanation is that binding effects the fluorescent lifetime, as for bivalent binding experiments.

Polymer binding and E/M ratio

Histidine polymers showed a much larger effect on the ΔE/M ratio than the smaller model complexes. For all three mixed vesicle systems, poly-L-histidine caused the excess E/M ratio to increase and then decrease back to the initial value over the polymer concentration range nano- to micromolar. The ΔE/M$_{max}$ value was much larger for poly-L-histidine binding compared to the small molecule complexes. For instance, comparison of ΔE/M$_{max}$ values for 1,4-bisimidazole to poly-L-histidine binding to 5% PSIDA/SOPC vesicles shows an increase from 0.02 to 0.2. The increase in the E/M value can be explained by many more ligand-lipid interactions than for smaller histidine-containing compounds. Alternatively, a larger effect on the fluorescent lifetime could also explain the data.

An increase followed by a decrease in surface bound ligand-receptor species with increasing ligand concentration is predicted from binding models developed for multivalent receptor-ligand binding on cell surfaces [27]. The amount of surface multivalent bound lipids, or "receptors" is predicted to increase to a maximum value as poly-L-histidine binds to multiple lipids. After this maximum value, the number of ligand cross-linked lipids eventually decreases back to monovalent ligand-bound lipids. This behavior is also

predicted for bivalent binding (Equation 4). Polyvalent histidine ligands, such as poly-L-histidine with at least 80 histidine residues/polymer, would be expected to form many contacts with metal-chelating lipids, effectively crosslinking the lipids, thereby causing an increase in the number of excimers.

The qualitative features of poly-L-histidine binding showed an increase in $\Delta E/M$ and then a decrease in $\Delta E/M$ ratio when copper is present as concentration of poly-L-histidine is increased. The same type of behavior is seen for all 5 mol% PSIDA-Cu^{2+} mixed bilayers at roughly the same poly-L-histidine concentration for vesicles between 20-10 μM total lipid. In contrast, poly-L-histidine added to Ca^{2+}-loaded vesicles shows a slight change in the E/M ratio, similar to the changes in $\Delta E/M$ observed for monovalent binding. Since the concentration at which the $\Delta E/M_{max}$ value occurs for poly-L-histidine (0.01 μM) is lower than for 1,4-bisimidazole (2 μM) for vesicles at the same concentration, the avidity of poly-L-histidine is higher for the bilayer than 1,4-bisimidazole. Since poly-L-histidine can bind to the membrane through multiple affinity interactions, the $\Delta E/M$ behavior could be described as increasing poly-L-histidine binding causing metal-chelating lipids to form into domains. After more poly-L-histidine has bound, the binding valency remains the same, yet the polymer binding is more evenly distributed resulting in no enriched lipid domains.

Previous studies of labeled phosphatidic acid mixed bilayers and poly-L-lysine binding showed an increase in the exchange frequency of nitroxide-labeled lipids and a large increase in the thermal transition due to poly-L-lysine binding [39]. Only half of the poly-L-lysine residues were able to bind to the bilayer, as determined through spin labeling studies. Crystallized domains in the lipid bilayer were imaged using freeze-etch prepared samples and TEM microscopy. Thus, polymer binding can have a very large-scale, macroscopic effect on the bilayer.

Additional fluorescence microscopy measurements on mixed 5% PSIDA/ 95% SOPC monolayers were made by Dr. Kevin Maloney [40]. Before poly-L-histidine

addition, no fluorescent domains were visible at the excimer wavelength. When Cu^{2+} was added to the subphase or the lipids were pre-metallated with Cu^{2+}, fluorescent patches composed of bound poly-L-histidine could be observed when suitable filters were used to view the excimer wavelength. Poly-L-histidine has no effect on fluorescence of the monolayer when metal was not present. Thus, poly-L-histidine appears to bind through multiple lipids since both changes in $\Delta E/M$ measured with vesicles and fluorescence microscopy of monolayers show a specific change in the excimer fluorescence when Cu^{2+} is present and little change when Ca^{2+} is present.

Both results with polymer-induced changes in fluorescent properties of monolayers and vesicles are consistent with multivalent binding of the poly-L-histidine to the bilayer through Cu^{2+}-coordination. Yet there could be other explanations for the change in the $\Delta E/M$ value. It is unclear whether the polymer is able to strip the metal from the bilayer to cause the decrease in $\Delta E/M$ to baseline or whether the binding of poly-L-histidine reverts to evenly distributed binding. When the polymer concentration is the same order of magnitude as the metal concentration there is an excess of histidine residues capable of chelating the metal ion. Removal of the metal ion would have a large effect on the E/M ratio and the lifetime, as shown in Chapter 2. Since changes in the lifetime were observed with the much smaller 1,4-bisimidazole molecule, the poly-L-histidine might also affect the lifetime through changes in the diffusivity of the lipids due to poly-L-histidine-induced binding.

The effect of poly-L-histidine can not be solely driven by aggregation of the vesicles through polymer-driven inter-vesicle crosslinking, although crosslinking was previously observed with poly-L-lysine binding to negatively-charged vesicles [41]. No visible turbidity effects were observed at the low dilutions of vesicles used in our studies. The magnitude of the E/M increase was affected by vesicle concentration and could reflect some inter-vesicle cross-linking by the polymer. However, a maximum value followed by a decrease back to baseline is observed for all dilutions of vesicles indicating that the

qualitative increase in excimers is similar. When the change in vesicle $\Delta E/M$ is combined with results from monolayer fluorescence microscopy we find that the results are consistent with multiple lipid coordination, even if aggregation complicates the vesicle $\Delta E/M$ results.

The concentration of the maximum $\Delta E/M$ upon polymer association can be compared to the maximum $\Delta E/M$ value of the bis-imidazole and peptide compounds at the same vesicle concentration. When the concentration of added poly-L-histidine is scaled by the maximum number of histidines per polymer (80), by multiplying the origin of Figure 4.22, we see that the magnitude of E/M maximum value for poly-L-histidine scales over the same concentration of ligand where bis-imidazole shows a $\Delta E/M$ maximum effect (8.0 vs. 2.0 μM). The picture that emerges from vesicle and monolayer measurements is specific polymer-driven lipid reorganization.

CONCLUSIONS

By monitoring the excimer to monomer ratio of pyrene-labeled metal-chelating lipids, changes in the lipid bilayers due to ligand binding through metal coordination could be followed. Simple models were used to compare the E/M data for different histidine compounds. Molecules containing two histidines were contacted with metal-chelating pyrene-labeled vesicles to determine if a compound with only two histidines could bring two lipid molecules together resulting in an excess excimer "signal". Selective enhancement of the excimer to monomer ratio due to ligand binding occurred when copper was present. Mixed vesicle systems composed of 5% PSIDA-Cu^{2+} lipid and 95% phospholipid also showed increases in the excimer to monomer ratio upon divalent and trivalent peptide addition. The magnitude of the E/M increase could not be increased by doubling the concentration of pyrene probe in the bilayer. Histidine-rich polymers showed a much larger effect on the E/M ratio that occurred at lower macromolecule concentration. We propose that the fluorescently-labeled metal-chelating vesicles provide a sensitive assay

of a ligand's ability to organize the lipid bilayer through specific metal-histidine coordination.

EXPERIMENTAL

Formation of fluorescently-labeled metal-chelating vesicles

Stock solutions of highly pure (>99%) lipids were prepared in volumetric flasks in chloroform (HPLC grade). Phospholipids were obtained from Avanti Polar Lipids. PSIDA was synthesized by Darryl Sasaki and found to be pure by elemental analysis and NMR. Typically, 10 μmoles total of lipid was measured using volumetric pipettes into a 12 ml conical glass centrifuge tube. The chloroform was evaporated under Argon atmosphere or evaporated under aspirator vacuum while rotating on a Buchi rotary evaporator fitted with a septum. The coated tubes were dried 12 hr. under high vacuum. 3 ml of [20 mM MOPS, 0.1M NaCl, pH 7.5] buffer was added to the tube and the solution heated above the highest lipid components melting transition while capped with a septum. The mixture was probe tip sonicated for 12-15 minutes in ice under Argon atmosphere using a Heat Systems (now Misonic) horn sonicator at level 4, 50% output, 25-35 Watts. The solutions were observed to be clear or slightly opalescent indicating very small vesicles. The titanium fragments were removed by centrifugation at 11,000 rpm for 20 minutes in a microfuge. The vesicles were used only for 3 days and remained clear in solution for months if no metal was present.

Size distribution of typical PSIDA/DSPC vesicles

The size distribution of the vesicles before metallation were measured on a Northrop & Leeds quasi-elastic light scattering apparatus with a argon laser as light source. The vesicle solution was compared to MOPS buffer at 25 °C at 90° scattering angle.

Refractive index of PBS, clear scatterers and a size cutoff of 6 μ was assumed at 25°C. The commercial software was used to analyze the data to produce a size distribution. The mean diameter was found to be 44 nm with a size range of 60 nm. This is considered to be a very broad distribution of vesicles. The vesicle size distribution was asymmetric starting at approximately 22 nm.

Fluorescence experiments

Vesicle stock solutions were diluted 1:150, 1:500 or 1:1000 for fluorescence experiments to prevent turbidity effects due to inter-vesicle cross linking by macromolecule. UV absorption of vesicle samples at 1:500 dilution showed no absorption spectra due to turbidity (300 nm). A Shimadzu RF-540 spectrofluorimeter fitted with temperature controlled bath was used for fluorescence intensity measurements. For a typical experiment, the vesicles were diluted in MOPS buffer to make a final volume of 3 ml solution and placed in a quartz cuvette. The excitation wavelength was 346 nm with excitation and emission slits set at 5 nm. The chart speed was 10 mm /min. The signal to noise of the machine was periodically checked and found to be S/N ≈ 100 (Raman band of H_2O). The water Raman emission band did not exceed the emission intensity of pyrene for any lipid concentration used. Similar fluorescence emission spectra were also obtained on a SLM 4800 instrument (SLM Instruments).

Vesicles were metallated during fluorescence experiments using the change in E/M due to specific metal binding to monitor metallation [Chapter 2]. The metal concentration deemed saturation was determined by adding enough metal to cause the decrease in E/M to be 0.1 unit above the value shown in (Chapter 2, Table 3) so as not to have excess metal present. Presence of excess metal during ligand titration would decrease the overall change in E/M ratio since free metal competitively binds to histidine-rich compounds in solution. For comparison to the fluorescence metallation procedure, PSIDA/DSPC/cholesterol vesicles were metallated with 4-fold excess of copper chloride to PSIDA lipid and dialyzed

against buffer (3 ml vesicles against 300 ml buffer) for three hours. The E/M behavior for dialyzed, metallated-cholesterol vesicles was identical to vesicles metallated in the cuvette.

Ligands containing histidines were added directly to the same sample cell and the intensities at 377 nm and 470 nm measured from the analog (paper) output. The experimental error was determined by adding buffer to sample cells and measuring the change due to different aliquots of buffer. This error was comparable to the error determined from averaged E/M measurements during metallation studies of vesicles.

Preparation of 1,4-bisimidazole

1,4-bisimidazole was synthesized by Dr. Sean D. Plunkett [42]. The methyl ester group was cleaved off in MeOH with KOH at 50 °C for 24 hr. by Dr. Darryl Sasaki. The compound was filtered and recrystallized 4 times in EtOH. The crystals were dried at 50 °C in a vacuum oven and analyzed by ^{1}H NMR and elemental analysis. 1,4-bisimidazole was obtained as the di-hydrochloride, monohydrate ($C_{15}H_8N_4O_3Cl_2$) (calculated 14.81 %N, 48.27 %C, 4.88 %H), found 14.43 %N, 46.92 %C, 4.49 %H, MW 373.24 g/mole.

Differential scanning calorimetry of bis-imidazole bound to PSIDA mixed vesicles

Small unilamellar vesicles were formed as for the fluorescence experiments by probe tip sonication. The total lipid concentration was between 1.4-4.0 mM total lipid and was determined using phosphate assay [43]. The scan rate used was 45 °C/hr which was found (Chapter 2) to have no kinetic limitations. Reversible thermal transitions were shown by scanning at least twice for each sample . In general, the second scan was used for the figures (Chapter 2).

Samples of metal-loaded vesicles with excess 1,4-bisimidazole (1.5 fold excess relative to PSIDA) were used in a Microcal (Northampton, MA) MCS DSC under external computer control. The raw data were acquired normalized by the scanrate and the baseline

subtracted using Microcal Origin software. The transition temperature ($\Delta C_{p,max}$) was obtained directly from the data directly since the baseline was linear.
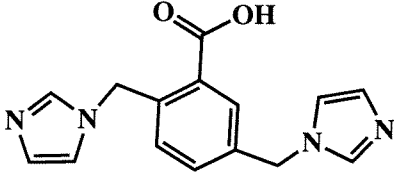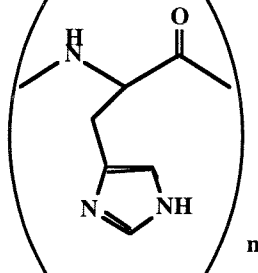
Fluorescence lifetime measurements

A YAG laser fitted with an oscillating shutter was used for pulsed lifetime experiments [11]. The instrument response at 25°C was acquired using 100% SOPC vesicles diluted 1:1000 in MOPS buffer to control for light scattering. The excitation was set at 355 nm. Monomer lifetime was acquired by using emission wavelength 397 nm (second vibronic band of monomer) with a 385 nm cutoff filter and neutral density filters with slits 1 mm in the double beam monochromator. Excimer lifetime was acquired by using an emission wavelength of 470 nm. with 385 nm cutoff and neutral density filters with 0.5 mm slit on the outside and 1 mm slit in the middle monochromator slit. Metal solution was added to the cell with rapid stirring.

The data were deconvoluted using a bi-exponential decay using the instrument response function. The minimum lifetime deemed faster than the response time of the machine is 5 ns [44]. Thus, lifetimes lower than 5 nanoseconds are artifacts of the fitting algorithm or represent fluorescence lifetimes faster than the resolution of the instrument. A bi-exponential decay was chosen because there is a faster lifetime component. χ^2 values of less than 4×10^{-4} were deemed acceptable for reporting.

Table 4.1. Structures of model compounds used in binding studies to metal-chelating, pyrene-labeled vesicles

Compound	Number of "Histidines"	Structure
1,4-bisimidazole	2	
Porcine Renin Substrate	2	N-Ac-Asp-Arg-Val-Tyr-Ile-**His**-Pro-Phe-**His**-Leu-Leu-Val-Tyr-Ser-COOH
Human Renin Substrate	3	N-Ac-Asp-Arg-Val-Tyr-Ile-**His**-Pro-Phe-**His**-Leu-Val-Ile-**His**-Asn-COOH
Poly-L-Histidine	80-92	

Table 4.2. Binding parameters obtained for non-linear least squares fits of single-site model (Equation 2) with experimental $\Delta E/M$ versus total 1,4-bis concentration added to fluorescently-labeled metal-chelating vesicles with different composition. Binding constants from fits were to be used to compare effect of multivalent binding on $\Delta E/M$ ratio.

Vesicle composition	K_{app} (M^{-1})	$\Delta(E/M)_{max}$	χ^2 ($\times 10^{-3}$)
5% PSIDA/DSPC	$1.9 \pm 0.8 \times 10^6$	0.16 ± 0.02	1.8
2.5% PSIDA/47.5% DSPC/ 50% cholesterol	$2.5 \pm 0.6 \times 10^6$	0.03 ± 0.02	0.089

Table 4.3. Binding parameters obtained from fits of human Renin peptide binding to pyrene-labeled, chelating mixed vesicles at pH 7.5. Single site model (Equation 2) used to fit data to get binding parameters.

5% PSIDA in	K_{app} (M^{-1})	$\Delta(E/M)_{max}$	χ^2 $(x\ 10^{-3})$
DSPC	$2.5 \pm 0.3 \times 10^6$	0.55 ± 0.01	3.5
SOPC	$9.4 \pm 2.5 \times 10^6$	0.02 ± 0.002	0.1

Table 4.4. Parameters determined deconvolution of time-resolved fluorescence lifetime measurements using a bi-exponential fit. Excitation at 355 nm; 385 cutoff filter with acquisition over 1.25 μsec. Data were deconvoluted from instrument response function determined with 100% SOPC vesicles. 5% PSIDA/95% SOPC vesicles [total lipid] = 3.2 μM in [20 mM MOPS, 100 mM NaCl, pH 7.5] at 25 °C.

5% PSIDA-Cu^{2+}/95% SOPC vesicles +	Monomer Lifetime 397 nm (nanoseconds)	Excimer Lifetime 470 nm (nanoseconds)
vesicles	33 ± 5	41 ± 5
vesicles + imidazole (5.2 μM imidazole)	35 ± 5	40 ± 5
vesicles + 1,4-bisimidazole (2.0 μM bisimidazole)	46 ± 5	63 ± 5
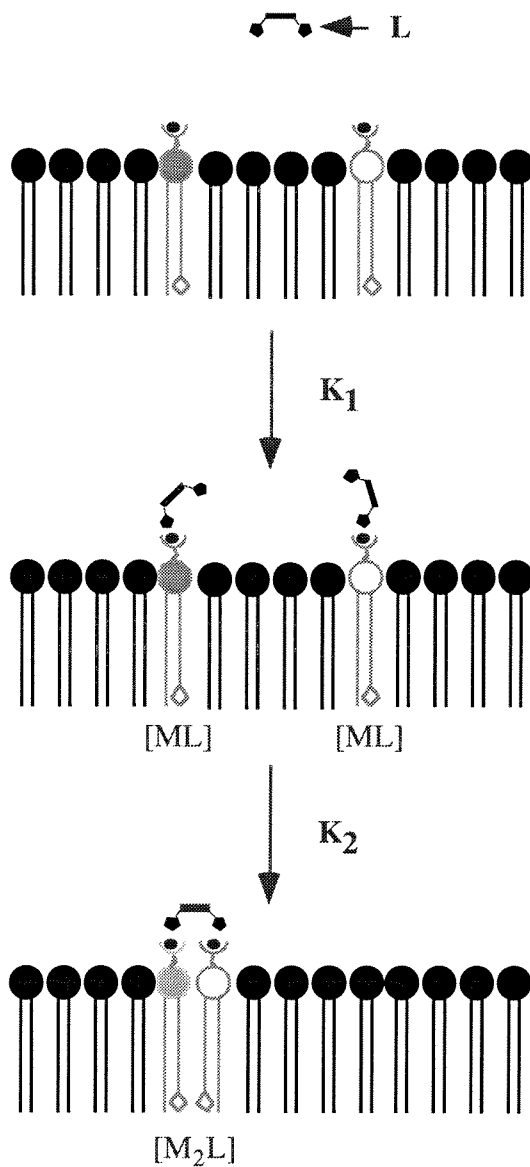
Figure 4.1. Equilibrium species that can form with a bivalent bis-histidine ligand [L] binding to metal-chelating IDA lipids in a synthetic bilayer. Solid, filled chelating lipids represent excited state monomer and open chelating lipid represents ground state monomer. Formation constants for monovalent [ML] and bivalent [M₂L] bound species are indicated.
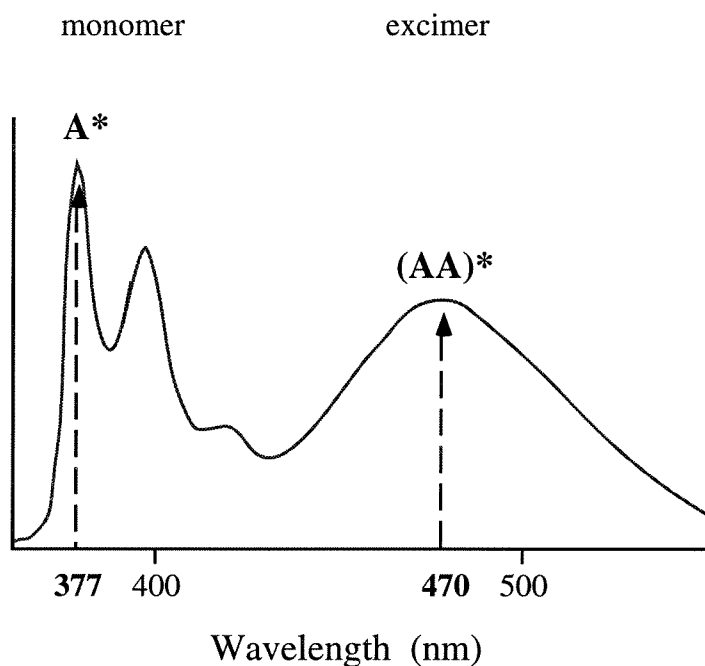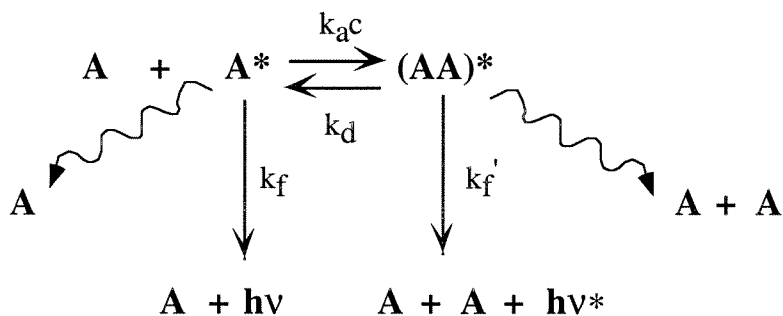
Figure 4.2. Kinetic scheme for excimer formation [30]. The pathways with straight arrows show processes that result in fluorescence. Shown below is a representative steady-state fluorescence emission spectrum showing pyrene-labeled lipids mixed with phosphatidyl choline lipids incorporated into vesicles is shown to illustrate the peaks measured to determine monomer and excimer intensity.

No ligand

$(E/M)_0$

M   G   E

+ ligand

E/M

E   E   M   G   M
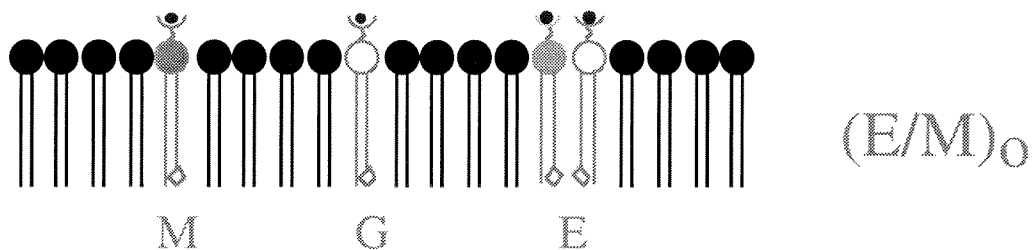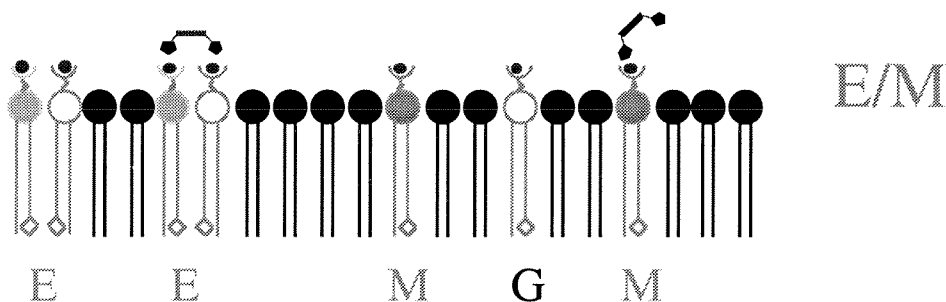
Excess Excimer

$$\Delta E/M = E/M - (E/M)_0$$

Figure 4.3. Pictorial explanation of excess excimer to monomer ratio ($\Delta E/M$). The species that contribute to membrane fluorescence before ligand addition M = monomer, E = excimer. Bivalent ligand bound to lipids contribute to the excimer and while monovalent bound species will contribute to monomer fluorescence. $\Delta E/M$ reflects the excess excimers that are due to ligand binding.
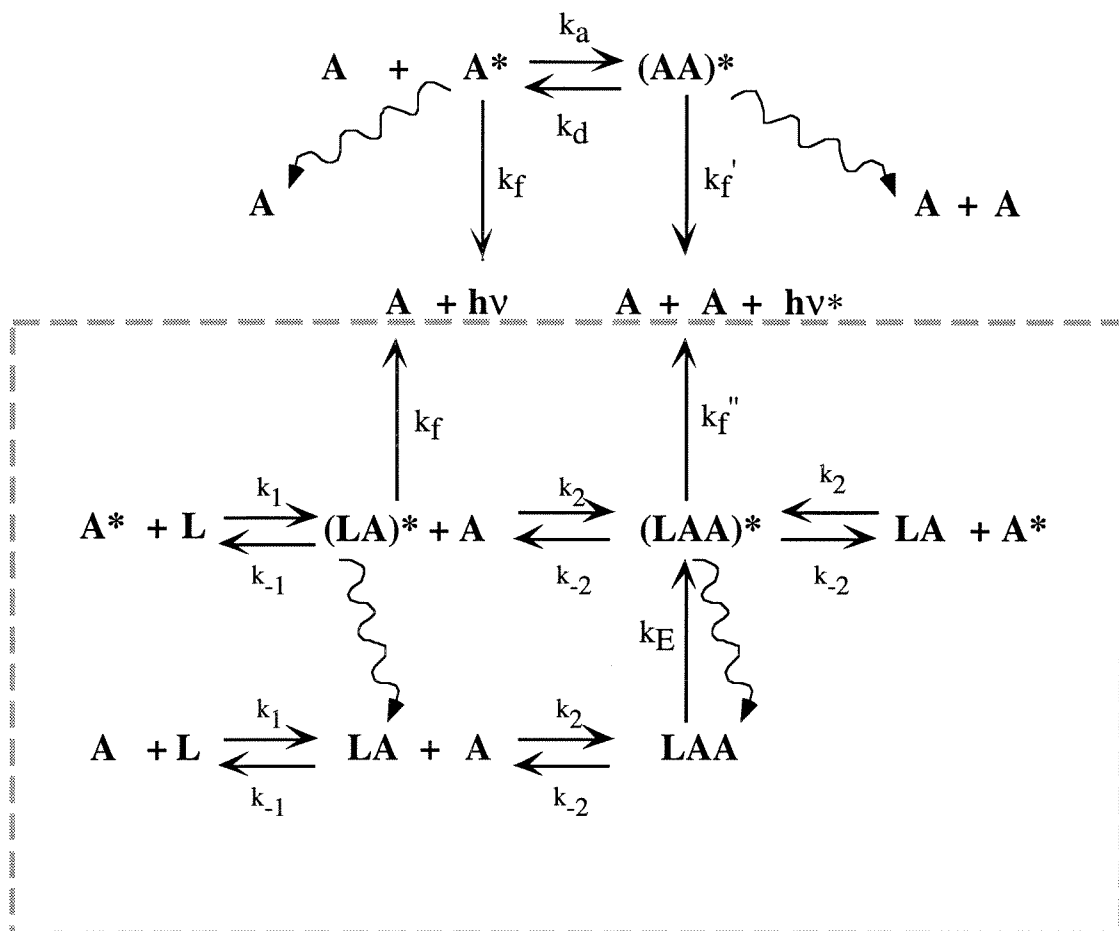
Figure 4.4. Kinetic scheme showing excimer and monomer fluorescent species formed upon bivalent ligand binding. Fluorescent excited state species are indicated with an asterisk. Self-quenching pathways are indicated with undulating arrow. Species in box are due to ligand binding to pyrene-labeled lipid A.
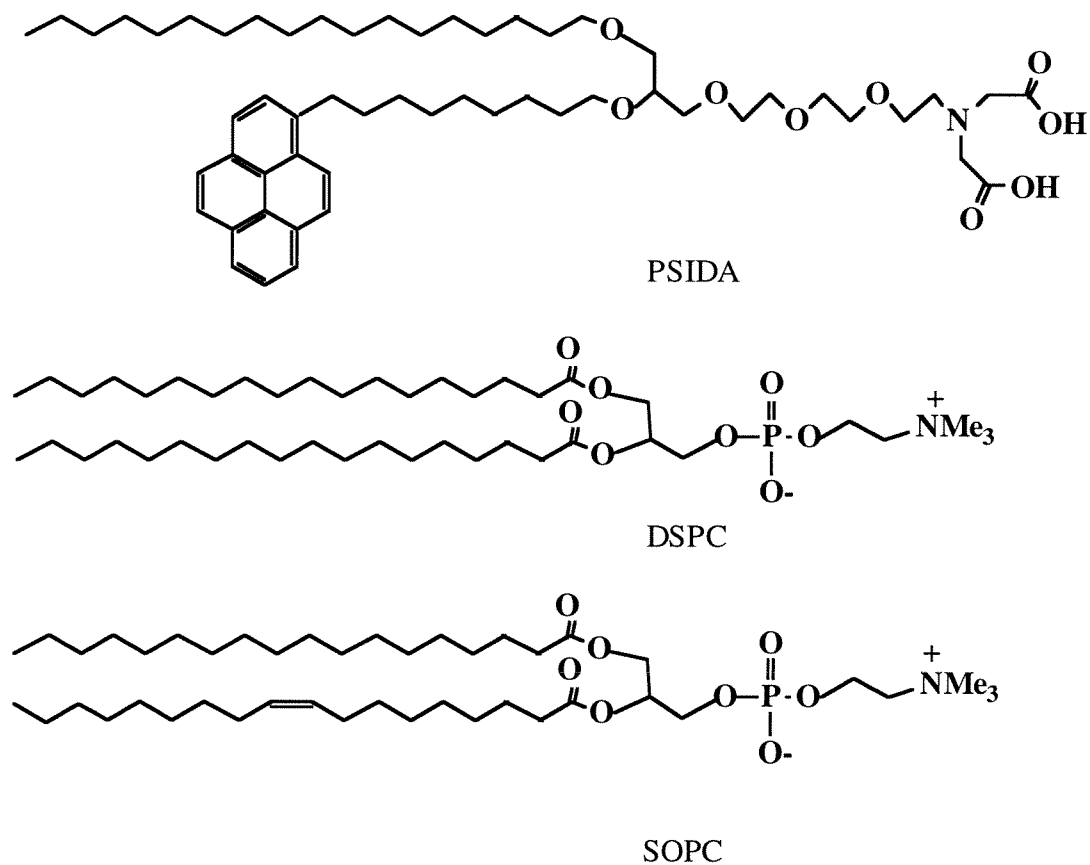
Figure 4.5. Lipids used to form fluorescently-labeled vesicles. The three lipids are PSIDA, DSPC and SOPC (Chapter 2).
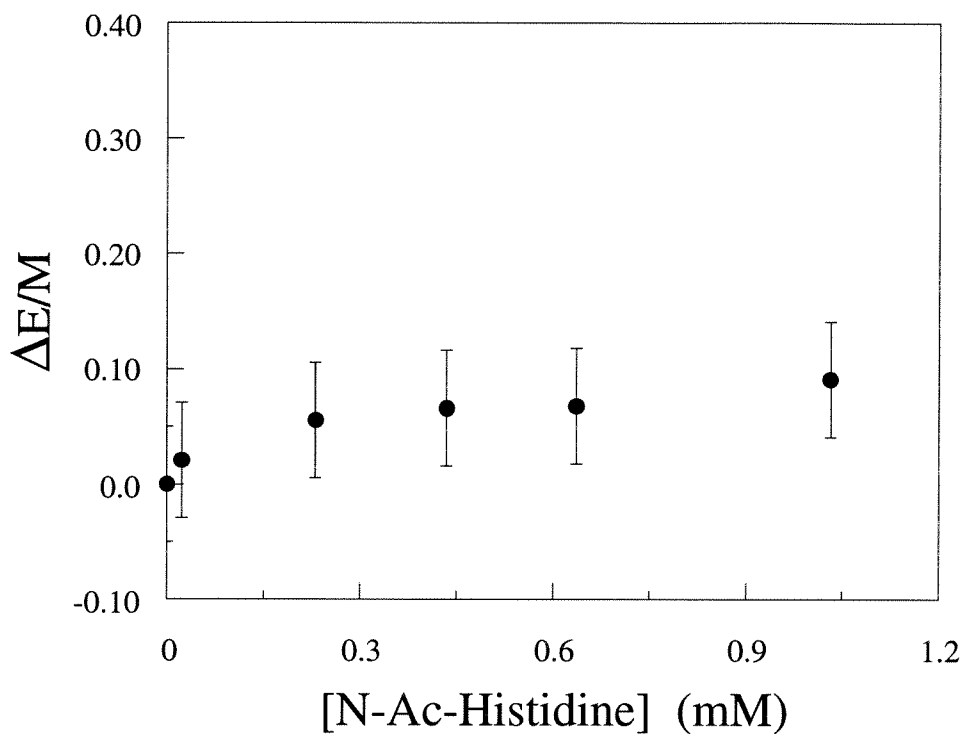
Figure 4.6. Change in fluorescence E/M due to binding of N-acetyl histidine added to 5% PSIDA/ 95% DSPC vesicles [20 μM total lipid] in buffer [0.02M MOPS, 0.1M NaCl, pH 7.5] at 25 °C. Copper [2.2 μM] added to vesicles in cuvette; $(E/M)_0$ = 0.23.
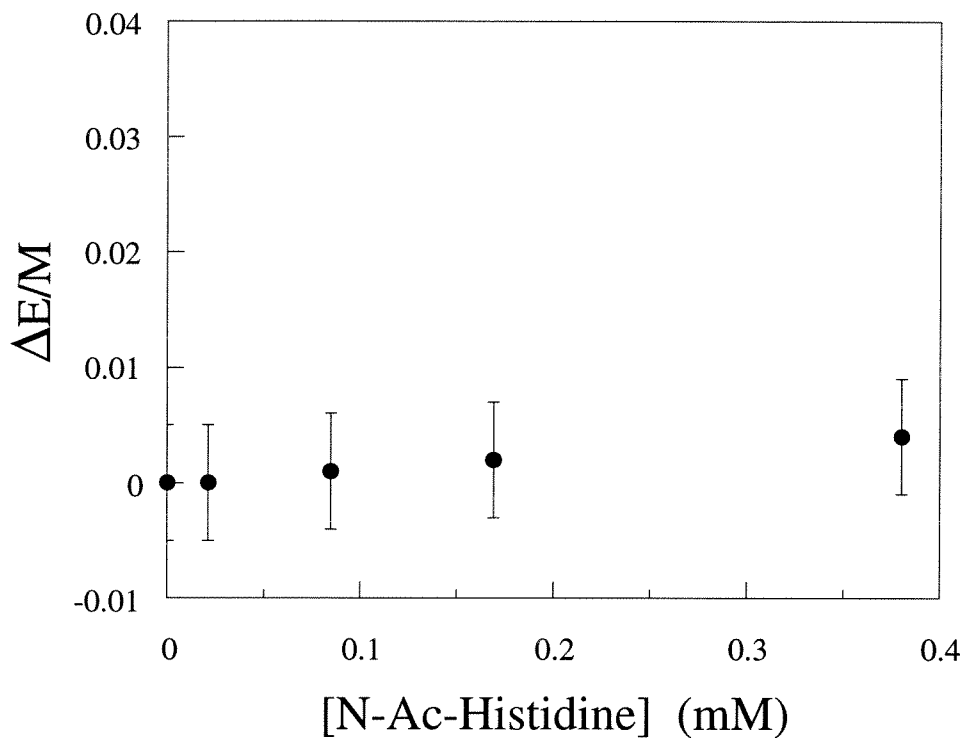
Figure 4.7. Change in fluorescence E/M due to binding of N-acetyl histidine to 2.5 mol%/ 47.% DSPC/ 50% cholesterol vesicles [40 μM total lipid] at pH 7.5 in [20 mM MOPS, 0.1M NaCl] buffer. Vesicles were metallated with 1.2 μM $CuCl_2$; ; $(E/M)_o = 0.07$.
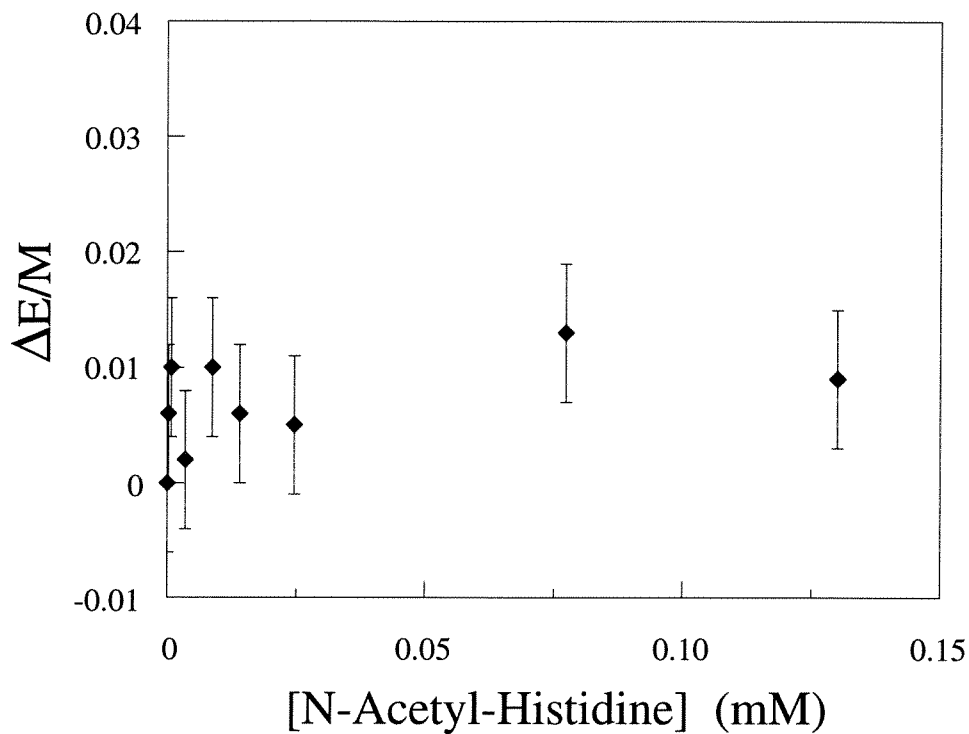
Figure 4.8. Change in fluorescence E/M due to binding of N-acetyl-histidine to 5% PSIDA/ 95% SOPC vesicles, added $[CuCl_2]$ = 0.14 μM; $(E/M)_o$ = 0.18. N-acetyl histidine added to [6.8 μM total lipid]. Vesicle solutions made in buffer [20 mM MOPS, 100 mM NaCl, pH 7.5] at 25 °C.
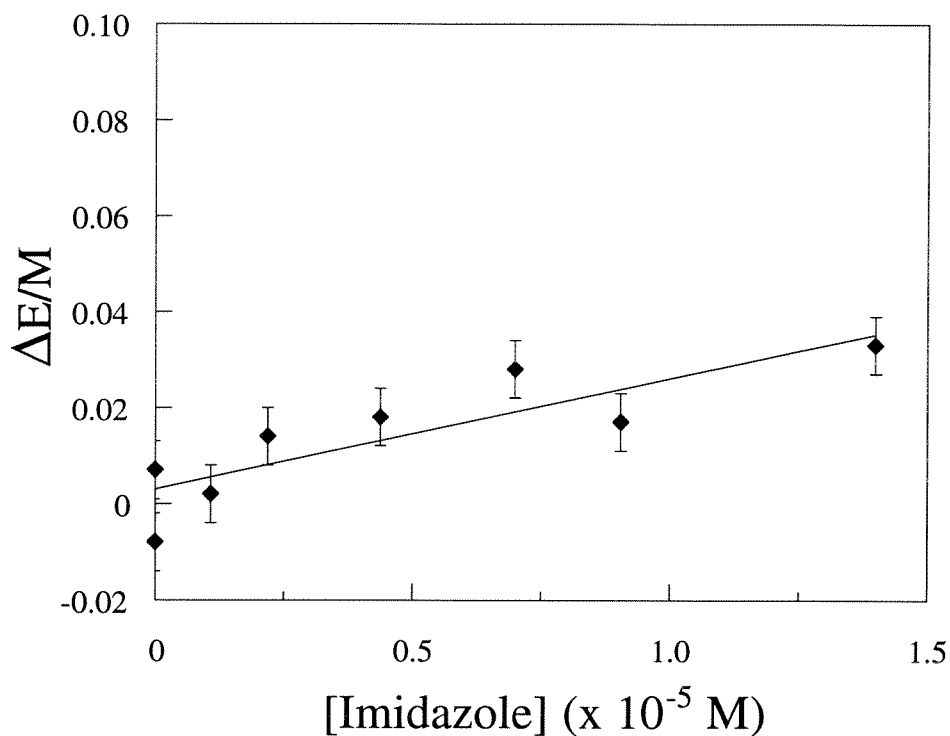
Figure 4.9. Change in fluorescence E/M due to binding of imidazole 5% PSIDA-Cu^{2+} /95% SOPC vesicles. Metal added to vesicles in cuvette, $[CuCl_2]$ = 2.2 μM at 25 °C in [20 mM MOPS, 100 mM NaCl, pH 7.5] buffer; $(E/M)_o$ = 0.18.
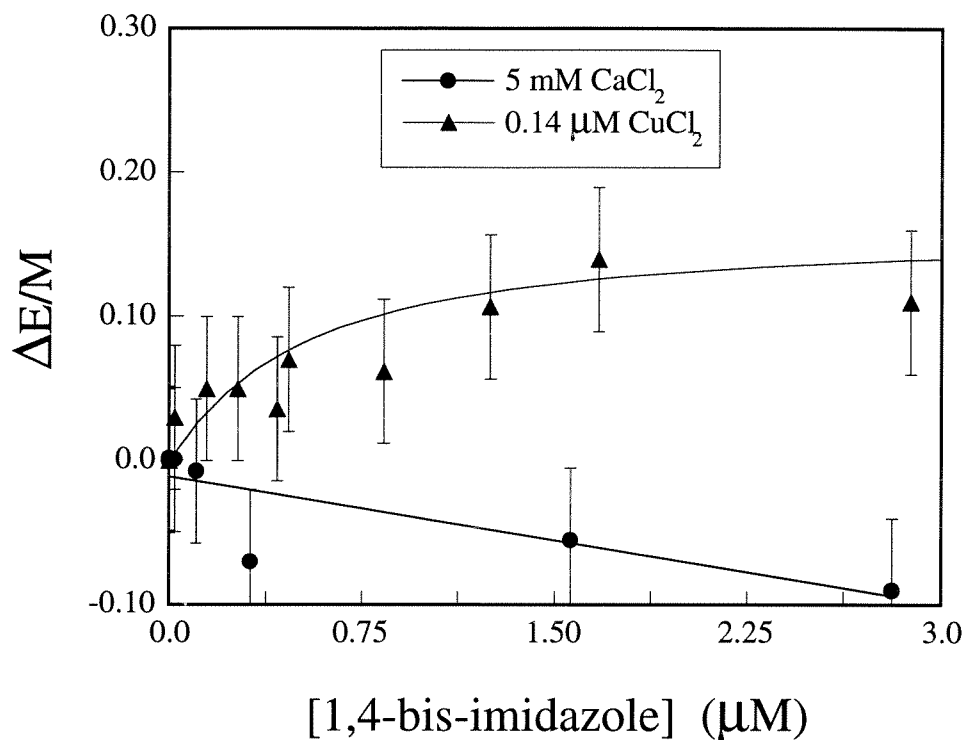
Figure 4.10. Change in fluorescence E/M due to binding of 1,4-bisimidazole to 5% PSIDA/ 95% DSPC vesicles [2.8 mM total lipid] and subsequent effect of excess E/M. Data shown is fitted with a single site binding model, Equation 2. Binding parameters obtained from fits are in Table 4.2. For Cu^{2+} metallated vesicles $(E/M)_o = 0.39$ and for Ca^{2+} $(E/M)_o = 0.55$.
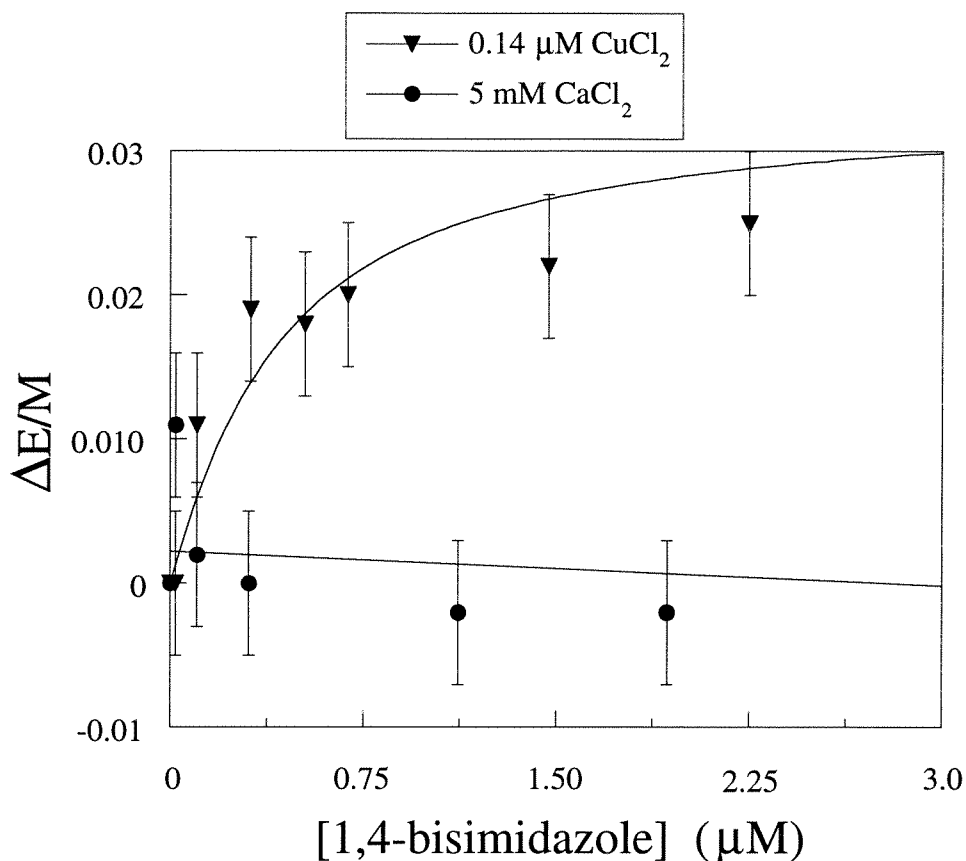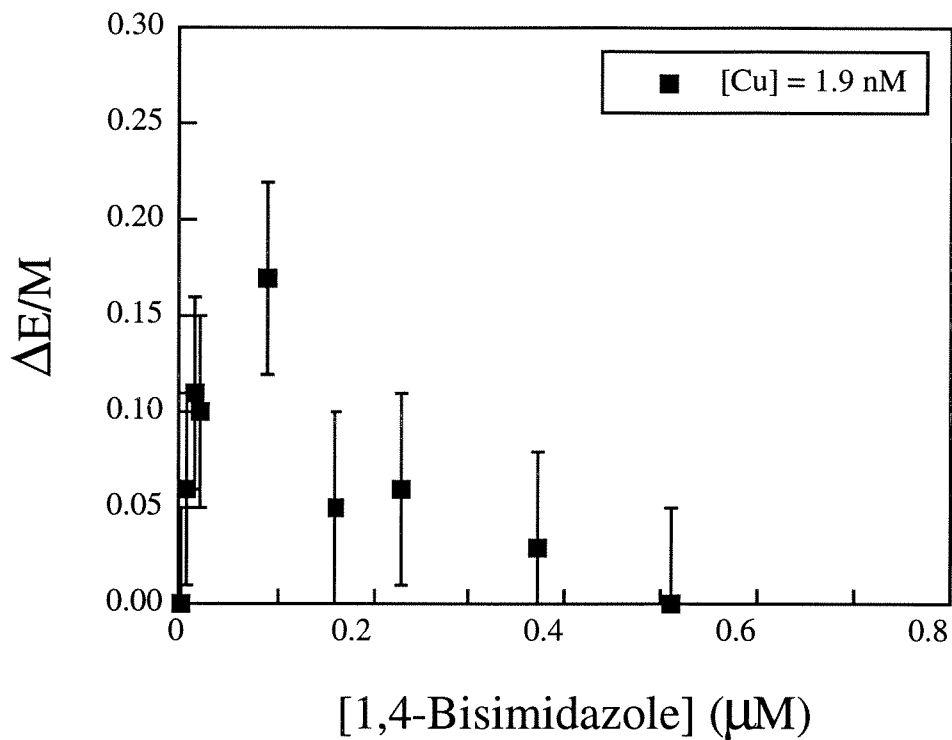
Figure 4.11. Change in fluorescence E/M due to binding of 1,4-bisimidazole added to 2.5% PSIDA/ 47.5% DSPC/ 50% cholesterol vesicles. $CuCl_2$ added to pre-formed vesicles [6.1 μM total lipid]. Data shown is fitted with a single site binding model, Equation 2. Binding parameters obtained from fits are in Table 4.2. For Cu^{2+} metallated vesicles $(E/M)_o = 0.12$ and for Ca^{2+} vesicles $(E/M)_o = 0.11$.
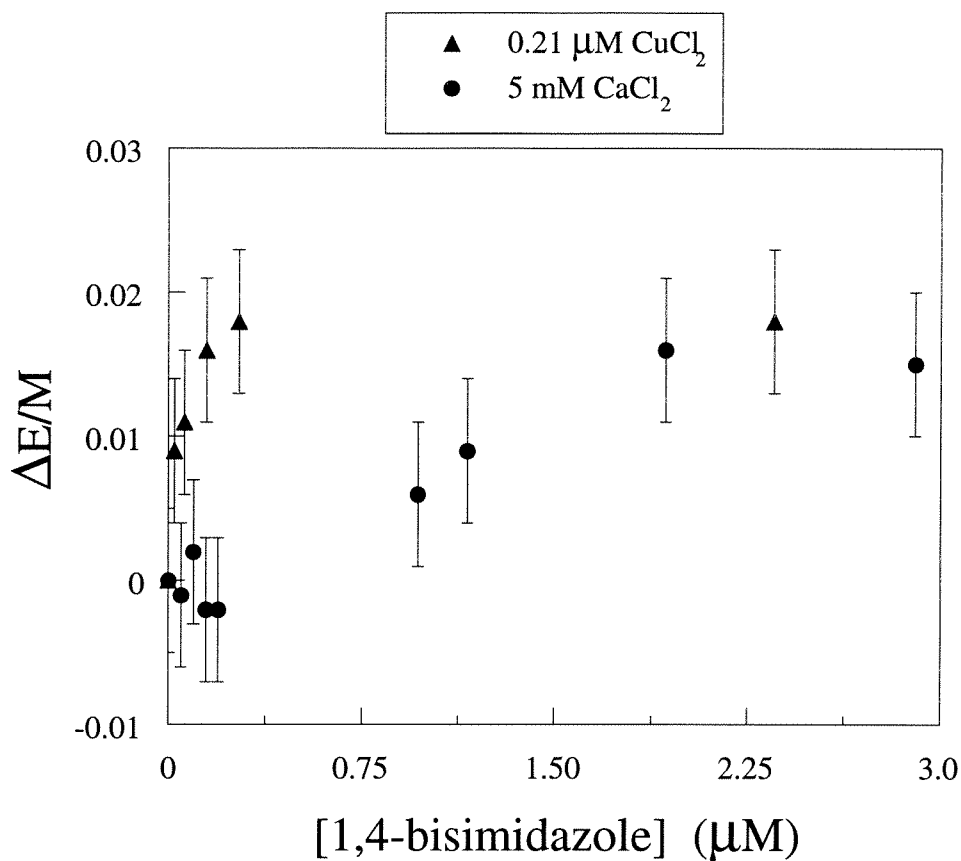
Figure 4.12. Change in fluorescence E/M due to binding of 1,4-bisimidazole added to 5% PSIDA/ 95% SOPC vesicles excess E/M ratio [7.8 μM total lipid]. For Cu^{2+} metallated vesicles $(E/M)_o = 0.26$ and for Ca^{2+} vesicles $(E/M)_o = 0.18$.
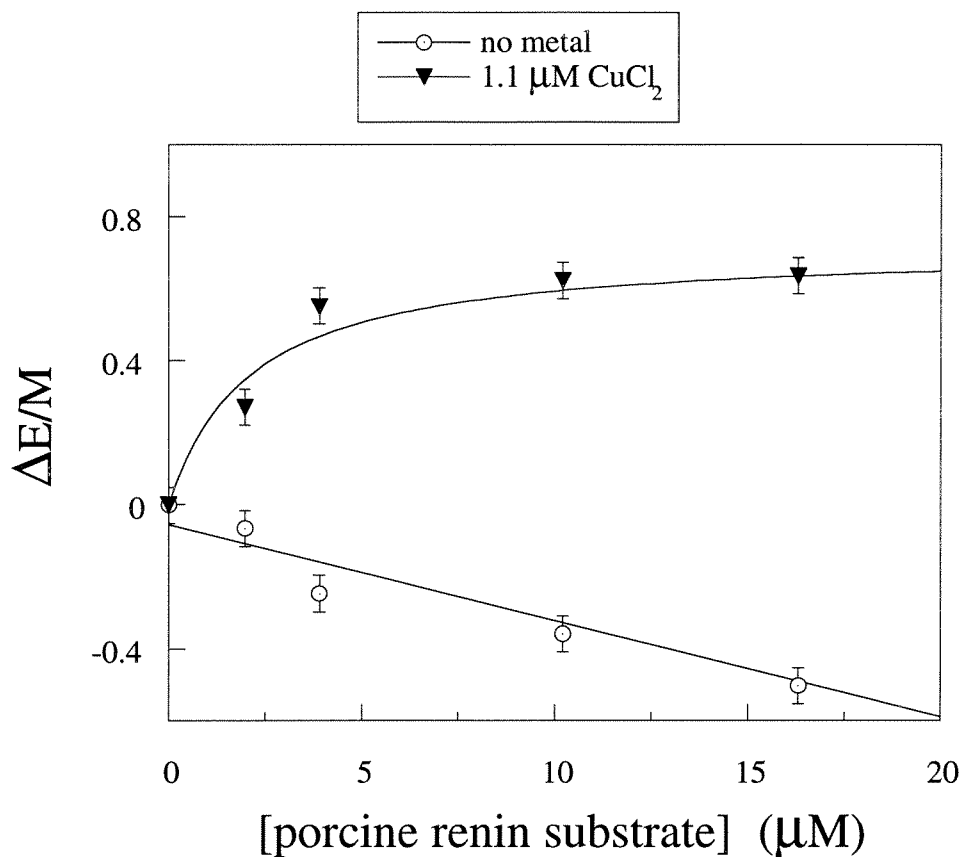
Figure 4.13. Change in fluorescence E/M due to binding of 1,4-bisimidazole to 10% PSIDA/ 90% DSPC vesicles. Metal concentration as indicated at 25 °C in [20 mM MOPS, 100 mM NaCl, pH 7.5] buffer; $(E/M)_o = 0.83$
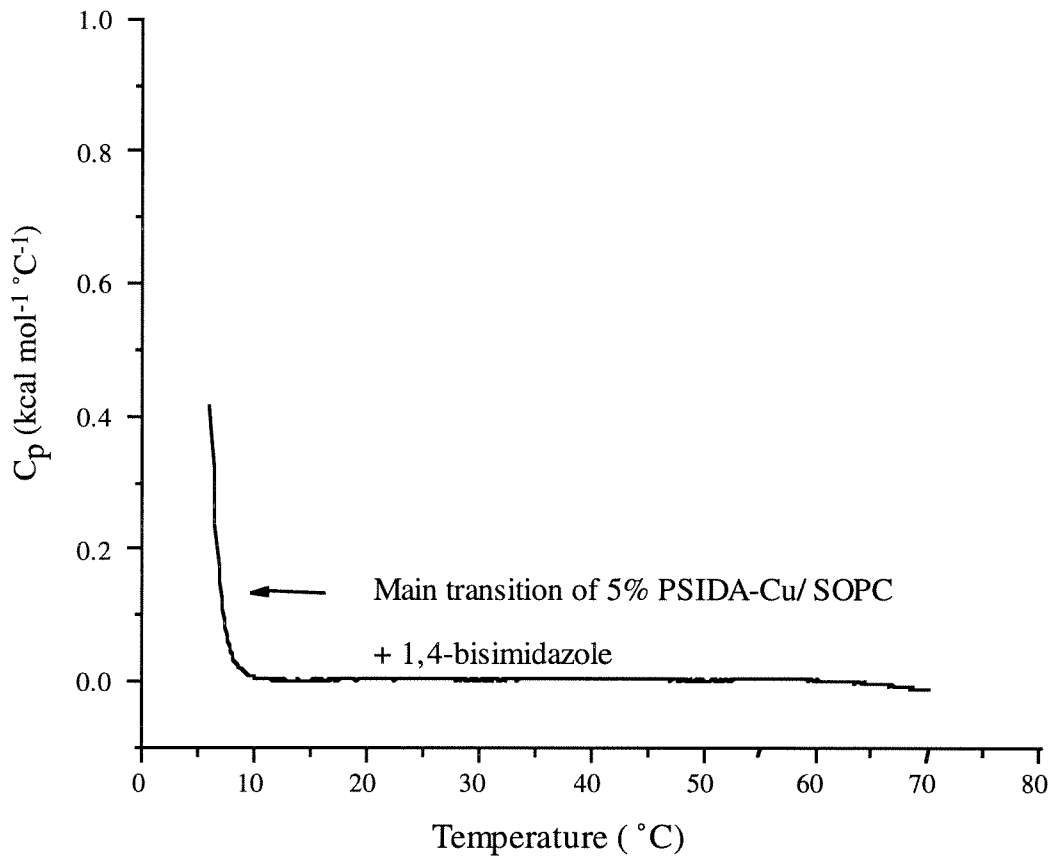
Figure 4.14. Thermal transition of 1,4-bisimidazole added to 5% PSIDA/ 95% SOPC small unilamellar vesicles using differential scanning calorimetry. 1.5 excess of 1,4-bisimidazole added to pre-formed vesicles. Due to instrument limitations, the main transition temperature occurs below the start temperature and is indicated by the arrow. Scan rate was 45 °C/hr.
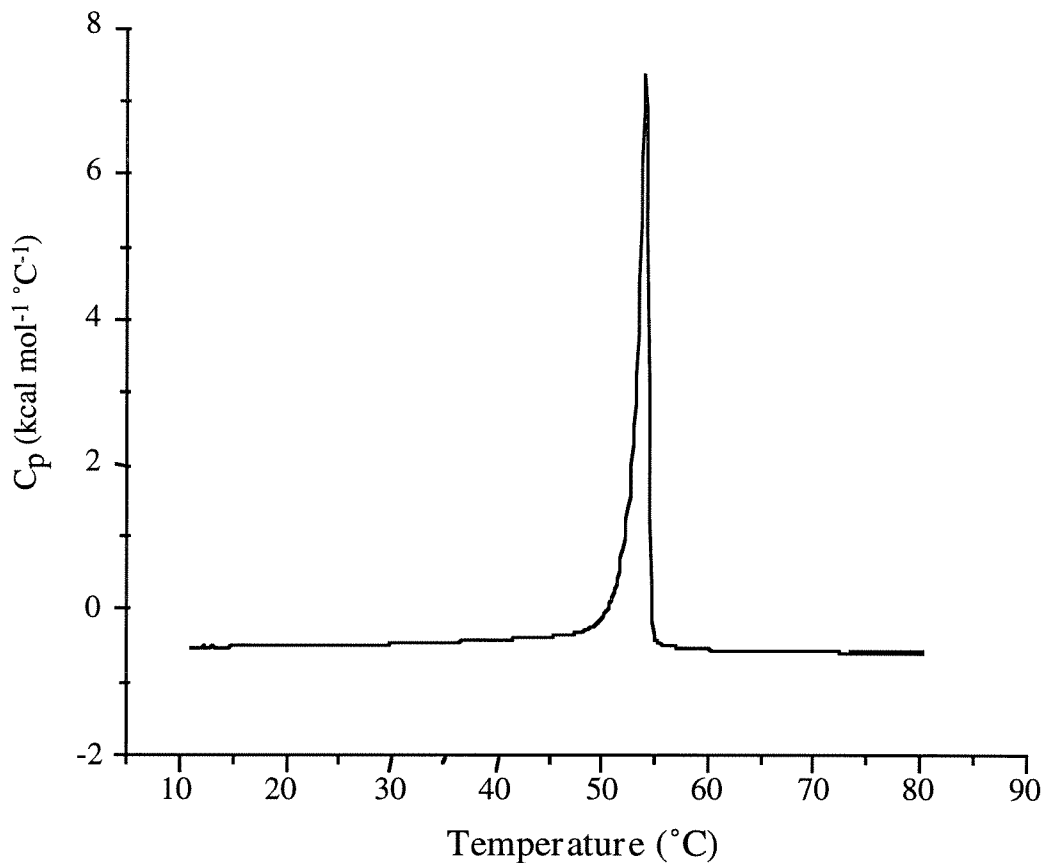
Figure 4.15. Thermal behavior of 1,4-bisimidazole added to 5% PSIDA-Cu^{2+}/ 95% DSPC small unilamellar vesicles using differential scanning calorimetry showing transition at 54.04 °C. 1.5 excess of 1,4-bisimidazole added to pre-formed vesicles. Transition temperature of metallated MLV vesicles lacking 1,4-bisimidazole is 54.3 °C. Scan rate was 45 °C/ hr, $\Delta H_{cal} = 12.8$ kcal/mole.
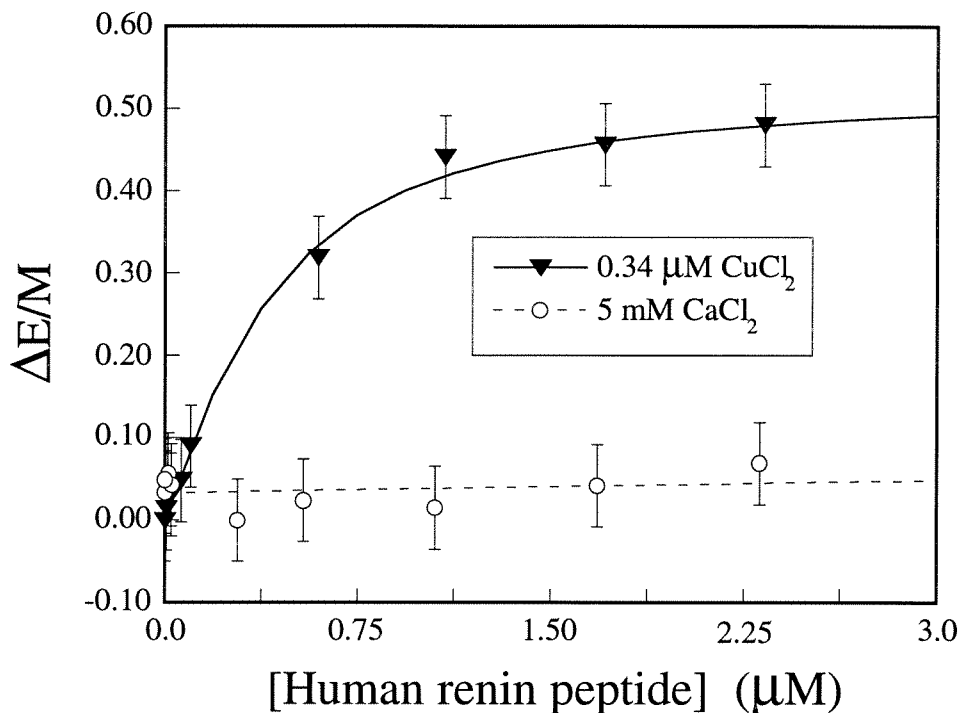
Figure 4.16. Change in fluorescence E/M due to binding of porcine renin peptide binding to 5% PSIDA/ 95% DSPC vesicles. Excess E/M ratio fitted with single-site model for benefit of the reader. For Cu^{2+} metallated vesicles, $(E/M)_o = 0.25$; and for unmetallated vesicles, $(E/M)_o = 1.77$. Metal concentrations added to pre-formed vesicles are indicated, [19 μM total lipid] at 25 °C in [20 mM MOPS, 100 mM NaCl, pH 7.5] buffer.
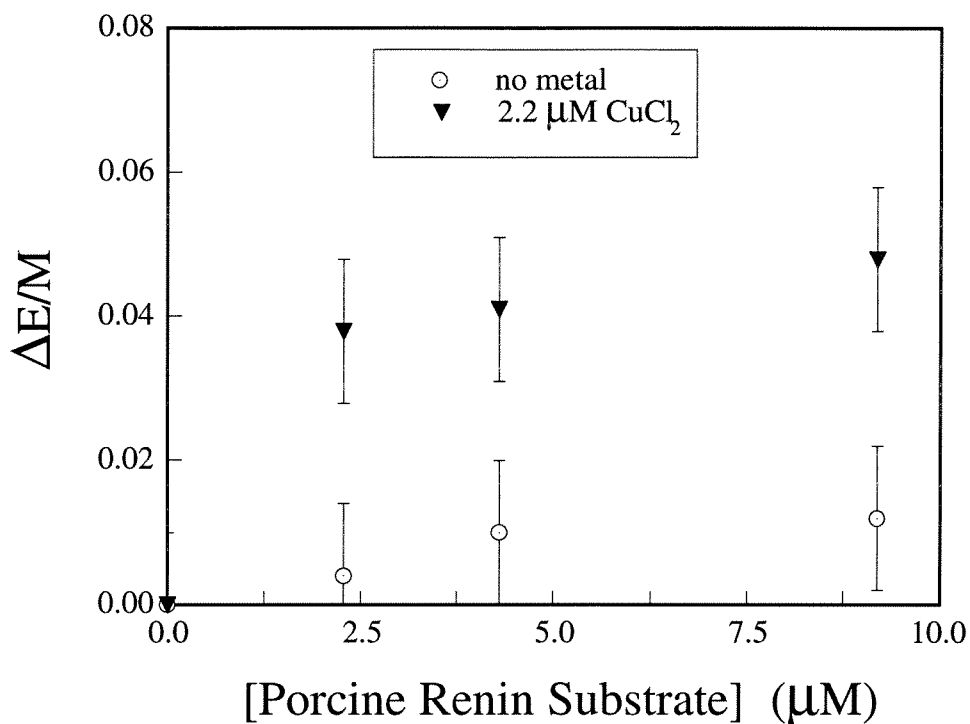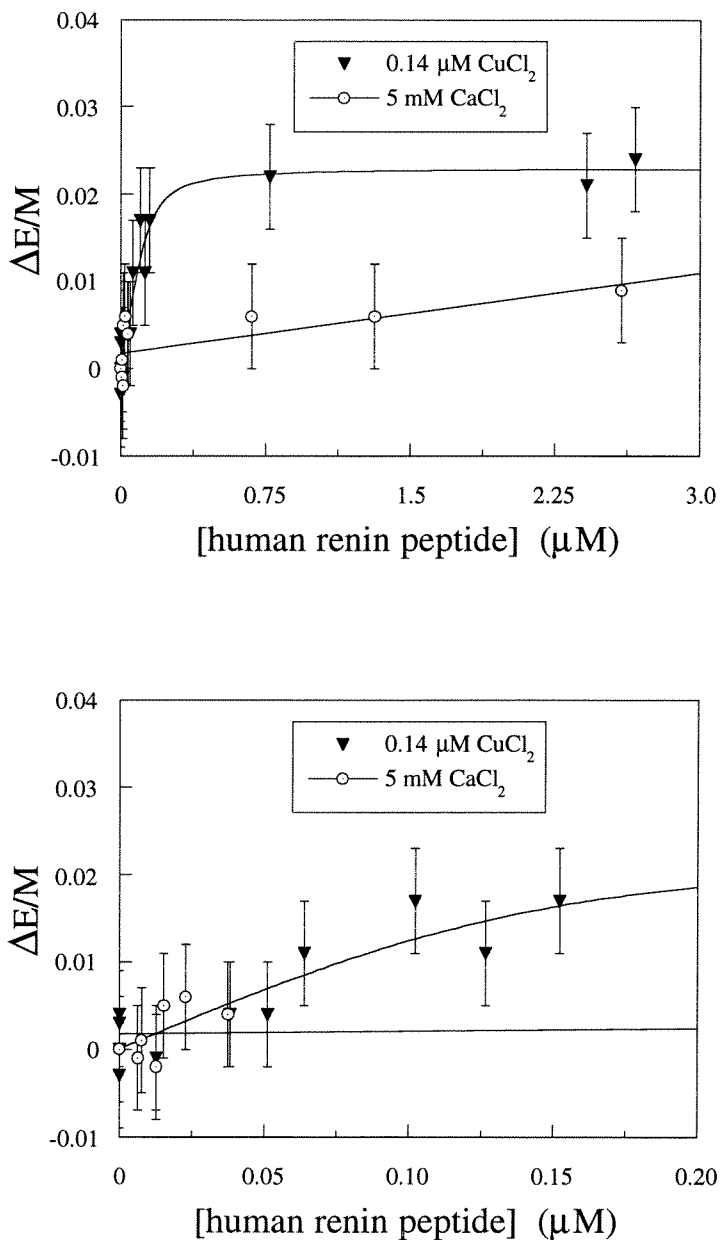
Figure 4.17. Change in fluorescence E/M due to binding of porcine renin peptide added to 2.5% PSIDA/ 47.5% DSPC / 50% cholesterol vesicles. Metal concentrations added to pre-formed vesicles are indicated at 25 °C in [20 mM MOPS, 100 mM NaCl, pH 7.5] buffer. For Cu^{2+} metallated vesicles $(E/M)_o = 0.07$ and for unmetallated vesicles $(E/M)_o = 0.10$.
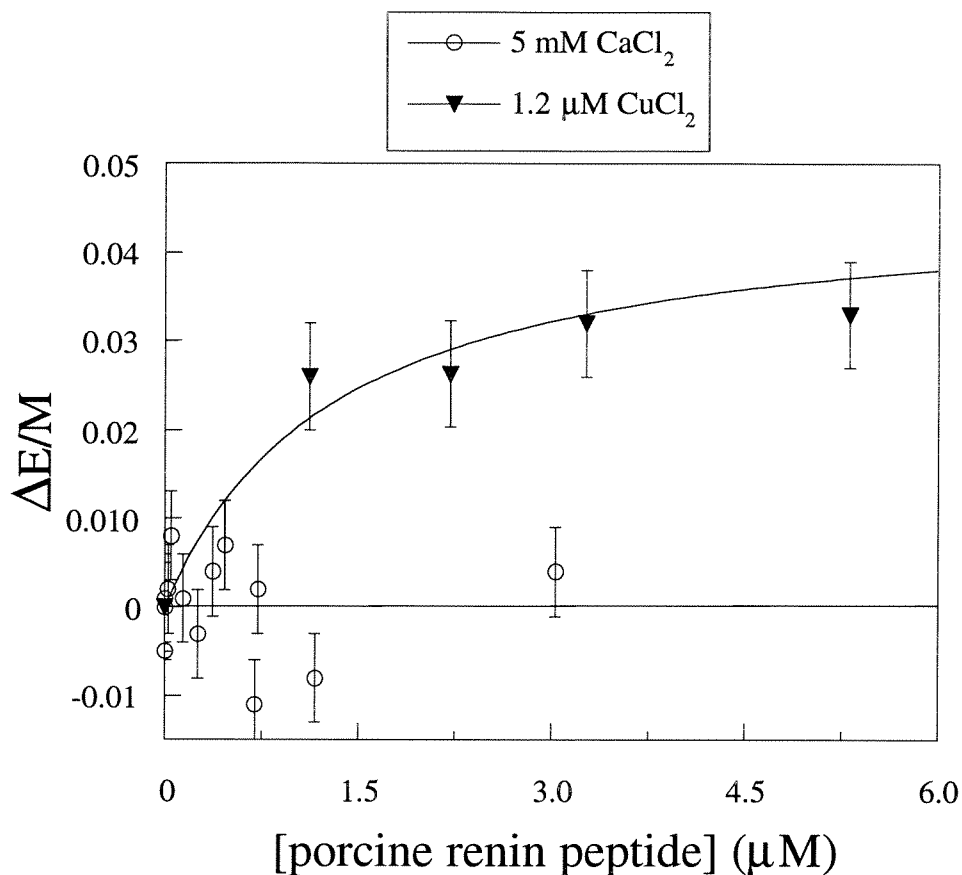
Figure 4.18. Change in fluorescence E/M due to binding of porcine renin peptide to 5% PSIDA/ 95% SOPC vesicles loaded with copper. Single-site fit is shown for benefit of the reader. For Cu^{2+} metallated vesicles $(E/M)_o = 0.17$ and for Ca^{2+} $(E/M)_o = 0.21$. Metal concentrations added to pre-formed vesicles are indicated at 25 °C in [20 mM MOPS, 100 mM NaCl, pH 7.5] buffer.

Figure 4.19. Change in fluorescence E/M due to binding of human renin peptide added to 5% PSIDA/ 95% DSPC vesicles. Excess E/M shown fitted with a single-site binding isotherm (Equation 2) to compare fitting parameters to other vesicle compositions (Table 4.3). Total lipid, [5.8 μM total lipid] with metal concentration as indicated at 25 °C in [20 mM MOPS, 100 mM NaCl, pH 7.5] buffer. For Cu^{2+} metallated vesicles $(E/M)_o$ = 0.37 and for Ca^{2+} vesicles $(E/M)_o$ = 0.74.
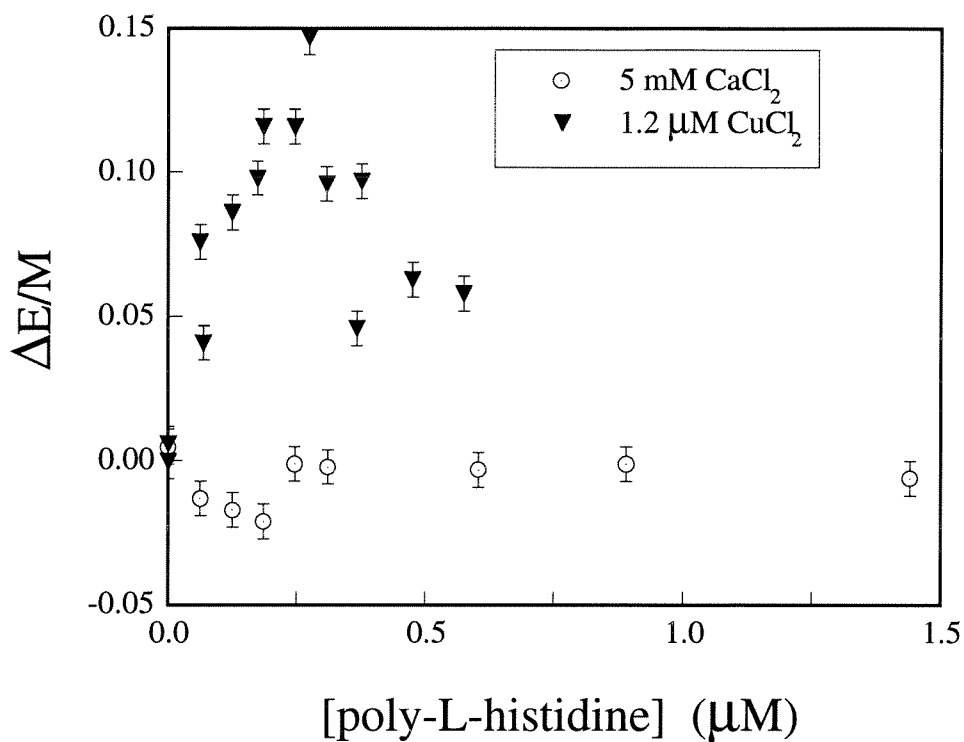
Figure 4.20. Change in fluorescence E/M due to binding of human renin peptide added to 5% PSIDA/ 95% SOPC vesicles. Excess E/M shown fitted with a single-site (Equation 2) binding isotherm to compare fitting parameters to other ligands (Table 4.3). Total lipid [12.8 μM total lipid] at 25 °C in [20 mM MOPS, 100 mM NaCl, pH 7.5] buffer. For Cu^{2+} metallated vesicles $(E/M)_o = 0.15$ and for Ca^{2+} metallated vesicles $(E/M)_o = 0.21$.

Figure 4.21. Change in fluorescence E/M due to binding of poly-L-histidine to 5% PSIDA/ 95% SOPC vesicles with Cu^{2+} and Ca^{2+}. Vesicle concentrations was 16 μM total lipid, at 25 °C in [20 mM MOPS, 100 mM NaCl, pH 7.5] buffer. For Cu^{2+} metallated vesicles $(E/M)_o = 0.17$ and for Ca^{2+} $(E/M)_o = 0.21$.
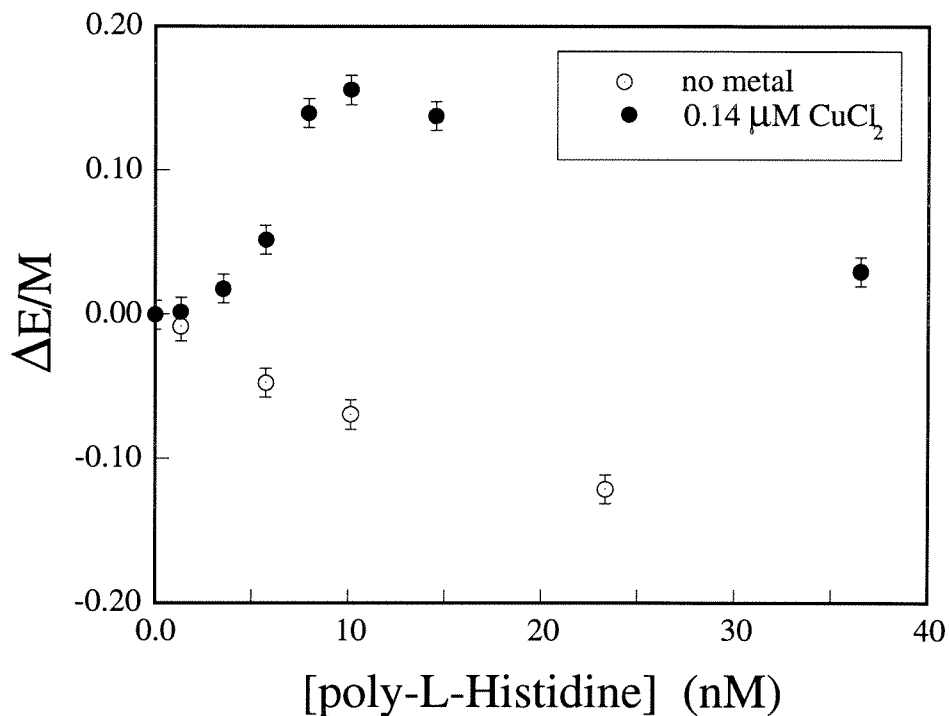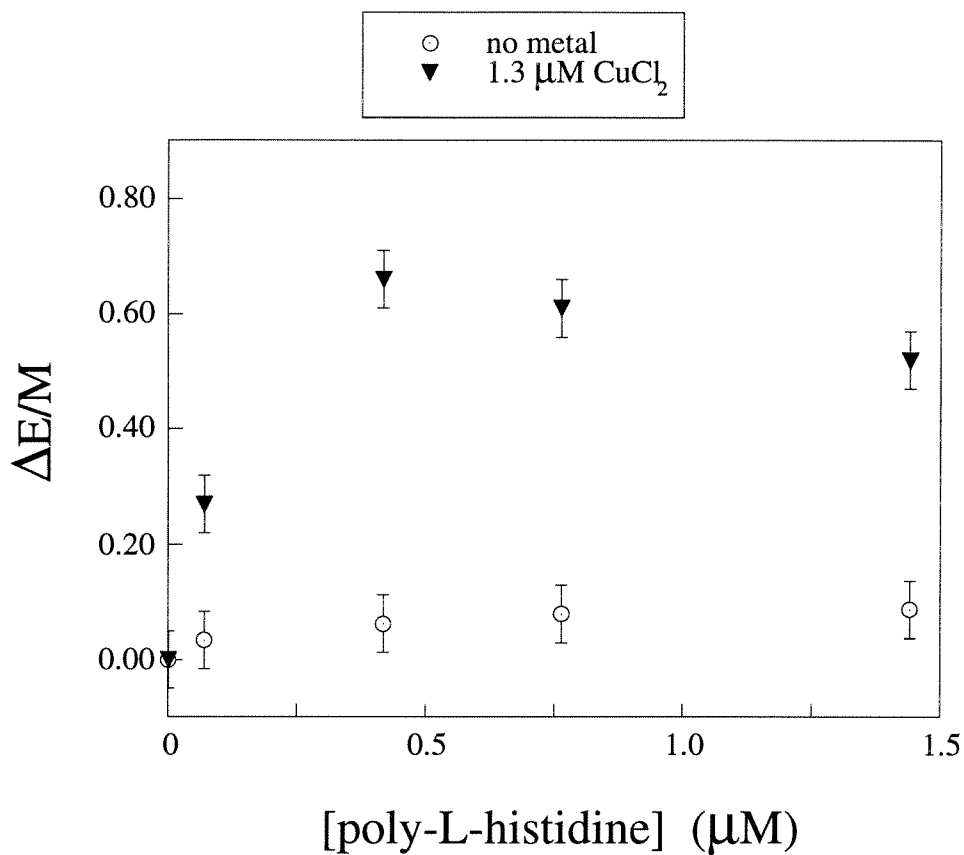
Figure 4.22. Change in fluorescence E/M due to binding of poly-L-histidine to 5% PSIDA/ 95% SOPC vesicles with Cu^{2+} and no metal. Lipid concentration was [7.6 μM total lipid] at 25 °C in [20 mM MOPS, 100 mM NaCl, pH 7.5] buffer. For Cu^{2+} metallated vesicles $(E/M)_o = 0.19$ and for unmetallated vesicles $(E/M)_o = 0.39$.

Figure 4.23. Change in fluorescence E/M due to binding of poly-L-histidine to 5% PSIDA/ 95% DSPC vesicles. Poly-L-histidine addition to 5% PSIDA/ 95% DSPC vesicles [19 μM total lipid] at 25 °C in [20 mM MOPS, 100 mM NaCl, pH 7.5] buffer. For Cu^{2+} metallated vesicles $(E/M)_o = 0.26$ and for unmetallated vesicles $(E/M)_o = 0.43$.

Figure 4.24. Change in fluorescence E/M due to binding of poly-L-histidine to 5% PSIDA/ 95% DSPC vesicles. Poly-L-histidine added to [5.7 μM total lipid] at 25 °C in [20 mM MOPS, 100 mM NaCl, pH 7.5] buffer. Ca^{2+}-loaded vesicles at 19 μM total lipid. For Cu^{2+} metallated vesicles $(E/M)_o = 0.40$ and for Ca^{2+} metallated vesicles $(E/M)_o = 0.21$.

Figure 4.25. Change in fluorescence E/M due to binding of poly-L-histidine to 2.5% PSIDA/ 47.5% DSPC/ 50% cholesterol vesicles. Poly-L-histidine addition to [10.7 μM total lipid] at 25 °C in [20 mM MOPS, 100 mM NaCl, pH 7.5] buffer. For Cu^{2+} metallated vesicles $(E/M)_o = 0.08$ and for Ca^{2+} metallated vesicles $(E/M)_o = 0.09$.
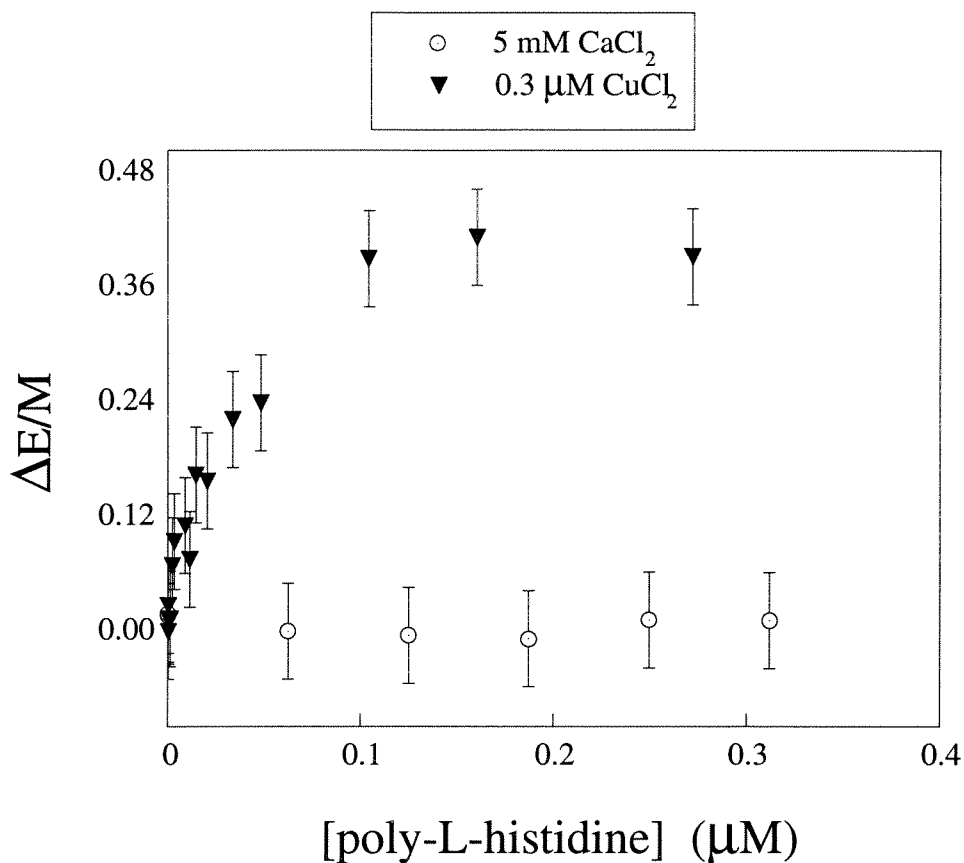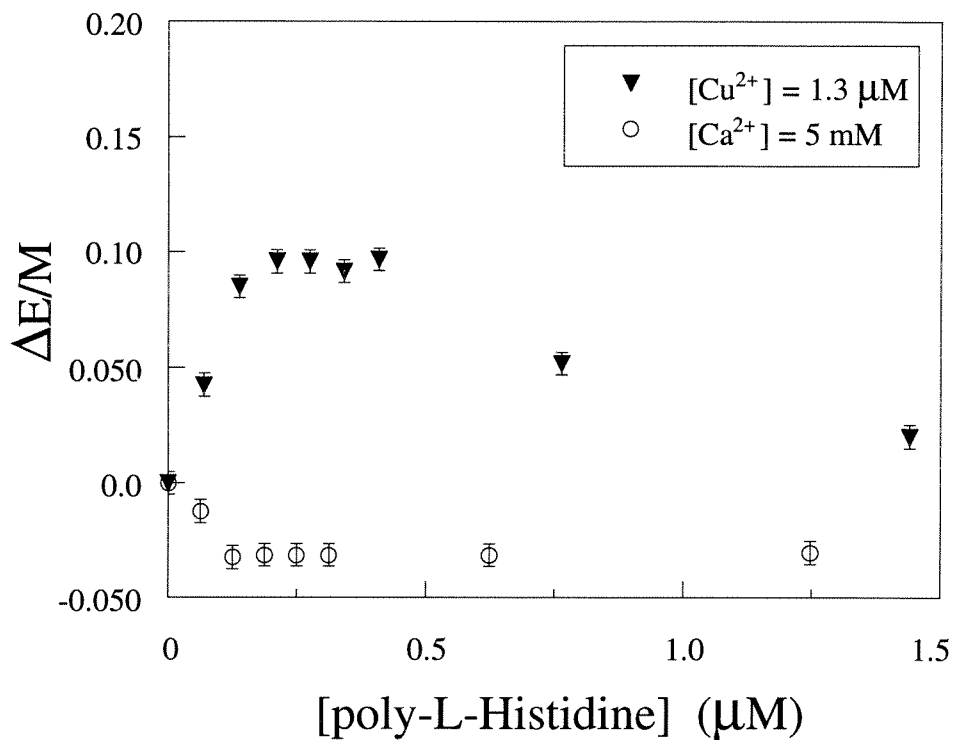
Figure 4.26. Change in fluorescence E/M due to binding of poly-L-histidine to 5% PSIDA/ 95% SOPC vesicles with Cu^{2+} and no metal. Vesicle concentration was 2.8 μM total lipid at 25 °C in [20 mM MOPS, 100 mM NaCl, pH 7.5] buffer. For Cu^{2+} metallated vesicles $(E/M)_o = 0.07$ and for unmetallated vesicles $(E/M)_o = 0.09$.

APPENDIX
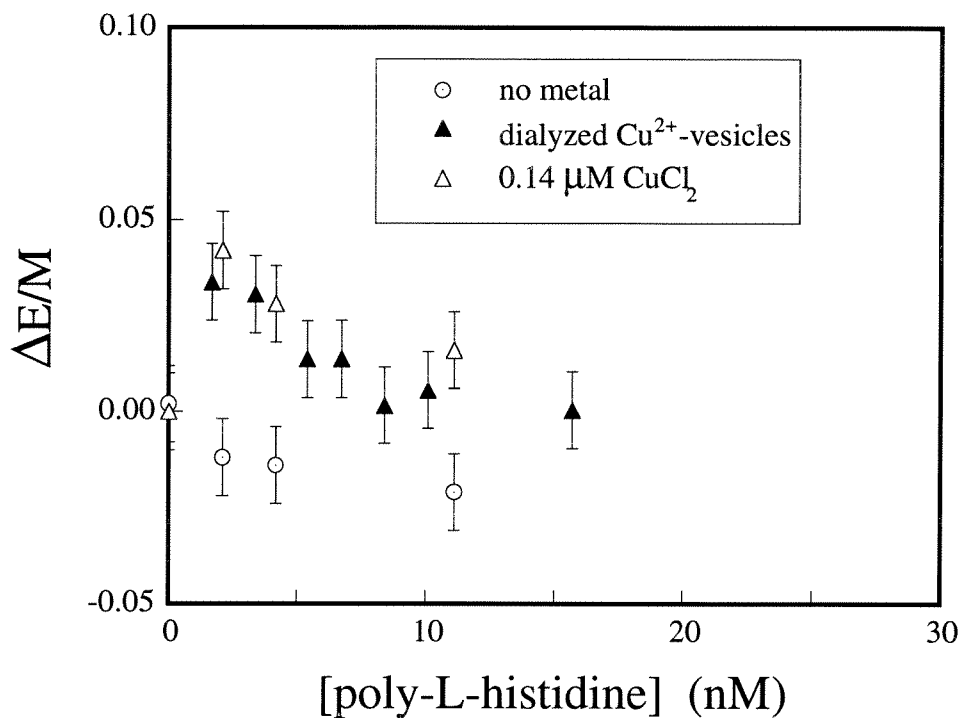
Table 4.5. Effect of photobleaching on 5% PSIDA/SOPC vesicles at 25 °C. E/M ratio is the intensity ratio between wavelengths 470 nm/ 377 nm.

Time (min.)	E/M
1	0.23
10	0.25
20	0.24
40	0.25
70	0.25
120	0.25
204	0.25
300	0.25

Analysis of single site binding

The following curve fit definition was used in the Macro Library of Kaleidagraph to fit the data using Kaleidagraph's internal Marquadt algorithm. M_t was determined from the concentration of added metal to each sample, a0 is the $\Delta E/M_{max}$ value, b0 is the dissociation constant.

```
;TOTAL ADDED LIGAND AND METAL SINGLE SITE BINDING MODEL
;mt is total metal concentration
;a0 is ΔE/M, b0 is Kd
;
root(mt,b) = ( sqrt( mt*mt - (2*mt*x) +\
2*mt*(b<0 ? 0.01:b) + \
((b<0 ? 0.01:b)^2) + (2*(b<0 ? 0.01:b)*x) + x*x));
;
Langtot(mt,a0,b0) = ((1/(2*mt))*( (a<0 ? 0.5:a)*(mt+x+ \
(b<0 ? 0.01:b) - root(mt,b) ) ))\;
a=a0\;b=b0;
;
```

Analysis of sequential binding

The following curve fit definition was used in the Macro Library of Kaleidagraph to fit the data using Kaleidagraph's internal Marquadt algorithm. M_t was determined from the total concentration of metal in each sample, a0 is the $\Delta E/M_{max}$ value, b0 is the lumped dimensionless crosslinking constant, K_2M_t.

```
;PERELSON & DELISI, [L]>>Mt
;
del2() = ( ((5.2e3*x)/((1+ 5.2e3*x)^2))* (a<0 ? 100:a));
;
Perelson(a0, b0) = (b<0 ? 1:b)*( (2*del2()+ \
1)/(4*del2()) - \
( sqrt(1+(4*del2())) )/(4*del2())  )\;
a=a0\;b=b0;
;
```

REFERENCES

1. Eichmann, K. *Angew. Chem. Int. Ed. Engl.* **1993**, *32*, 54-63.

2. Ahlers, M.; Müller, W.; Reichert, A.; Ringsdorf, H.; Venzmer, J. *Angew. Chem. Int. Ed. Engl.* **1990**, *29*, 1269-1285.

3. Ringsdorf, H.; Schlarb, B.; Venzmer, J. *Angew. Chem. Int. Ed. Engl.* **1988**, *27*, 113-158.

4. Fischer, B.; Heyn, S. P.; Egger, M.; Gaub, H. E. *Langmuir* **1993**, *9*, 136-140.

5. Goldstein, B. and Dembo, M.; In *Cell Surface Dynamics: Concepts and Models*; A. S. Perelson, C. DeLisi and F. W. Wiegel, Eds.; Marcel Dekker, Inc.: New York, 1984; pp 277-328.

6. Mallik, S.; Plunkett, S.D.; Dhal, P.K.; Johnson, R.D.; Pack, D.W.; Shnek, D.R.; Arnold, F.H. *New J. Chem.* **1994**, *18*, 299-304.

7. Penner, R. M. *Scanning Microscopy* **1993**, *7*, 805-813.

8. Kumar, A.; Biebuyck, H.A.; Whitesides, G.M. *Langmuir* **1994**, *10*, 1498-1511.

9. Parkinson, B. *Acs Symposium Series* **1992**, *499*, 76-85.

10. McCloskey, M. A.; Poo, M. *J. Cell. Biol.* **1986**, *102*, 2185-2196.

11. Lakowicz, J. R. *Principles of Fluorescence Spectroscopy*; Plenum Press: New York, 1983, pp 1-429.

12. Förster, Th. and Kasper *Z. Phys. Chem. N.F.* **1954**, *1*, 275-277.

13. Galla, H. J. and Hartmann, W. *Chem. Phys. Lipids.* **1980**, *27*, 199-219.

14. Somerharju, P. J.; Virtanen, J. A.; Eklund, K. K.; Vainio, P.; Kinnunen, P. K. J. *Biochemistry* **1985**, *24*, 2773-2781.

15. Cheng, K. H. ;. R.; L.; Liu, L.I.; Somerharju, P.; Sugar, I.P. *Biophys. J.* **1994**, *67*, 902-913.

16. Haverstick, D. M. and Glaser., M. *Biophys. J.* **1989**, *55*, 677-682.

17. Wiener, J. R. ;. P.; R.; Barenholz, Y.; Wagner, R.R. *Biochemistry* **1985**, *24*, 7651-7658.

18. Yechiel, E. and Edidin, M. *J. Cell. Biol.* **1987**, *105*, 755-760.

19. Jones, M. E. and Lentz, B.R. *Biochemistry* **1986**, *25*, 567-574.

20. Freire, E.; Markello, T.; Rigell, C.; Holloway, P. W. *Biochemistry* **1983**, *22*, 1675-1680.

21. Lehtonen, J. Y. and Kinnunen, P. K. J. *Biophys. J.* **1995**, *68*, 525-535.

22. Meers, P.; Daleke, D.; Hong, K.; Papahadjopoulos, D. *Biochemistry* **1991**, *30*, 2903-2908.

23. Shnek, D. R.; Pack, D.W.; Sasaki, D.Y.; Arnold, F.H. *Langmuir* **1994**, *10*, 2382-2388.

24. Kubalek, E. W.; Legrice, S. F. J.; Brown, P. O. *J. Struct. Biol.* **1994**, *113*, 117-123.

25. Schmitt, L; Dietrich, C.; Tampe, R. *J. Amer. Chem. Soc.* **1994**, *116*, 8485-8491.

26. Sinha, P. C.; Saxena, V. K.; Nigam, N. B.; Srivastava, M. N. *Indian J. Chem.* **1989**, *28A*, 335-336.

27. Perelson, A.S. and DeLisi, C. *Math. Biosci.* **1980**, *48*, 71-110.

28. Birks, J. B.; Dyson, D. J.; Munro, I. H. *Proc. Roy. Soc. (Lond.) Ser. A* **1963**, *275*, 575-588.

29. Martell, A. E., Smith, P.M. *Critical Stability Constants*; Plenum Press: New York, 1974; Vol. 6.

30. Galla, H.-J. and Sackmann, E. *Biochim. Biophys. Acta* **1974**, *339*, 103-115.

31. McElhaney, R. M. *Chem. Phys. Lipids* **1982**, *30*, 229-259.

32. Lakowicz, J. R. *Principles of Fluorescence Spectroscopy*; Plenum Press: New York, 1983, pp 1-429.

33. Schroeder, F. M.; Jefferson, J. R.; Kier, A. B.; Knittel, J.; Scallen, T. J.; Wood, W. G.; Hapala, I. *P.S.E.B.M.* **1991**, *196*, 235-252.

34. Mallik, S.; Johnson, R.D.; Arnold, F.H. *J. Amer. Chem. Soc.* **1994**, *115*, 2518-2520.

35. Fendler, J. *Membrane Mimetic Chemistry.* **1982**, John Wiley & Sons: New York, p137.

36. Tocanne, J.-F.; Dupou-Cézanne, L.; Lopez, A. *Prog. Lipid Res.* **1994**, *33*, 203-237.

37. Marsh, D.E. *CRC Handbook of Lipid Bilayers*, CRC Press, Boca Raton, 1990, pp 168-169,

38. Galla, H.-J. and Sackmann, E. *Biochim. Biophys. Acta* **1974**, *339*, 103-115.

39. Hartmann, W. and Galla, H.-J. *Biochim. Biophys. Acta* **1978**, *509*, 474-490.

40. Shnek, D.R.; Maloney, K.M.; Arnold, F.H. *Manuscript in preparation.*

41. Gad, A. E.; Bental, M.; Elyashiv, G.; Weinberg, H.; Nir, S. *Biochemistry* **1985**, *24*, 6277-6282.

42. Plunkett, S.D. *Ph.D. Thesis.* California Institute of Technology, Pasadena, CA, 1995.

43. Morrison, W. R. *Anal. Biochem.* **1964**, *7*, 218-224.

44. *personal communication*, Winkler, J. California Institute of Technology.

Chapter 5. Titration calorimetry studies of model complex binding to

metal-chelating vesicles

INTRODUCTION

Simultaneous multipoint attachment of a macromolecule to a surface is difficult to determine through most analytical spectroscopic techniques. This problem has been probed using excited-state dimer formation between fluorescently-labeled lipids (Chapter 4). Excimer fluorescence is produced upon collision of pyrene-labeled lipids diffusing in labeled-lipid membranes. Upon binding of multi-histidine compounds to these lipids, increases in the excimer to monomer ratio were observed. The increase in the ratio was believed to be due to excess collisions of labeled lipids induced by binding of the multivalent ligand to multiple lipids. However, the fraction of membrane-bound ligand was not measured directly by the fluorescence technique. An independent measure of the affinity of multivalent histidine ligands for lipid bilayers should show an increase in the apparent binding affinity over monovalent controls, supporting the fluorescence measurements.

Measurement of binding equilibria between proteins and vesicles is a difficult problem due to the vesicles' small size, usually requiring labeling of either the vesicle or protein with fluorescent or radioactive probes. Lipid-bound ligand is determined from a mass balance between the total ligand and the free ligand concentration, usually by spectroscopic determination of concentration of free ligand. Certain small molecules may be impossible to label, further complicating efforts to determine binding equilibria. Since the labeling process itself may introduce moieties which may interfere with the binding equilibrium, a method that could be used without chemical modification of interesting ligands would be very desirable.

Binding equilibria between small or large molecules can be followed through measurement of differential heat effects at constant temperature, through isothermal titration calorimetry (ITC) [1]. At least three ITC instruments have been designed to measure the incremental heat produced upon association of a ligand with a macromolecule [2]. The heat evolved due to binding is determined by monitoring changes in the heat capacity between

the stirred sample cell and a reference cell as ligand is injected into the sample cell. Recently, isothermal titration calorimetry has been used with peptide and protein binding to lipid vesicles to quantify association constants through fitting of heat changes due to binding [3]. Since it is relatively hard to completely separate proteins or small molecules from vesicles using conventional ultracentrifugation [4], and other techniques require chemical labeling which may introduce hydrophobic residues that interfere with surface binding, calorimetry offers a convenient approach to determine association constants.

Titration calorimetry is the most convenient technique to investigate binding of peptides and proteins to lipid vesicles since the two components need only be combined, and very little peptide is required for each experiment [3]. Since chemical or fluorescent labeling is unnecessary, the experiment is quick and straightforward. Very concentrated vesicles must be used, however. Isothermal titration calorimetry (ITC) is the only available method to study the binding effect of inhibitors to membrane proteins directly without radio-labeling or chemical addition of a fluorescent moiety [5]. Seelig has investigated both hydrophobic peptides [6] and hydrophilic [7] small molecule binding to phosphatidyl choline vesicles. Other titration calorimetry studies of proteins association negatively-charged lipid vesicles have shown the association parameters obtained are comparable to association parameters obtained from dialysis measurements or spectrophotometric measurements [8,9,10]. We wish to apply isothermal titration calorimetry to measure the binding of histidine-rich compounds to metal-chelating vesicles.

Metal binding and ligand binding to metal-chelating vesicles were studied using isothermal titration calorimetry to determine binding constants, enthalpy of binding, and stoichiometry. Model complexes of iminodiacetate-chelated-Cu^{2+} (Cu^{2+}IDA) and imidazole were first studied using ITC to determine if the calorimetry data agreed with published stability constants from potentiometry. After establishing that heat effects due to binding measured by ITC reflect the association between chelated metal ions and nitrogen compounds, imidazole was added to metal-chelating mixed vesicles to determine the

association parameters. Because the presence of the charged interface often shifts binding equilibria of charged molecules due to electrostatic effects [11], imidazole binding to mixed vesicles was investigated as a control for possible interfacial effects. For comparison to previous fluorescence measurements, 1,4-bisimidazole, containing two rigidly-linked histidine residues, was added to chelating-bilayers and the binding parameters determined. The shape and the stoichiometry of the binding isotherm for the bifunctional histidine molecule was very different than for single point binding for metal-chelating, fluorescently-labeled vesicles. Thus, calorimetric investigations of binding equilibria yield important quantitation of affinity of histidine-rich compounds for the bilayer. Additionally, since the calorimetry measurements allow calculation of both ΔH of binding as well as $\Delta G = -RT \ln K$, effects on the entropy of binding, ΔS, can be determined from the same measurement. We expect that entropy of binding will allow comparison of lipid organization and multipoint attachment.

CALCULATIONS

The heat measured, q (μcals), for each injection i into the sample cell relative to the (i-1) injection is related to the change in enthalpy, $\Delta H_i = H - H_o$, due to the binding of the ligand L to the total macromolecule M_t (M) present in the calorimeter [12]. The reference state is taken to be the free ligand in solution.

$$q = M_t[(\overline{H} - \overline{H}_o)_i - (\overline{H} - \overline{H}_o)_{i-1}] \qquad [1]$$

The heat evolved for each injection is due to the formation of bound species and can be mathematically related to equations of multiple binding equilibria. The heat evolved due to binding in the sample cell is directly related to the fractional bound species $M_k L_j$ composed of k macromolecules in the cell at the start of the experiment, M, able to bind j

ligands L. M_t is the total macromolecule in the cell before ligand is injected. The heat measured for each injection is directly related to the bound macromolecule or each term in the binding partition function. It is necessary to use the fraction of each species j bound to determine the heat q for each micro-injection of ligand L_t added to the sample volume, V_o [1].

$$q = M_t V_o \sum_j n_j \Delta H_j \theta_j \qquad [2]$$

θ_j is the fraction of bound species. The heat of each injection is therefore dependent on the progress of each θ_j, each bound species. We can relate each injection heat to a function of the following parameters: stoichiometry, n_j; enthalpy of binding, ΔH_j; and association constant, K_j; to the total added ligand, L_t, and total macromolecule, M_t. Thus, it is necessary to write equilibrium expressions for each fraction of bound species, θ_j , in solution to fit the measured heats to molar ratio of added ligand to macromolecule.

Single site binding model

Since the quantity of ligand added to the cell is known, rather than the free concentration, the binding isotherms must be developed in terms of total ligand, L_t, and macromolecule, M_t. For the association of single macromolecule with a monovalent ligand, the concentration of bound species is related to the total species by the equilibrium association [13].

$$K = \frac{\theta}{(1-\theta)[L]}$$
$$L_t = [L] + n\theta M_t \qquad [3]$$

The fraction bound, θ, is obtained from these two equations in terms of total added ligand concentration, L_t; macromolecule concentration in cell, M_t; association constant, K (M^{-1}); and stoichiometry, n; and the binding enthalpy, ΔH (kcal/mol). The expression for $n\theta Mt$ in terms of L_t and M_t is inserted into Equation 2 and yields the incremental heat of binding for any concentration of ligand added to the titration calorimeter.

$$q = \frac{nM_t \Delta H V_o}{2}\left[1 + \frac{L_t}{nM_t} + \frac{1}{nKM_t} - \sqrt{\left(1 + \frac{L_t}{nM_t} + \frac{1}{nKM_t}\right)^2 + \frac{4L_t}{nM_t}}\right] \quad [4]$$

For each injection the integrated heat is fit with the function for $q(M_t,L_t,n,K,\Delta H)$ in terms of the adjustable parameters n, K, and ΔH.

Since the system is not closed, some of the solution leaks above the adiabatic shield of the calorimeter. Assuming that all the heat is measured before the extra volume passes above the shield, an additional equation must be developed to adjust for this physical situation. The theoretical heat due to binding, q, must be corrected due to change in volume, dV_i, upon ligand injection. The difference in measured heat, $\Delta q(i)$, and theoretical heat of binding, Equation [4], can be as much as 50% of the total heat. Therefore, the volume correction is applied using the equation below for each injection.

$$\Delta q(i) = q(i) + \frac{dV_i}{V_o}\left[\frac{q(i) + q(i-1)}{2}\right] - q(i-1) \quad [5]$$

The heat difference between the i and (i-1) injection are fitted with $\Delta q(i)$ using the Marquadt algorithm developed in the commercial Origin™ software.

Sequential binding model

Sequential binding of a ligand L to a macromolecule M can be written using the following equilibrium expression. In the case of imidazole, two imidazoles can bind to one chelated copper.

$$K_1 = \frac{[ML]}{[M][L]}$$

$$K_2 = \frac{[ML_2]}{[M][L]^2} \qquad\qquad [6]$$

$$K_j = \frac{[ML_j]}{[M][L]^j}$$

Sequential binding of ligand to macromolecule M_t in the titration cell produces fraction of j bound species, F_j, shown below.

$$F_j = \frac{K_1 K_2 \ldots K_i [L]^j}{1 + K_1[L] + K_1 K_2 [L]^2 + \ldots + K_1 K_2 \ldots K_j [L]^j} \qquad\qquad [7]$$

Each F_j represents the fraction of sequentially bound ligand to form each $[ML_j]$ species. Sequential binding of two imidazoles to one copper has been assumed based on chromatography experiments [14]. The imidazole ITC data were fitted with this mechanism for experiments using model $Cu^{2+}IDA$ compounds as well as $PSIDA$-Cu^{2+} vesicles. The commercial software Origin™ uses a bisection method to find the fraction of each species bound and then uses the equation to fit the data with the adjustable parameters K_1, K_2 and ΔH_i, ΔH_2 to obtain the heat of each injection q.

$$q = M_t V_o (F_1 \Delta H_1 + F_2 [\Delta H_1 + \Delta H_2]) \qquad\qquad [8]$$

This model implicitly assumes that stoichiometry for the sequential binding model is n = 1 for all binding reactions. The linkage of each binding reaction is left undefined and non-equivalent. As for the single-site binding model, the heat that the machine measures due to change in volume must be corrected with Equation 5. The heat difference between the i and (i-1) injection are fitted with the above equations using the Marquadt algorithm with the commercial Origin™ software.

RESULTS & DISCUSSION

Metal binding to vesicles

Small unilamellar vesicles were made from a metal-chelating, fluorescently-labeled lipid, PSIDA, and either DSPC or SOPC lipids shown in Figure 5.1. Mixed vesicles composed of PSIDA and DSPC were shown to exhibit interesting changes in their fluorescence properties upon metal binding (Chapter 2). Metal binding studies of mixed PSIDA/SOPC vesicles at 25 °C, pH 7.5 were carried out to determine if the fluorescence changes measured in Chapter 2 paralleled the association constants measured through calorimetry. $MnCl_2$ was added to 5% PSIDA/ 95% SOPC vesicles (Figure 5.2) to determine the association constant and enthalpy using titration calorimetry. $MnCl_2$ was chosen instead of $CuCl_2$ because titration calorimetry is limited to measuring binding constants below $\sim 10^8$ M^{-1}. The raw differential heat capacity in Figure 5.2 for each injection (a) is shown plotted over the integrated heat data divided by moles of ligand injected (b). Data were fitted with a single-site binding model (Equation 4) assuming that each chelating lipid binds one metal ion.

The binding energetics of Mn^{2+} ions to PSIDA/SOPC vesicles were compared to that of the model N-linked complex, N-methyliminodiacetate, in solution. The stability constant of Mn^{2+} for N-methyliminodiacetic acid (MIDA) in solution is $10^{5.4}$ M^{-1} at 25 °C, compared to $K_a = 10^{11.0}$ M^{-1} for Cu^{2+} [15]. The values of ΔH and ΔS and $\Delta G = -RT \ln K_{app}$

of binding should reflect any re-organization of the lipids upon metal binding. Fits of the titration calorimetry curves using the single site model [Equation 4] yielded $\Delta H_{bind} = 1.2$ kcal/mol, $K_a = 3.35 \times 10^4$ M^{-1}, $n = 1.01$. The data showed a saturation at 1:1 total estimated total $[PSIDA]_T$ chelating moiety to added Mn^{2+} (assuming PSIDA mole fraction 0.05). The data were uncorrected for the difference of metal concentration at the vesicle surface due to the electric double layer, since the measurements were made in 0.1 M NaCl and the amount of charged lipid (PSIDA) at the interface was low (0.05 mole fraction). Fits of the data (Figure 5.2) showed the binding constant was an order of magnitude lower than for Mn^{2+} binding to MIDA in solution. This result shows that the affinity of the lipid for the metal ion is lowered by an order of magnitude due to interfacial pH effects or due to steric limitations.

ITC has been used to investigate the binding enthalpy of metal ion association to negatively-charged phospholipid vesicles, usually showing endothermic enthalpy of binding. ITC binding studies of Ca^{2+} or La^{2+} to mixed phosphatidylserine vesicles showed that the enthalpy was positive [16]. As in these other lipid system, the enthalpy of Mn^{2+} binding to PSIDA lipids was found to be endothermic, similar to Mn^{2+} binding to MIDA, $\Delta H_{Mn \cdot MIDA} = 0.6$ kcal/mol, in solution [15]. Endothermic enthalpy of metal binding is consistent with previous studies of interfacial metal binding and metal binding to model chelating molecules.

One important question concerning metal ion association to interfaces is whether or not the metal binding induces changes in the phase properties of the lipid. The binding entropy should reflect such changes if they occur. The entropic contribution to binding, $\Delta S = 25$ cal $^{\circ}K^{-1}$ mol^{-1}, shows that metal binding is entropically favored, as it is in solution. Entropy of binding may be compared to the entropy of formation for the model chelate, $Mn^{2+}MIDA$, $\Delta S = 27$ cal $^{\circ}K^{-1}$ mol^{-1} at 25 $^{\circ}C$ [15]. The lipid composition was chosen such that the ambient temperature at which the isothermal titration experiment was performed would be above the phase transition temperature of the mixed vesicle. Thus, the lipids

would be in the liquid-crystalline phase, which has a great degree of disorder. Metal binding to the lipid headgroup is favored because of the chelate effect [17]. Also, metal binding changes the hydration of the PSIDA lipid, causing release of water which would also increase the entropy. Thus, metal binding to the bilayer is also entropically driven as seen for other examples of electrostatic metal association to lipid vesicles and model complex studies [18,19].

Imidazole binding to Cu^{2+}IDA

Heat effects for imidazole binding to a small metal chelate in solution, Cu^{2+}IDA, were determined using isothermal titration calorimetry. Data were taken at two temperatures, 25 (Figure 5.3) and 35 °C (Figure 5.4), in order to compare to stability constants obtained from potentiometry in 0.1 M NaCl at 35 °C [20]. The data were fitted using Equation 8 with number of ligands able to bind set at j = 2. From Figure 5.3 and Figure 5.4, it is readily seen that the integrated heats do not reach saturation at 1:1 stoichiometry. This is due to the ability of Cu^{2+}IDA to bind two imidazoles. This conclusion is supported by X-ray crystallography data that also shows Cu^{2+}IDA bound to two imidazoles [21]. The binding constants shown in Table 5.1 obtained at the two temperatures are representative of typical measurements, and the average χ^2 are shown to represent goodness of fit.

Small model complexes were investigated to show that titration calorimetry could be used to measure association constants for metal coordination to nitrogen ligands. The first binding constant of imidazole for Cu^{2+}IDA is extremely close to the value obtained from potentiometry. The value of the first association constant at 35 °C of 3.93 x10^3 (M^{-1}) determined from calorimetry is similar to the value 2.2 x10^3 (M^{-1}) obtained from potentiometry at 35 °C [20]. Previous measurements from binding of Cu^{2+}IDA to chromatographic supports at 25 °C are very similar to calorimetric data obtained from fits of enthalpy of imidazole binding to Cu^{2+}IDA (Table 5.1) at 25 °C. The association constant,

$K_1 \sim 5.2 \times 10^3 \, (M^{-1})$, obtained from ITC measurements at 25 °C, pH 7.5, is essentially the same as the values of imidazole coordination to IDA-Cu^{2+} TSK gel $K_1 = 5.4 \times 10^3 \, M^{-1}$ [14,22]. Thus, titration calorimetry yields binding parameters similar to measurements made previously by other techniques. From fits of calorimetry data the second binding constant was found to be smaller than the first binding constant, also observed for N-acetyl histidine binding to Cu^{2+}IDA-TSK gels [23].

The coordination enthalpy (Table 5.1) between imidazole and Cu^{2+}IDA is exothermic as was observed was observed using potentiometric measurements for Cu^{2+} and imidazole, $\Delta H = -7.5$ kcal/mole at 25 °C [15]. Comparing the binding enthalpy at the two temperatures shown in Table 5.1 shows that the enthalpy does not have a strong temperature dependence.

The association constants obtained from calorimetry do not include the assumption that only deprotonated imidazole is able to coordinate to chelated copper. Thus, the association constant, K_{app}, will be a function of pH. Using the pK_a of imidazole, $pK_a = 7.01$, at the experimental pH of 7.5 the fraction of protonated imidazole is calculated from the following equation to be ~ 0.25 [24].

$$f = \frac{10^{(pH - pK)}}{(1 + 10^{(pH - pK)})}$$

Thus, the amount of deprotonated imidazole able to bind to Cu^{2+}IDA is ~75 % of the total added. The heat of ionization of imidazole is known in 0.1M NaCl. However, in a calorimetry experiment the ionization heat is dependent on the ionization of the buffer. Thus, the apparent binding constant should be corrected for the heat of ionization of imidazole to obtain the intrinsic association constant, if desired. For our studies, the association constants were treated as apparent binding constants for comparison to binding data taken with small unilamellar vesicles at the same pH and buffer conditions. Since the

pH for all experiments was kept constant, the heat of ionization for imidazole would remain the same.

Sequential binding of imidazole to $Cu^{2+}IDA$ was assumed based on previous measurements of N-acetyl histidine coordination to chromatographic supports [23]. Since the parameters obtained from calorimetry agree closely with previously measured binding parameters, all calorimetry data of imidazole binding to vesicles were fitted with sequential binding model.

Binding of imidazole to metal-chelating vesicles

To determine if the binding of imidazole to chelated-Cu^{2+} on vesicle surfaces was affected by interfacial effects, binding of imidazole to metal-chelating vesicles composed of the fluorescently-labeled lipid PSIDA-Cu^{2+} and various matrix phospholipids was investigated. Since the fluidity of the vesicle affects the mixing of the PSIDA lipid, different vesicle formulations were used. The raw titration data of imidazole binding to vesicles are shown in Figure 5.5 (SOPC) and Figure 5.6 (DSPC/cholesterol). The data were fitted using a sequential binding model [Equation 8] and the results are shown in Table 5.2 for the SOPC and DSPC/cholesterol mixed vesicles.

Different mixed PSIDA vesicle compositions were investigated to compare to fluorescence measurements (Chapter 4). ITC binding data taken with PSIDA-Cu^{2+}/DSPC vesicles were found to be complicated by aggregation of the vesicles. Aggregates of 5% PSIDA / 95% DSPC vesicles were observed after sonication if 1.05 molar ratio of copper to total PSIDA lipid was present. Since not all of the surface area of the vesicles is available for association with the bivalent ligand, the result are not included because the concentration of accessible PSIDA-Cu^{2+} lipid would be uncertain, adversely affecting the accuracy of the stoichiometry from subsequent fits of the data.

The vesicles containing cholesterol are assumed to have the same mole fraction of PSIDA-Cu^{2+} as SOPC vesicles since the cholesterol is buried in the membrane. SOPC and

DSPC/cholesterol vesicles are fluid at 25 °C. Note that the integrated enthalpies (Figure 5.5,6) do not saturate at 1:1 binding molar ratio. This is again due to the fact that two imidazoles can coordinate to one chelated metal ion.

If binding of imidazole was somehow affected by placement of the IDA at the lipid interface, binding of imidazole to metal-chelating vesicles composed of the fluorescently-labeled lipid PSIDA and various phospholipids would yield different binding parameters. The first association constant was slightly lower (Table 5.2) for imidazole binding to vesicles than for imidazole binding to the model complex, Cu^{2+}IDA (Table 5.1). Since the binding parameters were very similar to values obtained with model complexes, interfacial effects on the binding of monovalent complexes do not appear to be important.

Binding of 1,4-bisimidazole to copper-loaded fluorescent vesicles

The water-soluble compound 1,4-bisimidazole (Figure 5.7) was added to metallated vesicles to determine if the binding behavior differed from that of imidazole. SOPC and cholesterol /DSPC vesicles in the concentration range of 3-10 mM showed calorimetry traces with values above the minimum experimentally measurable heat per injection (10 µcal).

The calorimetry data for 1,4-bisimidazole binding to mixed metal-chelating vesicles are shown in Figure 5.8 (SOPC) and Figure 5.9 (DSPC/cholesterol). The data were fit with Equation 4. Other more complex fits containing sequential binding of each histidine residue on the bivalent ligand did not represent the data within acceptable χ^2 values (χ^2 = 3000 mcal). The apparent binding constant, apparent enthalpy, and stoichiometry were obtained from these fits. The results for the two vesicle systems are given in Table 5.3. Association constants obtained for both vesicle compositions from fits of the calorimetry data were remarkably similar, since the fluidity of the bilayers was similar for cholesterol/DSPC and SOPC small unilamellar vesicles.

Now the binding behavior for imidazole to metal-chelating vesicles can be compared to binding of 1,4-bisimidazole. Imidazole binding proceeds through sequential binding of two imidazole to a single copper, while association of 1,4-bisimidazole would be expected to proceed through binding to two separate copper ions chelated by individual lipids. We propose that 1,4-bisimidazole would organize the bilayer by bringing two lipids physically near enough each other to enhance the population of excimers. Bis-imidazole can interact with the bilayer through two modes. Both of the 1,4-bisimidazole lipid bound species [PSIDA-Cu·Bisim] and [(PSIDA-Cu)$_2$·Bisim] will contribute to the binding enthalpy that the calorimeter detects.

Upon comparing binding data of 1,4-bisimidazole and imidazole we would expect to see an effect on three parameters determined from calorimetry. For 1,4-bisimidazole we would expect an increase in the apparent binding constant compared to imidazole association if both imidazole residues were simultaneously coordinated to individual lipids. Metal coordination is sufficiently strong that once one bivalent ligand binds, a second metal-bearing lipid will coordinate when it collides with the bivalent-lipid complex. Additionally, since one 1,4-bisimidazole can bind twice to two metallated lipids, the stoichiometry would be close to 0.5 (ligands per Cu^{2+}-lipid). Monovalent coordination of 1,4-bisimidazole would have stoichiometry of near one bisimidazole to one chelated-Cu^{2+} ion. Therefore, stoichiometry near 1 would be measured if multisite attachment were not occurring or at high bisimidazole concentrations. Since multivalent binding would be enthalpically driven, we would also expect an increase in the enthalpy of binding, ΔH compared to imidazole binding.

For both vesicle compositions, the apparent binding constant for 1,4-bisimidazole determined from fits of single site association is larger by an order of magnitude (Table 5.3) than the first binding constant of imidazole for Cu^{2+}PSIDA mixed vesicles (Table 5.2). Since the 1,4-bisimidazole molecule is larger (8 Å diameter) than imidazole, it is assumed that sequential binding of two bis-imidazoles to a single copper is sterically unfavorable.

The binding constants are on the order of 10^5 (M^{-1}) which is consistent with two-point attachment to individual lipids since the monovalent controls have a first binding constant of 10^3 (M^{-1}). Such an increase in binding magnitude over monovalent controls can be rationalized using a simple ring closing argument for the bis-imidazole compound. The first binding between bis-imidazole and a lipid is presumed to be close to the first association constant of imidazole, $\sim 10^3$ M^{-1}. Ideally, the second binding to a second lipid thus could yield a binding constant orders of magnitude higher if there is not an entropic penalty of binding [25]. Re-organization of the lipids costs energy and should presumably reduce the total energetic gain due to multipoint binding. The entropic cost of re-organization can be rationalized from the thermodynamic parameters of binding derived from calorimetry.

The enthalpy of binding for 1,4-bisimidazole determined from fits of SOPC or DSPC/cholesterol vesicles [-16 kcal/mole] is approximately double that of the binding enthalpy for imidazole [-8 kcal/mole]. This is not surprising, since we expect some favorable enthalpic component upon coordinating to the second "histidine" of 1,4-bisimidazole. The entropy of binding is calculated from $\Delta G = -RT \ln K$. Changes in lipid reorganization should be reflected in the sign and magnitude of entropy of the system.

Lipid reorganization upon bis-imidazole binding would be expected to affect the magnitude of the entropic contribution. Entropies of binding of -43.7 and -34 cal $^{\circ}K^{-1}$ mol^{-1} were found for PSIDA/SOPC and PSIDA/DSPC/cholesterol vesicles. The entropy is large and strongly negative which could reflect unfavorable ordering of the bilayer by the bis-imidazole ligand. Thus, we may compare the entropy of binding due to bis-imidazole to the entropy of binding induced by imidazole which is also negative, but smaller $\Delta S = -8.2$ cal/$^{\circ}K$ mol. Thus, reorganization of the lipids induced by ligand could be reflected in the thermodynamic parameters of binding.

Stoichiometry determined from fits of 5% PSIDA-Cu/SOPC and 2.5% PSIDA-Cu^{2+}/47.5% DSPC/ 50% cholesterol vesicles (Table 5.3) was found to be close to 0.5 for

1,4-bisimidazoles per lipid. The uncertainty in stoichiometry could be due to differences in the sizes of the vesicles, but is most likely due to the difficulty of knowing the accessible concentration of PSIDA-Cu^{2+} for vesicle systems. The surface area available for binding is based on the assumption that the vesicles have 70% of the total lipid available for binding if they are small unilamellar vesicles. The size distribution of the vesicles may affect the surface area significantly if the size distribution is very large.

If a bis-imidazole ligand bound only to a single lipid then the stoichiometry would be closer to 1.0. Stoichiometry less than one is strong evidence for multipoint coordination of bis-imidazole to multiple lipids. Studies of PSIDA-Cu^{2+}/DSPC/cholesterol or PSIDA-Cu^{2+}/SOPC vesicles with bis-imidazole are consistent with bifunctional coordination. The control vesicles lacking metal showed only a small heat when imidazole (Figure 5.10) or bis-imidazole (Figure 5.11) is added, which indicates almost no non-specific binding. Additionally the heat of dilution was the same average value for each injection as for 1.25 mM bis-imidazole injected into buffer, indicating that the dilution of the ligand is very much smaller than the heat of binding through chelated-Cu^{2+} (Figure 5.12).

CONCLUSIONS

The favorable binding energetics found from titration calorimetry indicate that multiple lipids may be involved in ligand binding. Using the association constants derived from calorimetric investigations, the thermodynamic parameters of binding were determined and used to interpret the lipid binding mechanism. The association constants determined from heat effects of binding were an order of magnitude higher than for imidazole binding. Entropic effects of lipid reorganization were calculated from K_{app} and ΔH determined from calorimetry measurements of bivalent bisimidazole binding. The entropy for bivalent binding was much larger and negative than for monovalent binding, perhaps indicating lipid re-organization. Binding enthalpy of 1,4-bisimidazole determined through fits of single-site binding model was nearly double that of imidazole and

exothermic. Thus, the binding is energetically favorable, exothermically driven and consistent with possible lipid re-organization upon ligand binding.

After combining the equilibrium binding results of model complexes with fluorescence measurements from Chapter 4, our results support multivalent histidine coordination to the bilayer *via* multiple lipids. Fluorescence measurements of the E/M ratio support multiple-lipid coordination in certain cases, because the E/M ratio increased when multivalent histidine compounds were added to vesicles. Very small effects were observed when Ca^{2+} or no metal was present. The increase in the E/M ratio is expected if multivalent binding enhanced the number of labeled-lipid collisions, bringing the lipids near each other. The formation of labeled-lipid domains composed of poly-L-histidine visible under the fluorescence microscope at excimer wavelengths also strongly supports this conclusion. The model complex 1,4-bisimidazole was able to bind to the lipid bilayers with higher affinity than the monovalent controls, also indicating more favorable binding energy which can be explained by multiple lipid coordination.

From these studies, metal-chelating fluorescently-labeled lipids provide a simple system to mimic natural membrane receptors at the surface of cells that combine to send a signal upon ligand binding (E/M fluorescence) and membrane receptors that can form higher-affinity multivalent complexes (calorimetry measurements, protein binding experiments). Additionally, work in our group has shown that lipid-based metal-chelating materials will be useful for two dimensional protein crystallization and also specific targeting of histidine-rich compounds to lipid interfaces. Further studies with systems composed of fluorescently-labeled metal-chelating lipids are expected to provide insight into a ligand's ability to organize the bilayer and will be useful in measurements of ligand-driven membrane re-organization. For instance, resonance energy transfer between lipids combined with pyrene-labeled lipid measurements of E/M could further distinguish the structure of organized lipid-ligand complexes.

EXPERIMENTAL

Metal-chelating fluorescent lipids

Dr. Darryl Sasaki synthesized PSIDA according to the published procedure [26]. The lipids were stored at 4 °C in solid form. Solutions were made in volumetric flasks in $CHCl_3$ (HPLC grade). It was very important to keep the lipids from light since the solutions would turn brown upon overnight exposure. Therefore, the lipid solutions were stored at 4 °C in the dark. Phospholipids were obtained from Avanti Polar Lipids (> 99% purity).

Preparation of vesicles

Vesicles were prepared by probe tip sonication as described in Chapter 2. The vesicle solutions were centrifuged for 20 minutes at 11,000 rpm to remove titanium fragments from probe tip sonication. The vesicles were then allowed to fuse and or reorganize for 3 hr so that they reach an equilibrium size distribution. Vesicles undergoing fusion or other non-equilibrium processes would absorb heat and consequently prevent the heat feedback-controller from reaching an steady state temperature. The vesicle concentration was then determined after ITC by using a phosphate assay. The concentration of total iminodiacetate groups was then calculated by using the mole ratio (X = 0.05) of PSIDA lipid to total lipid. The total concentration of surface-accessible metal was assumed to be $(0.7)*[Cu]_T$ since the vesicles in the SUV regime have 70% of the total lipid on the outer leaflet of the bilayer [27]. Imidazole or 1,4-bisimidazole was weighed into volumetric flasks and dissolved in MOPS buffer with stirring (1-4 mM) in [20 mM MOPS, 100 mM NaCl, pH 7.5] buffer.

Metallation of vesicles

Since it was very time consuming to determine vesicle concentration after probe tip sonication, metal was added to MLV vesicles prior to sonication and the vesicles sonicated (except for cholesterol vesicles). Cholesterol vesicles can be metallated and free metal removed by dialysis, while other vesicle formulations, such as PSIDA/DSPC, do not disperse upon dialysis (Chapter 2). Concentrated $CuCl_2$ solutions were made in 0.1M NaCl. If the metal solution was made instead in MOPS buffer at pH 7.5, the metal would form a visible $[M^{2+}(OH)_2]_n$ precipitate. Metal solution was added so that the resulting stoichiometry between total metal and total PSIDA lipid added was 1.05. For SOPC/PSIDA or DSPC/PSIDA vesicles, metal was added (except for metal binding experiments) before sonication at the indicated molar ratio. The vesicles were sonicated and titanium fragments removed by centrifugation or filtering on a 0.2 μ syringe filter. SOPC vesicles would remain in solution with this slight excess of metal, while DSPC vesicles prepared with exactly the same metal concentration would be significantly more turbid.

Cholesterol vesicles were prepared and metal was added after titanium fragments had been removed. The vesicles were then dialyzed in 3000 MW cutoff dialysis tubing (3 ml of vesicles against 300 ml buffer) for three hours to remove free metal. The vesicles would form a clearer solution after dialysis.

Preparation of $Cu^{2+}IDA$ for calorimetry experiments

Since it is difficult to measure the concentration of $Cu^{2+}IDA$ below 1 mM using the extinction coefficient of $EDTA-Cu^{2+}$ [22], $Cu^{2+}IDA$ was prepared by re-crystallization and elemental analysis for calorimetry experiments. Stoichiometric $CuCl_2$ and iminodiacetate were added to ddH_2O, and the pH adjusted with HCl to 7.0. EtOH was added until cloudiness developed. The $Cu^{2+}IDA$ complex precipitated along with other neutral

complexes. The precipitate was dried and then recrystallized twice in EtOH. The blue crystals were dried at 25 °C under vacuum and analyzed by elemental analysis. $Cu^{2+}IDA$ was obtained as the di-hydrate ($C_4H_9NO_6Cu$) (calculated 6.07 %N, 20.83 %C, 3.93 %H, 27.54 %Cu), found 5.85 %N, 20.46 %C, 3.82 %H, 28.18 %Cu, MW 230.66 g/mole.

Preparation of 1,4-bisimidazole for calorimetry experiments

1,4-bisimidazole was generously donated by Dr. Sean D. Plunkett. The methyl ester group was cleaved off in MeOH with KOH at 50 °C for 24 hr. by Dr. Darryl Sasaki. The compound was filtered and recrystallized 4 times in EtOH. The crystals were dried at 50 °C in a vacuum oven and analyzed by elemental analysis. 1,4-Bisimidazole was obtained as the di-hydrochloride, monohydrate ($C_{15}H_8N_4O_3Cl_2$) (calculated 14.81 %N, 48.27 %C, 4.88 %H), found 14.43 %N, 46.92 %C, 4.49 %H, MW 373.24 g/mole.

Isothermal titration calorimetry experiments

All experiments were performed on a Microcal (Northampton, MA) MCS computer controlled titration calorimeter. The sample cells were jacketed by a temperature controlled Neslabs RTE-111 water bath (Newington, NH). The water bath was set 10 °C lower than the temperature setpoint. Performance of the machine was determined by reproducing RNAse binding to 2'CMP data within 10% error [13]. For a typical titration experiment, the temperature setpoint was set 0.5 °C lower than the expected value, since the calorimeter overshoots the setpoint by at least this amount. The sample cell and reference cell were rinsed with buffer at least four times before filling with the compounds used for ITC experiments. This is necessary because the cells contained ddH2O which is not buffered. Lipid samples or $Cu^{2+}IDA$ complexes were placed into the sample cell, and buffer was placed in the reference cell while carefully dispersing bubbles. A 250 µl or 100 µl syringe (Microcal) was filled with ligand, and all bubbles were removed by depressing the plunger several times and refilling the syringe. The impeller of the syringe was rinsed with buffer

and then rinsed with excess sample cell solution. The syringe was placed into the cell and the autostart feature was used so that the system would be fully equilibrated before the run started. Typically, the concentration in the cell and syringe was chosen such that 24 injections would exceed the expected stoichiometry for the binding equilibria, assuming a binding constant using a computer program EXPHELP© donated by Microcal. If possible, binding data were taken over an order of magnitude range of vesicle or $Cu^{2+}IDA$ concentration to investigate any association phenomena. Several concentrations were used when possible to determine if binding parameters were affected by possible aggregation. Since the concentrations of lipid vesicle in the cell had to be greater than 3 mM vesicle concentration as determined from estimates of the binding parameters, the concentration range was limited with vesicle samples due to materials limitations.

The data were analyzed after concentration was determined by the Origin curve fitting algorithm or fits that are shown in Calculations. The first point of integrated enthalpy was ignored in fits because the stepping motor controlling injection would not grip the syringe properly, and caused an incomplete injection. Fits to the data were deemed acceptable if the χ^2 values were lower than 3000 calories between predicted heat and measured. If possible the average of several measurements was used to obtain the average binding constants for a concentration range. To determine concentration after experiments with vesicles, the phosphate content of vesicles was measured using a molybdate-based phosphate assay (see Chapter 3, Experimental). For experiments with small molecules such as $Cu^{2+}IDA$, concentration was not measured since the compound had been analyzed for purity using elemental analysis.

Table 5.1. Binding parameters obtained from sequential binding fits of isothermal titration calorimetry data showing binding of imidazole to $Cu^{2+}IDA$. $[Cu^{2+}IDA]$ was kept between 0.2 to 2.0 mM in MOPS buffer. Imidazole was 8-fold more concentrated in the syringe than the $Cu^{2+}IDA$ concentration. The raw and fitted ITC data are shown in Figure 5.3 (25 °C) and Figure 5.4 (35 °C). For comparison, the first binding constant of imidazole for $Cu^{2+}IDA$ from potentiometry at 35 °C is shown below the data from calorimetry.

Temperature (°C)	K_1 (M^{-1})	K_2 (M^{-1})	$\Delta H°_1$ (kcal/mole)	$\Delta H°_2$ (kcal/mole)	χ^2 (cal)
25 ± 0.5	5.19 ± 0.07 x 10^3	362 ± 5	-7.89 ± 0.03	-10.9 ± 0.13	135
35 ± 0.5	3.93 ± 0.09 x 10^3	319 ± 8	-7.31 ± 0.05	-10.0 ± 0.25	260
Stability constants determined from potentiometry					
35 [20]	2.23 ± 0.01 x 10^3	891 ± 1	—	—	—

Table 5.2. Binding parameters from ITC obtained from fits of imidazole binding data to PSIDA mixed metallated vesicles at 25.2 ± 0.5 °C using [Equation 8]. The total vesicle concentration was determined through phosphate assay and was typically between 2-10 mM in MOPS buffer [0.02M MOPS, 0.1M NaCl, pH 7.5] and is shown below the corresponding vesicle composition.

5% PSIDA-Cu mixed with	K_1 (M^{-1})	K_2 (M^{-1})	ΔH_1 (kcal/mole)	ΔH_2 (kcal/mole)
(total $[PO_4]_T$ concentration)				
95% SOPC (6.4 mM)	3.0 ±0.06 x 10^3	820 ± 10	-8.57 ± 0.09	-11.0 ± 0.4
47.5% DSPC/ 50% cholesterol (9.1 mM)	5.4 ±0.73 x 10^3	450 ± 60	-6.25 ± 0.3	-3.3 ± 6.3

Table 5.3. Binding parameters obtained from 1,4-bisimidazole binding to PSIDA-Cu^{2+} mixed small unilamellar vesicles. Data fitted with single site binding model [Equation 4] with $\chi 2$ values less than 3000 cal. The data are shown in Figure 5.8 and Figure 5.9. Data taken at 25 ± 0.5 °C in [20 mM MOPS, 100 mM NaCl, pH 7.5] with lipid concentrations as indicated in Figure 5.8 and Figure 5.9 with 1,4-bisimidazole in syringe (0.5-2 mM).

5% PSIDA in	n	K_{app} $(x\ 10^4\ M^{-1})$	ΔH (kcal/mole)
DSPC/cholesterol	0.54 ± 0.10	8.52 ± 0.96	-19.79 ± 0.05
SOPC	0.41 ± 0.05	8.62 ± 0.73	-16.78 ± 0.05

PSIDA

DSPC
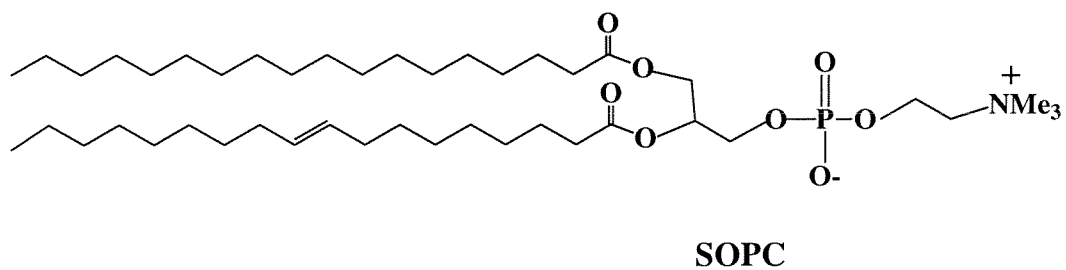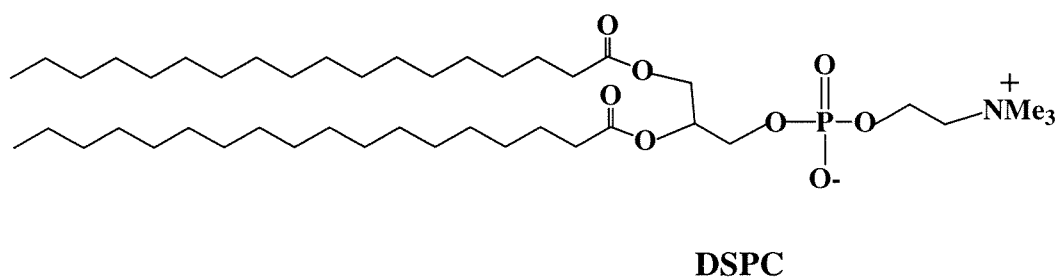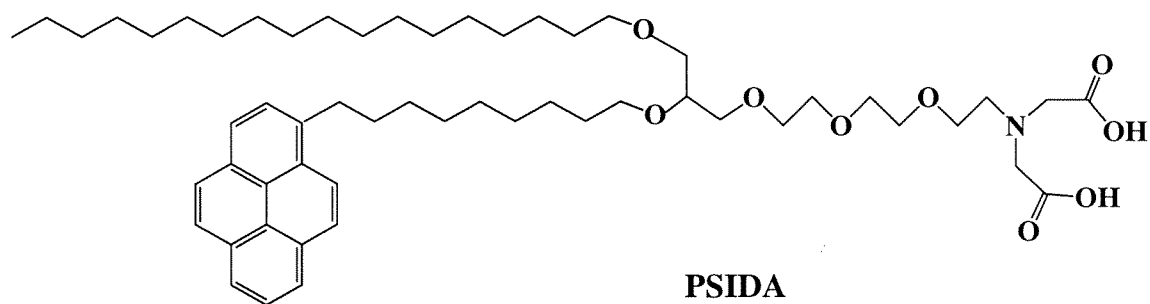
SOPC

Figure 5.1. Chemical structures of lipids used to make vesicles.
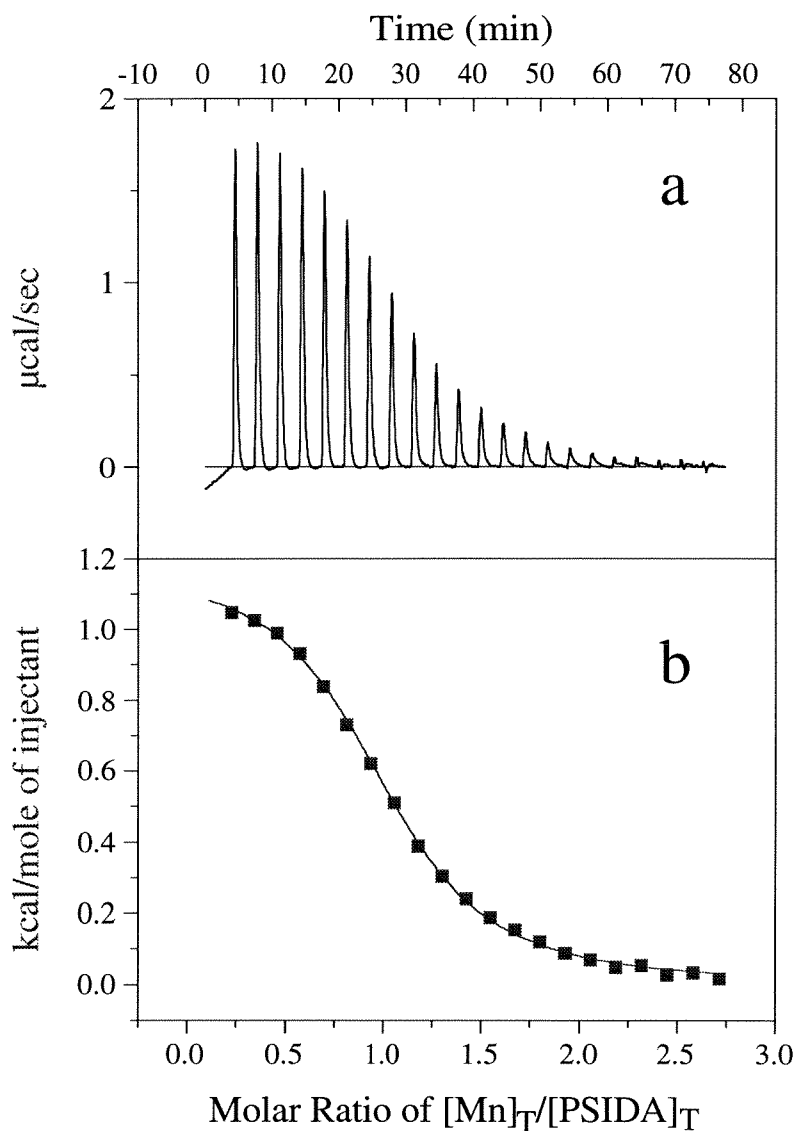
Figure 5.2. MnCl$_2$ binding to 5% PSIDA/ 95% SOPC vesicles (a) at 25 °C in buffer [20 mM MOPS, 100 mM NaCl, pH 7.5]. Integrated heat data (b) fitted with single-site binding model yielding stoichiometry n = 1.01 ± 0.01, K$_{app}$ = 3.32 ± 0.14 x 10^4 M^{-1}, ΔH = 1.18 kcal mol^{-1}. Lipid in cell, [PSIDA]$_T$ = 0.36 mM; ligand in syringe, [MnCl$_2$] = 5.37 mM; total lipid [PO$_4$]$_T$ = 7.8 mM.
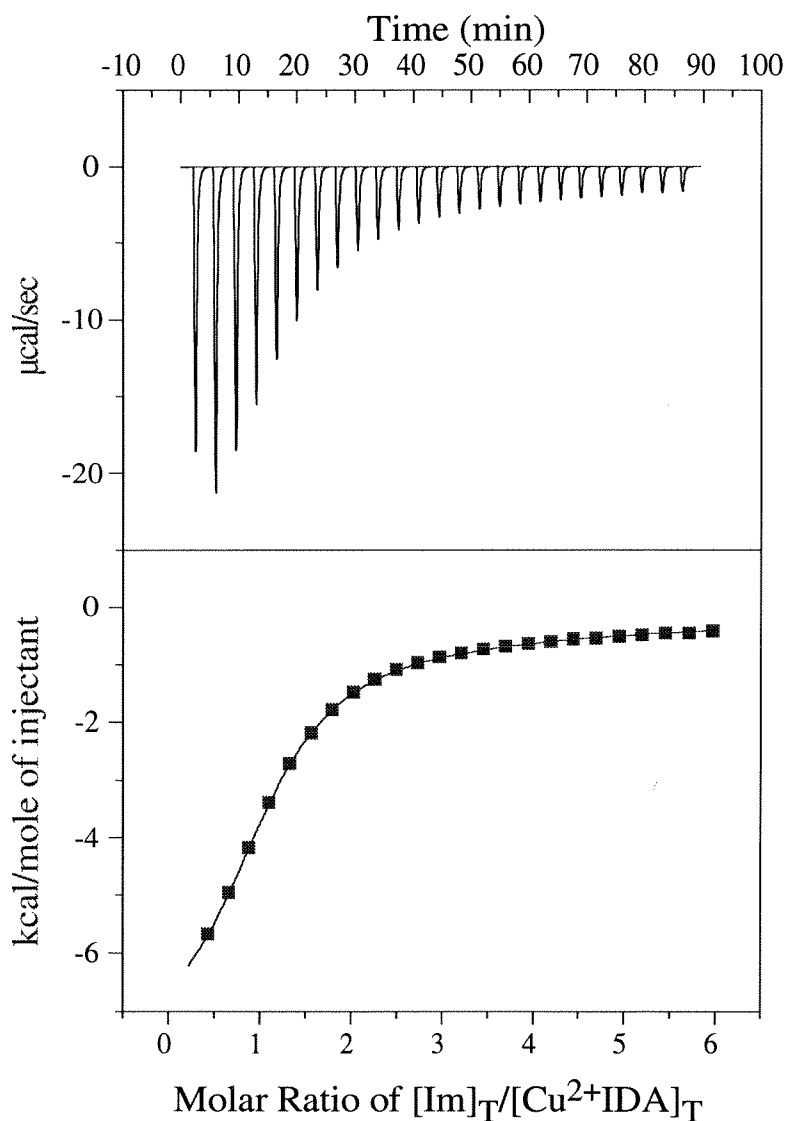
Figure 5.3. Isothermal calorimetry data showing binding of imdazole to Cu²⁺IDA at 25.2 ± 0.5 °C in [20 mM MOPS, 0.1 M NaCl, pH 7.5] buffer. [Cu²⁺IDA] = 0.5 mM in sample cell. Data fitted with Equation 8. Fitting parameters shown in Table 5.1.
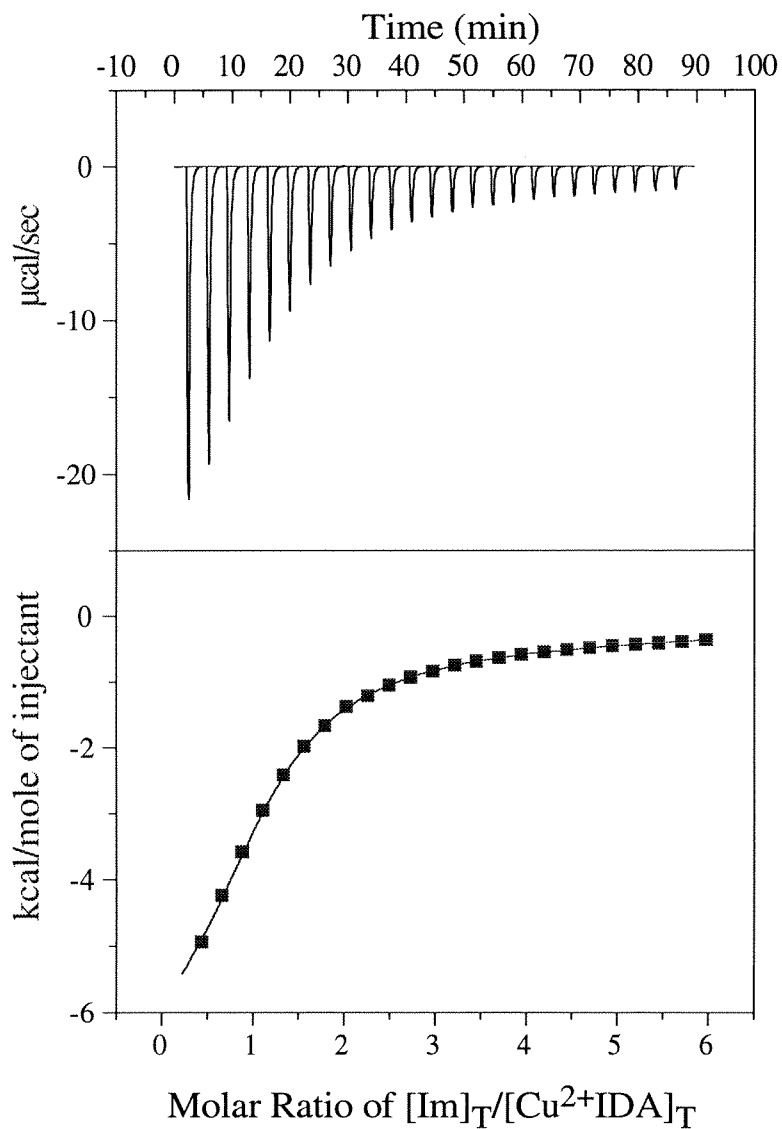
Figure 5.4. Isothermal calorimetry data showing binding of $Cu^{2+}IDA$ with imidazole at 35.2 ± 0.5 °C. $[Cu^{2+}IDA] = 0.5$ mM, in cell; [Imidazole] = 5mM, in syringe in MOPS buffer, pH 7.5. Data fitted with Equation 8. Fitting parameters shown in Table 1.
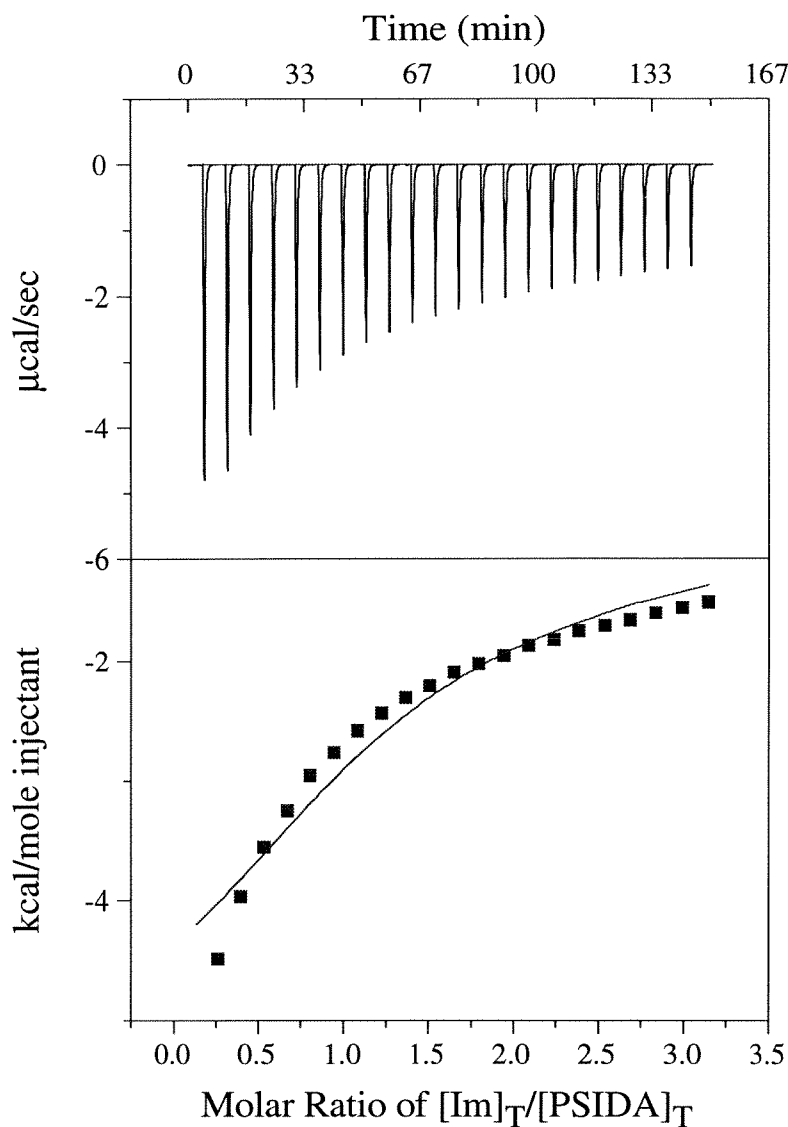
Figure 5.5. Titration calorimetry of imidazole binding to 2.5% PSIDA/ 47.5% DSPC/ 50% cholesterol vesicles [9.0 ± 3.2 mM total lipid phosphate] at 25.2 ± 0.4 °C. The vesicles were metallated and dialyzed prior to the experiment and fitted with Equation 8. Binding parameters are shown in Table 5.2.
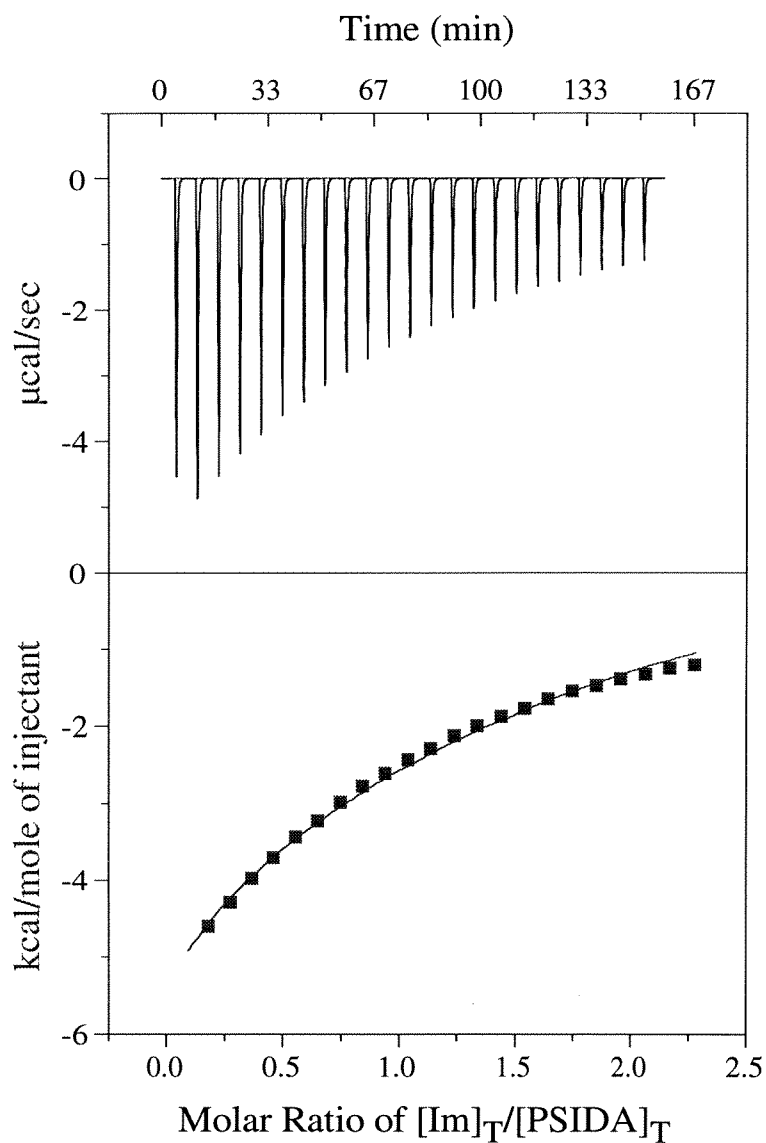
Figure 5.6. Titration calorimetry data showing binding of imidazole to 5% PSIDA-Cu^{2+} / 95% SOPC small unilamellar vesicles. Phosphate concentration of lipids was 6.4 ± 0.4 mM and total accessible copper was assumed to be 0.7 total PSIDA lipid, [PSIDA-Cu^{2+}] = 0.22 ± 0.02. Data are fitted with Equation 8. Fitting parameters are shown in Table 5.2.
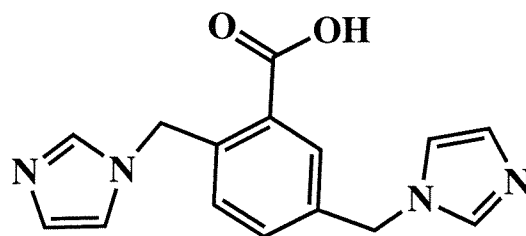
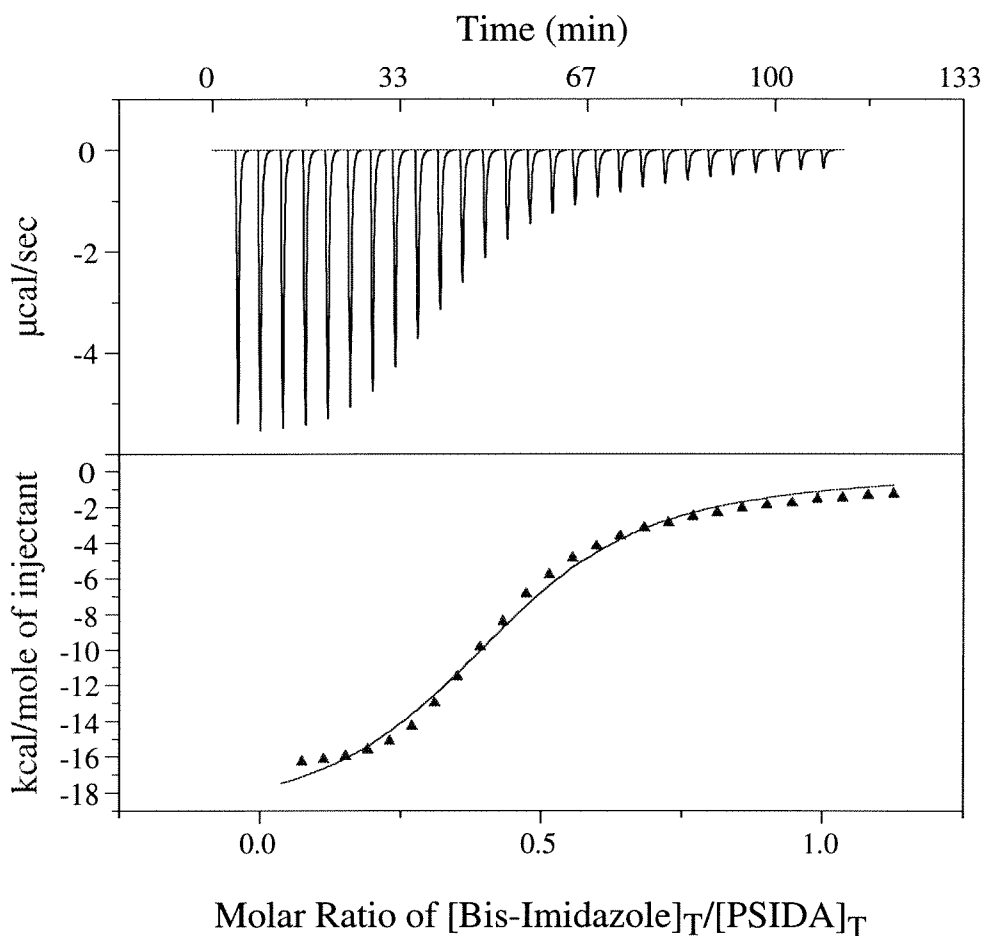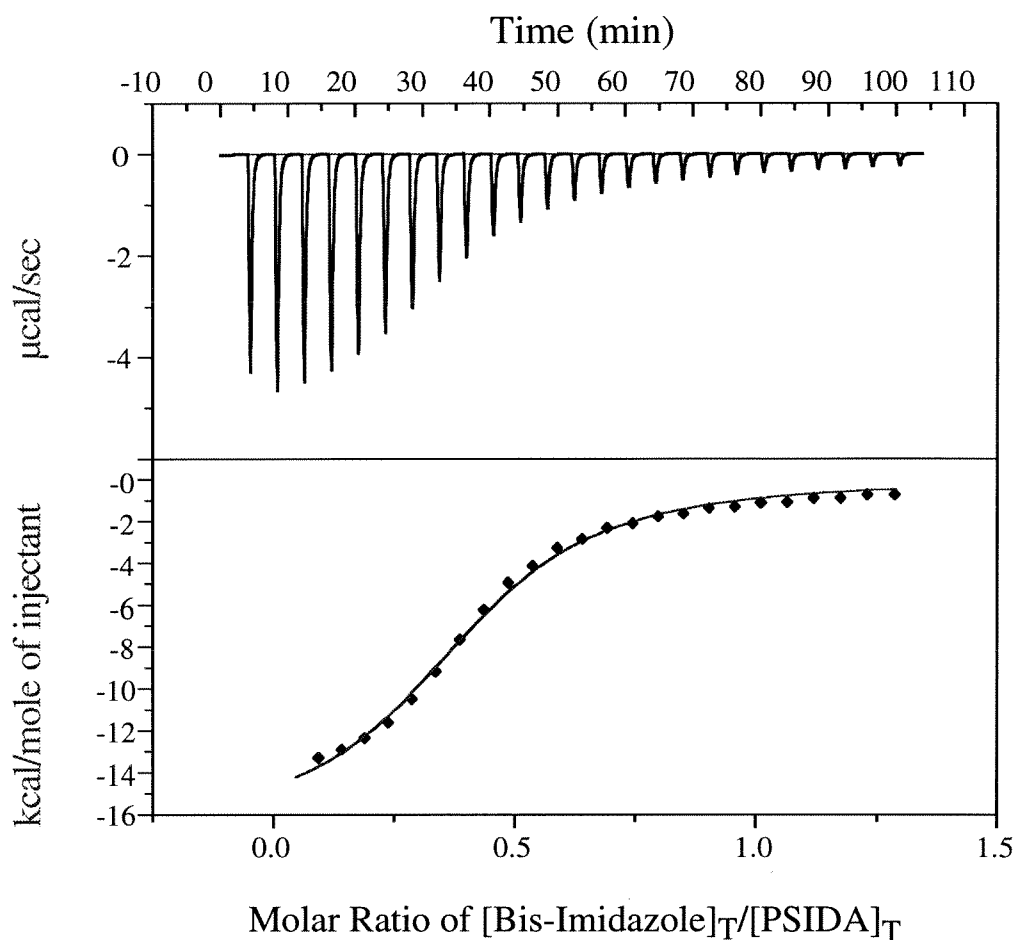**1,4-Bisimidazole**
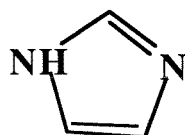
Imidazole

**Figure 5.7.** Structure of imidazole and 1,4-bisimidazole used in ITC binding experiments.

Figure 5.8. Titration calorimetry data showing binding of 1,4-bisimidazole to 2.5% PSIDA-Cu^{2}/47.5% DSPC/ 50% cholesterol small unilamellar vesicles at 25.2 ± 0.4 °C in MOPS buffer pH 7.5. Data are fitted with Equation 4. Lipid concentration of total accessible copper was $[PSIDA]_T$ = 0.18 ± 0.01 mM estimated from phosphate assay; [1,4-Bisimidazole] = 1.109 mM, in syringe. Binding parameters shown in Table 5.3.
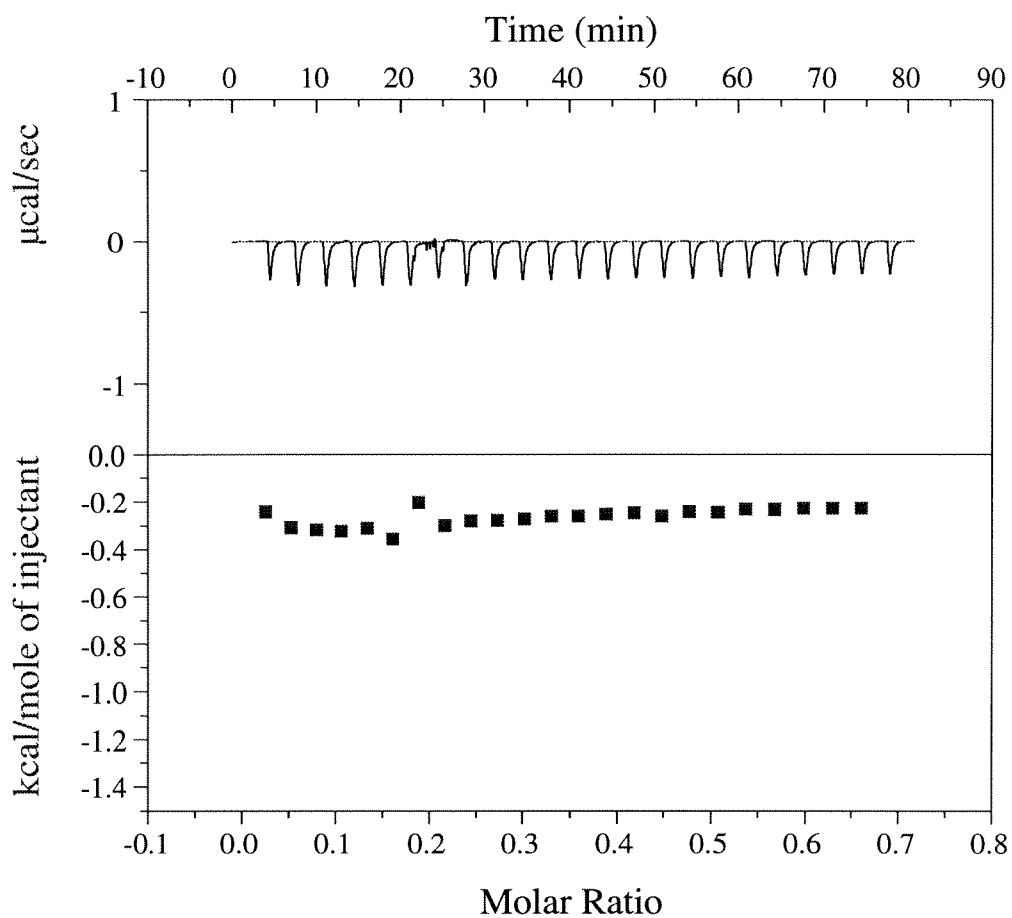
Figure 5.9. Titration calorimetry data showing 1,4-bisimidazole added to 5% PSIDA-Cu^{2+} / 95% SOPC small unilamellar vesicles taken at 25 ± 0.4 °C in MOPS buffer at pH 7.5. Data are fitted with Equation 4. $[PSIDA]_T = 0.18 \pm 0.01$ mM in cell, estimated from phosphate assay; [1,4-bisimidazole] = 1.109 mM, in syringe. Fitting parameters are shown in Table 5.3.
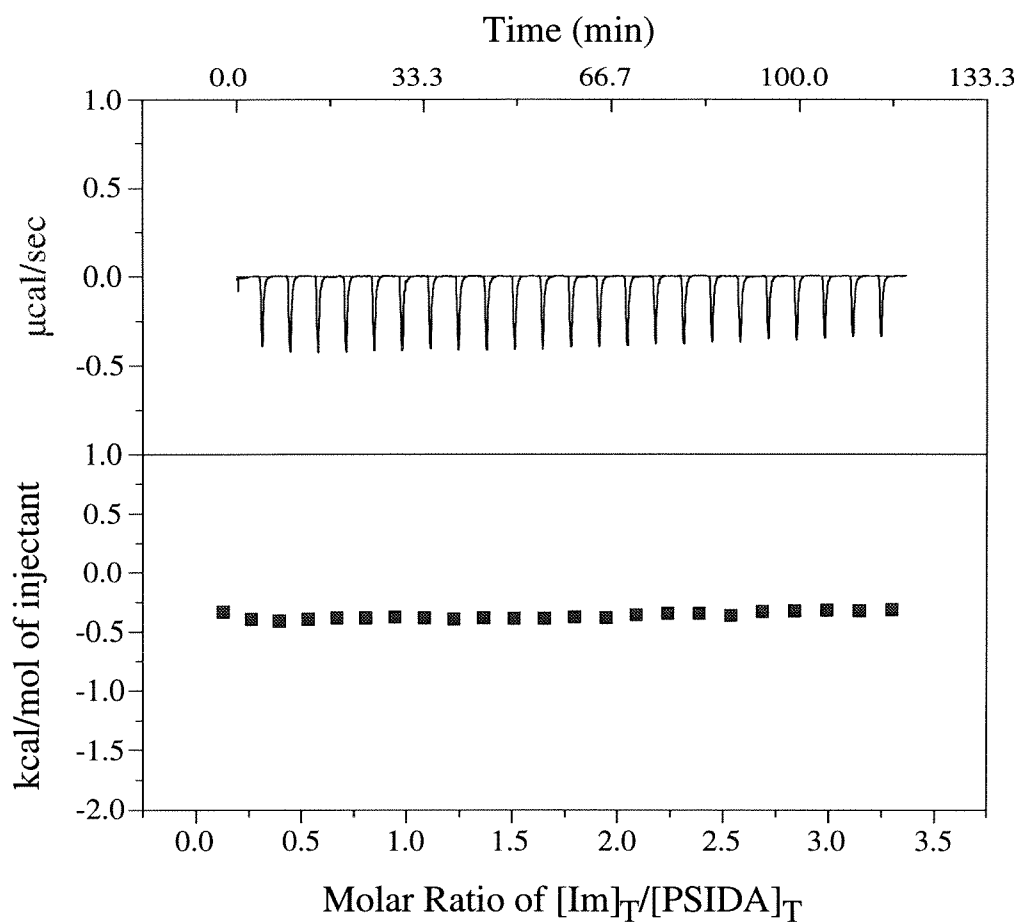
Figure 5.10. Control showing titration calorimetry of imidazole injected into 2.5% PSIDA/ 47.5% DSPC/ 50% cholesterol vesicles lacking metal at 25.2 ± 0.5 °C, at pH 7.5 in MOPS buffer. The uniform heat produced upon each injection indicates that the imidazole does not partition into the vesicle.
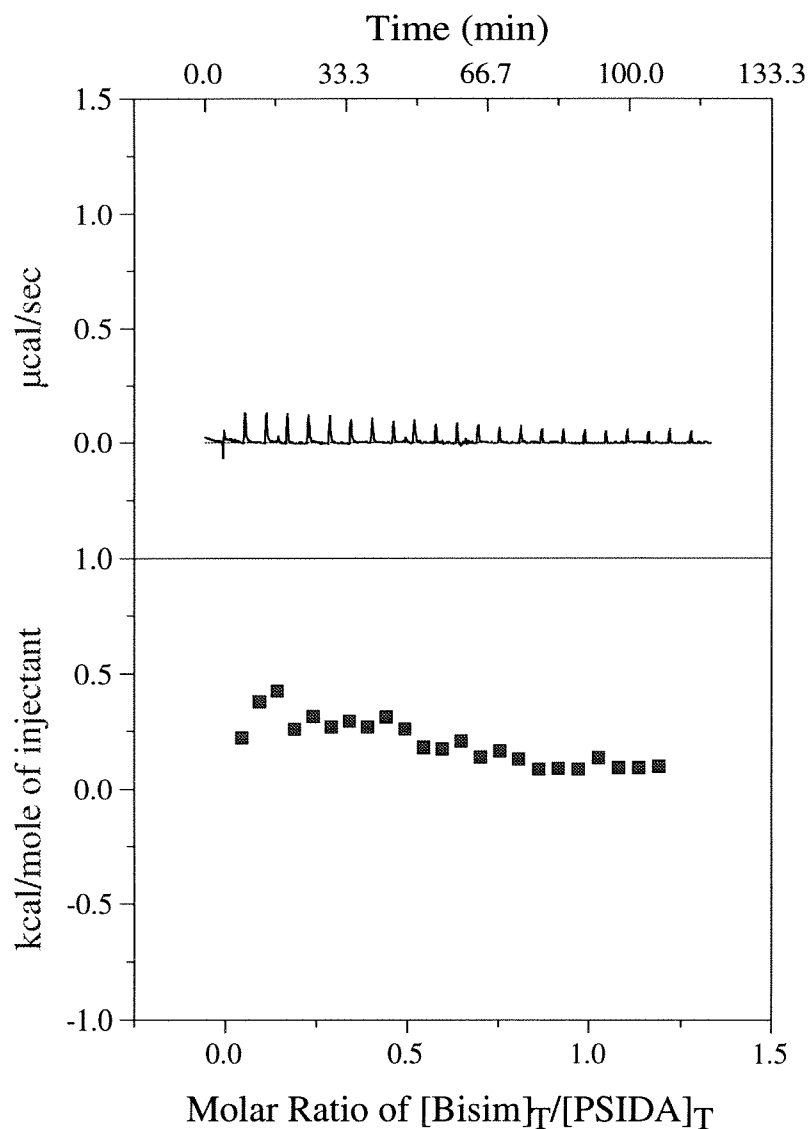
Figure 5.11. Control showing 1,4-bisimidazole injected into unmetallted cholesterol vesicles at 25.2 °C in MOPS buffer, pH 7.5. Vesicles placed in calorimeter cell [total lipid $PO_4]_T$ = 8.34 ±0.95 mM; ligand in syringe [1,4-bisimidazole] = 1.25 mM, in syringe. Average heat per injection found to be 279 cal/mole; 3.5 μcal/injection.

Figure 5.12. Titration calorimetry control showing dilution heat of imidazole [3.46 mM] added to buffer at 25.2 ± 0.4 °C. The averaged heat per injection was -10 μcal/injection; 346 cal/mole imidazole.
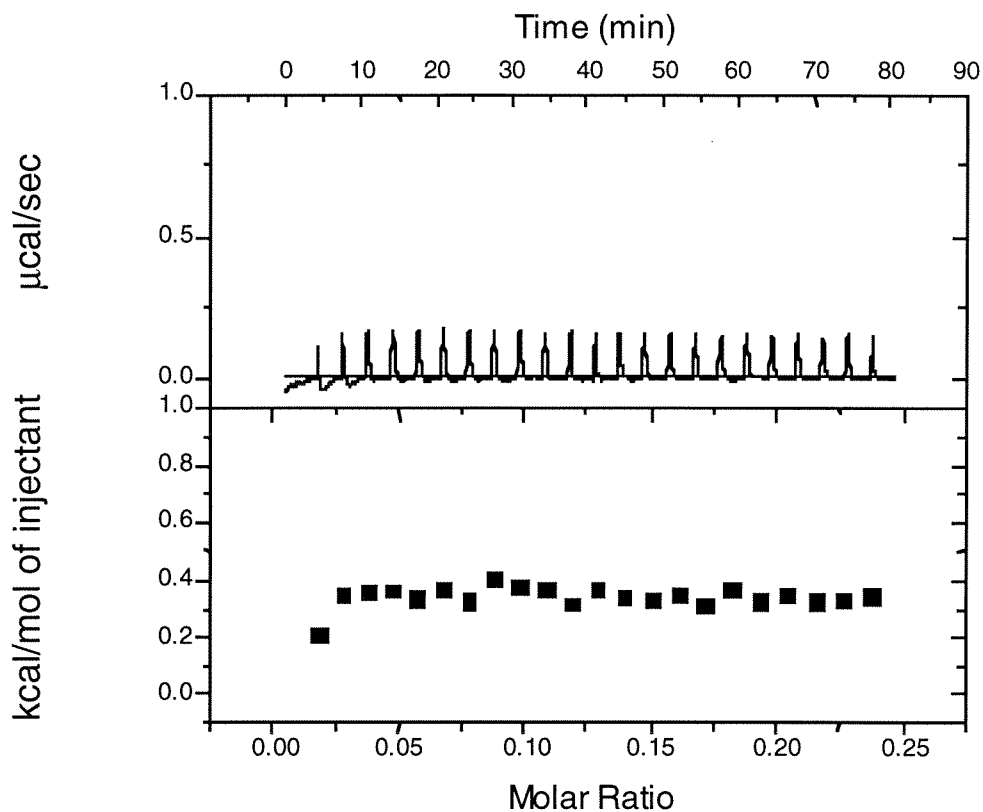
Figure 5.13. Dilution control of 1,4-bisimidazole injected into MOPS buffer at 25.2 °C. [1,4-bisimidazole] = 1.25 mM in MOPS buffer in syringe. Dilution heat is close to Figure 5.10 (0.4 kcal/mole injectant; -4.3 μcal/injection).

REFERENCES

1. Friere, E.; Mayorga, O. L.; Straume, M. *Anal. Chem.* **1990**, *62*, 950A-959A.

2. Wadsö, I. *Themal and Energetic Studies of Cellular Biological Systems.* James, A. M., Ed., Wright Publishers: Bristol, 1987, pp. 34-67.

3. Cooper, A. and McAuley-Hecht, K. E. *Phil. Trans. R. Soc. Lond. A* **1993**, *345*, 23-35.

4. Barenholz, Y.; Gibbes, D.; Litman, B.J.; Goll, J.; Thompson, T.E.; Carlson, F.D. *Biochemistry* **1977**, *16*, 2806-2810.

5. Miller, K. R. and Cistola, D.P. *Molec. Cell. Biochem.* **1993**, *123*, 29-37.

6. Seelig, J.and Ganz, P. *Biochemistry* **1991**, *30*, 9354-9359.

7. Seelig, J.; Nebel, S.; Ganz, P.; Bruns, C. *Biochemistry* **1993**, *32*, 9714-9721.

8. Zhang, F. and Rowe, E. S. *Biochim. Biophys. Acta* **1994**, *1193*, 219-225.

9. Plager, D. A. and Nelsestuen, G.L. *Biochemistry* **1994**, *33*, 7005-7013.

10. Montich, G.;. Scarlata, S.; Mclaughlin, S.; Lehrmann, R.; Seelig, J. *Biochim. Biophys. Acta* **1993**, *1146*, 17-24.

11. McLaughlin, S. *Annu. Rev. Biophys. Chem.* **1989**, *18*, 113-136.

12. Wyman, J.; Gill, S. J. *Binding and Linkage: Functional chemistry of biological macromolecules;* University Science Books: Mill Valley, 1990, pp p. 185.

13. Wiseman, T.; Williston, S.; Brandts, J.F.; Lin, L.-N. *Anal. Biochem.* **1989**, *179*, 131-137.

14. Johnson, R. D. *Ph.D. Thesis*, California Institute of Technology, **1995**.

15. Martell, A. E., Smith, P.M. *Critical Stability Constants*; Plenum Press: New York, 1974; Vol. 6.

16. Lehrmann, R. and Seelig, J. *Biochim. Biophys. Acta* **1994**, *1189*, 89-95.

17. Cotton, F.A.; Wilkinson, G. *Advanced inorganic chemistry; a comprehensive text,* 3d ed.; Interscience Publishers: New York, 1972

18. Mosior, M. and. McLaughlin., S. *Biochim. Biophys. Acta* **1992**, *1105*, 185-187.

19. Mosior, M. and McLaughlin, S. *Biochemistry* **1992**, *31*, 1767-1773.

20. Sinha, P. C.; Saxena, V.K.; Nigam, N.B.; Srivastava, M.N. *Ind. J. Chem.* **1989**, *28A*, 335-336.

21. Dung, N. H.; Viossat, B.; Busnot, A.; Zafra, A. G. S.; Perez, J. M. G.; Gutierrez, J. N. *Inorg. Chim. Acta* **1990**, *169*, 9-12.

22. Todd, R. *Ph.D. Thesis*, California Institute of Technology, **1993**.

23. Todd, R. J.; Johnson, R. D.; Arnold, F. H. *J. Chromatography* **1994**, *662*, 13-26.

24. van Holde, K.E. *Physical Biochemistry,* Prentice-Hall Inc.: Engelwood Cliffs, NJ, , 1985, p77.

25. Jencks, W. P. *Proc. Natl. Acad. Sci. USA* **1981**, *78*, 4046-4050.

26. Ng, K.; Pack, D.W.; Sasaki, D.Y.; Arnold, F.H. (submitted to *Langmuir*).

27. Fendler, J. *Membrane Mimetic Chemistry* , John Wiley & Sons: New York, 1982, pp121-132.